DISS. ETH NO. 24850

Initiation and Regulation of Integrin-Mediated Adhesion to Fibronectin in Fibroblasts

A thesis submitted to attain the degree of

DOCTOR OF SCIENCES of ETH ZURICH

(Dr. sc. ETH Zurich)

presented by

Nico Strohmeyer

Dipl. Nat., Technische Universität Bergakademie Freiberg

born on 02.05.1986

citizen of

Federal Republic of Germany

accepted on the recommendation of

Prof. Dr. Daniel J. Müller

Prof. Dr. Reinhard Fässler

Prof. Dr. Michael Nash

2018

To my wife and family

Research is what I'm doing when I don't know what I'm doing.

Wernher von Braun

Zusammenfassung

Für die korrekte physiologische Funktion von Geweben sind spezifische adhäsive Interaktionen zwischen Zellen und der extrazellulären Umgebung essentiell. Die primären Zelladhäsionsrezeptoren für viele extrazelluläre Strukturproteine, wie Kollagene, Fibronektin und Laminine sind Integrine. Diese binden an die extrazellulären Strukturproteine und koppeln sie über Adapterproteine an das Zytoskelett. Dadurch werden Zellen an der extrazellulären Matrix verankert. Wenn Integrine an Strukturproteine binden, bilden sie kleine Adhäsionscluster, welche im Verlauf der Adhäsionsformation zu großen fokalen Adhäsionen reifen. Während dieser Reifung wird die Verbindung zwischen Adhäsionsclustern und extrazellulären Strukturproteinen durch eine Vielzahl von intrazellulären Proteinen stabilisiert. Der Prozess der Adhäsionsreifung wird durch viele intra- und extrazelluläre Faktoren reguliert, unter anderem durch physikalischen Parameter der extrazellulären Umgebung und verschiedene intrazelluläre Signalkaskaden. Allerdings ist nicht bekannt welchen Einfluss physikalische Parameter der Umgebung oder der Zelle auf die Adhäsionsinitiierung durch Integrine haben. Weiterhin ist nicht bekannt, ob und wie sich verschiedene Integrine gegenseitig im Prozess der Adhäsionsinitiierung in ihrer Funktion beeinflussen. Mittels Rasterkraftmikroskopie-basierte Einzelzell-Kraftspektroskopie (SCFS) kann die Adhäsionsstärke während der Adhäsionsinitiierung quantitativ bestimmt werden. Dafür wird eine Zelle an einen Kraftsensor, den Cantilever, angebracht und an ein Substrat, welches eine proteinbeschichtete Oberfläche, eine andere Zelle oder ein Gewebe sein kann, angenähert, bis die Zelle mit diesem in Kontakt ist. Nach einer bestimmten Adhäsionszeit wird die Zelle zurückgezogen und vom Substrat abgelöst. Während des Ablösens der Zelle wird die maximale Kraft, welcher die Zelle widerstehen kann, bevor sie sich vom Substrat ablöst und die Bindungsstärke einzelner Adhäsionsrezeptoren bestimmt.

Eine Einschränkung der Rasterkraftmikroskopie-basierten SCFS, ist ein geringer experimenteller Durchsatz und damit verbunden ein hoher Zeitaufwand um statistisch aussagekräftige Ergebnisse zu erlangen. Ein Grund dafür ist, dass es bislang keine einfache experimentelle Möglichkeit gibt, Adhäsionsparameter einzelner Zellen für verschiedene Substrate zu bestimmen. Daher haben wir eine Maske entwickelt, welche erlaubt einen Untergrund mit vier verschiedenen Substraten zu beschichten. Diese Maske ist einfach zu produzieren, ermöglicht den direkten Vergleich von Adhäsionsbildung einer Zelle auf verschiedenen Substraten und minimiert so experimentelle Zeit und Kosten.

Um eine Zelle an den Kraftsensor des Rasterkraftmikroskops anzuheften, müssen adhärente Zellen zuerst von einer Zellkulturschale abgelöst werden. Das wird in der Regel durch den Einsatz der Protease Trypsin, welche Proteine an der Zelloberfläche verdaut, in Verbindung mit dem Entfernen von Adhäsions-essentiellen Ionen erreicht. Welchen Einfluss das Ablösen der Zellen von der Kulturschale auf die nachfolgenden, sehr sensitiven Adhäsionsexperimente hat, war bisher nicht bekannt. Unsere Experimente zeigen, dass das Ablösen der Zellen durch das

Entfernen von Ionen keinen systematischen Einfluss auf die nachfolgenden Adhäsionsmessungen hat. Jedoch führt das Ablösen mit Trypsin von Fibroblasten zu einer deutlichen Erhöhung der Adhäsionskraft zu Fibronektin in den nachfolgenden Adhäsionsexperimenten. Allerdings ist die Adhäsionskraft, nach einer Erholungsphase der Fibroblasten von etwa 45 Minuten nach dem Ablösen, auf dem Niveau der Zellen die durch das Entfernen von Ionen Abgelöst wurden. Somit hat auch die Ablösung der Zellen mit Trypsin nach etwa 45 Minuten keinen Einfluss mehr auf die Adhäsionsexperimente. Allerdings deuten diese Ergebnisse darauf hin, dass mittelfristig die Adhäsion zu bestimmten Substraten, wie in diesem Fall Fibronektin, von bestimmten Zelltypen durch das Ablösen mit Trypsin beeinflusst werden.

Adhäsion von Fibroblasten zu Fibronektin wird hauptsächlich durch zwei verschiedene Integrine, α5β1 und αVβ3 Integrine, initiiert. Allerdings ist weitgehend unbekannt, wie beide Integrine die Adhäsionsinitiierung regulieren. Unsere Experimente zeigen, dass beide Integrine um das Binden an Fibronektin konkurrieren. Auf Grund höherer Bindungskinetik und/oder besserer Stabilisierung der αVβ3 Integrine durch Adapterproteine binden αVβ3 Integrine an Fibronektin schneller als α5β1 Integrine. Nachdem sie an ihren Liganden gebunden haben, bilden αVβ3 Integrine kleine Adhäsionscluster, welche weiter reifen. Durch das Rekrutieren diverser intrazelluläre Proteine zu den Adhäsionsclustern initiieren αVβ3 Integrine Signale, welche über eine große Reichweite das Binden von α5β1 Integrine an Fibronektin fördern. Weiterhin wird die Clusterbildung von Fibronektin-gebundenen α5β1 Integrine beschleunigt, was zu einer schnelleren Verstärkung der Verbindung zwischen Zelle und extrazellulärer Matrix führt. Der Signalweg zwischen αVβ3 und α5β1 Integrine setzt sich aus verschiedenen Proteinen, einschließlich Proteinen die das Zytoskelett regulieren.

Während Fibroblasten Adhäsion zu Fibronektin aufbauen, müssen neu gebildete Adhäsionspunkte extra- und intrazellulär generierten Kräften widerstehen können. Um Erkenntnisse zu bekommen, wie Fibroblasten die initiale Adhäsion in Reaktion auf unterschiedliche mechanische Belastungen regulieren, haben wir Fibroblasten mit unterschiedlichen Geschwindigkeiten von Fibronektin separiert und die maximale Kraft, der sie widerstehen können, quantifiziert. Unsere Resultate zeigen, dass Fibroblasten, welche für etwa zwei Sekunden in Kontakt mit Fibronektin sind, ihre Adhäsion in Reaktion auf mechanische Belastung regulieren. Bei niedriger bis mittlerer mechanischer Belastung an neu formierten Adhäsionen, bilden α5β1 Integrine und Fibronektin „catch bonds“, welche durch eine längere Bindungsdauer bei mechanischer Belastung gekennzeichnet sind. Abhängig von diesen catch bonds initiieren α5β1 Integrine ein sehr schnelle Signalkaskade (unter 0.5 Sekunden), welche über zwei Kinasen (focal adhesion kinase und src kinase) die Bindung anderer Integrine an Fibronektin bedingt. Weiterhin ist für die Reaktion auf mechanische Belastung die Verbindung zwischen Integrinen und dem Zytoskelett, sowie Proteine die Aktin polymerisieren wichtig. Wenn die mechanische Belastung an den neu gebildeten Adhäsionen zu hoch wird, können keine zusätzlichen Integrine an Fibronektin gebunden werden und die Adhäsionsverstärkung schlägt fehl.

Summary

For the proper physiological function of tissues, specific adhesive interactions between cells and the extracellular environment are essential. The main cell adhesion receptors for many extracellular structural proteins, such as collagens, fibronectin and laminins are integrins. These bind to the extracellular structural proteins and couple them via adapter proteins to the cytoskeleton. This anchors cells to the extracellular matrix. When integrins bind to structural proteins, they form small adhesion clusters that mature into large focal adhesions in the course of the adhesion formation. During this maturation, the connection between adhesion clusters and extracellular structural proteins is stabilized by a variety of intracellular proteins. The process of adhesion maturation is regulated by many intracellular and extracellular factors, including physical parameters of the extracellular environment and various intracellular signaling cascades. However, the influence of physical parameters of the environment or the cell have on adhesion initiation by integrins is largely unknown. Furthermore, it is not known whether and how different integrins influence each other's function in the process of adhesion initiation. Atomic force microscopy (AFM)-based single-cell force spectroscopy (SCFS) can be used to quantify the adhesion strength during adhesion initiation. For this purpose, a cell is attached to a force sensor, the AFM-cantilever. The cantilever-bound cell is approached onto a substrate, which can be a protein-coated surface, another cell or a tissue, until the cell is in contact with it. After a certain adhesion time, the cell is withdrawn and detached from the substrate. As the cell is withdrawn from the substrate, the maximum force that the cell can withstand before it detached from the substrate and the binding strength of individual adhesion receptors are quantified.

A limitation of the atomic force microscopy-based SCFS, is a low experimental throughput and an extended experimental time to obtain statistically reliable results. One reason for this is that no simple experimental method exists that allows to characterize adhesion parameters of a single cell to multiple substrates. Therefore, we have developed a mask that allows to coat a surface with four different substrates. This mask is easy to produce, allows direct comparison of cell adhesion formation on different substrates, thereby minimizing experimental time and cost.

To attach a cell to the force sensor of the AFM, adherent cells must first be detached from a cell culture dish. This is typically achieved by the use of the protease trypsin, which digests proteins on the cell surface, in combination with the removal of adhesion-essential ions. The influence cell detachment from the culture dish on the subsequent, very sensitive adhesion experiments, was not previously known. Our experiments show that detachment of cells by the removal of ions has no systematic influence on the adhesion measurements. However, detachment of fibroblasts with trypsin results in a marked increase in the adhesion force to fibronectin in subsequent adhesion experiments. However, after a recovery time of about 45 minutes after detachment from the cell culture dish, the adhesion force of fibroblasts is at the level of the cells which have been detached by the removal of ions. Thus, the detachment of the cells with trypsin

after about 45 minutes has no influence on the adhesion experiments. However, these results indicate that adhesion of certain cell types to certain substrates, such as fibronectin in this case, will be affected by detachment with trypsin.

Adhesion of fibroblasts to fibronectin is primarily initiated by two different integrins, α5β1 and αVβ3 integrins. However, it is largely unknown how these integrins regulate adhesion initiation. Our experiments show that both integrins compete for binding to fibronectin. Due to higher binding kinetics and/or better stabilization of the αVβ3 integrins by adapter proteins, αVβ3 integrins bind to fibronectin faster than α5β1 integrins. After binding to their ligands, αVβ3 integrins form small adhesion clusters that mature in larger adhesion clusters. By recruiting diverse intracellular proteins into the adhesion clusters, αVβ3 integrins initiate signals that promote the binding of α5β1 integrins to fibronectin over long distances. Furthermore, the clustering of fibronectin-bound α5β1 integrins is accelerated, resulting in a faster enhancement of the cell-extracellular matrix linkage. The signaling pathway between αVβ3 and α5β1 integrins consists of several proteins, including proteins that regulate the cytoskeleton.

While fibroblasts build adhesion to fibronectin, newly formed adhesions must withstand extra- and intracellularly generated forces. To gain insight into how fibroblasts regulate initial adhesion in response to different mechanical loads, we have separated fibroblasts at different speeds from fibronectin and quantified the maximum force they can withstand. Our results show that fibroblasts, which were in contact with fibronectin for about two seconds, regulate their adhesion in response to mechanical load. At low to moderate mechanical load on newly formed adhesions, α5β1 integrins and fibronectin form catch bonds, which are characterized by an increased bond lifetime under mechanical stress. Depending on these catch bonds, α5β1 integrins initiate a very fast signaling cascade (less than 0.5 seconds), which causes the binding of other integrins to fibronectin via two kinases (focal adhesion kinase and src kinase). Furthermore, for the reaction to mechanical stress, the connection between integrins and the cytoskeleton, as well as proteins that polymerize actin important. If the mechanical load on the newly formed adhesions overcomes a threshold, no additional integrins can be bound to fibronectin and the adhesion enhancement fails.

Table of Content

1. Introduction

1.1. Cell Adhesion

Cell adhesion is crucial for the three-dimensional structure of all multicellular organisms, as it assembles single cells into a complex architecture found in tissue. Specific adhesive interactions between two cells or cells and the extracellular matrix (ECM) are fundamental for cellular communication, tissue organization and embryonic development. Thus, specific cell adhesion mechanisms translate basic genetic information into three-dimensional tissues and are essential for the correct physiological function of organs. However, cell adhesion is also employed to maintain or retrieve physiological homeostasis, for example in immune responses or wound healing. Cell adhesion is usually mediated by three functional complexes; the ECM, adhesion receptors that connect the cell to the ECM and intracellular proteins that connect the adhesion receptor to the cytoskeleton. Adhesion receptors are typically transmembrane proteins that are classified into different families depending on structure and function, including integrins, cadherins, proteoglycan superfamilies and selectins[1-4]. Adhesion receptors respond to cellular signaling, but also themselves induce intracellular signaling pathways, which regulate a wide variety of cellular properties and processes, including the adhesive and mechanical state of cells[5-8]. Due to the complexity of adhesion mechanisms and their essential roles in tissue maintenance, a wide variety of diseases are associated with impaired cell adhesion[9-12].

1.2. The Extracellular Matrix and Fibronectin

A fundamental component to the formation and the physiological function of a three-dimensional tissue is the ECM, which is a heterogeneous meshwork of fibrillar and non-fibrillar components. Proteoglycans and fibrous proteins, essentially collagens, laminins and fibronectin form a hydrated gel and are the main components of the ECM. Cells within the tissue form the ECM during development, maintain it during health, remodel it during adaption and repair it in response to a disease or during wound healing[13]. The ECM provides biochemical and biophysical cues to cells within the ECM, which influence cell proliferation, growth and differentiation within the tissue[14]. The composition and topography of the ECM is generated by a dynamic interplay of cellular components and the protein microenvironment that makes the ECM in each tissue unique[15].

One of the most abundant and ubiquitous ECM protein is fibronectin (Figure 1-1). It is produced and secreted by various cell types as a dimer comprised of two large monomers with a molecular mass of 230-270 kDa. For dimerization, fibronectin monomers are connected by two disulfide bonds at their C-termini. Fibronectin monomer are modularly build proteins consisting of repeating type I, II and III domains. Whereas all type I and type II domains are stabilized by

intra-chain disulfide bonds, the type III modules do not contain disulfide bonds and are hence more flexible. Fibronectin contains multiple functional regions that facilitate the binding of growth factors, structural proteins, such as collagens, fibrinogen as well as other fibronectin molecules, and present multiple binding sites for cell adhesion receptors[16,17]. Due to alternative splicing of the fibronectin gene, twenty different isoforms of monomeric fibronectin are expressed in humans and twelve in mice[18]. In many vertebrates, alternative splicing of fibronectin occurs by exon skipping of the extradomain B (between FNIII7 and FNIII8) and A (between FNIII11 and FNIII12) as well as a structurally more complex exon subdivision of module V (between FNIII14 and FNIII15)[18,19].

Cell adhesion to fibronectin is facilitated by multiple integrin binding sites found in different modules, but mainly in FNIII9 and FNIII10 (Figure 1-1)[16]. Thereby, the tripeptide arginylglycylaspartic acid (RGD) in the FNIII10 module[20] is essential for integrin binding to fibronectin[21]. In addition to binding the RGD motif, some integrins bind to the sequence PHRSN in the FNIII9 module, also called synergy site, which is in close proximity to the RGD motif. Although mutations in the synergy site lead to impaired function of specific integrins[22-25], mice carrying a mutation in the synergy site suffer from only minor defects[26]. This indicates that the function of the synergy site can be fibronectin-intrinsically rescued. However, a deletion of the whole fibronectin gene has severe impacts on cell adhesion, mesodermal migration and cell differentiation, resulting in embryonic lethality[27].

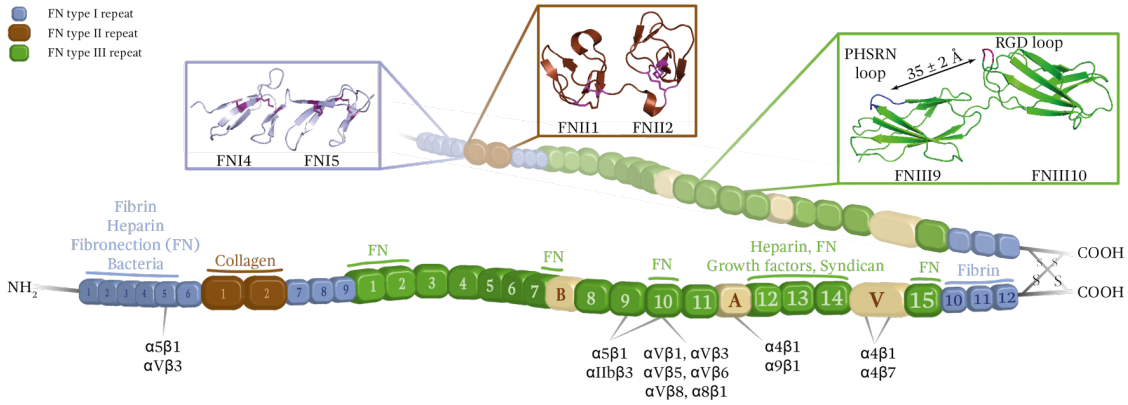

Figure 1-1 Scheme of the modular structure of a fibronectin dimer. Fibronectin is built from three different repeating modules (type I, blue; type II, brown; type III, green). The sites of alternative splicing (extradomains A, B and the variable 'V' domain) are shown in ochre. Integrin binding sites are indicated as well as binding domains for syndicans, growth factors, fibronectin, collagen, fibrin, heparin and bacteria. Structures of exemplary modules are drawn using PyMOL with coordinates from PDB (type I 1FBR, type II 1h8p, type III 1FNF).

The assembly of fibronectin matrices is a complex and cell driven process[28]. Fibronectin dimers are excreted by cells in a compact globular conformation, which is stabilized by intra-fibronectin interactions (Figure 1-2a)[29]. This conformation protects cryptic binding sites for other fibronectin proteins. Soluble fibronectin does not form fibrils even at high concentrations, which is of high importance in body fluids such as blood. Fibronectin fibril formation is initiated when integrins on the cell surface interact with RGD and the PHSRN motif of the soluble

fibronectin dimer. Adaptor proteins connect integrins and hence also the globular fibronectin to the actin cytoskeleton. The integrin-mediated cytoskeleton connection transmits myosin II-dependent tensile forces to the fibronectin dimer leading to a stretching of the bound fibronectin molecule. The fully extended fibronectin dimer is 90 to 160 nm long and has a diameter of 2-3 nm (Ref. 30,31).

Due to conformational changes and stretching of fibronectin molecules, cryptic inter-fibronectin interaction sites are unraveled leading to fibronectin self-assembly and fibril formation (Figure 1-2b)[32,33]. The C-terminal disulfide bonds in fibronectin dimers are essential to form fibrillar structures[34] and for the incorporation into fibronectin matrices[35]. Initially, the assembly of fibronectin by intermolecular interactions leads to the formation of small fibers at the cell periphery (Figure 1-2c) with a length of <700 nm and a diameter of 2-5 nm (Ref. 36,37). Recently, a recurring fibronectin pattern in newly formed native fibrils was determined with a periodicity of ~95 nm on average (ranging from 60 to 130 nm)[30]. Subsequent fibril maturation depends on two processes; an integrin-dependent incorporation of fibronectin into the fibers[38] and an integrin-independent recruitment of soluble fibronectin[39]. Thereby, the integrin-dependent maturation of fibronectin fibrils depends on cell-mediated contractile forces[32,40-44]. These forces maintain the extended conformation of the dimer[44] and reversibly unfold the type III repeats[45-47], which exposes cryptic binding sites and increases the binding of soluble fibronectin[43]. During maturation, fibronectin fibers grow in size and loose the periodicity[30]. Altogether, the formation and maturation of fibronectin matrices are mechano-sensitive processes that depend on cell-mediated tensile forces exerted on fibronectin molecules by integrins.

In tissue, the ECM composition and posttranslational modification of the components tightly control the mechanical properties of the ECM[48,49]. Cells respond to forces applied to their integrin-mediated adhesions by regulating expression of collagens, fibronectins and metalloproteinases, which together control the mechanical state of the ECM[50-54]. The tensional state of the ECM regulates the interaction of its components, as it has been shown that collagen I preferentially interacts with relaxed fibronectin, and upon binding shields fibronectin form excessive tensile forces[55]. Moreover, stretched cells assemble very dense matrices enriched in collagen fibers[52], with a directional matrix assembly along the axis of the applied force[56]. Together fibronectin and collagen fibers confer mechanical strength to tissues. Hence, mechanical force regulates the ECM at two levels. First, forces applied to cells, either by extracellular mechanical stress or cellular contractility, regulate ECM protein production and the secretion of ECM remodeling proteins. Second, the assembly of fibrils and their polymerization is directly affected by mechanical forces. Different tissues have different mechanical properties, which depend on the composition and remodeling of the ECM is remodeled as well as on cells present in the tissue. Consequently, alterations in the tissue specific mechanical properties result in impaired functionality of the tissue[57-59].

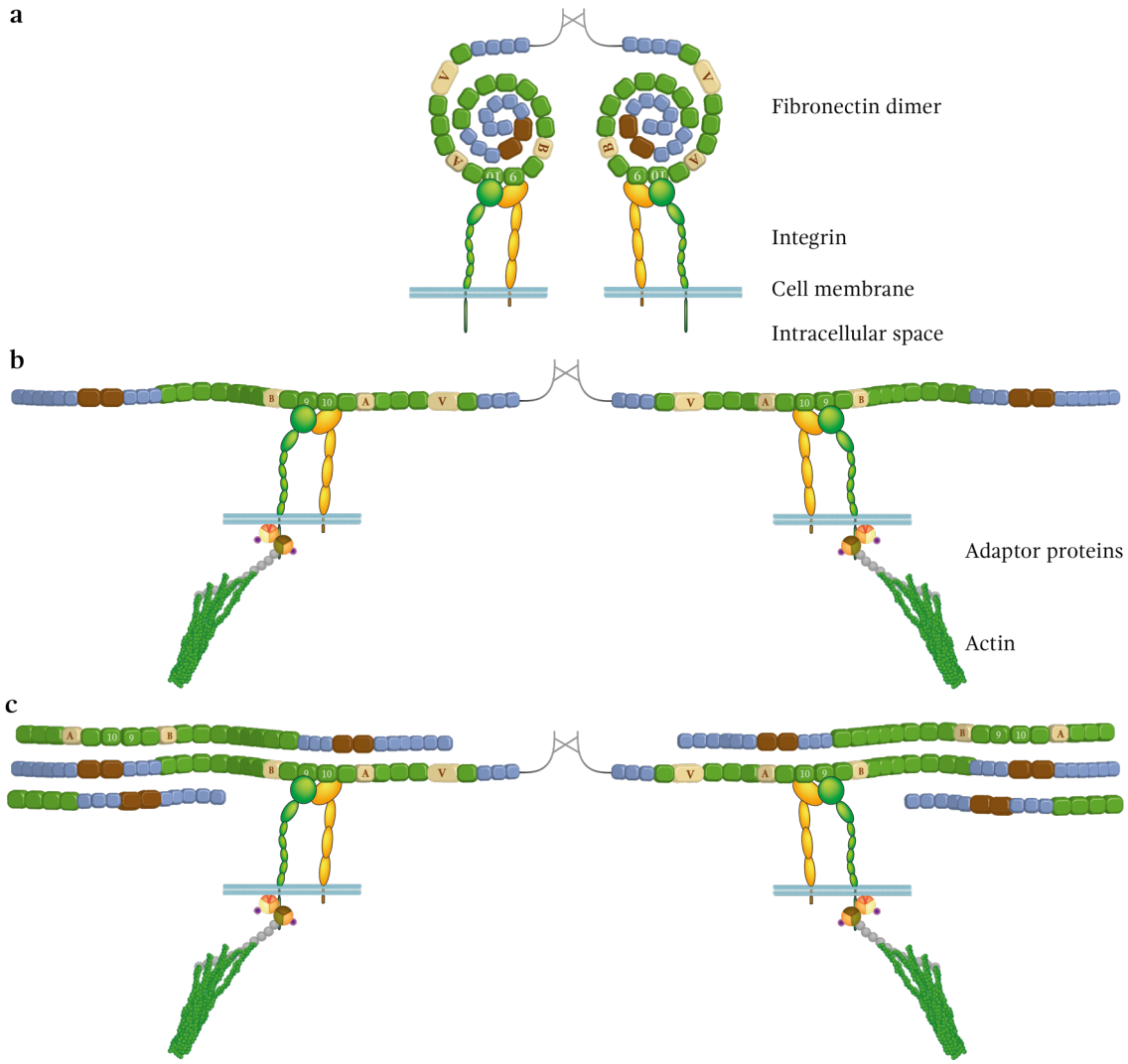

Figure 1-2 Fibronectin assembly. a) The globular fibronectin dimer is bound by integrins at the ninth and tenth type III repeat. b) The binding induces the coupling of integrins to the actin cytoskeleton *via* adaptor proteins. Contractility of the actin-cytoskeleton induces conformational changes of the fibronectin dimer. The elongation and partial unfolding of the fibronectin molecules exposes cryptic fibronectin binding sites, which c) induces fibril formation. Image redrawn form Mao *et al.*[17]

1.3. Integrins

The main mediators of adhesion to the ECM in metazoans cells are integrins. These are heterodimeric, transmembrane proteins and consist of an α and β subunit (Figure 1-3a). In order to attach cells to their surroundings, integrins link their extracellular ligand to the intracellular cytoskeleton. Since integrins cannot directly bind the cytoskeleton, adaptor proteins are recruited to the intracellular domain of integrins[60,61]. These adaptor proteins form a physical platform for a cohort of other scaffold and signaling proteins, which are recruited to the intracellular domains of integrins during adhesion formation. This large protein assembly, collectively called the adhesome, initiates a wide variety of signaling cascades[62,63]. The tensional state of integrin-mediated adhesion, varies the composition of the adhesome[64] and as a consequence, different signaling cascades are triggered. Therefore, integrins transmit biochemical and biomechanical

signals of the extracellular space into cells. Integrin mediated adhesion and related signaling are key elements in development, immune responses and hemostasis. Integrin dysregulation and modification in their signaling are involved in cancer and various other diseases[65].

1.3.1. Evolution and Complexity of Integrins

Whereas no homologs of integrins were discovered in plants, fungi or prokaryotes, the simplest metazoans, sponges and cnidarian, have integrins[66]. *Caenorhabditis elegans* express two different integrins, comprised of one β and two α subunits and orthologues of the two integrins are found in drosophila and vertebrates, although vertebrates expanded this set of integrins. Thereby, one set of integrins binds the RGD motif, found in fibronectin and the second set facilitates the binding to laminins in the basement membrane. Besides these two classes, vertebrates developed collagen-binding, leukocytes specific and a pair of related integrins. Extensive genome research discovered eighteen α and eight β subunits in mice and humans, which assemble twenty-four different integrins (Figure 1-3b)[21]. While most integrins bind their ligand at the β-subunit, all collagen-binding and some laminin-binding integrins have an additional domain inserted into the α-subunit that is required for ligand binding (Figure 1-3b). Although different integrins bind the same ligands[67], the physiological function of individual integrins is different (Table 1-1)[21,68]. Hence, integrin depletion leads to different phenotypes in mice ranging from developmental problems to organ defects and immune system defects[69], some of which can be related to human diseases[70]. The depletion of certain integrin subunits is lethal, which illustrates the importance of integrins for metazoans. For example, depletion of the β1 subunit leads to early embryonic lethality in mice[71].

Integrin mediated adhesion complexity is further increased by the plethora of intracellular proteins that are recruited to the intracellular tails[62,65,72]. The adhesome consists of over 200 different proteins, including various adaptor proteins that connect integrins to the cytoskeleton and bind other scaffold proteins, actin regulators and multiple signaling molecules. A quarter of these adhesome proteins evolved before integrins, implying different functions of these proteins before their contribution to adhesion regulation[72]. Over 60% of the adhesome proteins reside mainly connected to integrins, whereas the rest is transiently located in the adhesion site[65]. Most of the adhesome proteins that are evolutionary older than integrins belong to the transient class and fulfill a variety of other cellular functions[72]. Recently a consensus adhesome of 60 proteins was defined as the core integrin mediated adhesion machinery[63]. However, the exact composition and the resulting functions of an adhesome depend on the maturation of adhesion, integrins that are located in the adhesion site and, on the tension applied to the adhesion site[62-64].

Table 1-1 Integrins and their ligands[73]

	LN	TSP	FN	OPN	VN	TNC	FBN	FG	COL	ICAM	VCAM	LAP-TGFβ	CAD
α1β1	✓								✓				
α2β1	✓	✓							✓				
α3β1	✓	✓											
α4β1		✓	✓	✓							✓		
α5β1			✓	✓									
α6β1	✓												
α7β1	✓												
α8β1			✓	✓	✓	✓							
α9β1				✓		✓					✓		
α10β1	✓								✓				
α11β1									✓				
αVβ1			✓	✓								✓	
αDβ2										✓	✓		
αLβ2										✓			
αMβ2								✓		✓			
αXβ2								✓	✓	✓			
αVβ3		✓	✓	✓	✓	✓	✓	✓				✓	
αIIbβ3		✓	✓		✓			✓					
α6β4	✓												
αVβ5				✓	✓								
αVβ6			✓	✓								✓	
α4β7			✓	✓							✓		
αEβ7													✓
αVβ8												✓	

LN – laminin; TSP – thrombospondin; FN – fibronectin; OPN – osteopontin; VN – vitronectin; TNC – tenascin; FBN – fibrillin; FG – fibrinogen; COL – collagen; I-CAM – intracellular adhesion molecule; VCAM – vascular cell adhesion molecule; LAP-TGF-β – latent associated peptide-transforming growth factor beta; CAD – cadherin

1.3.2. Integrin Structure and Conformations

Although the size varies among different integrins, both subunits have a large extracellular domain with about 1100 and 750 amino acids for the α- and β-subunit, respectively (corresponding to a length of ~19 nm), a single transmembrane helix and a short, mostly unstructured intracellular tail of about 50 amino acids (~8 nm, Figure 1-3a)[74,75]. The additional extracellular domain in collagen binding integrins that is required for ligand binding is composed of about 200 amino acids and extends the extracellular domain to about ~23 nm. To form an integrin heterodimer, both subunits are non-covalently associated. The main dimerizing interactions are found in the extracellular domain close to the ligand binding site, with varying residues in the subunit interface among different integrins[75].

The extracellular domain of the α-subunit consists of two calf domains, forming the leg region, a thigh domain and a β-propeller domain. The latter two form the head region of the α-subunit (Figure 1-3a). In nine α-subunits an αI-domain is inserted into the β-propeller with a flexible linker between these subunits. In addition to the α-subunit-specific flexibility in the

linker between the αI-domain and the β-propeller, all α-subunits have two main regions of flexibility that allow extensive intra-molecular motion[76]. One is the linker between the β-propeller and the thigh and the other is the linker between the thigh and the calf1 domain, also known as the 'knee' of the α-subunit. The β-subunit consists of a βI-domain, which is embedded in a hybrid domain, together forming the head of the β-subunit, followed by four epidermal growth factor (EGF) domains and a β-tail domain, which are together referred to as the leg region. Like α-subunits, β-subunits have flexible linkers between some domains as well. One of them is the 'knee', which located between EGF1 and EGF2. Since the link between the hybrid and the first EGF domain also allows intra-molecular movement, the β-subunit seems to be more flexible than the α-subunit.

The first crystal structures of αVβ3 integrins without ligand showed the extracellular domain of the heterodimer in a bent conformation (Figure 1-3c)[77], which was confirmed by structures of αVβ3 integrins with ligand[78], αIIbβ3 and αXβ2 integrins[79,80]. Further, negatively stained electron microscopy images showed integrins predominately in the bent conformation[79-81]. This conformation sterically impairs ligand binding[76], by locating the binding pocket in the head domains close to the cell membrane. However, due to the flexibility of the integrin subunits, varying degrees of bending within the heterodimer were observed. This suggests different conformations of integrins in the range from fully bent to fully extended on the cell surfaces. In the latter conformation the ligand binding site is located away from the cell membrane[76,82,83]. Using antibodies against specific integrin conformations confirmed that integrins can adopt multiple quaternary structures on the cell membrane[83-85]. Whereas retaining integrins in this closed, bent conformation leads to compromised cell adhesion, arresting integrins in the extended conformation induces ligand binding, showing that this conformation has a high affinity for the ligand[86]. The transition of integrins from the low- to the high-affinity state includes the unbending of the extracellular domain to an upright heterodimer with associated legs, followed by leg separation and swing-out of the hybrid domain in the β-subunit (Figure 1-3c). While in the bent conformation, the transmembrane domains of both subunits are associated and stabilize the bent integrin conformation, current models of integrin affinity changes show a transmembrane domain separation to obtain the high affinity integrin conformation. A further requirement for the transition to the high affinity state of integrins is the disruption of a salt-bridge between the intracellular domains of both subunits. Due to this separation, especially the intracellular domain of the β-subunit can interact with multiple proteins that stabilize the active conformation of the integrin. Hence, integrins have to undergo massive changes in the intra-molecular structure to change their affinity state form low in the bent conformation to high in the upright conformation.

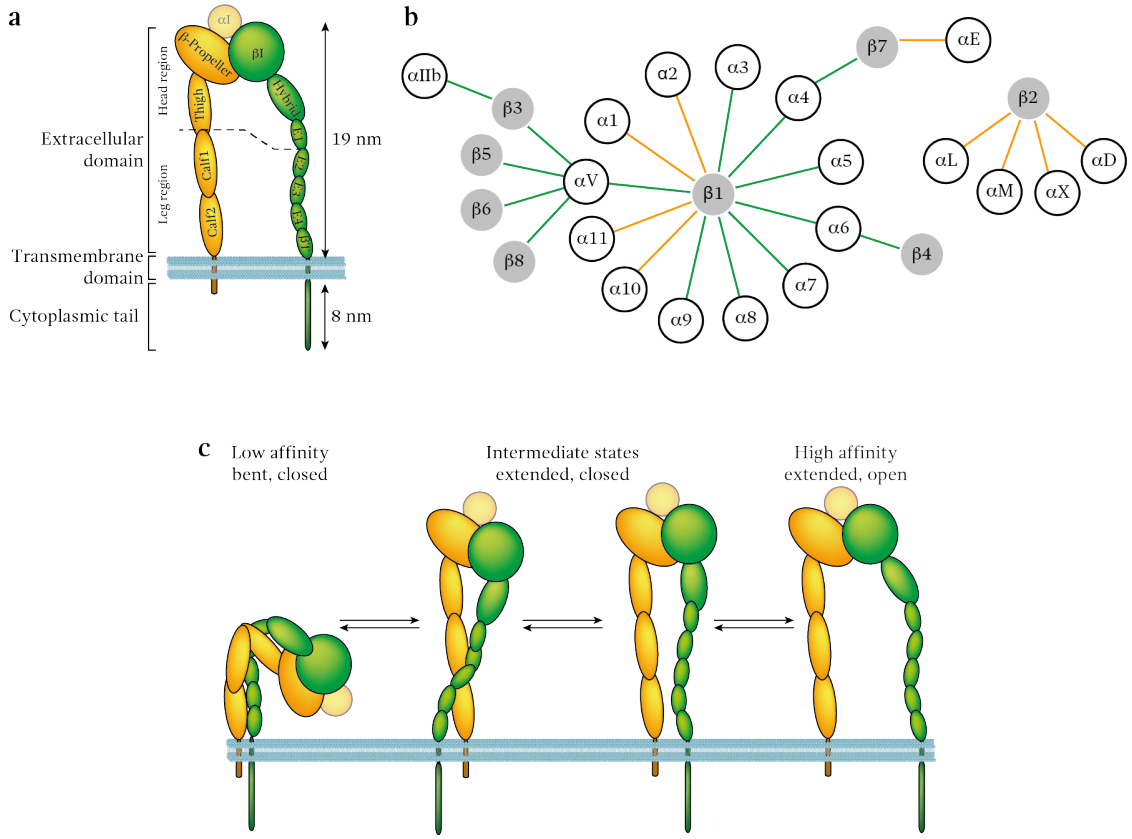

Figure 1-3 Integrin structure, composition and conformation dictate ligand binding. a) Integrins are transmembrane heterodimers, composed of an α- (yellow) and a β- (green) subunit. Each subunit contains multiple domains, with multiple flexible linkers between the subunits. In general, four regions of the integrins are distinguished: the head and leg region, the transmembrane domain and the intracellular tails. By structure, two classes of integrins are distinguished: αI-containing and –missing integrins. b) In mammals 18 α- and 8 β-subunits form 24 different integrins. Integrins that contain an αI-domain (connected by orange line) bind the ligand at the α-subunit and αI-domain missing integrins (green line) bind the ligand at the β-subunit. c) Integrins can adopt different conformations, which have different affinities for ligands. The bent conformation (left) places the ligand binding site close to the membrane, sterically hindering ligand binding. In this conformation, often called 'bent, closed', the integrin is inactive, due to low ligand affinity. In the upright but closed conformation (middle), the integrin can readily bind the ligand, however, integrin legs are still together. This conformation is often called 'extended, closed' conformation. Upon ligand binding, the integrin legs are separated, which allows intracellular proteins to bind. This conformation, called 'extended, open', has the highest ligand affinity.

Conformational changes of integrins are not driven by biochemical energy supply and thus, it is very likely that integrins are in constant motion on the cell surface. It has been proposed, that the flexibility of integrins leads to a spontaneous unbending of integrins, which would be sufficient for ligand binding[76,79,86-88]. Due to the lack of real-time observations, the range of motion without external ligands or intracellular proteins binding to the tails, is not clear. Contrary, integrins on the cell surface that are not bound to a ligand are proposed to maintain the bent conformation with only a very few in the high affinity state[89]. However, the mechanism by which the unbending is stimulated and integrins switch to the high affinity conformation is not clear. Although the upright conformation has the highest affinity for the ligand[81,83,89], it is still under debate which conformation of integrins can bind the ligand with sufficient affinity to drive integrins in the fully active state. It has been proposed, that only upright integrins can bind the ligand, however, ligand binding has been reported in the bend, closed conformation[90].

1.3.3. Integrin Ligand Binding

A very important step in transition from non-ligated to ligated integrin is the swing-out of the hybrid domain relative to the βI-domain upon leg separation (Figure 1-4)[76,91-93]. In the bent conformation, any movement of the hybrid domain is impaired, indicating that the unbending is essential prior to ligand binding[76]. For ligand binding eight distinct steps are required, which include a complex remodeling of the integrin head[82]. The swing-out of the hybrid domain induces conformational changes that ultimately leads to the downward movement of an α-helix in the βI-domain (Figure 1-4). This downward movement remodels the ligand binding site from a closed to an open conformation. Since integrin ligand binding requires divalent cations, especially magnesium, the ligand binding site is called 'metal-ion dependent adhesion site' (MIDAS). It is flanked by two additional cation binding sites which coordinate calcium[93]. While one of this cation binding site is coordinated with an inhibitory calcium ions, called adjacent to metal ion-dependent adhesion site (ADMIDAS), the second is a positive regulatory site and is called ligand induced metal ion-binding site (LIMBS)[77,78,94-96]. The conformational changes in the βI-domain remodel these two metal ion binding sites, which results in an increased affinity for the ligand and finally in firm ligand binding[88,97]. Coordination of manganese in the ADMIDAS induces structural changes of the βI-domain that lead to the high affinity conformation of the ligand binding site[94].

For integrins containing an αI-domain, this domain is the major ligand binding site, with a similar ligand binding mechanism as found for the βI-domain (Figure 1-4). Conformational changes, specifically a final downward movement of helix α7 in the αI-domain affect the affinity for the ligand binding site. Comparable to the βI-domain, ligand binding is dependent on Mg^{2+} and hence, the ligand binding site is also called MIDAS[75,97,98]. Since the αI-domain is not associated with the hybrid domain of the β-subunit, the hybrid domain swing-out is not directly causing the conformational change of in the αI-domain. Hence, the ligand affinity regulation in the head domain due to the global integrin conformation change requires an additional step in integrins containing an αI-domain. A glutamic acid (Glu) residue in the linker between the α7-helix of the αI-domain and the β-propeller is required for the high affinity conformation of the αI-domain[99,100]. It has been proposed that this Glu residue acts as an intrinsic ligand for the βI-domain MIDAS and their interaction induces a downward movement of the α7-helix in the αI-domain, shifting the αI-domain to the high affinity conformation[100,101].

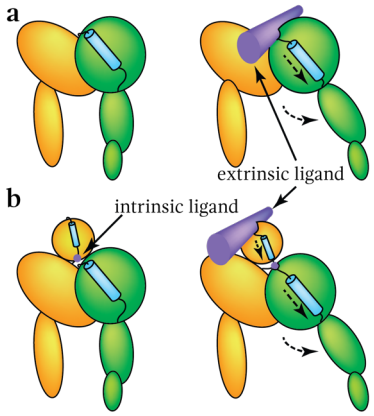

Figure 1-4 Conformational changes in the head region regulates ligand affinity. Illustration of the conformational changes in the βI-domain upon hybrid domain swing out. As a result of the swing out, the α7 helix (blue) moves downward inducing rearrangements in the binding pocket. a) integrin in the extended, closed and extended, open state without an αI-domain inserted. b) In integrins containing an αI-domain have an intrinsic ligand in the flexible linker that binds into the binding pocket of the βI-domain. This induces a similar conformational change in the αI-domain (downward movement of the α7 helix, shown in blue) as in the βI-domain and rearranges the binding pocket. Figure inspired by Campbell *et al.*[98]

The unbending of integrins and the swing-out of the hybrid domain, which together induce changes for ligand affinity are mechanical processes changing the orientation of domains in respect to the protein. It was proposed that forces applied to integrins, either from tension applied from the ligand binding site or from intracellular forces transduced to the integrin by the actin cytoskeleton *via* adaptor proteins can drive these conformational changes[102]. Indeed it has been shown that force applied to integrins can induce and stabilize the upright, high affinity conformation[103-105]. An unbending of integrins by externally applied force at the integrin head has been proposed in integrins with or without the αI-domain[104,105]. Hence, it is suggested that mechanical forces applied to integrins impact the conformational equilibrium and may induce the unbending of integrins.

1.4. Adaptor Proteins Regulate Integrin Function

Integrin intracellular tails, especially those of the β-subunit, are very flexible and capable of binding various cytoplasmic proteins of different function. Thereby, some of these proteins directly modulate the ligand binding of integrins[60,68]. While certain proteins maintain integrins non-ligated, other proteins maintain and/or induce the high affinity conformation of integrins. Talin and kindlin, two prominent examples, are indispensable for maintaining integrins bound to a ligand in the high affinity state[106]. When either of both proteins is depleted, cells have major adhesion deficiencies and mice, depleted from these proteins show developmental defects resulting in embryonic lethality[60]. Besides the maintenance of the high affinity state, talin and kindlin together are suggested to intracellularly induce conformational changes of integrins in hematopoietic cells[107].

1.4.1. Talin

Talin is a large protein composed of about 2500 amino acids[60,107,108]. Genetic studies showed talin to be conserved in all metazoans and to have a general importance in integrin function. Two isoforms, talin 1 and talin 2, are expressed in mammals with 74% identity and 86% similarity. Talin contains an N-terminal FERM domain with about 400 amino acids known as the talin head and a C-terminal region with about 2000 amino acids known as talin rod. Talin head

and rod are connected by an unstructured linker (Figure 1-5a). FERM domains are found in various proteins that connect transmembrane proteins to the cytoskeleton, such as protein 4.1, ezrin, radixin and moesin and usually contain three subdomains (F1-F3)[109]. Talin's FERM domain is atypical since it contains a fourth subdomain (F0), which is a duplicate of the F1 subdomain (Ref. 110). Three subdomains of talin's FERM domain (F1-F3) bind to phosphatidylinositol 4,5-bisphosphate (PIP2) containing membranes[110-113], localizing talin to the membrane and extending the talin head domain[113]. Importantly, to stabilize or inducing the high affinity conformation of integrins one subdomain of the FERM domain (F3) binds to two motifs in cytoplasmic domain of integrin β-subunits. The first is a membrane-proximal NPxY motif and the second is an α-helical region between the membrane and the NPxY motif[112,114-116]. When the FERM domain interacts with integrin β-tails, a salt bridge is formed between the F3 subdomain and a conserved aspartic acid (Asp) residue in the membrane-proximal region of integrin β-tails. This interaction is likely to disrupt the inhibitory salt bridge between the intracellular domains of the α- and the β-subunit and hence contributes to the conformational changes that increase integrin affinity[112]. However, talin binding to the β-tail alone is not sufficient to induce the high affinity conformation of integrins. Interactions of basic residues in the talin head with the cell membrane are essential for integrin function[110,112,113], indicating that a physical anchorage of the β-tail to the membrane and a consequent fixation of the β-subunit transmembrane domain is required for the integrin to remain in the high affinity conformation. A variety of other proteins bind to the talin head domain (Figure 1-5a), including actin[117,118], Rap1[110,119], focal adhesion kinase (FAK), phosphatidylinositol phosphate kinase type Iγ (PIPKIγ), T-cell lymphoma invasion and metastasis 1 (TIAM1), as well as Rap1-GTP-interacting adaptor molecule (RIAM)[60]. The talin rod, which is also crucial for integrin function, consists of 13 helix bundles (R1-R13) all of which contain four or five α-helices[120,121], and contains binding sites for several cytoplasmic proteins. These include two binding sites for actin[117,122,123], RIAM[124,125], paxillin[107], Kank1 and Kank2 (Ref. 126,127) and a controversial second integrin binding site[123,128]. Multiple vinculin binding sites were characterized in talin, most of which are cryptic in a relaxed state of talin[120].

As talin is a key protein to integrin function, its localization, integrin binding and conformation is tightly regulated. Talin can adopt an extended and a globular conformation (Figure 1-5b)[121]. These conformations have functional impact, whereas only the extended but not the globular conformation of talin can readily bind to the β-tail of integrins. In the globular conformation, the head domain interacts with the rod domain which inhibits the interaction with the integrin and the cell membrane. Thereby, F3 in the FERM domain interacts strongly with R9 and additionally F2-F3 interact with R1-R2, which sterically hinders the interaction with β-tail and the membrane binding, respectively[129-131]. The concept of talin auto-inhibition is consistent with the observation that a large ratio of talin is found in the cytosol[132], that it is translocated to adhesion sites when activated by Rap1 (Ref. 133-135) and that a tail-truncated version of talin leads

to a higher quantity of integrins in the high affinity state on the cell surface[114,136]. Whether talin continuously changes conformation and talin activation results from a shift of conformational equilibrium or whether talin has to be converted into the active conformation is not known. However, proteins that induce active talin are PIP2 (Ref. 137), RIAM[124,134,135], Gα13 (Ref. 138), and Kank2 (Ref. 126). Besides the conformation of talin also the binding of other proteins to talin is tightly regulated. For example, actin binding to the rod at both binding sites is impaired by the flanking regions, which are released when talin is stretched[139,140]. Further, the cryptic vinculin binding sites require a partial unfolding of the protein to be exposed, which is driven by forces trasmitted to talin by actin[141]. Hence, actomyosin induced forces affect the conformation of talin and hence talin binding to integrins[142] as well as vinculin and actin binding[122].

1.4.2. Kindlin

In the last decade, it became apparent that another family of FERM-domain containing proteins, termed kindlins, is required to maintain the high affinity conformation of integrins (Figure 1-5b). The kindlin family has three isoforms (kindlin1-3) that are expressed tissue-specifically[61,143]. Sequence alignment shows similar domain organization as found in the talin head domain[144]. Like talin, kindlin has an atypical FERM domain with an additional F0 subdomain. A major structural difference to the talin head domain is a pleckstrin homology (PH) domain inserted into the F2 subdomain. Although the structure of full length kindlin was not yet determined, recently the structure of truncated kindlin was solved, in which highly flexible regions were deleted[145]. The FERM domain of kindlin adopts a classical cloverleaf-like structure and localizes kindlin to the membrane by interactions of the PH domain, F0 and F1 domain with anionic lipids[146-148]. As in talin, the interaction of kindlin with the cell membrane is required for integrin function[149]. The F3 subdomain directly interacts with a membrane-distal NxxY motif in the β-tail, which essential for the high affinity conformation of integrins[150-152].

Besides being required to maintain the active conformation of integrins, the functionality of kindlin is poorly understood. However, kindlin has been shown to directly interact with integrin-linked kinase (ILK)[153-156], which in turn binds to actin *via* parvin[157,158]. Recently it has been also suggested that kindlin directly binds actin[159] as well as the actin polymerizing Arp2/3 complex[149]. This suggest that kindlin is not only important for integrin-ligand binding, but also for the integrin-actin connection and for cytoskeleton dynamics at the adhesion site. In addition. kindlin recruits paxillin to the adhesion site[106,149,160], which regulates integrin mediated adhesion by the phosphorylation of multiple signaling proteins[161,162]. This indicates that kindlin is an adaptor protein with multiple, yet unknown functions. Although, the full range of kindlin functions and its activation of kindlin as well as the interplay with talin remains to be elucidated, kindlin emerges as an important hub for multiple signaling proteins, which are required for integrin-mediated adhesion.

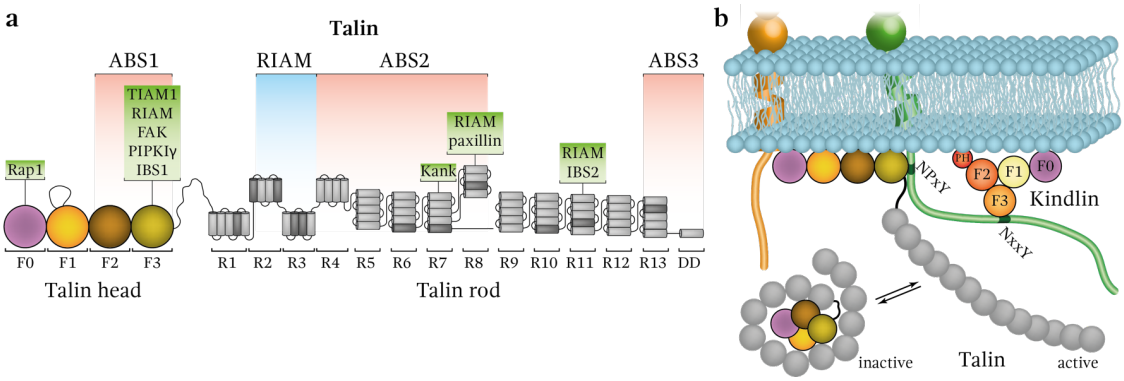

Figure 1-5 Talin and Kindlin are required for integrin ligand binding. a) Talin is composed of an atypical FERM domain (F0 - F3), commonly called the head domain that is connected by a flexible linker to the rod domain, containing 13 helix bundles (R1 – R13) and a dimerization helix (DD). Each helix bundle contains four or five helices (shown in grey). The interaction sites with other proteins are shown, whereas dark grey helices contain vinculin binding sites, which are partially cryptic. b) Two conformations of talin are known, an inactive and active conformation. Only in the active conformation, talin stabilizes integrins in the high affinity state. Active talin can interact with the membrane and the integrin β-tail at the membrane proximal NPxY motif and a membrane proximal helix. To maintain the active conformation of integrins, kindlin is required. Similar to talin, kindlin has an atypical FERM domain that interacts with the integrin β-tail. Structurally, the talin head domain and kindlin are similar, however, kindlin has an inserted PH domain. Kindlin interacts with a membrane distal NxxY motif in the integrin β-tail.

1.4.3. Integrin Inactivation

Since integrin functionality is tightly regulated, not only the active conformation can be stabilized by intracellular proteins, but also the inactive, low affinity state. It can be maintained or induced by proteins that associate with the intracellular domains of integrins. Mostly, these proteins bind either the β-tail[163-165] or conserved regions of the α-tail[166,167], thereby preventing the binding of the integrin activators, such as kindlin and talin. Filamin and docking protein 1 (DOK1) are prominent integrin inactivators. Both compete with talin for binding the membrane proximal NPxY motif. Integrin cytoplasmic domain-associated protein 1 (ICAP1) interacts with the distal NxxY motif in the β1-integrin cytoplasmic tail and hence impairs the binding of kindlin[168,169]. SHANK-associated RH domain interacting protein (SHARPIN) and mammary-derived growth inhibitor bind to the intracellular tail of the α-subunit[69]. Apart from competitive binding of cytoplasmic proteins to the tails of integrins, phosphorylation of specific residues at the β-tail can maintain or induce the bent, closed conformation of integrins. The phosphorylation of the tyrosine residue the NxxY motifs leads to an inhibition of talin or kindlin binding and promotes the binding of DOK1 (Ref. 170,171). Altogether, the low affinity state of integrins can be maintained by either direct protein-protein interaction, or by phosphorylation of the β-tail, which ultimately impairs the binding of talin and/or kindlin.

1.5. The Life of Integrins

In cells, whether embedded in a tissue or migratory, integrin adhesion sites are not static, but constantly remodeled. During migration, adhesion sites form at the leading edge, with single integrins which cluster into nascent adhesions that anchor membrane protrusions to the ECM. In these adhesions, an increasing number of adhesome proteins are recruited to the cytoplasmic integrin tails. Thereby, particular adhesome proteins are directly recruited to integrins, while other proteins are recruited upon actomyosin induced forces applied to adhesions. Although the majority of nascent adhesions is turned over, a small number of these adhesions mature into large focal adhesions at the tip of actin bundles or stress fibers. Since integrin adhesion sites are rather stationary or slightly sliding in respect to their extracellular binding site, focal adhesions translocate either to the center of the cell or to the rear during cell movement. Long-lived, highly elongated adhesions that are translocated to the center adhesions, called fibrillar adhesions, have a remodel adhesome and are important for ECM rearrangement and fibronectin assembly. At the rear of migratory cells, large focal adhesions are disassembled, integrins are internalized and transported to the leading edge.

1.5.1. Integrin Clustering and Nascent Adhesion Formation

Changes in the affinity of integrins were proven to be physiologically relevant, however, the physiological role of integrin avidity regulation has been long debated[172,173]. Upon ligand binding integrins form clusters with a diameter of about 100 nm that contain about 50 ligand bound integrins[174]. How these micro clusters are formed is still not fully understood, but it emerges that multiple factors are relevant for the clustering. The multivalency of ECM ligands with a maximum distance of 60 nm (Ref. 175) induces integrin clustering simply by localizing multiple integrins in proximity[176,177]. Also bulky membrane-bound glycoproteins, the glycocalyx, are thought to contribute to clustering of integrins[178]. The glycocalyx extends up to 80 nm into the extracellular space, thereby hindering integrins, which protrude 19 or 24 nm in the extended conformation into the extracellular space, from binding. Consequently, non-bound integrins are funneled into regions of existing adhesion sites, where the spatial hindrance for integrin binding is reduced due to the binding of other integrins[178]. Very important for integrin clustering are the initially recruited adaptor proteins talin and kindlin. The C-terminal α-helix of talin is a dimerization domain (DD, Figure 1-5a), which ultimately induces integrin dimerization (Figure 1-6)[140,179]. Hence, talin is not only required for integrin affinity changes but also for the regulation of avidity. Recently, the structure of kindlin was resolved, showing kindlin forming homodimers[145]. The deletion of key sequences for dimerization, which flank the PH domain, leads to a hampered integrin activation, which suggests that kindlin dimerization has an important role in the physiological function of integrins. Although the observed dimerization is very slow[145], dimerization of kindlin *in vivo* may be enhanced, however this remains unclear. In very early adhesion assembly, talin and kindlin were found in a stoichiometry of one to two

molecules, indicating that two talin molecules connect two kindlin dimers[180]. Hence, the interplay of kindlin and talin is essential for integrin function and initial clustering, which is enhanced by multivalency of ECM ligands and the glycocalyx.

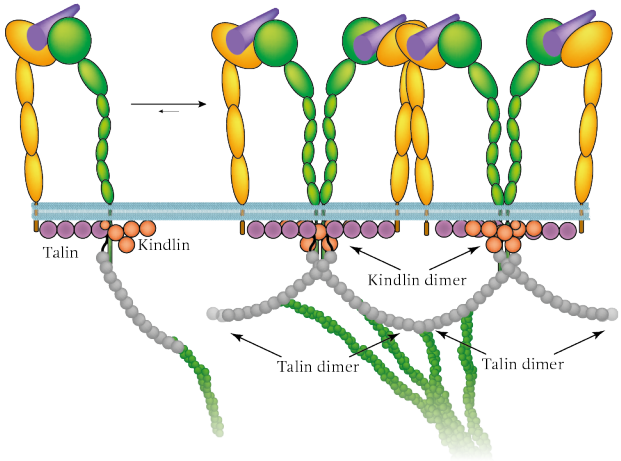

Figure 1-6 Integrin clustering. Initial integrin clustering is induced by multivalent ECM ligands. Upon ligand binding, talin and kindlin associate to the integrin β-tails. Both adaptor proteins form homo-dimers, inducing the association of integrins at the cytoplasmic domains. Thereby, the dimers of talin are formed by the interaction of two dimerization helices in the rod domains and kindlin dimerizes by interactions of two F2 domains.

The assembly of nascent adhesion is a complex process, which requires tight biochemical and biophysical regulation. Multiple adhesome proteins are quickly recruited to the cytoplasmic tail of clustered integrins, including focal adhesion kinase (FAK), vinculin, paxillin and the Src kinase family. There are indications that FAK plays a central role in the assembly and maturation of nascent adhesions. Although FAK depleted cells can adhere and initiate actin driven cell spreading[181,182], nascent adhesions do not undergo the typical maturation cycle[181]. It was shown that FAK promotes talin localization to nascent adhesions[182], thereby stabilizing more integrins in the active conformation[183] and connecting nascent adhesions to the actin cytoskeleton[184], which in combination results in early cell adhesion strengthening[183]. Although it was suggested that FAK directly binds to integrin β-tails, it recently was shown that FAK is recruited to adhesion sites by kindlin [106,185], which in turn was shown to occur in a complex with integrins directly upon ligand binding[180]. Paxillin, also recruited to integrins by kindlin, is phosphorylated by FAK and acts as hub for multiple signaling networks that induce cell spreading and adhesion maturation[162]. This phosphorylation seems to be important for integrin function as impeding the interaction between FAK and paxillin decreases cell adhesion and migration[185]. Due to the signaling initiated by both proteins, the actin polymerizing Arp2/3 complex, recruited to the adhesion site by either kindlin or FAK is activated[149,186]. With the recruitment of paxillin, FAK and the Arp2/3 complex cell membrane protrusions are induced by actin dynamics that apply forces to nascent adhesions.

1.5.2. Adhesion Maturation and Adhesome Formation

The coupling of nascent adhesions to dynamic actin spatially and temporally regulates the maturation or disassembly of the nascent adhesions[187]. Most nascent adhesions have a short lifetime, which correlates with the polymerization rate of actin. Nascent adhesions are usually stable for around one minute before being disassembled and recycled. Nascent adhesions are

disassembled as they are disconnected from actin due to actin de-polymerization by cofilin at the transition zone between lamellipodium and lamellum[188]. However, a small number of nascent adhesions grow towards the leading edge along α-actinin containing actin fibers into large focal adhesions (Figure 1-7). This maturation of nascent into focal adhesions depends on myosin II-induced actin contractility, which applies a force to the adhesion site. Integrin adaptor proteins, predominately talin, transmit the forces generated by actomyosin to integrins, which are thereby tilted in focal adhesions[189]. The application of myosin II-dependent forces to adhesions induces the recruitment of vinculin to the adhesions site, which reinforces the connection of integrins to actin. During maturation, adhesion sites develop a distinct layered structure (Figure 1-7b)[190,191]. Signaling proteins, including paxillin and FAK, localize to the cytoplasmic domains of integrin and reach about 30 nm into the intracellular space. This layer of proteins is commonly called 'signaling' layer. The 'actin regulatory layer' containing actin and actin associated proteins, including α-actinin is localized intracellularly 50 nm away from the cell membrane[190,192]. Talin plays a key structural role in the nano-scale architecture of focal adhesions as it bridges the distance between the cytoplasmic domains of integrins and the actin regulatory layer, by directly binding integrin β-tails and actin[193]. Not surprisingly, vinculin that reinforces the connection of adhesions to actin localizes primarily to the talin rod domain[190]. As the proteins in this layer transmit forces from the actomyosin cortex to the adhesion site and forces often regulate their function, this intermediary layer is often named 'force transduction layer'[190,192]. Further, focal adhesions are vertically structured along their horizontal axis. At the elongation site of focal adhesions, FAK-dependent tyrosine phosphorylation of paxillin is highest, providing a scaffold for phosphotyrosine-binding proteins[194]. In contrast, at the opposing site actin binding proteins are concentrated. At the periphery of focal adhesions, called the adhesion belt, Kank is recruited, which partially decouples the adhesion site from tension induced by the actomyosin cortex[126]. Thereby the binding of Kank to talin induces adhesion slippage and hence might regulate focal adhesion growth. It is likely that other proteins have a distinct spatial distribution and/or a gradient of biochemical state, *i.e.* phosphorylation, to regulate the growth of focal adhesions, however, these mechanisms are still poorly understood.

Since focal adhesions usually contain several different integrin classes, the role of single integrin types and their interplay in adhesion formation and adhesome assembly is of interest. For fibronectin-binding integrins it was shown that α5β1 and αVβ3/β5 integrins, which are usually found together in focal adhesions, form morphologically different adhesions and distinct actin structures when they are expressed exclusively[195]. Although adhesions formed by different integrins share a core adhesome[63], differences in the recruited adhesome proteins lead to functional differences. For instance, adhesions formed by α5β1 integrins generate myosin II-driven contractility and Arp2/3 complex assembled branched actins structures, while αVβ3/β5 integrins adapt to the tension by activating GEF-H1 and the actin polymerizing machinery mDia, which leads to the formation of unbranched thick actin stress fibers[195]. Thus, the interplay of

α5β1 and αVβ3/β5 integrins in focal adhesions allows cells to adapt to the rigidity of the extracellular environment[195]. However, how signaling induced by either of these integrins regulates the formation of mixed adhesion sites as well as the role of biophysical parameters in the regulation of these integrins is currently unknown.

Although focal adhesions are stable adhesion sites, proteins in adhesions are highly dynamic. Talin and kindlin stabilize the active conformation of integrins and hence integrins are mainly immobilized[196]. However, partially integrins in focal adhesions diffuse either freely or confined with integrin class dependent dynamics[196]. Many intracellular proteins, including talin, kindlin, FAK, paxillin, vinculin and ILK are not constantly bound and undergo frequent exchange with the cytoplasmic pool[197-199]. The binding and unbinding rate of adhesome proteins in many cases depends on the tension that is applied to the adhesion by the actomyosin cortex[198]. Thus, forces applied to adhesions regulate not only the composition of the adhesome but also the rate of protein turnover in the adhesome.

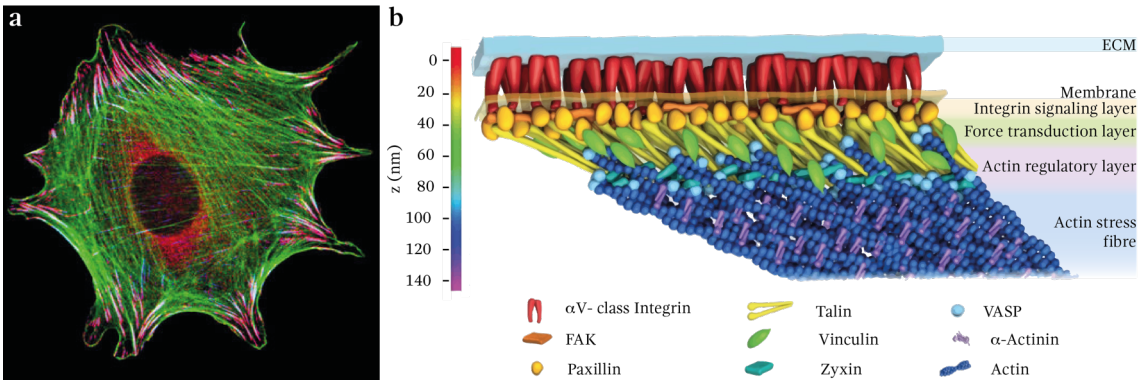

Figure 1-7 Focal adhesion architecture. a) In spread cells, large and elongated focal adhesions (red) are found at the tips of actin stress fibers (green). b) Focal adhesions have distinct vertical structure with a signaling layer within ~30 nm of the membrane, followed by a force transduction layer and the actin regulatory layer. Images a) taken from Einstein[200] and b) adapted from Kanchanawong *et al.*[190]

1.5.3. Adhesion Disassembly and Integrin Recycling

Integrin-mediated adhesions are frequently disassembled, either at the edge of the lamellum or at the rear of a migrating cell[201]. Microtubules play an important role in adhesion disassembly, as their depolymerization stabilizes focal adhesions by preventing their disassembly[202,203]. Upon re-polymerization of microtubules, focal adhesions are synchronously disassembled and integrins are internalized. Inhibition of kinesin-1, a motor protein involved in protein trafficking along microtubules, leads to the same phenotype of adhesion stabilization as microtubule depolymerization, indicating a critical role for kinesin-1 in adhesion disassembly and turnover[204]. FAK is also involved in adhesion disassembly by binding growth factor receptor-bound protein 2 (Grb2), which promotes recruitment of dynamin to adhesion sites. This complex is responsible for integrin internalization, thereby inducing adhesion disassembly[202]. It was proposed that α5β1 integrins are internalized in an upright conformation with associated FAK and Src at the β-tail, which are recycled at the leading edge of migrating cells[203]. FAK depletion

leads to an increased number of focal adhesions and massive stress fibers that stabilize focal adhesions[202,203,205]. Thus, it is likely that FAK induced signaling lowers actin contractility, thereby reduces stress fiber formation and ultimately destabilizes focal adhesions[205]. FAK and Src signaling hve been shown to be involved in adhesion disassembly at the rear of a migrating cell by increasing actin contractility[206]. Thus, FAK seems to be a key player in adhesion disassembly with diverse and spatially varying functions.

1.6. Integrin-Mediated Mechanotransduction

Many physiological processes depend on mechanical information about the extracellular environment, which cells can probe by applying forces to the ECM, and then transducing these into the cell as biochemical signals. For example, bone development and remodeling relies on the release of bone modulators by connexin hemichannels in osteocytes, which are regulated by bone fluid shear stress sensed and transduced by α5β1 integrins. In the last decade it became apparent that physical parameters of the environment, detected by integrins, dictate the lineage commitment of stem cells[207]. In general, it emerges that mechanotransduction is indispensable for embryonic development *in vivo*[208]. Applying forces to integrin adhesion sites induces many signaling cascades and cellular processes.

1.6.1. Forces Regulate Integrin Binding

Bonds between integrins and their ligands have to withstand high forces that are applied either from the extracellular environment or by actomyosin contractility. Forces impact the dissociation of integrin-ligand bonds and may also regulate the binding rate of integrins to their ligand. Fibronectin-ligated α5β1 integrins have a prolonged bond lifetime when the force applied to the bond increases, a phenomenon called catch bond[209]. Catch bonds formed by α5β1 integrins and fibronectin require the binding of the integrin to the RGD domain and the synergy site in fibronectin[22,210,211]. Hence, mechanically loaded α5β1 integrins can withstand higher forces and have an increased lifetime in tensioned adhesion sites. Cyclic instead of static mechanical loading of α5β1 integrin-fibronectin bonds increases the bond lifetime drastically already at low levels of applied force (~ 10 pN)[210]. However, if forces applied to a α5β1 integrin-ligand bond overcomes a certain threshold (> 30 pN), the bond properties transition to that of a slip bond[211], in which the lifetime of the bond decreases exponentially with increasing applied force. Changes in bond properties are suggested to regulate α5β1 integrin mediated signaling, as FAK seems to be only activated by α5β1 integrins when they form a catch bond with fibronectin[22]. This shows a fine tuning of α5β1 integrin-ligand binding and signaling by force that is applied to the bond. In mixed focal adhesions containing αVβ3 and α5β1 integrins, αVβ3 integrins localize in areas of high tension, whereas α5β1 integrins reside in regions with lower tension[195]. Although αVβ3 integrins were reported to bind less strong to fibronectin compared to α5β1 integrins[212], recent studies indicate that αVβ3 integrins may form stronger bonds with fibronectin than α5β1

integrins[104,195]. Although a catch bond behavior of αVβ3 integrins has not been observed, it was suggested recently that force drives the unclasping and prevents the collapsing of αVβ3 integrins, thereby regulating the binding kinetics and dissociation rates of αVβ3 integrins[104]. In adherent endothelial cells, flow induced shear stress regulates integrin binding. When cells are subjected to shear stress, the high affinity state of α5β1, αVβ3 and α2β1 integrins can be induced[213-215]. However, which integrins are regulated depends on the substrate endothelial cells adhere to, and thus on the class of bound integrins[213]. Cells adherent to collagen can induce the binding of additional α2β1 integrins, and correspondingly, cells adherent to fibronectin or fibrinogen induce the high affinity state of α5β1 and αVβ3 integrins in response to shear stress[213]. In fact, there are indications that α2β1 integrins under tension may suppress the high affinity conformation of α5β1 integrins. Shear stress induced integrin-ligand engagement depends on a signaling within seconds that includes the activation of Src, which forms a complex with FAK, and Phosphatidylinositol-3-OH kinase (PI3K), which is known to be involved in integrin activation[213,216,217]. It is likely that mechanical control of integrin ligand binding kinetics, including binding rate and dissociation rates, is a general feature of integrins[218].

1.6.2. Actin Regulation by Force

Cells remodel their actin cytoskeleton upon the application of force. For example, endothelial cells under flow induced shear stress align their cytoskeleton along the direction of flow[216,219]. Further, when cells cannot generate traction forces, due to a soft extracellular environment or inhibited cell contractility, actin structures are fundamentally different. A prominent effect when lacking the ability to generate forces is a perturbed development and maintenance of thick actin stress fibers that interconnect focal adhesions[195,220]. Externally applied forces, induced by stretching of substrates induces actin remodeling[221], also on soft substrates[222]. However, on soft substrates static stretching does not stimulate actin remodeling or cell spreading, whereas cyclic application of force induces actin stress fiber formation. The response to cyclic stretching is optimal at a certain amplitude and frequency of stretching, indicating that the transduction of mechanical cues are limited by a force and time threshold. In order to maintain the adhesion-actin connection at high forces, vinculin reinforces the binding of talin to actin. Thereby, vinculin forms an asymmetric catch bond with actin that moves to the cell center[223]. Hence, not only are adhesion sites modulated by force, but also the actin cytoskeleton dynamics and actin connection of adhesion sites. The induction of actin remodeling with stress fiber formation leads to cell stiffening[224-226]. The current hypothesis is that in mechanically loaded cells, whether shear stressed, stretched or indented, the actin cytoskeleton first rearranges, which then triggers signaling cascades that induce an active response to the applied mechanical cues.

1.6.3. Mechanosensitive Adhesome Proteins

When force is applied to an adhesion site, multiple adhesome proteins are recruited[227], many of which respond to force and are involved in transducing actomyosin generated forces to the adhesion site or extracellular tension to the cytoskeleton. The best studied adhesome protein involved in mechanotransduction is talin. Upon recruitment of talin to integrins, talin binds actin at the C-terminal actin binding site (ABS3). The binding of actin to the second actin binding site the talin rod (ABS2) in relaxed talin is inhibited by flanking helix bundles (R2-R3 and R9; Ref. 139). It has long been speculated that the conformation of talin changes under force and that force modulates talin function[228]. Indeed, forces of about 30 pN applied to the first three helix bundles (R1-R3) induced their unfolding, thereby exposing cryptic vinculin binding sites, which results in increased vinculin binding to talin (Figure 1-8)[229,230]. Although all helix bundles can be mechanically unfolded[231], in the full length talin rod domain one helix bundle (R8) is insensitive to force[232]. Talin unfolding has a mechanical hierarchy. The R3 helix bundle unfolds at about 5 pN as the first mechano-sensor in talin and all other domains unfold sequentially at forces between 10 and 20 pN, thereby exposing additional vinculin binding sites[232,233]. Further, forces applied to talin and subsequent vinculin binding to the helix bundles R2-R3 seem to reduce the repression of actin binding to ABS2 (Ref. 139). This results in a stronger connection of the adhesion site to actin and higher forces applied to talin[234]. Recently it has been shown that the actin binding to ABS2 induces a vinculin dependent force gradient across talin[235]. When the force applied to talin exceeds 25 pN, the helix bundle R3 undergoes a helix-to-coil transition, resulting in the unbinding of vinculin from talin[232]. Importantly, when the force is released from talin, it folds back into the non-stretched conformation[233]. Hence, talin acts as a force buffer in adhesions, which is supported by the report that the length of talin fluctuates between 80 and 350 nm *in vivo*[236]. Thereby, vinculin binds optimally to talin when talin is extended to 180 nm (Ref. 237). Thus, protein binding to talin is tightly regulated by force. Low to medium forces stretch and/or partially unfold talin, promoting vinculin binding to talin and subsequent actin binding at ABS2, whereas high forces lead to helix-to-coil transition that result in vinculin unbinding and tension reduction.

Although forces regulate the binding of other proteins to talin, talin does not directly translate biophysical cues into biochemical signals. However, forces applied to other adhesome proteins regulate their catalytic activity and hence, these proteins transform forces in biochemical signals. As a prominent example, FAK is required for physiological force transduction and adhesion regulation in response to extra- or intracellular forces (Figure 1-8)[238-240]. Similar to talin, FAK occurs in an auto-inhibited state, in which the FERM domain binds to the kinase domain, thereby sterically hindering the catalytic activity of FAK. The N-terminal FERM domain binds to the talin head as well as PIP2-rich membranes. The C-terminal focal adhesion targeting (FAT) domain binds to paxillin, which indirectly binds to actin. There are indications, that the binding of the FERM domain to PIP2 rich membranes destabilizes the auto-inhibited state of

FAK and induces auto-phosphorylation, which is required for signaling transduction[241]. Further, the indirect connection to the actin cytoskeleton may apply pulling forces of the actin cytoskeleton to FAK, which lead to conformational changes and an opening of the catalytic pocket of the kinase domain[242,243]. The rapid (< 0.3 s) phosphorylation of Src by FAK upon externally applied forces to fibronectin binding integrins[244,245] indicates the regulation of FAK activity by forces. There is no indication, that Src activation is directly modulated by force, as it does not bind to actin and is therefore not subjected to force. A substrate of Src, p130Cas (Cas) is phosphorylated in response to externally applied forces by stretching (Figure 1-8), which induces the phosphorylation of the talin activating protein Rap1. Hence, the stretching induced phosphorylation of Cas leads to adhesion maturation and growth by inducing ligand engagement of integrins[124,246]. Besides the before mentioned force sensitive proteins, it is likely that many other proteins in the adhesome are functionally regulated by force, thereby regulating cell adhesion and migration in response to different biophysical parameters.

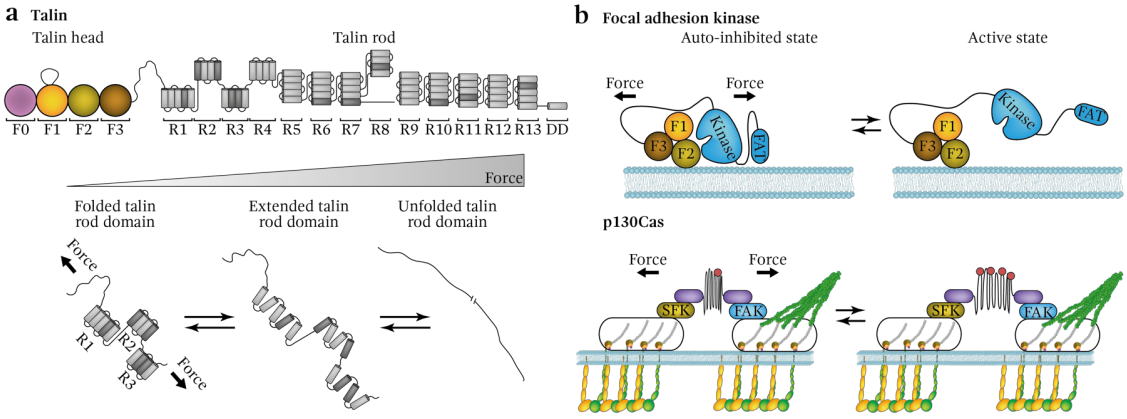

Figure 1-8 Forces regulate adhesome proteins in structure and function. a) Talin is the best studied mechanosensitive proteins in the adhesome. Forces transduced by actin or the extracellular environment induces the stretching and unfolding of the rod domain. Due to this, the cryptic vinculin binding sites are exposed. Forces above 25 pN induce a helix-to-coil transformation of R3, leading to the unbinding of vinculin. b) FAK and p130Cas, force induced conformational changes increase the catalytic activity by the change of accessibility of the kinase domain or the phosphorylation state (red dots), respectively.

1.6.4. The Molecular Clutch Model

In migrating cells, newly formed membrane protrusions initiated by rapid actin polymerization at free filament ends push out the membrane at the leading edge (Figure 1-9). This requires the anchorage of filaments to an immobile object that opposes the pushing force of the actin polymerization. Is the filament not anchored, actin polymerization at the leading edge of the cell induces a rearward movement of actin, a process known as actin retrograde flow[247]. Integrin-mediated adhesions couple newly formed filaments *via* adhesome proteins to the stationary ECM and hence, apply a traction force to the ECM, which results in a net forward movement of the cell[248]. When integrin adhesion sites are not connected to actin, the retrograde flow is high and traction forces are low. The coupling of integrins to actin in migrating cells is conceptually described in the molecular clutch model (Figure 1-9)[249-251]. In this model, talin connects integrins

to actin and is indispensable for the clutch. The clutch is reinforced by wvinculin, which is also crucial for the full functionality of the clutch[249].

The molecular clutch model discribes a highly dynamic system that responds to a wide range of extracellular rigidities. On soft substrates, the rate of force increase across talin is low due to a high elasticity of the substrate (Figure 1-9). Thus, the loading rate is lower on talin than on the integrin-ligand bond and hence, the integrin unbinds from the ligand before the integrin-actin connection is reinforced and actin-mediated forces can be transmitted to the adhesion[249]. With increasing rigidity, the loading rate of talin increases and, above a certain threshold, is higher than the integrin-ECM dissociation rate. Thereby, talin is stretched and/or partially unfolded, which induces vinculin binding and adhesion reinforcement, ultimately resulting in higher traction forces and higher migration speeds of cells (Figure 1-9). It has been shown that upon depletion of talin cells exert a biphasic traction force response to increasing

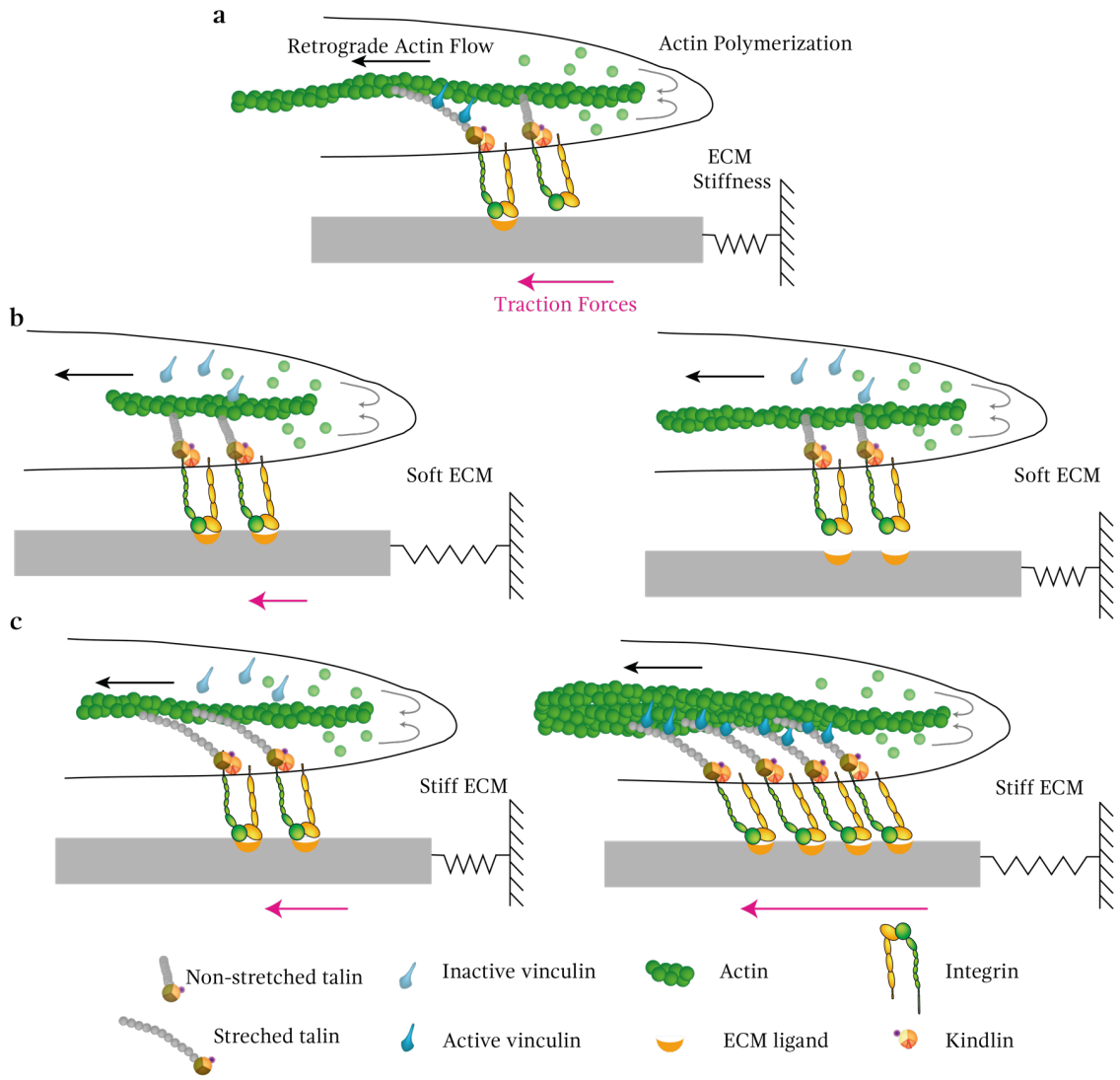

Figure 1-9 The molecular clutch model. a) A schematic overview of the molecular clutch model. b) On soft substrates, the loading rate of talin is lower than the unbinding rate of integrins from their ligand. This leads to the dissociation of the integrin from the ligand before adhesion reinforcement. c) On stiff substrates, talin is stretched and partially unfolded, which recruits vinculin and reinforces the adhesion site. Figure redrawn from Swaminathan *et al.*[253]

rigidities[249]. This indicates that other adhesome proteins may be involved in the clutch, especially in the transition of low forces, with a likely candidate being kindlin. Destabilization of the clutch, for example by Kank binding to talin and thereby competing with vinculin binding, leads to a weaker actin-talin connection[126]. Thereby, traction forces on the adhesions are lowered and hence, adhesion slippage is induced. The clutch model describes how force generation affects the adhesion connection to actin and with the unbinding behavior of integrins during adhesion initiation. However, how forces regulate the binding behavior of different integrins and their subsequent signaling during adhesion formation is not known. Possible cross-regulation of integrins, as shown in focal adhesions[195,252], during adhesion initiation may also regulate early adhesions. This thesis aims at addressing these fundamental questions.

1.7. Characterizing Cell Adhesion and Tensional States

Due to the importance of cell adhesion and related cellular processes, the interaction of adhesion receptors and their ligands are studied extensively using various methods[254-257]. Due to the lack of a method, to directly quantify cell-surface interaction strength, the characterization of cell adhesion is limited to measuring forces required to detach cells from their substrate or to measure forces that are applied intracellular or extracellular at adhesion sites. To characterize these different aspects of cell adhesion, several approaches were developed over the last decades, reaching from very crude washing assays to methods that can quantify piconewton forces that mechanically stretch single molecules.

1.7.1. Bulk Adhesion Characterization Methods

One of the earliest methods developed to characterize cell adhesion employs shear forces resulting from liquid flow to detach cells from a substrate. Thereto, cells are seeded onto a substrate of interest and are allowed to initiate adhesion. Subsequently, loosely bound or non-adherent cells are washed off and the number of remaining cells is quantified. With this crude assay, different cell adhesion molecules were discovered and it has given valuable insight in basic cell adhesion mechanisms, such as basic understanding of mechanotransduction in endothelial cells. However, reproducibility and quantitative read-outs are poor. Advancements of washing essays, *i.e.* spinning disc devises, minimized the variability of forces applied to the cells, thereby allowing the analysis of important adhesion mechanisms and basic mechanobiological processes. However, shear forces acting on cells depend not only on the velocity of the liquid but also on the size and the shape of cells. Therefore, the forces applied to cells in such experiments cover a wide range and are challenging to quantify. Hence, other methods were developed that detect the forces applied to cells and very precisely quantify forces required to detach cells from a substrate of interest.

1.7.2. Single-Cell Adhesion Measurements

Different single-cell force spectroscopy (SCFS) methods were developed over the last decades to quantitatively characterize deadhesion processes of single cells from biotic or abiotic substrates, cells or tissues[258,259]. In these experiments, an immobilized single cell is first brought into contact with and subsequently separated from a substrate of interest while force sensitive device, such as optical or magnetic tweezers, micropipettes, or atomic force microscope (AFM), provide information about forces and energies of the attachment and detachment process[256,260,261]. SCFS usually allows a precise control of the experimental setting, including the contact time and force of the probed cell and the substrate of interest, thereby providing reproducible experimental conditions.

Optical and magnetic tweezers are rarely used to characterize cell adhesion due to their restricted force range between 0.1 and 200 pN (Ref. 262). In a widely used approach using micropipettes, a cell is partially aspirated into a pipette and brought into contact with a ligand-coated microsphere that is coupled to a force sensor. The force sensor is usually a swollen red blood cell with known physical parameters, which itself is partially aspirated into a second micropipette. Monitoring the position of the microsphere allows the precise determination of the force acting on it during the separation. This method is sensitive enough to characterize the binding properties of single adhesion receptors[210,211,263]. The forces that can be detected with this method range up to 1 nN, which is, however, not sufficient to characterize adhesion of a whole cell.

AFM-based SCFS (Figure 1-10) overcomes these force limits as the choice of different force sensors, *i.e.* AFM cantilevers, allows a large force range from ≈ 10 pN to > 100 nN to be measured[256,259,261,264,265]. To characterize forces with AFM, the deflection of the cantilever is monitored by a laser that is reflected from the cantilever onto a photodiode that is either position sensitive or segmented (Figure 1-10a). After determining the spring constant of the used cantilever[266], the deflection of the cantilever is translated into force using Hook's law. To probe adhesion characteristics of a single cell it is attached to a tipless cantilever (Figure 1-10b). This is facilitated by cantilever coating with either specific adhesion receptor ligands, antibodies or non-specific adhesives. The cantilever-bound cell is then approached either onto a protein-coated substrate, another cell, tissue explant or biomaterial. During the approach, the stiffness of the probed cell can be characterized when the cell is pushed onto the substrate[261,267-270]. After a given contact time during which the cell is allowed to initiate adhesion, the cantilever is retracted until cell and substrate are fully separated and the corresponding force acting on the cantilever is recorded throughout the experiment. Thereby, the force acting on the cantilever is usually displayed in dependence of distance between cantilever and substrate (force-distance curve) or the duration of the experiment (force-time curve). Thanks to the wide force

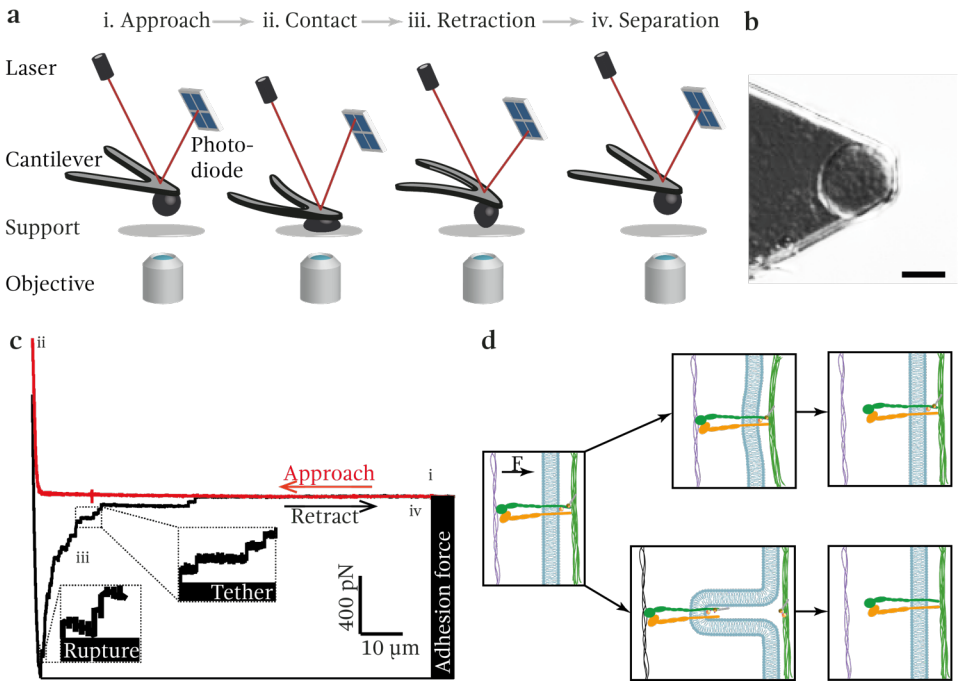

Figure 1-10 Scheme of atomic force microscopy-based single cell force spectroscopy. a and b) To use a single cell as a probe it is bound to a tipless AFM cantilever (scale bar, 10 µm). a) (i and ii) The cantilever is approached onto a protein-coated substrate until a preset contact force is reached. After a defined contact time (ii), the cantilever is retracted until the cell is fully separated from the substrate (iii and iv). During approach and retraction, the cantilever deflection and thus, the force acting on the cell is recorded in force-distance curves. c) Force distance curves show different features: In the approach curve (red) the cantilever deflection correlates with the stiffness of the cell and is called contact stiffness. The retraction curve (black) records the adhesion force of the cell, which represents the maximum downward force deflecting the cantilever and thus the force needed to detach cell and substrate. After recording the maximum adhesion force, single receptor unbinding events are observed. d) Rupture events are recorded when the adhesion receptor-ligand bond of a cytoskeleton-linked adhesion receptor fails. Tether events are recorded when a membrane tether is extruded from the cell membrane with the adhesion receptor at its tip (tethers). In the latter case attachment of the adhesion receptor to the cytoskeleton is either too weak to resist the mechanical stress applied or non-existent[264,278,284].

range that is covered by AFM-based SCFS, cell adhesion can be quantified from the level of an entire cell to the contribution of single adhesion receptors (Figure 1-10c). The detachment process quantitatively describes the force at which the cell starts to detach from the substrate, commonly called adhesion force. After the adhesion force is overcome, multiple smaller unbinding events are observable in force-distance curves, which correlate to the unbinding of single or clustered adhesion receptors from their ligands (Figure **1-10**d)[258,259,261,264,271]. In rupture events describe the unbinding of adhesion receptors from their ligand upon exposure of mechanical stress without membrane extraction[271-276]. These unbinding events can be used to extract the maximum force that an adhesion receptor-ligand bond can bear[259,267,272]. Tether events describe the extraction membrane tether, which are anchored to the substrate by one or multiple adhesion receptors[264,277,278]. Since the extension of tethers does not depend on the strength of the receptor-ligand bond, but characterizes mechanical properties of the cell cortex and cell membrane tension[273,275,278-283], forces recorded in these events do not quantify the adhesion receptor-ligand interaction directly. However, the lifetime of these tethers strongly depends on the

anchorage of the tether to the substrate and thus on the receptor-ligand interaction[273,275,283]. In the later separating phase between cell and substrate, the cell body is not in contact with the substrate anymore and cell adhesion is exclusively mediated by tethers[273].

1.7.3. Traction Force Measurements

Besides characterization of the force that is required to detach cell from a substrate, the tensional states of the whole cell and its adhesion sites are key elements of cell adhesion. Tensional states can be evaluated using traction force measurements. All traction force measurements are conceptually simple; cells or tissues are grown on flexible substrates, which are deformed by forces exerted by these cells/tissues[254,257]. Using the information of the substrate deformation, usually obtained by optical microscopy, and the physical parameters of the deformed substrate, traction forces can be calculated. To quantify subcellular traction forces, small fluorescent beads (diameter $\leqq$ 1 µm) are embedded in elastic ECM protein-coated polyacrylamide hydrogels or polydimethylsiloxane surfaces[285,286]. The substrate stiffness is tunable, achieved by varying degrees of crosslinking, and can thereby mimic different physiologically relevant environments. Although the concept is simple, the calibration of substrate stiffness and the calculation of traction forces are rather complicated. A different approach to measure traction forces is the use of small, vertical cantilevers that are usually made of silicon. Such pillars range from 0.25 to 10 µm in diameter and can quantify subcellular traction forces as well. Calculating traction forces is commonly easier for pillar, as Hook's law can be applied after determining the spring constant of the pillars[254,257]. However, pillar substrates have a distinct surface structure that may influence cellular behaviors, which has to be taken into account. All two-dimensional traction force methods employ materials that cannot be biodegraded by cells, however, ECM remodeling and degradation is relevant for the traction profiles of cells *in vivo*[287,288]. Moreover, experiments on two-dimensional surfaces reduces the complexity of the natural, three-dimensional matrix, in which cells are embedded in tissue. Hence, in the last decade a great effort was made to develop three-dimensional hydrogels, in which three-dimensional traction forces of cells could be quantified. These hydrogels are built of different backbones, such as poly(ethylene glycol) or polysaccharides, that allow conjugation with ECM proteins and variation of gel stiffness, which is regulated by the crosslinking density[254,257]. However, changing the mechanical properties of these gels induces changes in porosity, medium diffusion and mass transport. In these hydrogels, the crosslinking can be designed to be cleavable by cells, similar to the native ECM and hence, cells can control the stiffness of the gels[289], which mimics natural ECM conditions but increases the complexity of force calculations due to constantly changing physical parameters of the gel. Although two- and three-dimensional traction force microscopy provided valuable insights in mechanobiological processes, it requires new biomaterials, in which biochemical, structural and mechanical features can be tuned independently.

1.7.4. Molecular Tension Sensors

To address tension that is transmitted by single proteins, molecular sensors have been developed in the last years. These sensors are built as a molecular spring that connects either a fluorophore and a quencher or a Förster resonance energy transfer (FRET) fluorophore pair. The spatial arrangement of tow fluorophores or fluorophore and quencher are designed in a way that the application of strain to the spring changes the emission spectra of the fluorophores[290-292]. To translate the shift in the emission spectra of the fluorophores to forces, molecular tension sensors have to be carefully calibrated. Tension sensors can be either decorated with a ligand for an adhesion receptor and coupled to a stiff extracellular substrate, to address the tension applied to ligands by specific adhesion receptors, or they can be introduced into intracellular proteins, quantifying the tension that is applied to specific adhesome proteins. Extracellular tension sensors are often build from DNA-hairpins[293], peptide sequences[290] or whole proteins[294] that are partially or fully unfolded when tension is applied. Intracellular tension sensors are usually the protein of interested that is genetically modified to contain fluorophore pairs. In case the protein of interest is not sufficiently stretched by the applied tension, a molecular spring can be inserted between the fluorophore pair. It is noteworthy that all molecular tension sensors only provide information about the magnitude of the force but not the direction.

1.8. References

1. Pokutta, S. & Weis, W. I. Structure and Mechanism of Cadherins and Catenins in Cell-Cell Contacts. *Annu. Rev. Cell Dev. Biol.* **23,** 237–261 (2007).
2. McEver, R. P. & Zhu, C. Rolling cell adhesion. *Annu. Rev. Cell Dev. Biol.* **26,** 363–396 (2010).
3. Zaidel-Bar, R. Cadherin adhesome at a glance. *J. Cell Sci.* **126,** 373–378 (2013).
4. Winograd-Katz, S. E., Fässler, R., Geiger, B. & Legate, K. R. The integrin adhesome: from genes and proteins to human disease. *Nat. Rev. Mol. Cell Biol.* **15,** 273–288 (2014).
5. Crossin, K. L., Prieto, A. L., Hoffman, S. & Jones, F. S. Expression of adhesion molecules and the establishment of boundaries during embryonic and neural development. *Exp Neurol* **109,** 6–18 (1990).
6. Meager, A. Cytokine regulation of cellular adhesion molecule expression in inflammation. *Cytokine Growth Factor Rev.* (1999).
7. Hynes, R. O. Integrins: versatility, modulation, and signaling in cell adhesion. *Cell* **69,** 11–25 (1992).
8. Sutherland, A. E., Calarco, P. G. & Damsky, C. H. Developmental regulation of integrin expression at the time of implantation in the mouse embryo. *Development* **119,** 1175–1186 (1993).
9. Gumbiner, B. M. Cell adhesion: the molecular basis of tissue architecture and morphogenesis. *Cell* **84,** 345–357 (1996).
10. Kreidberg, J. A. & Symons, J. M. Integrins in kidney development, function, and disease. *Am. J. Physiol. Renal. Physiol.* **279,** F233–F242 (2000).
11. Halbleib, J. M. & Nelson, W. J. Cadherins in development: cell adhesion, sorting, and tissue morphogenesis. *Genes Dev.* **20,** 3199–3214 (2006).
12. Barone, V. & Heisenberg, C.-P. Cell adhesion in embryo morphogenesis. *Curr. Opin. Cell. Biol.* **24,** 148–153 (2012).
13. Lu, P., Takai, K., Weaver, V. M. & Werb, Z. Extracellular Matrix Degradation and Remodeling in Development and Disease. *Cold Spring Harb Perspect Biol* **3,** a005058–a005058 (2011).

14. Schwartz, M. A., Schaller, M. D. & Ginsberg, M. H. Integrins: emerging paradigms of signal transduction. *Annu. Rev. Cell Dev. Biol.* **11,** 549–599 (1995).
15. Humphrey, J. D., Dufresne, E. R. & Schwartz, M. A. Mechanotransduction and extracellular matrix homeostasis. *Nat. Rev. Mol. Cell Biol.* **15,** 802–812 (2014).
16. Leiss, M., Beckmann, K., Girós, A., Costell, M. & Fässler, R. The role of integrin binding sites in fibronectin matrix assembly in vivo. *Curr. Opin. Cell. Biol.* **20,** 502–507 (2008).
17. Mao, Y. & Schwarzbauer, J. E. Fibronectin fibrillogenesis, a cell-mediated matrix assembly process. *Matrix Biol.* **24,** 389–399 (2005).
18. Pankov, R. Fibronectin at a glance. *J. Cell Sci.* **115,** 3861–3863 (2002).
19. Ffrench-Constant, C. Alternative Splicing of Fibronectin—Many Different Proteins but Few Different Functions. *Exp. Cell Res.* **221,** 261–271 (1995).
20. Pierschbacher, M. D. & Ruoslahti, E. Variants of the cell recognition site of fibronectin that retain attachment-promoting activity. *PNAS* **81,** 5985–5988 (1984).
21. Hynes, R. O. Integrins: bidirectional, allosteric signaling machines. *Cell* **110,** 673–687 (2002).
22. Friedland, J. C., Lee, M. H. & Boettiger, D. Mechanically activated integrin switch controls alpha5beta1 function. *Science* **323,** 642–644 (2009).
23. Aota, S., Nagai, T. & Yamada, K. M. Characterization of regions of fibronectin besides the arginine-glycine-aspartic acid sequence required for adhesive function of the cell-binding domain using site-directed mutagenesis. *J. Biol. Chem.* **266,** 15938–15943 (1991).
24. Chada, D., Mather, T. & Nollert, M. U. The Synergy Site of Fibronectin Is Required for Strong Interaction with the Platelet Integrin αIIbβ3. *Ann Biomed Eng* **34,** 1542–1552 (2006).
25. Nagae, M. *et al.* Crystal structure of α5β1 integrin ectodomain: Atomic details of the fibronectin receptor. *J. Cell Biol.* **197,** 131–140 (2012).
26. Benito-Jardón, M. *et al.* The fibronectin synergy site re-enforces cell adhesion and mediates a crosstalk between integrin classes. *eLIFE* **6,** e22264 (2017).
27. George, E. L., Georges-Labouesse, E. N., Patel-King, R. S., Rayburn, H. & Hynes, R. O. Defects in mesoderm, neural tube and vascular development in mouse embryos lacking fibronectin. *Development* **119,** 1079–1091 (1993).
28. McDonald, J. A. Extracellular matrix assembly. *Annu. Rev. Cell Biol.* **4,** 183–207 (1988).
29. Johnson, K. J., Sage, H., Briscoe, G. & Erickson, H. P. The Compact Conformation of Fibronectin Is Determined by Intramolecular Ionic Interactions. *J. Biol. Chem.* **274,** 15473–15479 (1999).
30. Früh, S. M., Schoen, I., Ries, J. & Vogel, V. Molecular architecture of native fibronectin fibrils. *Nat. Commun.* **6,** ncomms8275 (2015).
31. Engel, J. *et al.* Shapes, domain organizations and flexibility of laminin and fibronectin, two multifunctional proteins of the extracellular matrix. *J. Mol. Biol.* **150,** 97–120 (1981).
32. Baneyx, G., Baugh, L. & Vogel, V. Fibronectin extension and unfolding within cell matrix fibrils controlled by cytoskeletal tension. *PNAS* **99,** 5139–5143 (2002).
33. Pankov, R. *et al.* Integrin dynamics and matrix assembly: tensin-dependent translocation of alpha(5)beta(1) integrins promotes early fibronectin fibrillogenesis. *J. Cell Biol.* **148,** 1075–1090 (2000).
34. Schwarzbauer, J. E. Identification of the fibronectin sequences required for assembly of a fibrillar matrix. *J. Cell Biol.* **113,** 1463–1473 (1991).
35. Sottile, J. & Wiley, S. Assembly of amino-terminal fibronectin dimers into the extracellular matrix. *J. Biol. Chem.* **269,** 17192–17198 (1994).
36. Gudzenko, T. & Franz, C. M. Studying early stages of fibronectin fibrillogenesis in living cells by atomic force microscopy. *Mol. Biol. Cell* **26,** 3190–3204 (2015).
37. Chen, Y., Zardi, L. & Peters, D. M. P. High-resolution cryo-scanning electron microscopy study of the macromolecular structure of fibronectin fibrils. *Scanning* **19,** 349–355 (1997).
38. Fogerty, F. J., Akiyama, S. K., Yamada, K. M. & Mosher, D. F. Inhibition of binding of fibronectin to matrix assembly sites by anti-integrin (alpha 5 beta 1) antibodies. *J. Cell*

Biol. **111,** 699–708 (1990).
39. Sechler, J. L. Altered rate of fibronectin matrix assembly by deletion of the first type III repeats. *J. Cell Biol.* **134,** 573–583 (1996).
40. Danen, E. H. J., Sonneveld, P., Brakebusch, C., Fässler, R. & Sonnenberg, A. The fibronectin-binding integrins alpha5beta1 and alphavbeta3 differentially modulate RhoA-GTP loading, organization of cell matrix adhesions, and fibronectin fibrillogenesis. *J. Cell Biol.* **159,** 1071–1086 (2002).
41. Ulmer, J., Geiger, B. & Spatz, J. P. Force-induced fibronectin fibrillogenesis in vitro. *Soft Matter* **4,** 1998–2007 (2008).
42. Geiger, B., Bershadsky, A., Pankov, R. & Yamada, K. M. Transmembrane crosstalk between the extracellular matrix and the cytoskeleton : Article : Nature Reviews Molecular Cell Biology. *Nat. Rev. Mol. Cell Biol.* **2,** 793–805 (2001).
43. Zhong, C. *et al.* Rho-mediated Contractility Exposes a Cryptic Site in Fibronectin and Induces Fibronectin Matrix Assembly. *J. Cell Biol.* **141,** 539–551 (1998).
44. Smith, M. L. *et al.* Force-Induced Unfolding of Fibronectin in the Extracellular Matrix of Living Cells. *Plos Biol* **5,** e268 (2007).
45. Erickson, H. P. Reversible unfolding of fibronectin type III and immunoglobulin domains provides the structural basis for stretch and elasticity of titin and fibronectin. *PNAS* **91,** 10114–10118 (1994).
46. Gao, M., Craig, D., Vogel, V. & Schulten, K. Identifying Unfolding Intermediates of FN-III10 by Steered Molecular Dynamics. *J. Mol. Biol.* **323,** 939–950 (2002).
47. Oberhauser, A. F., Badilla-Fernandez, C., Carrion-Vazquez, M. & Fernandez, J. M. The Mechanical Hierarchies of Fibronectin Observed with Single-molecule AFM. *J. Mol. Biol.* **319,** 433–447 (2002).
48. Erler, J. T. & Weaver, V. M. Three-dimensional context regulation of metastasis. *Clin Exp Metastasis* **26,** 35–49 (2008).
49. Paszek, M. J. *et al.* Tensional homeostasis and the malignant phenotype. *Cancer Cell* **8,** 241–254 (2005).
50. Bershadsky, A. *et al.* Assembly and mechanosensory function of focal adhesions: experiments and models. *European Journal of Cell Biology* **85,** 165–173 (2006).
51. Schwartz, M. A. & DeSimone, D. W. Cell adhesion receptors in mechanotransduction. *Curr. Opin. Cell. Biol.* **20,** 551–556 (2008).
52. Chiquet, M., Renedo, A. S., Huber, F. & Flück, M. How do fibroblasts translate mechanical signals into changes in extracellular matrix production? *Matrix Biol.* **22,** 73–80 (2003).
53. Chiquet, M. Regulation of extracellular matrix gene expression by mechanical stress. *Matrix Biol.* **18,** 417–426 (1999).
54. Wang, J. H. C., Thampatty, B. P., Lin, J.-S. & Im, H.-J. Mechanoregulation of gene expression in fibroblasts. *Gene* **391,** 1–15 (2007).
55. Kubow, K. E. *et al.* Mechanical forces regulate the interactions of fibronectin and collagen I in extracellular matrix. *Nat. Commun.* **6,** ncomms9026 (2015).
56. Nguyen, T. D. *et al.* Effects of Cell Seeding and Cyclic Stretch on the Fiber Remodeling in an Extracellular Matrix–Derived Bioscaffold. *http://www.liebertpub.com/tea* **15,** 957–963 (2008).
57. Cox, T. R. & Erler, J. T. Remodeling and homeostasis of the extracellular matrix: implications for fibrotic diseases and cancer. *Disease Models & Mechanisms* **4,** 165–178 (2011).
58. Discher, D. E. Tissue Cells Feel and Respond to the Stiffness of Their Substrate. *Science* **310,** 1139–1143 (2005).
59. Levental, I., Georges, P. C. & Janmey, P. A. Soft biological materials and their impact on cell function. *Soft Matter* (2007).
60. Calderwood, D. A., Campbell, I. D. & Critchley, D. R. Talins and kindlins: partners in integrin-mediated adhesion. *Nat. Rev. Mol. Cell Biol.* **14,** 503–517 (2013).
61. Moser, M., Legate, K. R., Zent, R. & Fässler, R. The tail of integrins, talin, and kindlins. *Science* **324,** 895–899 (2009).
62. Horton, E. R. *et al.* The integrin adhesome network at a glance. *J. Cell Sci.* **129,** jcs.192054–5 (2016).
63. Horton, E. R. *et al.* Definition of a consensus integrin adhesome and its dynamics

during adhesion complex assembly and disassembly. *Nat. Cell Biol.* **17,** 1577–1587 (2015).
64. Schiller, H. B., Friedel, C. C., Boulegue, C. & Fässler, R. Quantitative proteomics of the integrin adhesome show a myosin II-dependent recruitment of LIM domain proteins. *EMBO Rep.* **12,** 259–266 (2011).
65. Winograd-Katz, S. E., Fässler, R., Geiger, B. & Legate, K. R. The integrin adhesome: from genes and proteins to human disease. *Nat. Rev. Mol. Cell Biol.* **15,** 273–288 (2014).
66. Whittaker, C. A. & Hynes, R. O. Distribution and evolution of von Willebrand/integrin A domains: widely dispersed domains with roles in cell adhesion and elsewhere. *Mol. Biol. Cell* **13,** 3369–3387 (2002).
67. Humphries, J. D., Byron, A. & Humphries, M. J. Integrin ligands at a glance. *J. Cell Sci.* **119,** 3901–3903 (2006).
68. Bouvard, D., Pouwels, J., De Franceschi, N. & Ivaska, J. Integrin inactivators: balancing cellular functions in vitro and in vivo. *Nature Publishing Group* **14,** 430–442 (2013).
69. Bouvard, D., Pouwels, J., De Franceschi, N. & Ivaska, J. Integrin inactivators: balancing cellular functions in vitro and in vivo. *Nat. Rev. Mol. Cell Biol.* **14,** 432–444 (2013).
70. Danen, E. Integrins: Signalling and Disease. *eLS* doi:10.1002/9780470015902.a0004022.pub3
71. Fassler, R. & Meyer, M. Consequences of lack of beta 1 integrin gene expression in mice. *Genes Dev.* **9,** 1896–1908 (1995).
72. Zaidel-Bar, R. Evolution of complexity in the integrin adhesome. *J. Cell Biol.* **186,** 317–321 (2009).
73. Humphries, J. D., Byron, A. & Humphries, M. J. Integrin ligands at a glance. *J. Cell Sci.* **119,** 3901–3903 (2006).
74. Anthis, N. J. & Campbell, I. D. The tail of integrin activation. *Trends in Biochemical Sciences* **36,** 191–198 (2011).
75. Arnaout, M. A., Mahalingam, B. & Xiong, J. P. Integrin structure, allostery, and bidirectional signaling. *Annu. Rev. Cell Dev. Biol.* **21,** 381–410 (2005).
76. Takagi, J., Petre, B. M., Walz, T. & Springer, T. A. Global Conformational Rearrangements in Integrin Extracellular Domains in Outside-In and Inside-Out Signaling. *Cell* **110,** 599–611 (2002).
77. Xiong, J.-P. *et al.* Crystal Structure of the Extracellular Segment of Integrin αVβ3. *Science* **294,** 339–345 (2001).
78. Xiong, J.-P. *et al.* Crystal Structure of the Extracellular Segment of Integrin αVβ3 in Complex with an Arg-Gly-Asp Ligand. *Science* **296,** 151–155 (2002).
79. Zhu, J. *et al.* Structure of a Complete Integrin Ectodomain in a Physiologic Resting State and Activation and Deactivation by Applied Forces. *Mol. Cell* **32,** 849–861 (2008).
80. Xie, C. *et al.* Structure of an integrin with an αI domain, complement receptor type 4. *EMBO J.* **29,** 666–679 (2010).
81. Chen, X. *et al.* Requirement of open headpiece conformation for activation of leukocyte integrin X 2. *PNAS* **107,** 14727–14732 (2010).
82. Zhu, J., Zhu, J. & Springer, T. A. Complete integrin headpiece opening in eight steps. *J. Cell Biol.* **201,** 1053–1068 (2013).
83. Schürpf, T. & Springer, T. A. Regulation of integrin affinity on cell surfaces. *EMBO J.* **30,** 4712–4727 (2011).
84. Su, Y. *et al.* Relating conformation to function in integrin α5β1. *Proc. Natl. Acad. Sci. U.S.A.* **113,** E3872–81 (2016).
85. Byron, A. *et al.* Anti-integrin monoclonal antibodies. *J. Cell Sci.* **122,** 4009–4011 (2009).
86. Su, Y. *et al.* Relating conformation to function in integrin α5β1. *Proc. Natl. Acad. Sci. U.S.A.* **113,** 201605074–E3881 (2016).
87. Askari, J. A., Buckley, P. A., Mould, A. P. & Humphries, M. J. Linking integrin conformation to function. *J. Cell Sci.* **122,** 165–170 (2009).
88. Campbell, I. D. & Humphries, M. J. Integrin structure, activation, and interactions. *Cold Spring Harb Perspect Biol* **3,** (2011).
89. Li, J. *et al.* Conformational equilibria and intrinsic affinities define integrin activation.

EMBO J. **36,** 629–645 (2017).
90. Adair, B. D. *et al.* Three-dimensional EM structure of the ectodomain of integrin αVβ3 in a complex with fibronectin. *J. Cell Biol.* **168,** 1109–1118 (2005).
91. Mould, A. P. *et al.* Conformational changes in the integrin beta A domain provide a mechanism for signal transduction via hybrid domain movement. *J. Biol. Chem.* **278,** 17028–17035 (2003).
92. Luo, B.-H., Takagi, J. & Springer, T. A. Locking the beta3 integrin I-like domain into high and low affinity conformations with disulfides. *J. Biol. Chem.* **279,** 10215–10221 (2004).
93. Xiao, T., Takagi, J., Coller, B. S., Wang, J.-H. & Springer, T. A. Structural basis for allostery in integrins and binding to fibrinogen-mimetic therapeutics. *Nature* **432,** 59–67 (2004).
94. Chen, J., Salas, A. & Springer, T. A. Bistable regulation of integrin adhesiveness by a bipolar metal ion cluster. *Nat Struct Biol* **10,** 995–1001 (2003).
95. Mould, A. P., Barton, S. J., Askari, J. A., Craig, S. E. & Humphries, M. J. Role of ADMIDAS cation-binding site in ligand recognition by integrin alpha 5 beta 1. *J. Biol. Chem.* **278,** 51622–51629 (2003).
96. Chen, J., Yang, W., Kim, M., Carman, C. V. & Springer, T. A. Regulation of outside-in signaling and affinity by the β2 I domain of integrin αLβ2. *Proc. Natl. Acad. Sci. U.S.A.* **103,** 13062–13067 (2006).
97. Luo, B.-H., Carman, C. V. & Springer, T. A. Structural Basis of Integrin Regulation and Signaling. *Annu. Rev. Immunol.* **25,** 619–647 (2007).
98. Campbell, I. D. & Humphries, M. J. Integrin structure, activation, and interactions. *Cold Spring Harb Perspect Biol* **3,** a004994–a004994 (2011).
99. Huth, J. R. *et al.* NMR and mutagenesis evidence for an I domain allosteric site that regulates lymphocyte function-associated antigen 1 ligand binding. *PNAS* **97,** 5231–5236 (2000).
100. Alonso, J. L., Essafi, M., Xiong, J.-P., Stehle, T. & Arnaout, M. A. Does the Integrin αA Domain Act as a Ligand for its βA Domain? *Current Biology* **12,** R340–R342 (2002).
101. Yang, W., Shimaoka, M., Salas, A., Takagi, J. & Springer, T. A. Intersubunit signal transmission in integrins by a receptor-like interaction with a pull spring. *PNAS* **101,** 2906–2911 (2004).
102. Chen, W. *et al.* Molecular Dynamics Simulations of Forced Unbending of Integrin αVβ3. *PLoS Comput Biol* **7,** e1001086 (2011).
103. Nordenfelt, P., Elliott, H. L. & Springer, T. A. Coordinated integrin activation by actin-dependent force during T-cell migration. *Nat. Commun.* **7,** ncomms13119 (2016).
104. Chen, Y., Lee, H., Tong, H., Schwartz, M. & Zhu, C. Force regulated conformational change of integrin αVβ3. *Matrix Biol.* (2016). doi:10.1016/j.matbio.2016.07.002
105. Chen, W., Lou, J., Evans, E. A. & Zhu, C. Observing force-regulated conformational changes and ligand dissociation from a single integrin on cells. *J. Cell Biol.* **199,** 497–512 (2012).
106. Theodosiou, M. *et al.* Kindlin-2 cooperates with talin to activate integrins and induces cell spreading by directly binding paxillin. *eLIFE* **5,** e10130 (2016).
107. Klapholz, B. & Brown, N. H. Talin – the master of integrin adhesions. *J. Cell Sci.* **130,** 2435–2446 (2017).
108. Critchley, D. R. & Gingras, A. R. Talin at a glance. *J. Cell Sci.* **121,** 1345–1347 (2008).
109. Tepass, U. FERM proteins in animal morphogenesis. *Curr. Opin. Genet. Dev.* **19,** 357–367 (2009).
110. Goult, B. T. *et al.* Structure of a double ubiquitin-like domain in the talin head: a role in integrin activation. *EMBO J.* **29,** 1069–1080 (2010).
111. Saltel, F. *et al.* New PI(4,5)P2- and membrane proximal integrin–binding motifs in the talin head control β3-integrin clustering. *J. Cell Biol.* **187,** 715–731 (2009).
112. Anthis, N. J. *et al.* The structure of an integrin/talin complex reveals the basis of inside-out signal transduction. - PubMed - NCBI. *EMBO J.* **28,** 3623–3632 (2009).
113. Elliott, P. R. *et al.* The Structure of the Talin Head Reveals a Novel Extended Conformation of the FERM Domain. *Structure* **18,** 1289–1299 (2010).
114. Calderwood, D. A. *et al.* The Talin head domain binds to integrin beta subunit

cytoplasmic tails and regulates integrin activation. *J. Biol. Chem.* **274,** 28071–28074 (1999).
115. García-Alvarez, B. *et al.* Structural Determinants of Integrin Recognition by Talin. *Mol. Cell* **11,** 49–58 (2003).
116. Wegener, K. L. *et al.* Structural Basis of Integrin Activation by Talin. *Cell* **128,** 171–182 (2007).
117. Hemmings, L. *et al.* Talin contains three actin-binding sites each of which is adjacent to a vinculin-binding site. *J. Cell Sci.* **109 (Pt 11),** 2715–2726 (1996).
118. Lee, H.-S. *et al.* Characterization of an Actin-binding Site within the Talin FERM Domain. *J. Mol. Biol.* **343,** 771–784 (2004).
119. Plak, K., Pots, H., Van Haastert, P. J. M. & Kortholt, A. Direct Interaction between TalinB and Rap1 is necessary for adhesion of Dictyostelium cells. *BMC Cell Biology 2016 17:1* **17,** 1 (2016).
120. Gingras, A. R. *et al.* Mapping and consensus sequence identification for multiple vinculin binding sites within the talin rod. *J. Biol. Chem.* **280,** 37217–37224 (2005).
121. Goult, B. T. *et al.* Structural studies on full-length talin1 reveal a compact auto-inhibited dimer: Implications for talin activation. *Journal of Structural Biology* **184,** 21–32 (2013).
122. Atherton, P. *et al.* Vinculin controls talin engagement with the actomyosin machinery. *Nat. Commun.* **6,** ncomms10038 (2015).
123. Gingras, A. R. *et al.* Structural determinants of integrin binding to the talin rod. *J. Biol. Chem.* **284,** 8866–8876 (2009).
124. Lee, H.-S., Lim, C. J., Puzon-McLaughlin, W., Shattil, S. J. & Ginsberg, M. H. RIAM activates integrins by linking talin to ras GTPase membrane-targeting sequences. *J. Biol. Chem.* **284,** 5119–5127 (2009).
125. Goult, B. T. *et al.* RIAM and Vinculin Binding to Talin Are Mutually Exclusive and Regulate Adhesion Assembly and Turnover. *J. Biol. Chem.* **288,** 8238–8249 (2013).
126. Sun, Z. *et al.* Kank2 activates talin, reduces force transduction across integrins and induces central adhesion formation. *Nat. Cell Biol.* **18,** 941–953 (2016).
127. Bouchet, B. P. *et al.* Talin-KANK1 interaction controls the recruitment of cortical microtubule stabilizing complexes to focal adhesions. *bioRxiv* 055210 (2016). doi:10.1101/055210
128. Rodius, S. *et al.* The talin rod IBS2 alpha-helix interacts with the beta3 integrin cytoplasmic tail membrane-proximal helix by establishing charge complementary salt bridges. *J. Biol. Chem.* **283,** 24212–24223 (2008).
129. Goult, B. T. *et al.* The structure of an interdomain complex that regulates talin activity. *J. Biol. Chem.* **284,** 15097–15106 (2009).
130. Goksoy, E. *et al.* Structural basis for the autoinhibition of talin in regulating integrin activation. *Mol. Cell* **31,** 124–133 (2008).
131. Zhang, H., Chang, Y.-C., Huang, Q., Brennan, M. L. & Wu, J. Structural and Functional Analysis of a Talin Triple-Domain Module Suggests an Alternative Talin Autoinhibitory Configuration. *Structure* **24,** 721–729 (2016).
132. Banno, A. *et al.* Subcellular Localization of Talin Is Regulated by Inter-domain Interactions. *J. Biol. Chem.* **287,** 13799–13812 (2012).
133. Lee, H.-S., Lim, C. J., Puzon-McLaughlin, W., Shattil, S. J. & Ginsberg, M. H. RIAM activates integrins by linking talin to ras GTPase membrane-targeting sequences. *J. Biol. Chem.* **284,** 5119–5127 (2009).
134. Yang, J. *et al.* Conformational activation of talin by RIAM triggers integrin-mediated cell adhesion. *Nat. Commun.* **5,** 5880 (2014).
135. Lagarrigue, F. *et al.* A RIAM/lamellipodin-talin-integrin complex forms the tip of sticky fingers that guide cell migration. *Nat. Commun.* **6,** 8492 (2015).
136. Ye, F. *et al.* Recreation of the terminal events in physiological integrin activation. *J. Cell Biol.* **188,** 157–173 (2010).
137. Martel, V. *et al.* Conformation, localization, and integrin binding of talin depend on its interaction with phosphoinositides. *J. Biol. Chem.* **276,** 21217–21227 (2001).
138. Schiemer, J. *et al.* Gα13 Switch Region 2 Relieves Talin Autoinhibition to Activate αIIbβ3 Integrin. *J. Biol. Chem.* **291,** 26598–26612 (2016).
139. Atherton, P. *et al.* Vinculin controls talin engagement with the actomyosin machinery.

Nat. Commun. **6,** 10038 (2015).
140. Gingras, A. R. *et al.* The structure of the C-terminal actin-binding domain of talin. *EMBO J.* **27,** 458–469 (2008).
141. del Rio, A. *et al.* Stretching single talin rod molecules activates vinculin binding. *Science* **323,** 638–641 (2009).
142. Lee, S. E., Kamm, R. D. & Mofrad, M. R. K. Force-induced activation of Talin and its possible role in focal adhesion mechanotransduction. *J. Biomech.* **40,** 2096–2106 (2007).
143. Rognoni, E., Ruppert, R. & Fässler, R. The kindlin family: functions, signaling properties and implications for human disease. *J. Cell Sci.* **129,** 17–27 (2016).
144. Goult, B. T. *et al.* The Structure of the N-Terminus of Kindlin-1: A Domain Important for αIIbβ3 Integrin Activation. *J. Mol. Biol.* **394,** 944–956 (2009).
145. Li, H. *et al.* Structural basis of kindlin-mediated integrin recognition and activation. *Proc. Natl. Acad. Sci. U.S.A.* **135,** 201703064 (2017).
146. Bouaouina, M. *et al.* A conserved lipid-binding loop in the kindlin FERM F1 domain is required for kindlin-mediated αIIbβ3 integrin coactivation. *J. Biol. Chem.* **287,** 6979–6990 (2012).
147. Liu, J. *et al.* Structural basis of phosphoinositide binding to kindlin-2 protein pleckstrin homology domain in regulating integrin activation. *J. Biol. Chem.* **286,** 43334–43342 (2011).
148. Perera, H. D. *et al.* Membrane Binding of the N-Terminal Ubiquitin-Like Domain of kindlin-2 Is Crucial for Its Regulation of Integrin Activation. *Structure* **19,** 1664–1671 (2011).
149. Böttcher, R. T. *et al.* Kindlin-2 recruits paxillin and Arp2/3 to promote membrane protrusions during initial cell spreading. *J. Cell Biol.* (2017). doi:10.1083/jcb.201701176
150. Harburger, D. S., Bouaouina, M. & Calderwood, D. A. Kindlin-1 and -2 directly bind the C-terminal region of beta integrin cytoplasmic tails and exert integrin-specific activation effects. *J. Biol. Chem.* **284,** 11485–11497 (2009).
151. Moser, M., Nieswandt, B., Ussar, S., Pozgajova, M. & Fässler, R. Kindlin-3 is essential for integrin activation and platelet aggregation. *Nat. Med.* **14,** 325–330 (2008).
152. Ma, Y.-Q., Qin, J., Wu, C. & Plow, E. F. Kindlin-2 (Mig-2): a co-activator of β3 integrins. *J. Cell Biol.* **181,** 439–446 (2008).
153. Fukuda, K. *et al.* Molecular Basis of Kindlin-2 Binding to Integrin-linked Kinase Pseudokinase for Regulating Cell Adhesion. *J. Biol. Chem.* **289,** 28363–28375 (2014).
154. Huet-Calderwood, C. *et al.* Differences in binding to the ILK complex determines kindlin isoform adhesion localization and integrin activation. *J. Cell Sci.* **127,** 4308–4321 (2014).
155. Montañez, E. *et al.* Kindlin-2 controls bidirectional signaling of integrins. *Genes Dev.* **22,** 1325–1330 (2008).
156. Böttcher, R. T., Lange, A. & Fässler, R. How ILK and kindlins cooperate to orchestrate integrin signaling. *Curr. Opin. Cell. Biol.* **21,** 670–675 (2009).
157. Legate, K. R., Montañez, E., Kudlacek, O. & Füssler, R. ILK, PINCH and parvin: the tIPP of integrin signalling. *Nat. Rev. Mol. Cell Biol.* **7,** 20–31 (2005).
158. Wickström, S. A., Lange, A., Montañez, E. & Fässler, R. The ILK/PINCH/parvin complex: the kinase is dead, long live the pseudokinase! *EMBO J.* **29,** 281–291 (2010).
159. Bledzka, K. *et al.* Kindlin-2 directly binds actin and regulates integrin outside-in signaling. *J. Cell Biol.* **213,** 97–108 (2016).
160. Gao, J. *et al.* Kindlin supports platelet integrin αIIbβ3 activation by interacting with paxillin. *J. Cell Sci.* jcs.205641 (2017). doi:10.1242/jcs.205641
161. Schaller, M. D. Paxillin: a focal adhesion-associated adaptor protein. *, Published online: 02 October 2001; | doi:10.1038/sj.onc.1204786* **20,** 6459–6472 (2001).
162. Turner, C. E. Paxillin and focal adhesion signalling. *Nat. Cell Biol.* **2,** E231–E236 (2000).
163. Chang, D. D., Wong, C., Smith, H. & Liu, J. ICAP-1, a novel beta1 integrin cytoplasmic domain-associated protein, binds to a conserved and functionally important NPXY sequence motif of beta1 integrin. *J. Cell Biol.* **138,** 1149–1157 (1997).
164. Kiema, T. *et al.* The Molecular Basis of Filamin Binding to Integrins and Competition with Talin. *Mol. Cell* **21,** 337–347 (2006).

165. Liu, J. *et al.* Structural mechanism of integrin inactivation by filamin. *Nature structural & molecular biology* **22,** 383–389 (2015).
166. Rantala, J. K. *et al.* SHARPIN is an endogenous inhibitor of [beta]1-integrin activation. *Nat. Cell Biol.* **13,** 1315–1324 (2011).
167. Nevo, J. *et al.* Mammary-derived growth inhibitor (MDGI) interacts with integrin α-subunits and suppresses integrin activity and invasion. *Oncogene* **29,** 6452–6463 (2010).
168. Brunner, M. *et al.* Osteoblast mineralization requires β1 integrin/ICAP-1–dependent fibronectin deposition. *J. Cell Biol.* **194,** 307–322 (2011).
169. Liu, W., Draheim, K. M., Zhang, R., Calderwood, D. A. & Boggon, T. J. Mechanism for KRIT1 Release of ICAP1-Mediated Suppression of Integrin Activation. *Mol. Cell* **49,** 719–729 (2013).
170. Oxley, C. L. *et al.* An Integrin Phosphorylation Switch THE EFFECT OF β3 INTEGRIN TAIL PHOSPHORYLATION ON DOK1 AND TALIN BINDING. *J. Biol. Chem.* **283,** 5420–5426 (2008).
171. Nevo, J. *et al.* Mammary-derived growth inhibitor (MDGI) interacts with integrin |[alpha]|-subunits and suppresses integrin activity and invasion. *Oncogene* **29,** 6452–6463 (2010).
172. Bazzoni, G. & Hemler, M. E. Are changes in integrin affinity and conformation overemphasized? *Trends in Biochemical Sciences* **23,** 30–34 (1998).
173. Carman, C. V. & Springer, T. A. Integrin avidity regulation: are changes in affinity and conformation underemphasized? *Curr. Opin. Cell. Biol.* **15,** 547–556 (2003).
174. Changede, R., Xu, X., Margadant, F. & Sheetz, M. P. Nascent Integrin Adhesions Form on All Matrix Rigidities after Integrin Activation. *Dev. Cell* **35,** 614–621 (2015).
175. Cavalcanti-Adam, E. A., Aydin, D., Hirschfeld Warneken, V. C. & Spatz, J. P. Cell adhesion and response to synthetic nanopatterned environments by steering receptor clustering and spatial location. *HFSP Journal* **2,** 276–285 (2008).
176. Kim, M., Carman, C. V., Yang, W., Salas, A. & Springer, T. A. The primacy of affinity over clustering in regulation of adhesiveness of the integrin αLβ2. *J. Cell Biol.* **167,** 1241–1253 (2004).
177. Petrie, T. A. *et al.* Multivalent Integrin-Specific Ligands Enhance Tissue Healing and Biomaterial Integration. *Sci Transl Med* **2,** 45ra60–45ra60 (2010).
178. Paszek, M. J. *et al.* The cancer glycocalyx mechanically primes integrin-mediated growth and survival. *Nature* **511,** 319–325 (2014).
179. Wang, P., Ballestrem, C. & Streuli, C. H. The C terminus of talin links integrins to cell cycle progression. *J. Cell Biol.* **195,** 499–513 (2011).
180. Bachir, A. I. *et al.* Integrin-Associated Complexes Form Hierarchically with Variable Stoichiometry in Nascent Adhesions. *Current Biology* **24,** 1845–1853 (2014).
181. Sieg, D. J., Hauck, C. R. & Schlaepfer, D. D. Required role of focal adhesion kinase (FAK) for integrin-stimulated cell migration. *J. Cell Sci.* **112,** 2677–2691 (1999).
182. Lawson, C. *et al.* FAK promotes recruitment of talin to nascent adhesions to control cell motility. *J. Cell Biol.* **196,** 223–232 (2012).
183. Michael, K. E., Dumbauld, D. W., Burns, K. L., Hanks, S. K. & García, A. J. Focal adhesion kinase modulates cell adhesion strengthening via integrin activation. *Mol. Biol. Cell* **20,** 2508–2519 (2009).
184. Serrels, B. *et al.* Focal adhesion kinase controls actin assembly via a FERM-mediated interaction with the Arp2/3 complex. *Nat. Cell Biol.* **9,** 1046–1056 (2007).
185. Deramaudt, T. B. *et al.* Altering FAK-Paxillin Interactions Reduces Adhesion, Migration and Invasion Processes. *PLoS ONE* **9,** e92059 (2014).
186. Swaminathan, V., Fischer, R. S. & Waterman, C. M. The FAK-Arp2/3 interaction promotes leading edge advance and haptosensing by coupling nascent adhesions to lamellipodia actin. *Mol. Biol. Cell* **27,** 1085–1100 (2016).
187. Choi, C. K. *et al.* Actin and α-actinin orchestrate the assembly and maturation of nascent adhesions in a myosin II motor-independent manner. *Nat. Cell Biol.* **10,** 1039–1050 (2008).
188. Oser, M. & Condeelis, J. The cofilin activity cycle in lamellipodia and invadopodia. *Journal of Cellular Biochemistry* **108,** 1252–1262 (2009).
189. Swaminathan, V. *et al.* Actin retrograde flow actively aligns and orients ligand-

engaged integrins in focal adhesions. *PNAS* **114,** 10648–10653 (2017).
190. Kanchanawong, P. *et al.* Nanoscale architecture of integrin-based cell adhesions. *Nature* **468,** 580–584 (2010).
191. Case, L. B. *et al.* Molecular mechanism of vinculin activation and nanoscale spatial organization in focal adhesions. *Nat. Cell Biol.* **17,** 880–892 (2015).
192. Case, L. B. & Waterman, C. M. Integration of actin dynamics and cell adhesion by a three-dimensional, mechanosensitive molecular clutch. *Nat. Cell Biol.* **17,** 955–963 (2015).
193. Liu, J. *et al.* Talin determines the nanoscale architecture of focal adhesions. *Proc. Natl. Acad. Sci. U.S.A.* **112,** E4864–73 (2015).
194. Zaidel-Bar, R., Milo, R., Kam, Z. & Geiger, B. A paxillin tyrosine phosphorylation switch regulates the assembly and form of cell-matrix adhesions. *J. Cell Sci.* **120,** 137–148 (2007).
195. Schiller, H. B. *et al.* β1- and αv-class integrins cooperate to regulate myosin II during rigidity sensing of fibronectin-based microenvironments. *Nat. Cell Biol.* **15,** 625–636 (2013).
196. Rossier, O. *et al.* Integrins β1 and β3 exhibit distinct dynamic nanoscale organizations inside focal adhesions. *Nat. Cell Biol.* **14,** 1057–1067 (2012).
197. Wolfenson, H. *et al.* A Role for the Juxtamembrane Cytoplasm in the Molecular Dynamics of Focal Adhesions. *PLoS ONE* **4,** e4304 (2009).
198. Lavelin, I. *et al.* Differential Effect of Actomyosin Relaxation on the Dynamic Properties of Focal Adhesion Proteins. *PLoS ONE* **8,** e73549 (2013).
199. Lele, T. P., Thodeti, C. K., Pendse, J. & Ingber, D. E. Investigating complexity of protein–protein interactions in focal adhesions. *Biochemical and Biophysical Research Communications* **369,** 929–934 (2008).
200. Eisenstein, M. Mechanobiology: A measure of molecular muscle. *Nature* **544,** 255–257 (2017).
201. Wehrle-Haller, B. Assembly and disassembly of cell matrix adhesions. *Curr. Opin. Cell. Biol.* **24,** 569–581 (2012).
202. Ezratty, E. J., Partridge, M. A. & Gundersen, G. G. Microtubule-induced focal adhesion disassembly is mediated by dynamin and focal adhesion kinase. *Nat. Cell Biol.* **7,** 581–590 (2005).
203. Nader, G., Ezratty, E. J. & Gundersen, G. G. FAK, talin and PIPKIγ regulate endocytosed integrin activation to polarize focal adhesion assembly. *Nat. Cell Biol.* **18,** 491–503 (2016).
204. Krylyshkina, O. *et al.* Modulation of substrate adhesion dynamics via microtubule targeting requires kinesin-1. *J. Cell Biol.* **156,** 349–360 (2002).
205. Schober, M. *et al.* Focal adhesion kinase modulates tension signaling to control actin and focal adhesion dynamics. *J. Cell Biol.* **176,** 667–680 (2007).
206. Webb, D. J. *et al.* FAK-Src signalling through paxillin, ERK and MLCK regulates adhesion disassembly. *Nat. Cell Biol.* **6,** 154–161 (2004).
207. Engler, A. J., Sen, S., Sweeney, H. L. & Discher, D. E. Matrix Elasticity Directs Stem Cell Lineage Specification. *Cell* **126,** 677–689 (2006).
208. Wozniak, M. A., Modzelewska, K., Kwong, L. & Keely, P. J. Focal adhesion regulation of cell behavior. *Biochimica et Biophysica Acta (BBA) - Molecular Cell Research* **1692,** 103–119 (2004).
209. Thomas, W. Catch Bonds in Adhesion. *Annu. Rev. Biomed. Eng.* **10,** 39–57 (2008).
210. Kong, F. *et al.* Cyclic Mechanical Reinforcement of Integrin–Ligand Interactions. *Mol. Cell* **49,** 1060–1068 (2013).
211. Kong, F., García, A. J., Mould, A. P., Humphries, M. J. & Zhu, C. Demonstration of catch bonds between an integrin and its ligand. *J. Cell Biol.* **185,** 1275–1284 (2009).
212. Roca-Cusachs, P., Gauthier, N. C., del Rio, A. & Sheetz, M. P. Clustering of α5β1 integrins determines adhesion strength whereas αvβ3 and talin enable mechanotransduction. *Proc. Natl. Acad. Sci. U.S.A.* **106,** 16245–16250 (2009).
213. Orr, A. W., Ginsberg, M. H., Shattil, S. J., Deckmyn, H. & Schwartz, M. A. Matrix-specific suppression of integrin activation in shear stress signaling. *Mol. Biol. Cell* **17,** 4686–4697 (2006).
214. Tzima, E., Del Pozo, M. A., Shattil, S. J., Chien, S. & Schwartz, M. A. Activation of

integrins in endothelial cells by fluid shear stress mediates Rho-dependent cytoskeletal alignment. *EMBO J.* **20,** 4639–4647 (2001).
215. Katsumi, A., Naoe, T., Matsushita, T., Kaibuchi, K. & Schwartz, M. A. Integrin activation and matrix binding mediate cellular responses to mechanical stretch. *J. Biol. Chem.* **280,** 16546–16549 (2005).
216. Tzima, E. *et al.* A mechanosensory complex that mediates the endothelial cell response to fluid shear stress. *Nature* **437,** 426–431 (2005).
217. Tzima, E., del Pozo, M. A., Shattil, S. J., Chien, S. & Schwartz, M. A. Activation of integrins in endothelial cells by fluid shear stress mediates Rho-dependent cytoskeletal alignment. *EMBO J.* **20,** 4639–4647 (2001).
218. Elosegui-Artola, A. *et al.* Rigidity sensing and adaptation through regulation of integrin types. *Nat. Mater.* **13,** 631–637 (2014).
219. Tzima, E. *et al.* Activation of Rac1 by shear stress in endothelial cells mediates both cytoskeletal reorganization and effects on gene expression. *EMBO J.* **21,** 6791–6800 (2002).
220. Hotulainen, P. & Lappalainen, P. Stress fibers are generated by two distinct actin assembly mechanisms in motile cells. *J. Cell Biol.* **173,** 383–394 (2006).
221. Gawlak, G. *et al.* Paxillin mediates stretch-induced Rho signaling and endothelial permeability via assembly of paxillin-p42/44MAPK-GEF-H1 complex. *FASEB J* **28,** 3249–3260 (2014).
222. Cui, Y. *et al.* Cyclic stretching of soft substrates induces spreading and growth. *Nat. Commun.* **6,** 6333 (2015).
223. Huang, D. L., Bax, N. A., Buckley, C. D., Weis, W. I. & Dunn, A. R. Vinculin forms a directionally asymmetric catch bond with F-actin. *Science* **357,** 703–706 (2017).
224. Matthews, B. D., Overby, D. R., Mannix, R. & Ingber, D. E. Cellular adaptation to mechanical stress: role of integrins, Rho, cytoskeletal tension and mechanosensitive ion channels. *J. Cell Sci.* **119,** 508–518 (2006).
225. Tavares, S. *et al.* Actin stress fiber organization promotes cell stiffening and proliferation of pre-invasive breast cancer cells. *Nat. Commun.* **8,** ncomms15237 (2017).
226. Icard-Arcizet, D., Cardoso, O., Richert, A. & Hénon, S. Cell Stiffening in Response to External Stress is Correlated to Actin Recruitment. *Biophys. J.* **94,** 2906–2913 (2008).
227. Schiller, H. B., Friedel, C. C., Boulegue, C. & Fässler, R. Quantitative proteomics of the integrin adhesome show a myosin II-dependent recruitment of LIM domain proteins. *EMBO Rep.* **12,** 259–266 (2011).
228. Ziegler, W. H., Liddington, R. C. & Critchley, D. R. The structure and regulation of vinculin. *Trends in Cell Biology* **16,** 453–460 (2006).
229. del Rio, A. *et al.* Stretching single talin rod molecules activates vinculin binding. *Science* **323,** 638–641 (2009).
230. Ciobanasu, C., Faivre, B. & Le Clainche, C. Actomyosin-dependent formation of the mechanosensitive talin–vinculin complex reinforces actin anchoring. *Nat. Commun.* **5,** ncomms4095 (2014).
231. Haining, A. W. M., Essen, von, M., Attwood, S. J., Hytönen, V. P. & del Río Hernández, A. All Subdomains of the Talin Rod Are Mechanically Vulnerable and May Contribute To Cellular Mechanosensing. *ACS Nano* **10,** 6648–6658 (2016).
232. Yao, M. *et al.* Mechanical activation of vinculin binding to talin locks talin in an unfolded conformation. *Scientific Reports* **4,** 4610 (2014).
233. Yao, M. *et al.* The mechanical response of talin. *Nat. Commun.* **7,** 11966 (2016).
234. Kumar, A. *et al.* Talin tension sensor reveals novel features of focal adhesion force transmission and mechanosensitivity. *J. Cell Biol.* **213,** 371–383 (2016).
235. Ringer, P. *et al.* Multiplexing molecular tension sensors reveals piconewton force gradient across talin-1. *Nature Methods* **4,** 2974 (2017).
236. Margadant, F. *et al.* Mechanotransduction In Vivo by Repeated Talin Stretch-Relaxation Events Depends upon Vinculin. *Plos Biol* **9,** e1001223 (2011).
237. Hu, X. *et al.* Cooperative Vinculin Binding to Talin Mapped by Time-Resolved Super Resolution Microscopy. *Nano Lett.* **16,** 4062–4068 (2016).
238. Zebda, N., Dubrovskyi, O. & Birukov, K. G. Focal Adhesion Kinase Regulation of Mechanotransduction and its Impact on Endothelial Cell Functions. *Microvascular Research* **83,** 71–81 (2012).

239. Tomakidi, P., Schulz, S., Proksch, S., Weber, W. & Steinberg, T. Focal adhesion kinase (FAK) perspectives in mechanobiology: implications for cell behaviour. *Cell Tissue Res.* **357,** 515–526 (2014).
240. Katsumi, A., Orr, A. W., Tzima, E. & Schwartz, M. A. Integrins in mechanotransduction. *J. Biol. Chem.* **279,** 12001–12004 (2004).
241. Herzog, F. A., Braun, L., Schoen, I. & Vogel, V. Structural Insights How PIP2 Imposes Preferred Binding Orientations of FAK at Lipid Membranes. *J Phys Chem B* **121,** 3523–3535 (2017).
242. Bell, S. & Terentjev, E. M. Focal Adhesion Kinase: The Reversible Molecular Mechanosensor. *Biophys. J.* **112,** 2439–2450 (2017).
243. Zhou, J. *et al.* Mechanism of Focal Adhesion Kinase Mechanosensing. *PLoS Comput Biol* **11,** e1004593 (2015).
244. Na, S. *et al.* Rapid signal transduction in living cells is a unique feature of mechanotransduction. *Proc. Natl. Acad. Sci. U.S.A.* **105,** 6626–6631 (2008).
245. Wang, Y. *et al.* Visualizing the mechanical activation of Src. *Nature* **434,** 1040–1045 (2005).
246. Sawada, Y. *et al.* Force Sensing by Extension of the Src Family Kinase Substrate, p130Cas. *Cell* **127,** 1015–1026 (2006).
247. Mitchison, T. J. & Cramer, L. P. Actin-Based Cell Motility and Cell Locomotion. *Cell* **84,** 371–379 (1996).
248. Wolfenson, H., Lavelin, I. & Geiger, B. Dynamic Regulation of the Structure and Functions of Integrin Adhesions. *Dev. Cell* **24,** 447–458 (2013).
249. Elosegui-Artola, A. *et al.* Mechanical regulation of a molecular clutch defines force transmission and transduction in response to matrix rigidity. *Nat. Cell Biol.* (2016). doi:10.1038/ncb3336
250. Elosegui-Artola, A. *et al.* Rigidity sensing and adaptation through regulation of integrin types. *Nat. Mater.* **13,** 631–637 (2014).
251. Mitchison, T. & Kirschner, M. Cytoskeletal dynamics and nerve growth. *Neuron* **1,** 761–772 (1988).
252. Schiller, H. B. & Fässler, R. Mechanosensitivity and compositional dynamics of cell–matrix adhesions. *EMBO Rep.* **14,** 509–519 (2013).
253. Swaminathan, V. & Waterman, C. M. The molecular clutch model for mechanotransduction evolves. *Nat. Cell Biol.* **18,** 459–461 (2016).
254. Polacheck, W. J. & Chen, C. S. Measuring cell-generated forces: a guide to the available tools. *Nature Methods* **13,** 415–423 (2016).
255. García, A. J. & Gallant, N. D. Stick and grip: measurement systems and quantitative analyses of integrin-mediated cell adhesion strength. *Cell Biochem Biophys* **39,** 61–73 (2003).
256. Taubenberger, A. V., Hutmacher, D. W. & Müller, D. J. Single-Cell Force Spectroscopy, an Emerging Tool to Quantify Cell Adhesion to Biomaterials. *Tissue Engineering Part B: Reviews* **20,** 40–55 (2014).
257. Roca-Cusachs, P., Conte, V. & Trepat, X. Quantifying forces in cell biology. *Nat. Cell Biol.* **12,** 299 (2017).
258. Benoit, M., Gabriel, D., Gerisch, G. & Gaub, H. E. Discrete interactions in cell adhesion measured by single-molecule force spectroscopy. *Nat. Cell Biol.* **2,** 313–317 (2000).
259. Helenius, J., Heisenberg, C.-P., Gaub, H. E. & Müller, D. J. Single-cell force spectroscopy. *J. Cell Sci.* **121,** 1785–1791 (2008).
260. Neuman, K. C. & Nagy, A. Single-molecule force spectroscopy: optical tweezers, magnetic tweezers and atomic force microscopy. *Nature Methods* **5,** 491–505 (2008).
261. Friedrichs, J. *et al.* A practical guide to quantify cell adhesion using single-cell force spectroscopy. *Methods* **60,** 169–178 (2013).
262. Neuman, K. C. & Nagy, A. Single-molecule force spectroscopy: optical tweezers, magnetic tweezers and atomic force microscopy. *Nature Methods* **5,** 491–505 (2008).
263. Evans, E., Ritchie, K. & Merkel, R. Sensitive force technique to probe molecular adhesion and structural linkages at biological interfaces. *Biophys. J.* **68,** 2580–2587 (1995).
264. Müller, D. J., Helenius, J., Alsteens, D. & Dufrêne, Y. F. Force probing surfaces of living cells to molecular resolution. *Nat. Chem. Biol.* **5,** 383–390 (2009).
265. Müller, D. J., Krieg, M., Alsteens, D. & Dufrêne, Y. F. New frontiers in atomic force

microscopy: analyzing interactions from single-molecules to cells. *Current Opinion in Biotechnology* **20,** 4–13 (2009).
266. Hutter, J. L. & Bechhoefer, J. Calibration of atomic-force microscope tips. *Rev. Sci. Instrum.* **64,** 1868 (1993).
267. Friedrichs, J., Helenius, J. & Müller, D. J. Stimulated single-cell force spectroscopy to quantify cell adhesion receptor crosstalk. *Proteomics* **10,** 1455–1462 (2010).
268. Krieg, M. *et al.* Tensile forces govern germ-layer organization in zebrafish. *Nat. Cell Biol.* **10,** 429–436 (2008).
269. Beckmann, J., Schubert, R., Chiquet-Ehrismann, R. & Müller, D. J. Deciphering teneurin domains that facilitate cellular recognition, cell-cell adhesion, and neurite outgrowth using atomic force microscopy-based single-cell force spectroscopy. *Nano Lett.* **13,** 2937–2946 (2013).
270. Dufrêne, Y. F., Martínez-Martín, D., Medalsy, I., Alsteens, D. & Müller, D. J. Multiparametric imaging of biological systems by force-distance curve-based AFM. *Nature Methods* **10,** 847–854 (2013).
271. Chu, C., Celik, E., Rico, F. & Moy, V. T. Elongated Membrane Tethers, Individually Anchored by High Affinity α4β1/VCAM-1 Complexes, Are the Quantal Units of Monocyte Arrests. *PLoS ONE* **8,** e64187 (2013).
272. Taubenberger, A., Cisneros, D. A., Puech, P.-H., Müller, D. J. & Franz, C. M. Revealing early steps of alpha2beta1 integrin-mediated adhesion to collagen type I by using single-cell force spectroscopy. *Mol. Biol. Cell* **18,** 1634–1644 (2007).
273. Riet, Te, J. *et al.* Dynamic coupling of ALCAM to the actin cortex strengthens cell adhesion to CD6. *J. Cell Sci.* **127,** 1595–1606 (2014).
274. Fichtner, D. *et al.* Covalent and Density-Controlled Surface Immobilization of E-Cadherin for Adhesion Force Spectroscopy. *PLoS ONE* **9,** e93123 (2014).
275. Krieg, M., Helenius, J., Heisenberg, C.-P. & Müller, D. J. A Bond for a Lifetime: Employing Membrane Nanotubes from Living Cells to Determine Receptor-Ligand Kinetics. *Angew. Chem. Int. Ed.* **47,** 9775–9777 (2008).
276. Siamantouras, E., Hills, C. E., Younis, M. Y. G., Squires, P. E. & Liu, K.-K. Quantitative investigation of calcimimetic R568 on beta cell adhesion and mechanics using AFM single-cell force spectroscopy. *FEBS Lett.* **588,** 1178–1183 (2014).
277. Benoit, M. & Gaub, H. E. Measuring cell adhesion forces with the atomic force microscope at the molecular level. *Cells Tissues Organs* **172,** 174–189 (2002).
278. Sheetz, M. P. Cell control by membrane–cytoskeleton adhesion. *Nat. Rev. Mol. Cell Biol.* **2,** 392–396 (2001).
279. Marshall, B. T. *et al.* Direct observation of catch bonds involving cell-adhesion molecules. *Nature* **423,** 190–193 (2003).
280. Sun, M. *et al.* Multiple Membrane Tethers Probed by Atomic Force Microscopy. *Biophys. J.* **89,** 4320–4329 (2005).
281. Krieg, M., Dunn, A. R. & Goodman, M. B. Mechanical control of the sense of touch by β-spectrin. *Nat. Cell Biol.* **16,** 224–233 (2014).
282. Vásquez, V., Krieg, M., Lockhead, D. & Goodman, M. B. Phospholipids that Contain Polyunsaturated Fatty Acids Enhance Neuronal Cell Mechanics and Touch Sensation. *Cell Reports* **6,** 70–80 (2014).
283. Teräväinen, T. P. *et al.* αV-integrins are required for mechanotransduction in MDCK epithelial cells. *PLoS ONE* **8,** e71485 (2013).
284. Evans, E. A. & Calderwood, D. A. Forces and bond dynamics in cell adhesion. *Science* **316,** 1148–1153 (2007).
285. Dembo, M., Oliver, T., Ishihara, A. & Jacobson, K. Imaging the traction stresses exerted by locomoting cells with the elastic substratum method. *Biophys. J.* **70,** 2008–2022 (1996).
286. Lee, J. Traction forces generated by locomoting keratocytes. *J. Cell Biol.* **127,** 1957–1964 (1994).
287. Kim, I. L., Khetan, S., Baker, B. M., Chen, C. S. & Burdick, J. A. Fibrous hyaluronic acid hydrogels that direct MSC chondrogenesis through mechanical and adhesive cues. *Biomaterials* **34,** 5571–5580 (2013).
288. Khetan, S. *et al.* Degradation-mediated cellular traction directs stem cell fate in covalently crosslinked three-dimensional hydrogels. *Nat. Mater.* **12,** 458–465 (2013).

289. Legant, W. R. *et al.* Measurement of mechanical tractions exerted by cells in three-dimensional matrices. *Nature Methods* **7,** 969–971 (2010).
290. Morimatsu, M., Mekhdjian, A. H., Adhikari, A. S. & Dunn, A. R. Molecular Tension Sensors Report Forces Generated by Single Integrin Molecules in Living Cells. *Nano Lett.* **13,** 3985–3989 (2013).
291. Grashoff, C. *et al.* Measuring mechanical tension across vinculin reveals regulation of focal adhesion dynamics. *Nature* **466,** 263–266 (2010).
292. Blakely, B. L. *et al.* A DNA-based molecular probe for optically reporting cellular traction forces. *Nature Methods* **11,** 1229–1232 (2014).
293. Wang, X. & Ha, T. Defining Single Molecular Forces Required to Activate Integrin and Notch Signaling. *Science* **340,** 991–994 (2013).
294. Galior, K., Liu, Y., Yehl, K., Vivek, S. & Salaita, K. Titin-Based Nanoparticle Tension Sensors Map High-Magnitude Integrin Forces within Focal Adhesions. *Nano Lett.* **16,** 341–348 (2016).

2. Increasing throughput of AFM-based single cell adhesion measurements through multi-substrate surfaces

Miao Yu[1,2*], Nico Strohmeyer[1*], Jinghe Wang[2], Daniel J. Muller[1], Jonne Helenius[1]

1. Department of Biosystems Science and Engineering, ETH Zurich, Mattenstrasse 26, 4058 Basel, Switzerland

2. Center for Precision Engineering, Harbin Institute of Technology, Harbin 150001, China

* Contributed equally

Correspondence: Jonne Helenius, jonne.helenius@bsse.ethz.ch

Keywords: Atomic force microscopy, cell adhesion, single-cell force spectroscopy, single cell assay, collagen I, laminin, fibronectin, PC3, MDCK, HeLa, fibroblasts

Published in *Beilstein J. Nanotechnol.* **6,** 157–166 (2015).

2.1. Abstract

Mammalian cells regulate adhesion by expressing and regulating a diverse array of cell adhesion molecules on their cell surfaces. Since cell types express distinct sets of cell adhesion molecules, substrate specific adhesion is cell type and condition dependent. Single-cell force spectroscopy is used to quantify the contribution of cell adhesion molecules to adhesion of cells to specific substrates at both cell and single molecule levels. However, the low throughput of single-cell adhesion experiments greatly limits the number of substrates that can be examined. In order to overcome this limitation by the ability to measure the adhesion of a cell to multiple substrates, we developed segmented PDMS masks. To verify the utility of the masks, the adhesion of four different cell lines, HeLa (Kyoto), prostate cancer (PC), mouse kidney fibroblast and MDCK, to three extracellular matrix proteins, fibronectin, collagen I and laminin 332, was examined. We found that the adhesion of each cell line tested to different matrix proteins was distinct; no two cell lines adhered equally to each of the proteins. The PDMS masks improved the throughput limitation of single-cell force spectroscopy and allow experiments that previously were not feasible. Since the masks are economical and versatility different assays can be improved.

2.2. Introduction

The regulated adhesion of mammalian cells with the extracellular matrix (ECM) and surrounding cells is crucial in biological processes such as cell migration, deviation cell growth, proliferation, migration, and apoptosis. Since impaired cell adhesion causes a wide range of diseases, the study of cell adhesion is an important field of research[1-5]. Cell adhesion is predominantly mediated by cell adhesion molecules (CAMs), which comprise different protein families, including integrins and cadherin[6]. Cells express and regulate CAMs in order to control whether, how strong and how long they adhere to surfaces they encounter[7-10]. Extracellular cues and intracellular signaling tightly regulated cell adhesion. Furthermore, outside-in signaling of CAMs regulate cellular processes including the adhesive properties of the cell[11]. Among CAMs, integrins dominantly facilitate adhesion of cells to ECM proteins. Integrins are heterodimers composed of non-covalently linked α- and β-subunits both of which consist of a large extracellular domain, short transmembrane domain, and cytoplasmic domain of variable length. In mammalian cells, the 18 α- and 8 β-subunits are known to form 24 different integrins which have specific, but overlapping, adhesion functions and often bind to more than one ECM protein[12]. To adopt their adhesion to the ECM, cells regulate the surface expression of integrins[13]. Importantly, cells differ in the adherence to various ECM proteins, and necessitate the investigation of the adhesive properties of the cells.

Atomic force microscopy (AFM)-based single-cell force spectroscopy (SCFS) provides a versatile tool to quantify the adhesion of single cell adhesion in conditions approaching physiological[14-16]. In AFM-based SCFS, a single cell is attached to a cantilever (Figure 2-1A,B), commonly facilitated by an adhesive coating (e.g. concanavalin A, poly-L-lysine or CellTak)[17-22]. The attached cell is lowered (approach) onto a substrate (Figure 2-1A(i)), which is a protein-coated surface, another cell or a biomaterial[23], until a set force is reached and kept stationary for a set time to allow the cell to form adhesive interactions (Figure 2-1A(ii)). During the subsequent raising (retraction) of the cantilever (Figure 2-1A(iii)), the force acting on the cell and the distance between cell and substrate is recorded in a force-distance curve (Figure 2-1C). The force range that can be detected with AFM-based SCFS is from ~10 pN up to ~100 nN[14], thereby SCFS allows both the overall cell adhesion and the contribution of single adhesion receptors to be quantified. During initial cantilever retraction the upward acting force on the cell increases until the force needed to initiate cell de-adhesion is reached, thereafter, unbinding events occur (Figure 2-1C). The maximum force is called adhesion force and is a measure of how strong the cell adhered to the substrate. Unbinding events correlate with the unbinding of either single or clustered CAMs and can be characterized as either rupture or tether events[15,17,20]. The analysis of these unbinding events may be used to characterize the strength of single bonds and cell membrane properties[17,24,25]. Examples of utility of SCFS include studies of the adhesion of two *Dictyostelium discoideum* cells *via* glycoproteins[26], dendritic cells *via* activated leukocyte cell adhesion molecules[17], Chinese hamster ovary cells to collagen I *via* $\alpha_2\beta_1$-integrins[22], pre-osteoblasts to

denatured collagen I *via* $\alpha_5\beta_1$-integrins and integrins containing α_v-subunits[27], Jurkat T cells to the vascular cell adhesion molecule VCAM-1 *via* $\alpha_4\beta_1$-integrins[28], and the contribution of galectins to the overall cell adhesion of MDCK cells to collagens[29]. In addition to studying the adhesion of cells to a substrate, the regulation of one CAM by another CAM has also been studied by SCFS. It was shown by SCFS, that collagen I binding integrins down-regulate the avidity of fibronectin binding integrins by an increased endocytosis in HeLa cells[30].

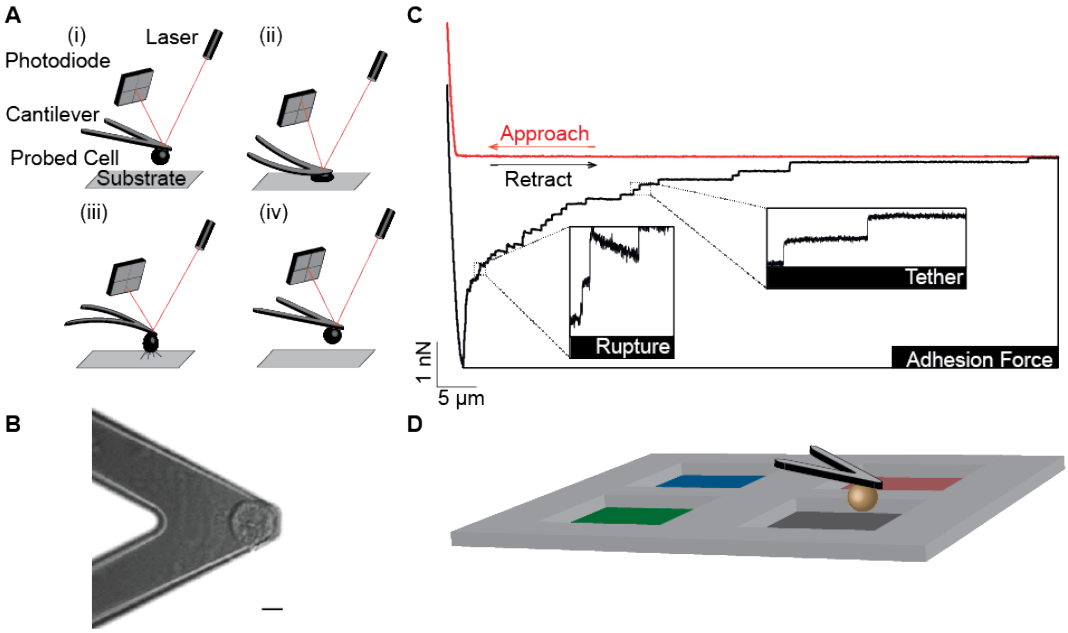

Figure 2-1 Depiction of AFM-based SCFS. (A and B) A single cell is bound to a tip-less AFM cantilever via a receptor specific or unspecific substrate (scale bar, 10 µm). (A) (i and ii) The cantilever bound cell is approached onto the substrate until a preset force recorded. After a contact time, (iii) the cantilever is retracted until the cell is fully detached from the substrate. During the experimental cycle, the deflection (force) of the cantilever and the distance between cell and surface is recorded in a force-distance curve. (C) Force-distance curves show distinct features: in the approach force-distance curve the deflection of the cantilever is recorded while the cell is pressed on the substrate; the retraction force-distance curve (black) records the adhesion force of the cell, which represents the maximum force acting on the cantilever and thus, the force needed to initiate the detachment of the cell from its substrate. Subsequently single receptor unbinding events are observed. Rupture events are recorded when the CAM-ligand bond of a cytoskeleton-linked CAM fails. Tether events are recorded when a membrane tether is extruded from the cell membrane with the CAM at its tip (tethers). In the latter case attachment of the CAM to the cytoskeleton is either too weak to resist the mechanical stress applied or non-existent. (D) To improve the throughput of SCFS experiments, a four-segmented coating mask is used, allowing adhesion force measurements with one cell to different adhesives substrates.

The classical SCFS set-up, where the adhesion of a cantilever bound cell to a substrate is probed has a limited throughput, because only one substrate is examined per cantilever. Therefore, an alternative method has been used to quantify the adhesive properties of several cells to using one cantilever. Thereto, in an upside-down assay, a ligand (e.g. ECM protein) functionalized cantilever or a cantilever with a functionalized bead is lowered on round or spread cells that are seeded on a Petri dish[31,32]. After the contact time the cantilever is retracted from the cell and the adhesion of the cell to the cantilever or bead is measured. Thereafter, the cantilever can be moved above another cell and the adhesion experiment cycle repeated. By this upside-down approach, several cells can be examined using one cantilever. However, a surface that has been

in contact with a cell may be contaminated with debris from the cell or restructured by the cell, especially after longer contact times[16,33]. Due to the limited surface areas at the ends of cantilevers and beads, the coating is compromised after a few measurements and the cantilever must be replaced to ensure consistent assay conditions.

An alternative method to increase throughput of adhesion measurements in the classical setup, is to microstructure the surface such that it presents areas having different properties. Examples used for SCFS include micro-structured surfaces with two different polymers[34], different nanoscale groves[35] and two different ECM proteins[36]. However, the equipment needed for these approaches are not common in laboratories.

To increase throughput, we choose to modify Petri dishes by adding four-segmented polydimethylsiloxane (PDMS) masks (Figure 2-1D). The four segments separate the Petri dish surface into four independent 4×4 mm^2 wells, which allow one dish to be coated with different substrates and, thus, characterization of the adhesion of the same cell to four substrates. The masks are thin enough to remain on the Petri dish while performing adhesion measurements. These multi-segmented substrates not only increases the rate at which SCFS measurements can be made but also improves their reliability and comparability, because the adhesion of cells of the same type can fluctuate considerably[37]. Therefore, the number of cells probed can be reduced. In addition, the masks decrease the coating area, save experimental material and improve experimental efficiency. We implemented the masks to characterize the adhesion of different cell lines to collagen I, fibronectin and laminin 332 and found that the cell lines had unique adhesion profiles, which likely reflect differences in the CAMs they expressed.

2.3. Results

2.3.1. PDMS masks for single-cell force spectroscopy

To increase throughput of AFM-based SCFS, we developed segmented PDMS masks (Figure 2-1D, Figure 2-2B) that allow the adhesion of one cell to different substrates to be characterized. Using a mask, four 16 mm^2 large and 150 µm deep wells (segments, Figure 2-2B) can be coated in one Petri dish and SCFS adhesion measurements performed with the same cell in each segment without removing the mask. Since the non-specific adhesion of different cell lines to either glass or PDMS varies, we developed two types of PDMS masks, where the protein-coat is either on a glass or PDMS surface. The mask type can be chosen to minimize the background adhesion of the cell line. The production process as well as the handling of the PDMS mask is described in the next sections. In addition, the characterization of surface topography, protein coating and microscopy utility of both types of PDMS masks is presented.

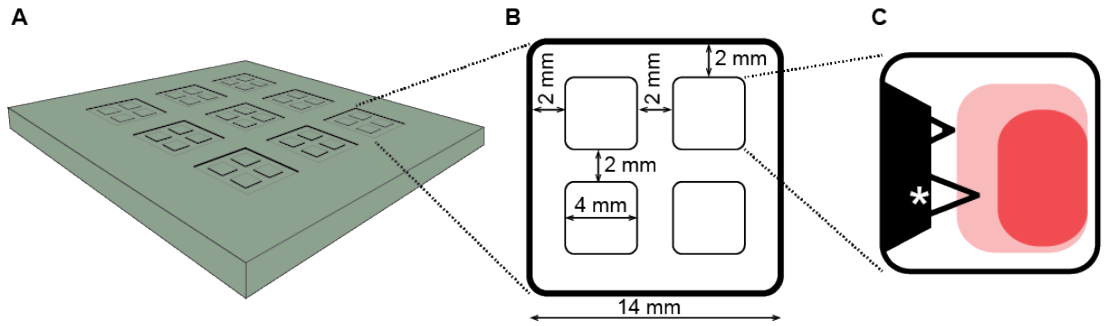

Figure 2-2 Technical details of the PDMS coating mask. (A) For the production of the PDMS masks, an aluminum mold is produced, with nine casting molds for PDMS masks. Dimensions of the masks are shown in (B). The height of the wells is 150 µm. (C) Accessible area with an AFM-cantilever (stared, NPO, Bruker) usually used for SCFS adhesion experiments. Dark red shows the recommended area where the PDMS masks do not interfere with the measurement, in pale red the area where are small interferences and in white areas measurements are not possible.

2.3.2. Characterization of protein coating on PDMS masks

To characterize the surface roughness and the protein coating on glass and PDMS surfaces were imaged using AFM. Several protein-coated surfaces of both PDMS and glass were imaged. Surfaces of protein-coated glass were smooth with height variations of ≈ 4 nm (Figure 2-3A). In contrast, the protein coated PDMS surfaces were rougher, with height differences of ≈ 80 nm (Figure 2-3B).

To verify that the surfaces were coated with proteins, we tried to physically remove the protein coating over a 10×10 µm^2 area of the sample by applying a high contact force (≈95 nN) during contact mode AFM imaging, i.e. to scratch the coating with the AFM cantilever. An area was scratched several times, before the scanning angle was rotated 90° and the same area was scratched several more times. After scratching, a 20×20 µm^2 area surrounding the scratched area was imaged. On the glass surface, the protein was removed from the scratched area (Figure 2-3A''). The protein-coating depth was 3.2±0.5 nm (n=5) for BSA and 4.5±0.4 nm (n=5) for collagen I (Figure 2-3C). The AFM images of PDMS coatings (Figure 2-3B and D) revealed an uneven surface with surface features exceeding 40 nm in height. These are caused by the copying of imperfections in the in the aluminum mold. Although the sensitivity of AFM imaging is high enough to detect protein coatings, the overall roughness of the surface masks thin protein layers, and thus we were likely not able to detect the presence of a scratched protein patch.

Since we were unable to confirm a protein coating on PDMS by the AFM scratching experiments, we coated glass and PDMS surfaces with fluorescent conjugated proteins used in the later adhesion study: Fluorescein isothiocyanate (FITC) conjugated BSA, rhodamine conjugated laminin, FITC conjugated collagen I and HiLyte488 conjugated fibronectin. For each protein, confocal images show near homogeneous surface signals when absorbed on both PDMS (Figure 2-3, E' to H') and glass (Figure 2-3, E to H). In a smaller area the fluorescence was bleached using either the 488 or 555 nm laser at full power. On both surfaces the fluorescence signal was

abolished, demonstrating that the ECM proteins coated the surfaces. Negative controls (uncoated glass or PDMS) showed background fluorescence that did not decrease with bleaching (data not shown). These experiments confirm homogenious protein coatings on glass surface and indicate PDMS surfaces were similarly coated.

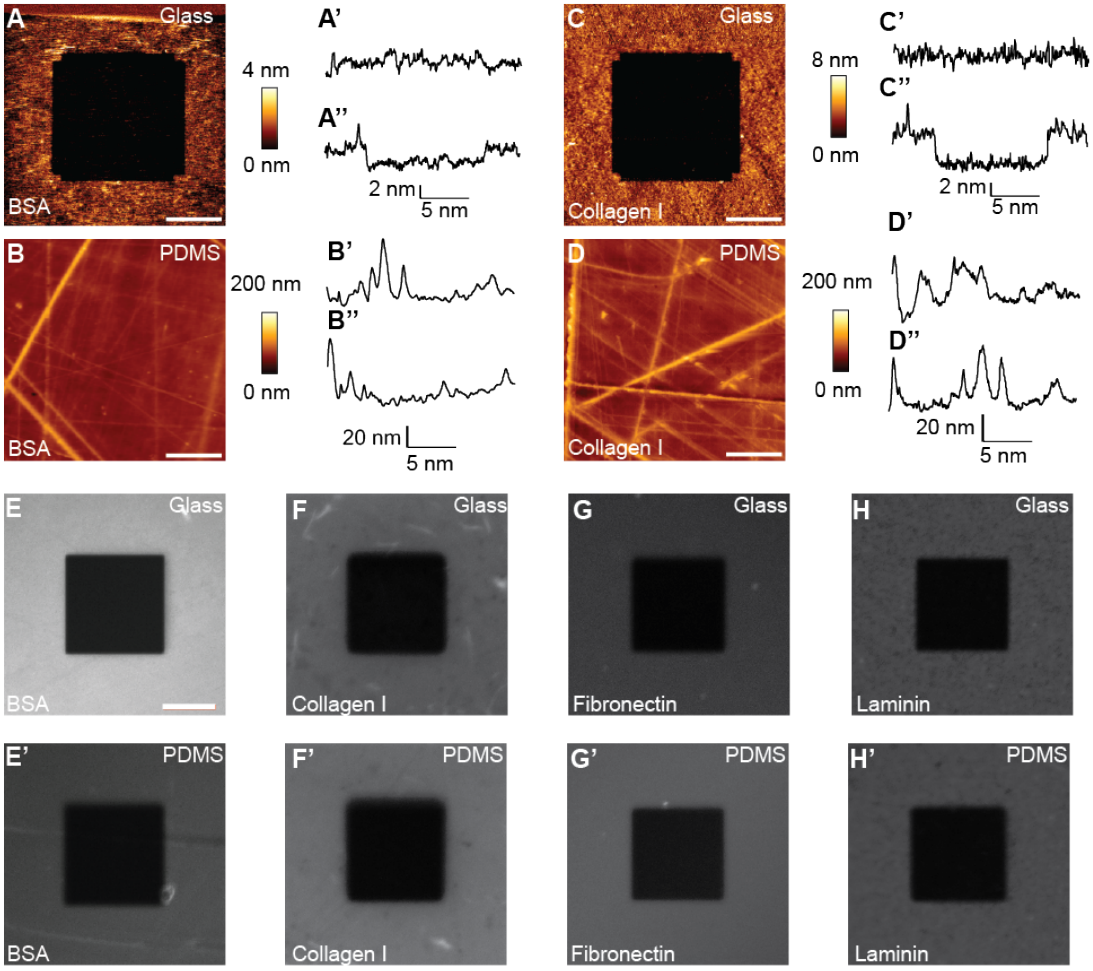

Figure 2-3 Surface characterization. Representative topographies of BSA and collagen I coated glass-surfaced (A and C, respectively) and PDMS-surfaced (B and D, respectively) wells. A 20 × 20 μm^2 area of the coated surface was AFM-imaged after a 10 x 10 μm^2 area was repeatedly scratched by contact mode AFM imaging using a high contact force. Images show a cavity in the scratched area for BSA (A) and collagen I (C) coated glass surfaces. The thicknesses of the coatings were similar, ≈3.5 nm for BSA and ≈4.5 nm for collagen (A'' and C''). The PDMS surface showed a rough surface with height differences of ≈80 nm (B and D). On PDMS the displacment of proteins by AFM scratching was not evident (B, B'' and D, D''). Scale bars, 5 μm. Since a protein coat was not demostrated, we coated PDMS-surfaced wells with fluorescently labled BSA (FITC), collagen I (FITC), fibronectin (rhodamine) and laminin (Hi-Lyte488) and imaged the glass (E-H, in order as listed) and PDMS (E'-F') surfaces. A 20 × 20 μm^2 area was bleached with maximum laser power before the 50 × 50 μm^2 area was imaged (E-H and E'-H'). Scale bar, 10 μm.

2.3.3. Accessibility of the coated area with cantilever bound cells.

The area at the bottom of a well accessible for SCFS is limited by the geometry of the mask and the AFM cantilever chip. If these come in contact with each other, the recorded force-distance curves will be corrupted or, worse, the AFM chip maybe displaced and the cantilever damaged. Both, the height of the coating mask and the 10° angle of the cantilever determine the

accessible area. Unfortunately, PDMS masks thinner then 150 µm are fragile and difficult to handle making the production of masked dishes cumbersome. The area suited for adhesion measurements is depicted in Figure 2-2C. Since the AFM chip must clear the chip-side of the mask approximately 1 mm of the area at the chip-side cannot be used for adhesion measurements (see Figure 2-2C, white area). How far the cantilever can be moved towards the side borders of the well is set by the position of the cantilever on the chip and how the chip is mounted. The tip-area is accessible until the cantilever makes contact with the mask. When the cantilever was too close to the chip boarder, both approach and retraction force distance curves showed a distinct bending in the base line force. When the cantilever was too close a side border, no obvious features was found in force-distance curves. The sensitivity of the cantilever was determined by pressing it to a surface either outside the mask or close to the tip-side border of a well.

2.3.4. Evaluation of the PDMS masks for light microscopy

Light microscopy is essential for many SCFS experiments. Therefore, we tested the optical behavior of the masks with PDMS surfaces. UV/VIS spectra of 1 mm thick PDMS slices showed that cured PDMS did not absorb light at wavelengths important for light microscopy (230 to 840 nm, data not shown). PDMS masks did not appear to reduce the quality of wide-filed and fluorescence images. However, the z-resolution and calibration will be sub-optimal since the optical density of the PDMS used, 1.415 as measured, does not match that of water. Furthermore, the working distance of the microscope objective must exceed the thickness of the PDMS bottom and, thus, these masks are not suited for short distance, high numerical aperture objectives, in case PDMS surface masks are used. Although the masks with PDMS surfaces show technical limitations in optical microscopy, they are usable for standard microscopy mostly used in combination with SCFS. If the PDMS-surfaced masks interfere with optical microscopy the masks with glass surfaces are recommended.

2.3.5. Comparison of non-specific adhesion force on glass and PDMS surfaces

In our experience, unspecific cell adhesion to clean glass is higher than the adhesion of cells to the ConA-coated cantilever. In order to attach cells to ConA-coated cantilevers, it was necessary to passivate glass surfaces onto which cells were pipetted. We found that both HeLa and PC3 cells also adhere to PDMS strongly (Figure 2-4). Therefore, it was necessary to passivate the PDMS surfaces. BSA is commonly used to block unspecific adhesion of cells to different surfaces[38]. To address unspecific cell adhesion we coated glass and PDMS surfaced wells with BSA. To our surprise, the adhesion of PC3 cells was higher to BSA when BSA was adsorbed on glass than when absorbed on PDMS (Figure 2-4). Thus, we decided to use PDMS surfaced masks in the following experiments. Furthermore, we pick up cells with the cantilever from BSA coated wells because the adhesion to BSA is lower than to the ConA-coated cantilevers.

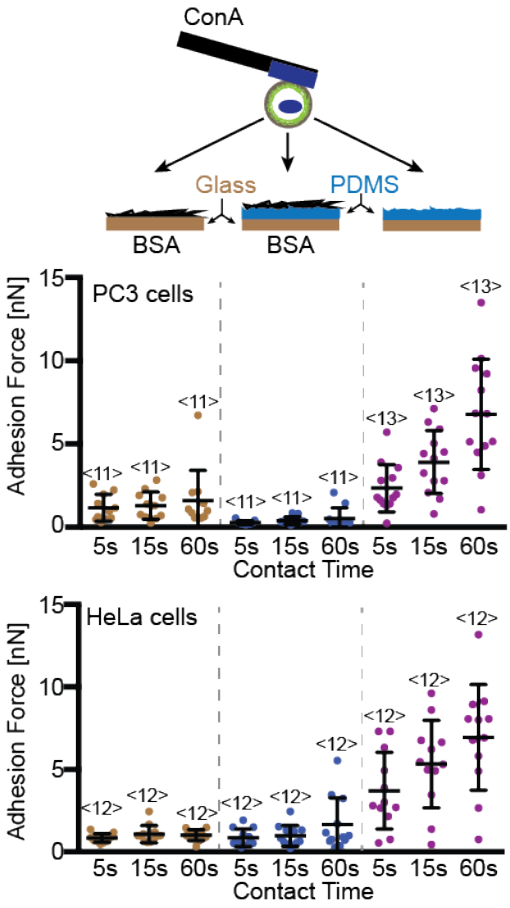

Figure 2-4 Comparisons of glass surface and PDMS surface masks. Top, depiction of the SCFS assay used to quantify the adhesion of PC3 and HeLa cells. Single cells were bound to ConA-coated cantilevers and approached to BSA-coated glass or PDMS and clean PDMS surface until a force of 2 nN was recorded. After the denoted contact time the cantilever was retracted to detach the cantilever bound cell and substrate. During retraction the adhesion force of cell and substrate was measured. Bottom, adhesion forces recorded for PC3 and HeLa cells during their detachment from substrates. Each dot represents the measurement of one cell with the number of cells assayed for each condition given by <n>. Indicated are the times (5, 15 and 60 s) the cell was in contact with the substrate before being detached. Bars mark mean force and standard deviation.

2.3.6. Cell line dependent adhesion to extracellular matrix proteins

To demonstrate that PDMS masks are a useful tool to increase throughput and comparability of results on different ECM proteins in SCFS we conducted a small adhesion force screen with four cell lines on three different ECM proteins. Thereto, we coated the wells in the PDMS coating masks with collagen I, fibronectin, and laminin 332. We evaluated cell adhesion of PC3, HeLa, mouse kidney fibroblast and MDCK cells to the different extracellular matrix proteins. The fourth well of the PDMS mask was coated with BSA from which cells were picked up. We measured the adhesion force to all three ECM proteins of at least 11 cells of measurements (Figure 2-5). It became apparent that every cell line has a unique fingerprint of cell adhesion to different ECM proteins. For example, PC3 cells showed similar adhesion to collagen I and fibronectin and a higher to laminin 332, while mouse kidney fibroblast showed each cell line. From the force-distance curves, we extracted the adhesion force for all very low adhesion to collagen I and laminin 332 but high adhesion to fibronectin. This indicates, that cell lines express different patterns of CAMs, in our study in particular integrins. Besides the cell line dependent forces observed, contact-time dependent strengthening also differed between cell lines, indicating difference in the dynamic regulation of adhesion. These results show, that the

PDMS masks can be used to find adhesive properties that distinguish different cell lines from each other and perhaps reflect unique cell line specific adhesion signatures.

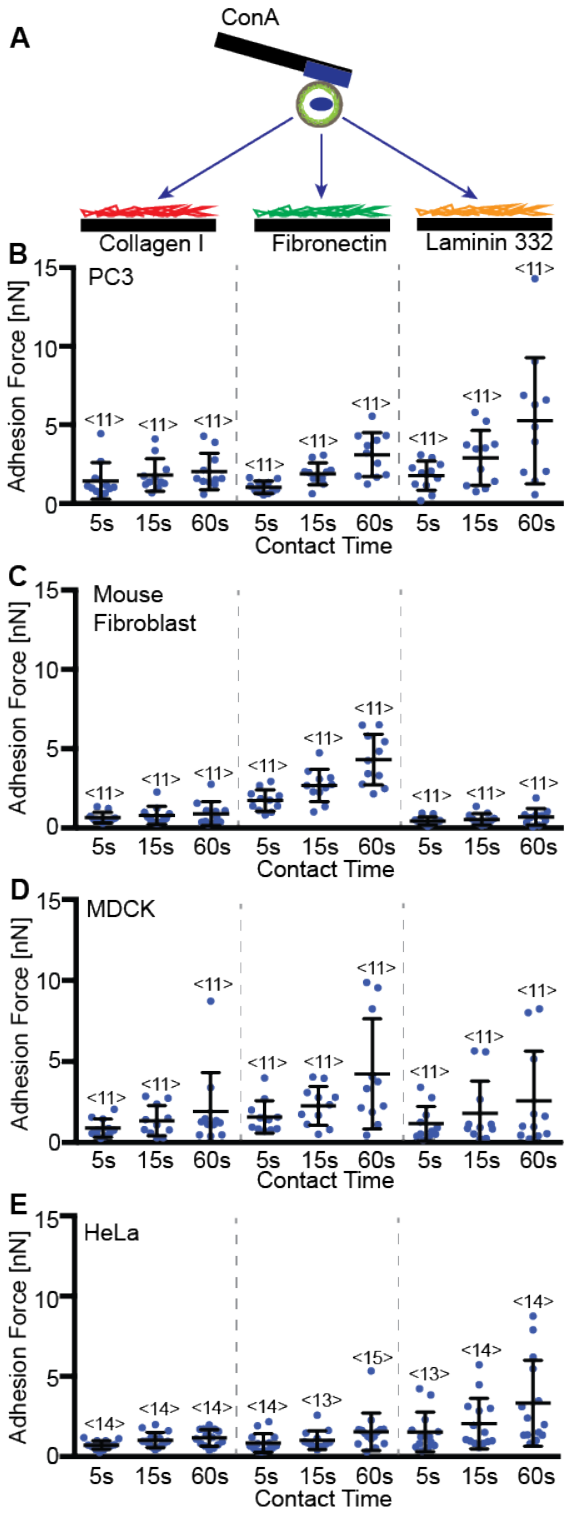

Figure 2-5 Cell line dependent adhesion of ECM proteins. (A) depiction of SCFS experimental setup, where the adhesion of a ConA bound cell is measured to different protein coated surfaces. Graphs of the adhesion forces measured for PC3 (B), mouse fibroblasts (C), MDCK (D) or HeLa (E) cells collagen I, fibronectin and laminin 332 coated PDMS surfaces after contact times of 5, 15 and 60 s. Each dot represents the measurement of one cell attached to ConA coated cantilevers. The number of cells assayed for each condition is given by <n>. Bars mark mean force and standard deviation.

2.4. Discussion

Adhesion is a fundamental aspect of both healthy and diseased cells. In the last decade, single cell adhesion studies have contributed to the understanding of adhesion proteins and their

regulation. AFM-based SCFS has been used to quantify adhesion of numerous cell types to a divers set of substrates, include ECM proteins, biomaterial and cell-cell adhesion proteins[14,15,26]. However, since only one cell can be examined at a time, the number of conditions that can be studied efficiently by SCFS is limited. To help alleviate this problem, we designed two kinds of PDMS masks that allow the characterizing cell adhesion of one cell to multiple adhesive substrates. The masks were cast in aluminum molds, which can be made in most mechanical workshops.

We characterized the masks with regard to surface topography, protein coating ability and applicability for light microscopy. While the PDMS surface was very rough compared to the glass surface, both could be coated well with proteins. The height variation of the PDMS surface, ≈80 nm, although small compared the size of cells examined, 15 µm, may be the cause of the differences in HeLa cell adhesion to BSA coated substrates observed in Figure 2-4. Other differences between glass and PDMS surface, such as hydrophobicity or the specifics of protein absorption, may also account for this difference. However, since the difference in adhesion to BSA only occurred for PC3 cells (Figure 2-4) and was minor compared to specific adhesion, we conclude that both glass and PDMS surfaces can be coated and used for cell adhesion measurements. Fluorescently labeled proteins adsorbed on glass and PDMS, which showed homogenous protein coatings on both surfaces (Figure 2-3), confirmed this. Further experiments showed that like glass-bottomed wells, PDMS-bottomed wells are suitable for light microscopy. Thus, neither mask lowered the quality of possible SCFS experiments, even in combination with light microscopy. If SCFS is combined with advanced light microscopy and objectives with small working distances and high numerical apertures we recommend to use glass surface mask.

Finally, we used the PDMS masks to characterize and compare the adhesion of four cell lines to collagen I, fibronectin and laminin 332. HeLa (Kyoto), PC3, mouse kidney fibroblast and MDCK cells where chosen based to their widespread use. The masks allowed us to profile the adhesion properties of the cells quickly and efficiently, requiring ≈2 days for each cell line. By measuring the adhesion of a single cell to different matrix proteins a smaller number of cells need to be assayed. These measurements show that cell lines have specific ECM proteins adhesion profiles. This is likely due to difference in their expression of integrins. To profile cell adhesion of different cell lines the used substrates could be readily extended to more ECM proteins and cell-cell adhesion proteins, such as E-cadherin. Further, contact times could be increased to address long term CAM regulation, which would increase the accuracy of the profiles. With the help of the PDMS coating masks a semi-automated adhesion measurement setup is feasible.

Our masks compare favorably to commercially available silicone masks, such as provided by Ibidi. The production of the mask is easy and commercially available equivalents are commonly expensive, the here-described mask only requires a mold, which can be easily produced in workshop and the PDMS components. Further, the usage of the mask is not limited to AFM-based SCFS, as the mask is only an example of possible dimensions and forms. For example,

migration or spreading experiments can be conducted on different proteins, as the masks are usable for light microscopy. Further examples where masks could be used include wound-healing assays and experiments that require more complex surface structures.

2.5. Experimental

2.5.1. Production of PDMS masks

To make PDMS masks a casting mold with cavities for nine masks was used (Figure 2-2A). For the mold, 150 µm deep cavities were machined in an 8 mm thick aluminum plate (for details see Figure 2-2B), which was then anodizing to harden its surface. To reduce clinging of PDMS to the mold, the mold was silanized overnight with 200 µL tridecafluoro-trichlorosilane in a vacuum chamber at room temperature. After silanization the mold was washed extensively with water and ethanol. It was important that the cavities were free from any residues before casting. PDMS elastomer (Sylgard 184, Dow Corning) was mixed in a 10:1 oil to base ratio. The mixture was placed in a vacuum chamber for 20 min to remove dissolved gases. About 2 ml of the uncured PDMS mixture was placed on top of the aluminum mold and spread uniformly over the mold using a straightedge. For glass surface masks only the cavities of the mold were filled and, importantly, the inner squares (future wells of the mask) were wiped free of PDMS. In contrast, to produce masks with PDMS-surface-wells, the entire top of aluminum mold was left covered with a thin PDMS layer. The mold was place at 80ºC for at least 2 hours fully cure the PDMS. After cooling, the glass-bottom masks were carefully lifted out of the cavities and excess PDMS removed from the edges of the wells. In contrast, PDMS-surface masks where cut out of the continuous PDMS layer before they were lifted off the mold. Subsequently, both types of masks were placed topside down in the middle of a glass bottom Petri dish (WPI) and any air bubbles were removed by gently pushing them out with tweezers before the dishes were placed at 80ºC for 20 min. To enhance the binding of the PDMS mask to the glass, both surfaces can be plasma cleaned in air for one minute before they are joined. However, PDMS surfaces become hydrophilic during plasma treatment, and thus, liquid coating drops spread over the masks. Storing the PDMS in air will restore the hydrophobicity of the surface.

2.5.2. Cell culture

PC3 cells were maintained in RPMI-1640 (Gibco-Life technologies) supplemented 1 mM sodium pyruvate; HeLa (Kyoto) and mouse kidney fibroblasts were maintained in DMEM GLUTAMAX supplemented with 10% (V/V) FCS; MDCK cells were maintained in MEM supplemented with 5% FCS. All media also contained 100 units/mL penicillin and 100 µg/mL streptomycin (both Gibco-Life technologies),

2.5.3. Protein functionalization of PDMS masks and cantilever

Before the PDMS or glass surface was coated with proteins, the Petri dish containing the PDMS masks was washed with ethanol and ultrapure water to remove any residue. After drying Petri dishes, 16 µL solutions of 160 µg/mL collagen I (Inamed Biomaterials), 50 µg /mL fibronectin (Merck), 50 µg /mL laminin 332 (Abcam) or 2%(W/V) BSA (Sigma) in PBS were added to separate wells and left to adsorb overnight at 4ºC. To minimize uncoated glass surfaces all wells were incubated with BSA for 30 minutes at room temperature. Glass and PDMS were coated with fluorescently labeled proteins as described for non-labeled proteins. The cantilever coating was performed as previous description [30]. In short, the cantilever were plasma-cleaned and incubated over night in 2 mg/mL ConA (Sigma) containing PBS at 4ºC.

2.5.4. Characterization of protein coatings

To characterize surface roughness and protein coatings of PDMS and glass-surfaced wells a NanoWizzard II AFM (JPK Instruments) mounted on an inverted microscope (Axio Observer.Zi, Zeiss) was used. AFM imaging was performed in intermittent contact mode with a V-shaped cantilever (SNL, Brucker) having a nominal spring constant of 0.58 N/m. First, an area of 20 × 20 µm^2 was imaged at a line rate of 0.7 Hz and with a resolution of 512 × 512 pixels. During the scan, the force acting on the surface was kept low by manually adjusting the drive voltage between 0.5 and 1 V, which compensated for the thermal drifts. AFM scratching was done in contact mode on an area of 10 × 10 µm^2 with a cantilever deflection of 8 V (≈95 nN), a line rate of 10 Hz and an image size of 128 × 128 pixels. After performing 10 scratches the scan direction was rotated 90º and another 10 scratches were performed. Thereafter, the original 20 × 20 µm^2 surface area was reimaged using the original AFM settings.

2.5.5. Single-cell force spectroscopy

For SCFS a CellHesion200 (JPK Instruments), mounted on an inverted optical microscope (Axio Observer.Z1, Zeiss) in a temperature controlled noise cancellation box was used. The temperature was set to 37 ºC throughout the experiments. 200 µm long tip-less V-shaped silicon nitride cantilevers having nominal spring constants of 0.06 N/m (NP-0, Bruker) were used for adhesion measurements. The spring constant of every cantilever was determined prior the experiment using the thermal noise method.

Prior to experiments cells grown to ~80% confluency were detached from culture flasks by trypsin/EDTA and washed off with measurement media (cell line specific media supplemented with 20 mM HEPES) containing 10% FCS. Cells were pelleted (420 g for 90 seconds) and re-suspended in measurement media. Petri dishes with PDMS masks were washed with measurement media to exchange coating buffers and remove loosely bound protein from the surface. Throughout the experiments the PDMS mask remained on Petri Dish. After a recovery

time of at least 45 minutes in measurement media [20] single cell suspensions were pipetted onto the BSA well and cells were allowed to settle. To attach a cell the calibrated and functionalized cantilever was lowered onto a cell with a velocity of 10 µm/s until a force of 5 nN was recorded and raised after remaining 5 seconds at a constant height. The presence of a cell at the apex of the cantilever was visually confirmed. Cantilever bound cells were incubated for 10 minutes to ensure firm binding on the cantilever. For adhesion measurements, single cantilever-bound cells were moved over the protein-coated wells and lowered onto the protein-coated surface with a velocity of 5 µm/s until a contact force of 2 nN was recorded. The cantilever was maintained at a constant height for 5, 15 or 60 seconds (contact time) and subsequently retracted for >90 µm at a speed of 5 µm/s until the cell was fully detached from the substrate. After each adhesion cycle, the cell was allowed to recover for a time at least equal to the contact time before a new adhesion cycle was performed. The area in which each cell adhesion was quantified was changed after ever experimental cycle performed. After quantifying cells adhesion with the three contact times, the cell was moved to another protein-coated well and adhesion measurements were repeated. To avoid possible systematic errors caused by substrate specific cell activation or deactivation, we varied the order in which cell adhesion to the substrates was measured. After adhesion measurements on all protein coatings, the cell was exchanged. The Petri dish was replaced after characterizing 4 cells on each coating. In case a cell showed morphological changes during the experiments it was discarded. Adhesion forces were extracted from force-distance curves using JPK data processing software.

2.5.6. Fluorescence microscopy and UV/VIS spectroscopy

Fluorescence microscopy was performed with an inverted confocal laser-scanning microscope (Axio Observer.Z1, LSM 700, Zeiss) equipped with a Plan apochromat 25x/0.8 water-immersion lens (Zeiss). FITC-albumin (Sigma), fibronectin-HiLyte488 (LuBioScience), laminin-rhodamine (LuBioScience) and FITC-collagen I (Sigma) were dissolved at 20 µg/ml in PBS and absorbed as described above. For fluorophore bleaching, the laser power of the 488 or 555 nm laser was set to the maximum intensity. A limited area (20 × 20 μm^2) was bleached using a single 156 × 156 pixels scan, before a 50 × 50 μm^2 image (448 × 448 pixels) was recorded at 4% laser intensity. UV/VIS spectrums were acquired using a NanoDrop 2000c (Thermo Scientific) of 1 mm thick PDMS slices.

2.6. Authors Contribution

N.S., D.J.M. and J.H. designed the experiments and wrote the paper. N.S. and J.H. developed the mask. M.Y. and N.S. performed most experiments and analyzed the data. All authors discussed the experiments, read and approved the manuscript.

2.7. Acknowledgements

We thank Mitasha Bharadwaj and Joost te Riet for their help developing and evaluating the masks and Paul Argast for developing the aluminum molds. We thank Hongxiang Wang for Ph.D supervising Miao Yu in Harbin Institute of Technology. The mouse kidney fiboblasts, MDCK and PC3 cell lines were kindly provided by Reinhard Fässler, Aki Manninen and the Oncology Group of the Institute for Surgical Research and Hospital Management at University Hospital Basel, respectively. The Swiss National Science Foundation (Grant 31003A_138063) and the NCCR Molecular Systems Engineering supported this work. Miao Yu was supported by the National Natural Science Foundation of China (51175124).

2.8. References

1. Winograd-Katz, S. E., Fässler, R., Geiger, B. & Legate, K. R. The integrin adhesome: from genes and proteins to human disease. *Nat Rev Mol Cell Biol* **15,** 273–288 (2014).
2. Hegde, S. & Raghavan, S. A Skin-depth Analysis of Integrins: Role of the Integrin Network in Health and Disease. *Cell Commun Adhes* **20,** 155–169 (2013).
3. Barone, V. & Heisenberg, C.-P. Cell adhesion in embryo morphogenesis. *Current Opinion in Cell Biology* **24,** 148–153 (2012).
4. El-Amraoui, A. & Petit, C. *Chapter 16 - Cadherin Defects in Inherited Human Diseases. Molecular biology of cadherins. Preface.* **116,** 361–384 (Elsevier Inc., 2013).
5. Gumbiner, B. M. *Cell adhesion: the molecular basis of tissue architecture and morphogenesis.* (Cell, 1996).
6. Juliano, R. L. Signal transduction by cell adhesion receptors and the cytoskeleton: functions of integrins, cadherins, selectins, and immunoglobulin-superfamily members. *Annu. Rev. Pharmacol. Toxicol.* **42,** 283–323 (2002).
7. Crossin, K. L., Prieto, A. L., Hoffman, S. & Jones, F. S. Expression of adhesion molecules and the establishment of boundaries during embryonic and neural development. *Experimental ...* **109,** 6–18 (1990).
8. Meager, A. Cytokine regulation of cellular adhesion molecule expression in inflammation. *Cytokine & growth factor reviews* (1999).
9. Hynes, R. O. Integrins: versatility, modulation, and signaling in cell adhesion. *Cell* **69,** 11–25 (1992).
10. Sutherland, A. E., Calarco, P. G. & Damsky, C. H. Developmental regulation of integrin expression at the time of implantation in the mouse embryo. *Development* **119,** 1175–1186 (1993).
11. Shen, B., Delaney, M. K. & Du, X. Inside-out, outside-in, and inside–outside-in: G protein signaling in integrin-mediated cell adhesion, spreading, and retraction. *Current Opinion in Cell Biology* **24,** 600–606 (2012).
12. Hynes, R. O. Integrins: bidirectional, allosteric signaling machines. *Cell* **110,** 673–687 (2002).
13. The Regulation of Expression of Integrin Receptors. **214,** 123–131 (1997).
14. Helenius, J., Heisenberg, C.-P., Gaub, H. E. & Müller, D. J. Single-cell force spectroscopy. *Journal of Cell Science* **121,** 1785–1791 (2008).
15. Müller, D. J., Helenius, J., Alsteens, D. & Dufrêne, Y. F. Force probing surfaces of living cells to molecular resolution. *Nat Chem Biol* **5,** 383–390 (2009).
16. Friedrichs, J. *et al.* A practical guide to quantify cell adhesion using single-cell force spectroscopy. *Methods* **60,** 169–178 (2013).
17. Riet, Te, J. *et al.* Dynamic coupling of ALCAM to the actin cortex strengthens cell adhesion to CD6. *Journal of Cell Science* **127,** 1595–1606 (2014).
18. Force and compliance measurements on living cells using atomic force microscopy (AFM). **6,** 1–9 (2004).
19. Fichtner, D. *et al.* Covalent and Density-Controlled Surface Immobilization of E-Cadherin for Adhesion Force Spectroscopy. *PLoS ONE* **9,** e93123 (2014).

20. Schubert, R. *et al.* Assay for characterizing the recovery of vertebrate cells for adhesion measurements by single-cell force spectroscopy. *FEBS Letters* 1–10 (2014). doi:10.1016/j.febslet.2014.06.012
21. Friedrichs, J., Helenius, J. & Muller, D. J. Quantifying cellular adhesion to extracellular matrix components by single-cell force spectroscopy. *Nature Protocols* **5,** 1353–1361 (2010).
22. Taubenberger, A., Cisneros, D. A., Puech, P.-H., Müller, D. J. & Franz, C. M. Revealing early steps of alpha2beta1 integrin-mediated adhesion to collagen type I by using single-cell force spectroscopy. *Mol. Biol. Cell* **18,** 1634–1644 (2007).
23. Taubenberger, A. V., Hutmacher, D. W. & Müller, D. J. Single-Cell Force Spectroscopy, an Emerging Tool to Quantify Cell Adhesion to Biomaterials. *Tissue Engineering Part B: Reviews* **20,** 40–55 (2014).
24. Krieg, M., Helenius, J., Heisenberg, C.-P. & Müller, D. J. A Bond for a Lifetime: Employing Membrane Nanotubes from Living Cells to Determine Receptor-Ligand Kinetics. *Angew. Chem. Int. Ed.* **47,** 9775–9777 (2008).
25. Benoit, M. & Gaub, H. E. Measuring cell adhesion forces with the atomic force microscope at the molecular level. *Cells Tissues Organs* **172,** 174–189 (2002).
26. Benoit, M., Gabriel, D., Gerisch, G. & Gaub, H. E. Discrete interactions in cell adhesion measured by single-molecule force spectroscopy. *Nat Cell Biol* **2,** 313–317 (2000).
27. Taubenberger, A. V., Woodruff, M. A., Bai, H., Müller, D. J. & Hutmacher, D. W. The effect of unlocking RGD-motifs in collagen I on pre-osteoblast adhesion and differentiation. *Biomaterials* **31,** 2827–2835 (2010).
28. Alon, R. *et al.* Alpha4beta1-dependent adhesion strengthening under mechanical strain is regulated by paxillin association with the alpha4-cytoplasmic domain. *The Journal of Cell Biology* **171,** 1073–1084 (2005).
29. Friedrichs, J. *et al.* Contributions of galectin-3 and -9 to epithelial cell adhesion analyzed by single cell force spectroscopy. *Journal of Biological Chemistry* **282,** 29375–29383 (2007).
30. Friedrichs, J., Helenius, J. & Müller, D. J. Stimulated single-cell force spectroscopy to quantify cell adhesion receptor crosstalk. *Proteomics* **10,** 1455–1462 (2010).
31. Kim, H., Arakawa, H., Osada, T. & Ikai, A. Quantification of cell adhesion force with AFM: distribution of vitronectin receptors on a living MC3T3-E1 cell. *Ultramicroscopy* **97,** 359–363 (2003).
32. Hyonchol, K., Arakawa, H., Osada, T. & Ikai, A. Quantification of fibronectin and cell surface interactions by AFM. *Colloids and Surfaces B:* **25,** 33–43 (2002).
33. Taubenberger, A., Franz, C. M. & Müller, D. J. Cellular Remodelling of Individual Collagen Fibrils Visualized by Time-lapse AFM. *Journal of Molecular Biology* **372,** 594–607 (2007).
34. Canale, C., Petrelli, A., Salerno, M., Diaspro, A. & Dante, S. A new quantitative experimental approach to investigate single cell adhesion on multifunctional substrates. *Biosensors & bioelectronics* **48,** 172–179 (2013).
35. Lamers, E. *et al.* Dynamic cell adhesion and migration on nanoscale grooved substrates. *Eur Cell Mater* **23,** 182–93– discussion 193–4 (2012).
36. Dao, L. *et al.* Revealing non-genetic adhesive variations in clonal populations by comparative single-cell force spectroscopy. *Exp. Cell Res.* **318,** 2155–2167 (2012).
37. Dao, L., Gonnermann, C. & Franz, C. M. Investigating differential cell-matrix adhesion by directly comparative single-cell force spectroscopy. *J. Mol. Recognit.* **26,** 578–589 (2013).
38. Lee, M. H., Brass, D. A., Morris, R., Composto, R. J. & Ducheyne, P. The effect of non-specific interactions on cellular adhesion using model surfaces. *Biomaterials* **26,** 1721–1730 (2005).

3. Assay for characterizing the recovery of vertebrate cells for adhesion measurements by single-cell force spectroscopy

Rajib Schubert[1,*], Nico Strohmeyer[1,*], Mitasha Bharadwaj[1], Subramanian P. Ramanathan[1], Michael Krieg[2], Jens Friedrichs[3], Clemens M. Franz[4], Daniel J. Muller[1]

1. Department of Biosystems Science and Engineering, ETH Zurich, Mattenstrasse 26, 4058 Basel, Switzerland

2. Department of Molecular and Cellular Physiology, Stanford University, Stanford, California 94305, USA

3. Leibniz Institute of Polymer Research Dresden, Institute for Biofunctional Polymer Materials, Hohe Str. 6, 01069 Dresden, Germany

4. Karlsruhe Institute of Technology (KIT), DFG-Center for Functional Nanostructures, Wolfgang-Gaede-Str. 1a, 76131 Karlsruhe, Germany

Correspondence: Daniel J. Muller, Tel: +41 61 387 33 07, Fax: +41 61 387 39 94, Email: daniel.mueller@bsse.ethz.ch

* Contributed equally

Keywords: Atomic force microscopy, collagen I, fibronectin, trypsin, EDTA, extracellular matrix

Abbreviations: AFM – atomic force microscopy, BSA – bovine serum albumin, CAMs – cell adhesion molecules, ConA – concanavalin A, ECM – extracellular matrix, GFP – green fluorescent protein, FD – force-distance, FCS – fetal calf serum, MYH9 – myosin heavy chain 9, PAR – protease-activated receptor, SCFS – single-cell force spectroscopy

Published in *FEBS Lett.* **588,** 3639–3648 (2014)

3.1. Abstract

Single-cell force spectroscopy (SCFS) is becoming a widely used method to quantify the adhesion of a living cell to a substrate, another cell or tissue. The high sensitivity of SCFS permits determining the contributions of individual cell adhesion molecules (CAMs) to the adhesion force of an entire cell. However, to prepare adherent cells for SCFS, they must first be detached from tissue-culture flasks or plates. EDTA and trypsin are often applied for this purpose. Because cellular properties can be affected by this treatment, cells need to recover before being further characterized by SCFS. Here we introduce atomic force microscopy (AFM)-based SCFS to measure the mechanical and adhesive properties of HeLa cells and mouse embryonic kidney fibroblasts while they are recovering after detachment from tissue-culture. We find that mechanical and adhesive properties of both cell lines recover quickly (<10 min) after detachment using EDTA, while trypsin-detached fibroblasts require >60 min to fully recover. Our assay introduced to characterize the recovery of mammalian cells after detachment can in future be used to estimate the recovery behavior of other adherent cell types.

3.2. Introduction

Specific adhesive interactions between cells and extracellular matrix (ECM) or between cells play crucial roles in cellular communication, tissue organization, embryonic development and wound healing. Accordingly, a wide variety of diseases is associated with impaired cell adhesion[1-4]. Animal cells sense and adhere to their extracellular environment *via* cell adhesion molecules (CAMs), which are typically transmembrane proteins. Specific interactions between CAMs and their extracellular ligands induce intracellular signaling pathways, which regulate the adhesive and mechanical properties of cells besides other cellular processes. CAMs are classified into different families, including integrins, cadherins and selectins[5-8]. To strengthen the cellular attachment to an extracellular substrate, multi-protein complexes anchor CAMs to the cytoskeleton. Key cytoplasmic adaptor proteins include talin, kindlin, vinculin and catenins[9-12]. Due to the general importance of cell adhesion, the interaction of CAMs and their ligands are studied extensively using various, yet mostly qualitative, methods[13,14]. However, as these qualitative methods can provide helpful insights, describing the adhesive interactions of cells in detail benefits greatly from measuring quantitative parameters such as cell adhesion forces, kinetics and energies.

Single-cell force spectroscopy (SCFS) offers the possibility to measure adhesive forces and energies of single cells adhering to a biotic or abiotic substrate, another cell or tissue[15,16]. SCFS methods are based on force sensing devices such as optical or magnetic tweezers, micropipettes, or atomic force microscopy (AFM)[14,17,18]. In these SCFS-based methods the cell is brought into contact with an adhesive substrate or another cell for a given contact time and then separated. While approaching and retracting the cell, the interaction forces are recorded and provide a quantitative measure of the adhesive interactions between cell and substrate. Among all currently available SCFS methods, AFM-based SCFS covers the largest dynamic force range from ≈10 pN to ≈100 nN that can be measured[16,18,19]. This wide range permits quantifying the adhesive force of an entire cell down to the adhesive force established by single CAMs. AFM-based SCFS attaches a single cell to the apex of a tipless AFM cantilever (Figure 3-1). To facilitate cell attachment, the cantilever is coated either with a substrate-mimicking ligand (*e.g.*, cell surface receptors or ECM proteins including collagens, laminins, or fibronectin), concanavalin A (ConA) to bind carbohydrates on the cell surface, antibodies, or an unspecific adhesive (*e.g.*, CellTak, poly-L-lysine)[15,20-32]. The cantilever-bound cell is then approached either to a protein-coated substrate, another cell, tissue explant or biomaterial. After a pre-determined contact time, during which the cell is allowed to initiate adhesion, the cantilever is retracted until cell and substrate are fully separated. During the approach and retraction cycle cantilever deflection (*e.g.*, force) and cell-substrate distance are recorded in so-called force-distance (FD) curves (Figure 3-1C). Analysis of the FD curves provides several quantitative insights into the cellular interaction with the substrate. The approach FD curve provides insight into the mechanical properties of the cell being pressed onto the substrate[18,26,33-35]. The retraction FD curve provides the maximum

detachment force, also called adhesion force, of the cell. However, two types of smaller unbinding events contained in the retraction FD curves correspond to the unbinding of single or clustered CAMs[15,16,18,19,36]. These unbinding events are frequently named rupture and tether events, and differ in the molecular scenarios leading to their emergence. In rupture events, the CAMs remain anchored to the actin-cytoskeleton and upon exposure of mechanical stress detach from their extracellular ligand[22,31,32,36-38]. If the anchorage to the cytoskeleton breaks before a CAM unbinds from the extracellular ligand or if the CAM has not been attached to the cytoskeleton in the first place, the CAM is pulled away from the cell cortex on the tip of a membrane tether[19,39,40]. In this so-called tether event, the tether is mechanically extended until the receptor-ligand bond breaks. The force required to extend a tether from the cellular membrane does not depend on the strength of the CAM-ligand bond but rather on mechanical properties of the cellular membrane (*e.g.*, bending rigidity, viscosity, and tension)[40], the velocity at which the tether is extracted from the membrane, and on cell membrane attachment to the cortical cytoskeleton. In rare cases, tether extension from the cellular membrane terminates when the tether fails or if the receptor is pulled out of the membrane[40,41]. In the later separating phase between cell and substrate, the cell body is not in contact with the substrate anymore and tethers exclusively mediate cell adhesion [31]. The analysis of tether unbinding events can provide information on the lifetime of single CAM bonds, the mechanical properties of the cell cortex, and cell membrane tension[31,37,40,42-45].

Although SCFS measurements and other methods applied to characterize cell adhesion provide quantitative and qualitative insights into cell adhesion, a drawback is that adherent cells must first be detached from culturing flasks in order to characterize their adhesion to a given substrate. Cells are commonly detached with trypsin and/or ethylenediaminetetraacetic acid (EDTA)[27,46,47]. Although some CAMs, such as $\alpha_2\beta_1$ integrin[14], are trypsin resistant, other CAMS such as cadherins are sensitive to trypsin cleavage[48]. Furthermore, other proteins involved in the initiation of cell adhesion may be indirectly activated by trypsin cleavage. For example, trypsin has been shown to cleave and activate protease-activated receptors (PARs), which regulate various cellular processes, including actomyosin cortex function and adhesion[49-51]. Moreover, trypsin cleaves proteoglycans, which can contribute to cell adhesion[52]. Because EDTA chelates divalent ions its presence can perturb calcium and magnesium dependent cellular processes[53,54]. Although some CAMs are not functionally dependent on divalent ions, many CAMs (*e.g.*, integrins and cadherins) require the availability of divalent ions for stably interacting with their ligand and, thus, are inhibited upon EDTA treatment. However, it is not entirely clear if and how EDTA and trypsin treatment affects subsequent cell adhesion measurements, especially directly after the cells have been detached from culture flasks. To circumvent this uncertainty, in many SCFS studies cells were explicitly left to recover for a certain

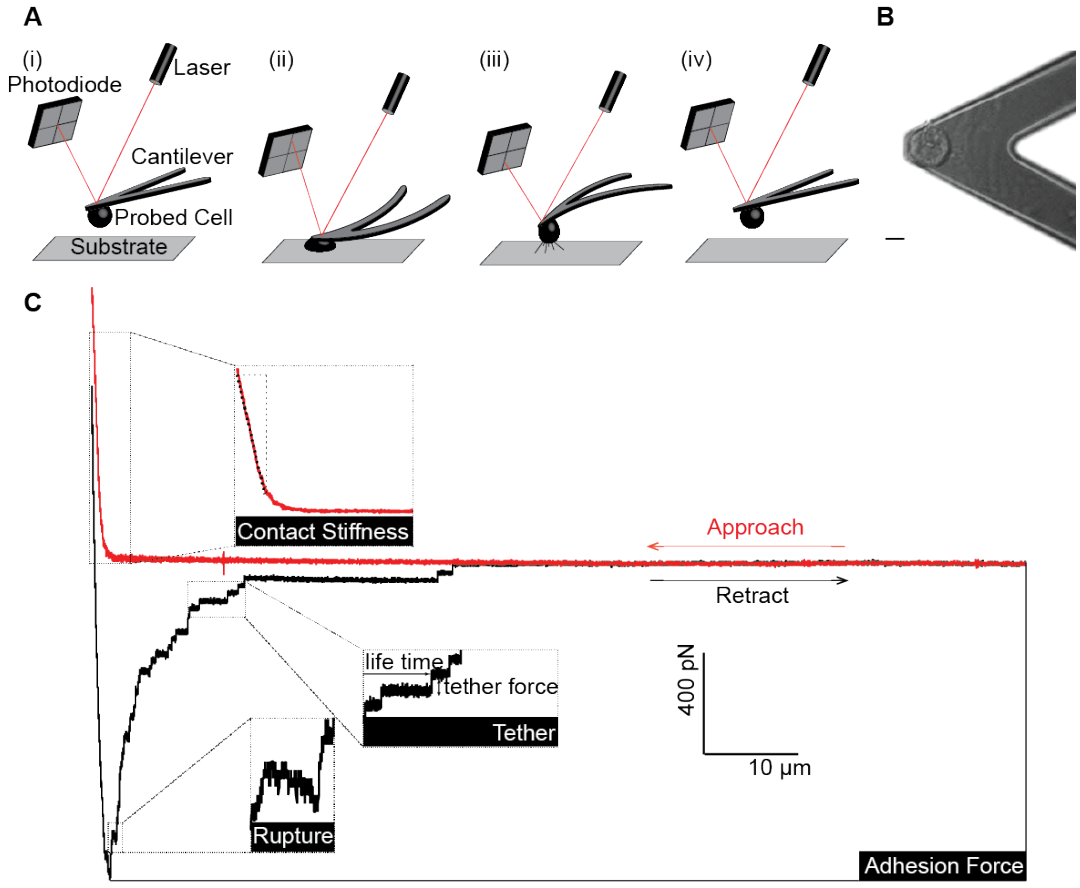

Figure 3-1 Scheme of AFM-based SCFS. (A and B) To use a single cell as a probe it is bound to a concanavalin A (ConA)-coated tipless AFM cantilever (scale bar, 10 µm). (A) (i and ii) The cantilever is approached onto a protein-coated substrate until a preset contact force is reached. After a defined contact time (ii), the cantilever is retracted until the cell is fully separated from the substrate (iii and iv). During approach and retraction, the cantilever deflection and thus, the force acting on the cell is recorded in force-distance (FD) curves. (C) FD curves show different features: In the approach FD curve (red) the cantilever deflection measured upon pressing the cell onto the substrate correlates with the stiffness of the cell and is called contact stiffness [33]. The retraction FD curve (black) records the adhesion force of the cell, which represents the maximum downward force deflecting the cantilever and thus the maximum force needed to detach cell and substrate. After recording the maximum adhesion force, single receptor unbinding events are observed. Rupture events are recorded when the CAM-ligand bond of a cytoskeleton-linked CAM fails. Tether events are recorded when a membrane tether is extruded from the cell membrane with the CAM at its tip (tethers). In the latter case attachment of the CAM to the cytoskeleton is either too weak to resist the mechanical stress applied or non-existent[19,40,41].

time after detachment from the cell culture flask before characterizing their adhesion properties[15,22,25,26,32-34,55-57]. However, to our best knowledge a systematic approach to characterize the recovery time needed to conduct reproducible cell adhesion experiments has not been published. Here we introduce a simple assay to characterize the recovery time of selected eukaryotic cell lines to recover mechanical and adhesive properties after being detached from culturing flasks. For this assay we first detach vertebrate cells using either EDTA or trypsin, then allow them to recover from the detachment process for different time ranges and subsequently use SCFS to quantify their adhesive properties to collagen I, fibronectin fragments and BSA. The experiments show that the recovery times of the cell lines depend on the detachment method and that trypsin treatment can highly upregulate cell adhesion to ECM proteins. After increased

waiting times cells return to a 'normal' adhesion mode that is not influenced by the agents used for detaching cells from culture flasks. The approach described can be used to determine the 'recovery time' after detachment of virtually any eukaryotic cell type whose adhesive properties are to be characterized. The described protocol can thus be implemented in every SCFS-based study to exclude effects of the cell detachment process on the outcome of the experiments.

3.3. Materials and Methods

3.3.1. Cell Culture

HeLa (Kyoto) cells and mouse kidney fibroblasts were maintained in DMEM (Gibco-Life technologies, NY, USA), supplemented with 10% (v/v) fetal calf serum (FCS, Sigma, Steinheim, Germany), 100 units/mL penicillin (Gibco-Life technologies) and 100 µg/mL streptomycin (Gibco-Life technologies). HeLa cells were grown on untreated and fibroblasts on fibronectin (Calbiochem-Merck, Darmstadt, Germany) coated tissue culture flasks (Jet BioFil, Guangzhou, China).

3.3.2. Expression and purification of fibronectin fragments

Fibronectin fragment $FN_{III}7\text{-}10$ and RGD-deleted fibronectin fragment $FN_{III}7\text{-}10\Delta RGD$ were expressed from plasmid pET15b-$FN_{III}7\text{-}10$ in *E.coli* BL21 (DE3) pLysS as described[58]. Briefly, cells were grown in Lennox L broth (Invitrogen, Carlsbad, USA) supplemented with 100 µg/mL of ampicillin (Sigma, Buchs, Switzerland) and 34 µg/mL chloramphenicol (Sigma) at 37°C. Expression was induced with 500 mM isopropyl thiogalactose (IPTG, Sigma) at optical density $(OD)_{600}$ = 0.6. Cells were harvested after 4 h, re-suspended in buffer (20 mM Tris-HCl, 150 mM NaCl, pH 8.0), and broken by sonication. Cell debris was removed by ultracentrifugation at 40'000xg for 45 min. The soluble protein fraction was bound to nickel-nitrilotriacetic acid resin (Protino® Ni-NTA Agarose, MACHEREY-NAGEL, Düren, Germany) for 2 h at 4°C. The resin was then loaded onto a column and washed with buffer (20 mM Tris-HCl, 150 mM NaCl, 10 mM imidazole, pH 8.0). $FN_{III}7\text{-}10$ was eluted with elution buffer (20 mM Tris-HCl, 150 mM NaCl, 500 mM imidazole, pH 8.0). Peak fractions were pooled and dialyzed against imidazole free buffer (20mM Tris-HCl, 150 mM NaCl, pH 8.0). The protein concentration was adjusted to 1.0 mg/mL with dialyzing buffer and aliquots were stored at -20°C.

3.3.3. Surface coating of cantilever and petri dishes

Cantilevers (NP-0, Bruker, USA) were prepared for cell attachment as described previously[27]. In short, cantilevers were plasma-cleaned prior to overnight incubation (at 4°C) in ConA (2 mg/mL, Sigma) in PBS. The glass bottoms of Petri dishes (35 mm FluoroDish, World Precision Instruments, US) were overlaid with a PDMS mask to allow four different coatings of the glass surface[31]. Three of the four PDMS framed glass surfaces were incubated overnight in PBS

at 4°C either with collagen I (160 µg/mL, Inamed Biomaterials, Fremont, CA), fibronectin fragment $FN_{III}7\text{-}10$ (50 µg/mL), RGD deleted fibronectin fragment $FN_{III}7\text{-}10\Delta RGD$ (50 µg/mL) or BSA (Sigma). The fourth segment was left uncoated.

3.3.4. SCFS

For SCFS a CellHesion 200 (JPK Instruments, Berlin, Germany) mounted on an inverted microscope (Observer.Z, Zeiss, Jena, Germany) was used[59]. During SCFS cells were maintained at 37°C using a temperature controlled incubator box (LIS, Basel, Switzerland). 200 µm long tipless V-shaped silicon nitride cantilevers having nominal spring constants of 0.06 N/m (NP-0, Bruker) were used for adhesion measurements. The spring constant of every cantilever was determined prior the experiment using the thermal noise method[60], which accuracy lies at ≈10% [61].

Overnight serum-starved fibroblasts and HeLa cells grown in 24 well plates (Thermo Scientific, Roskilde, Denmark) to confluency of ≈80% were washed with PBS and detached with either 200 µL of 15 mM EDTA (BioUltra Grade, Sigma) or 0.05 % (w/v) trypsin (Sigma), both in PBS, for four and two minutes, respectively. Detached cells were suspended in SCFS media (DMEM supplemented with 20 mM HEPES) containing 1% (v/v) FCS, pelleted and resuspended in serum free SCFS media. Throughout experiments the PDMS masks framing the four segments of glass surfaces remained on the Petri dishes. Each PDMS mask of a Petri dish was washed with SCFS media to exchange coating buffers and to remove weakly attached proteins of the individual glass segments. Cell suspensions were pipetted into the Petri dishes containing the substrate-coated glass supports and allowed to settle. To attach single cells, the apex of a calibrated, ConA functionalized cantilever was lowered with a velocity of 10 µm/s onto a cell until reaching a contact force of 3 nN. After 5 seconds contact, the cantilever was retracted from the Petri dish by 50 µm. Cells were incubated in SCFS media for different times to characterize cell adhesion after different recovery times. For adhesion experiments, cantilever bound cells were lowered onto a given substrate-coated glass segment with a velocity of 5 µm/s until reaching a contact force of 1 nN. The cantilever was maintained at this position (constant height) for 60 seconds and subsequently retracted with 5 µm/s for >90 µm until the cell detached from the substrate-coated glass segment. After detachment from the substrate segment the cell was allowed to recover for 60 seconds before probing adhesion to the next substrate-coated glass segment. A single cell was either used to probe adhesion for all three recovery times. As soon as the cell showed morphological changes (*e.g.* spreading on the cantilever) it was replaced. Cell Adhesion at recovery times >60 min were quantified using cells additional to those probed in earlier recovery times. Cells were never allowed to recover >90 min after detachment from the culture flask. Adhesion forces were extracted from FD curves using the JPK data processing software (JPK Instruments). Cell stiffness, rupture forces, and tether forces were analyzed using in-house build routines, which were based in Igor 6 (Wavemetric, Oregon, USA). Rupture and tether events were analyzed separate. They were distinguished upon the plateau slope before the rupture event, where tether plateaus had a

maximum angle of ~10° (Figure 3-1C). Statistical test were done in Prism (GraphPad, La Jolla, USA).

3.3.5. Confocal microscopy

To image F-actin and non-muscle myosin IIA, we used a HeLa cell line expressing human MYH9-GFP and Lifeact-mCherry. Geneticin (0.5 mg ml^{-1}, Life Technologies) and puromycin (0.5 µg ml^{-1}, Life Technologies) were used for antibiotic selection. An inverted confocal microscope (Observer.Z1, LSM 700, Zeiss) with a 63x/1.3 LCI Plan-Neofluar water immersion objective (Zeiss) was used. Cells were maintained at 37°C using a Petri dish heater (JPK Instruments). In all the representative images shown, contrast and brightness were adjusted to similar levels for visual comparison using Zeiss AxioVision software (Rel. 4.8).

3.4. Results

To characterize a potential influence of the detachment process of adherent cells from culture flasks on the cell's ability to re-establish adhesion, mouse kidney fibroblasts and HeLa cells were detached from flasks using either 15 mM EDTA or 0.05 % (w/v) trypsin. After a certain recovery interval in media, cells were non-specifically attached to tipless AFM cantilevers functionalized with concanavalin A (ConA). SCFS was then used to characterize the adhesion of an attached cell to different substrates (Figure 3-1). The parameters extracted from the approach and retract FD curves recorded in these experiments were contact stiffness of the cell pressed to the substrate, maximum adhesion force of the cell, and the force of the single rupture and tether events (Figure 3-1C). In the following paragraphs we will report how the cell detachment procedure from culture flasks affects each of these parameters.

3.4.1. Characterizing the contact stiffness of cells after detachment from culture flasks

To conduct adhesion measurements by SCFS, single cells attached to the AFM cantilever are pressed onto a substrate for a given contact force and time. Normally contact forces on the range of a few nN are chosen, which distribute over the entire contact area of cell and substrate and result in a relatively small contact pressure applied to the cell. For example, when pressing mouse kidney fibroblasts onto the substrate at a contact force of 1 nN, the contact area estimated from optical microscopy is 70.4 ± 12.2 $µm^2$ (average ± SD, n=8). This results in a contact pressure of 14.6 ± 2.8 N/m^2 (*e.g.*, Pa), which is much smaller than the typical intracellular pressure (≈10-10.000 Pa) generated by animal cells [62-64]. However, if the procedure applied to detach the cells from cell culture flasks significantly influences the mechanical properties of the cell, pressing a softer or stiffer cell onto the substrate at a given contact force results in different cell-substrate contact areas. Variations of the contact area can have a direct impact on the number of CAMs that could bind their ligands and establish adhesion. Accordingly, if the mechanical properties

of the cell would vary with the time after detachment from the culture flask this could have a considerable impact on the SCFS measurements.

Our SCFS experiments show that the contact stiffness of mouse kidney fibroblasts does not significantly change with increasing recovery time after detachment from the cell culture flask by trypsin (Figure 3-2). After EDTA detachment from the culture flasks, the mean contact stiffness of fibroblasts shows small variations of less than 20% (940 pN/µm to 1160 pN/µm) between different recovery times, and the contact stiffness of single cells distributed widely for each recovery time. We therefore consider this difference insignificant (P-values > 0.01).

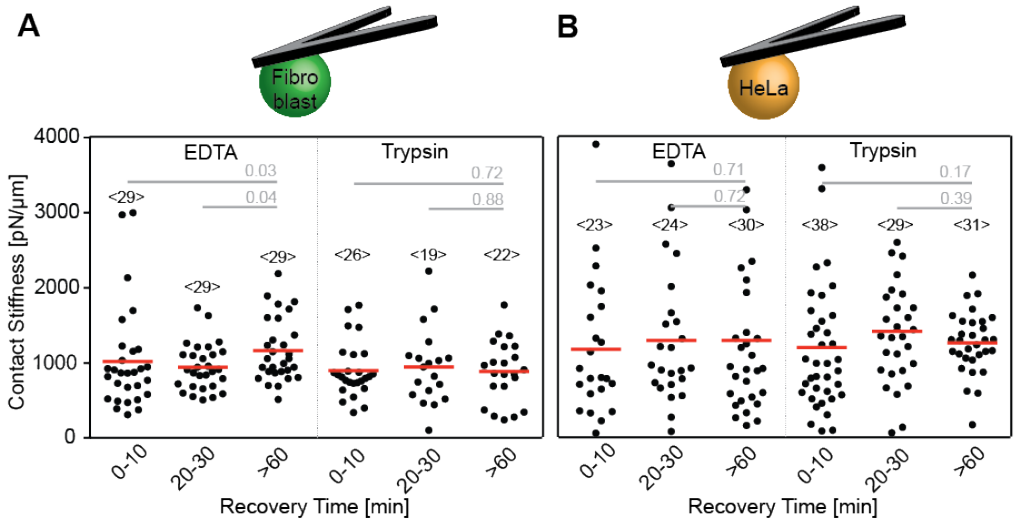

Figure 3-2 Contact stiffness of (A) mouse kidney fibroblasts and (B) HeLa cells for different recovery times after detachment from cell culture flasks. The contact stiffness was determined as depicted in Figure 3-1. SCFS experiments on different substrate coatings are combined for different recovery times. The recovery time denotes the time cells were allowed to recover after detachment from culture flasks using either EDTA or trypsin. Within this recovery time cell adhesion to the different substrates was characterized using SCFS. Each dot represents one SCFS measurement, approaching a single fibroblast or HeLa cell at 5 µm/s to the substrate until reaching a contact force of 1 nN. Red bars indicate average values. <n> gives the number of measurements for each condition. Mann-Whitney P-values (in gray) indicating the significance of measurements compared to those made after a recovery time of >60 min

The independence of contact stiffness on recovery time is also observed for HeLa cells detached by EDTA or trypsin. These measurements suggest that at the contact force applied and within the sensitivity of the SCFS measurements, detachment from the cell culture flasks by either EDTA or trypsin does not change the mechanical properties of the cell and, thus, not the contact area between cell and substrate.

3.4.2. Cortical actomyosin localization shows no significant changes during recovery after detachment from culture flasks

An AFM cantilever compressing a rounded cell by a few µm mainly measures the mechanical properties of the actomyosin cortex[65]. In the previous section we observed no changes of the contact stiffness of mouse embryonic kidney fibroblasts and of HeLa cells detached by trypsin or EDTA. Previous experiments suggest that the enrichment of cortical F-actin and myosin

II correlates with higher cell cortex tensions in interphase cells[66,67]. Thus, our SCFS results showing that the mechanical properties of cells remain unchanged over the entire recovery time course suggest that the actomyosin cortex of the cells remains unchanged as well. To further investigate whether this is indeed the case we imaged the dynamics of actin and myosin in HeLa cells stably expressing Lifeact-mCherry and MYH9-GFP after detachment from culture flasks using EDTA or trypsin (Figure 3-3). Regardless of the detachment method applied, the live cell confocal microscopy images revealed no significant elevation of F-actin or myosin IIA forming the actomyosin cortex thickness. The confocal microscopy images support the observation by SCFS that the cortical stiffness remained unchanged over the same time course.

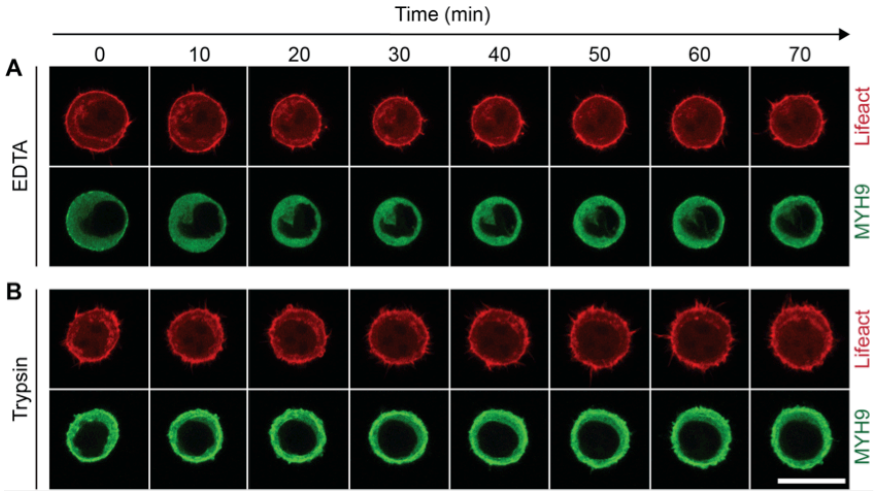

Figure 3-3 Tracking the actomyosin cortex after detachment with (A) EDTA or (B) trypsin. Confocal images of HeLa cells expressing mCherry labeled F-actin (Lifeact-mCherry, red) and GFP labeled myosin II (MYH9-GFP, green). Images were acquired every 10 minutes through the center of the cell. Cells were detached from cell culture flasks with 0.05% trypsin or 15 mM EDTA, and seeded in SCFS medium devoid of either trypsin or EDTA. Scale bar 20 µm, applies to all images.

3.4.3. Influence of recovery time on cell adhesion

Next, we investigated whether the adhesion force of mouse kidney fibroblasts or HeLa cells to different substrates depends on the detachment method from the culture flasks. For fibroblasts we used substrates featuring collagen I, a fibronectin type III fragment containing repeat 7-10 domains ($FN_{III}7$-10) and a fibronectin $FN_{III}7$-10 fragment lacking the integrin binding site ($FN_{III}7$-10ΔRGD). Whereas fibroblasts can specifically adhere to collagen I and to $FN_{III}7$-10 *via* integrins[68], they are unable to specifically adhere to $FN_{III}7$-10ΔRGD[58,69]. Thus, $FN_{III}7$-10ΔRGD was used as a control to characterize unspecific fibroblast adhesion. SCFS showed that the adhesion force of fibroblasts to the two specific substrates collagen I and $FN_{III}7$-10 does not depend on the recovery time of the cell if detached from culture flasks using EDTA (Figure 3-4A). Although adhesion forces to the $FN_{III}7$-10ΔRGD control substrate decreases slightly after >60 min of recovery, the averages differ only by about 200 pN resulting in lower significance levels. However, fibroblasts detached from culture flasks in the presence of 0.05 % (w/v) trypsin showed a different behavior. While adhesion of fibroblasts to collagen I did not depend on the

recovery time after trypsin-induced detachment, adhesion to the fibronectin fragments FN_{III}7-10 showed a clear time dependence. To our surprise, also the adhesion to the non-specific substrate (FN_{III}7-10 ΔRGD) was dependent on the recovery time. In both cases cell adhesion was at first strongly enhanced after detachment and only after recovery times >60 min showed values equal to those observed for fibroblasts detached from culture flasks using EDTA. This highlights that trypsin treatment to detach fibroblasts from cell culture flasks activates their adhesion to fibronectin. As fibroblast adhesion to the FN_{III}7-10ΔRGD control substrate can be seen as being unspecific the results suggest trypsin cleavage to slightly increase unspecific adhesion as well.

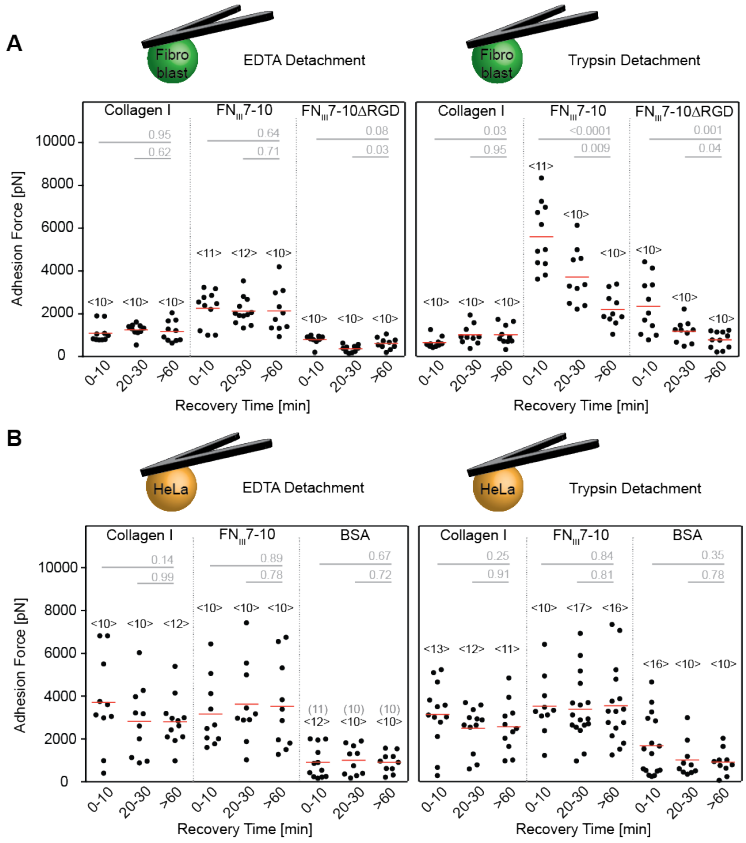

Figure 3-4 Adhesion force of (A) mouse kidney fibroblasts and (B) HeLa cells recorded after different recovery times from trypsin or EDTA treatment. Fibroblast adhesion forces were recorded to collagen I, fibronectin type III fragment containing repeats 7-10 (FN_{III}7-10), or the same fibronectin fragment lacking the RGD sequence (FN_{III}7-10ΔRGD). Adhesion forces of HeLa cells were recorded to collagen I, FN_{III}7-10, or BSA. Cantilever-bound cells pressed on the substrate with a force of 1 nN were allowed to initiate adhesion for 60 seconds prior to retraction. Each dot represents a single cell characterized. Red bars indicate average values. <n> gives the number of measurements and (n) the number of cells for each condition. Mann-Whitney P-values indicating the significance of the measurements compared to those made after a recovery time of >60 min given in gray.

Using HeLa cells we characterized adhesion to collagen I, FN_{III}7-10, and bovine serum albumin (BSA). As fibroblasts HeLa cells adhere to collagen I and FN_{III}7-10 specifically via integrins[26,70,71]. However the expression levels may be different and thus, also the adhesion differs from fibroblasts. In contrast to fibroblasts HeLa cells showed a relatively high adhesion to FN_{III}7-10ΔRGD coated substrates (data not shown). Thus, we used BSA as substrate, which is frequently used to suppress unspecific cell adhesion to the supporting glass surface[72,73]. The

adhesion force of HeLa cells to the three different substrates was largely independent on the detachment method (EDTA or trypsin) from culture flasks prior to SCFS measurements (Figure 3-4). These results highlight that the adhesive properties of different cell lines are differently affected by the procedure used to detach the cells from culture flasks.

3.4.4. Rupture events do not depend on recovery time

After having characterized the maximum cell adhesion force of fibroblasts and HeLa cells to different ECM substrates, we analyzed the rupture events recorded during cell-substrate detachment (Figure 3-5). These rupture events correspond to the breaking of individual or clusters of CAM-ligand bonds exposed to mechanical stress. Rupture events recorded for fibroblasts and HeLa cells detached from culture flasks using EDTA or trypsin prior SCFS did not show significant dependency on recovery time (Figure 3-5). This result may be seen in contradiction to the increased adhesion strength of fibroblasts to the fibronectin constructs, which depended strongly on the recovery time of the fibroblasts after trypsin treatment (Figure 3-4). However, because the strength of the single rupture events (median rupture force ≈50 pN with data points spreading from 15 to 400 pN) were not affected by trypsin (Figure 3-5) our result suggests that the increased fibroblast adhesion to $FN_{III}7$-10 originated from increased avidity (*e.g.,* availability of CAMs binding to fibronectin) rather than increased affinity (*e.g.,* binding strength of CAMs to fibronectin).

3.4.5. Tether forces do not depend on recovery time

Next, we characterized the forces required to extract single tethers from fibroblasts and HeLa cells while being detached from the three different substrates (Figure 3-6). Although the median tether forces statistically sometime depended on the recovery time after detachment from the culture flasks, the differences were very minor (<10 pN) compared to the spread of the data points (Figure 3-6). Thus, we do not consider the tether force differences as relevant for the detachment process using either EDTA or trypsin. Because the force required to extract tethers from cell membranes depends on the properties of the cell membrane and not on the CAM bond adhering the tether to the substrate, this result indicates that the properties of the cell membrane do not depend on the procedure used to detach the cells from the culture flasks.

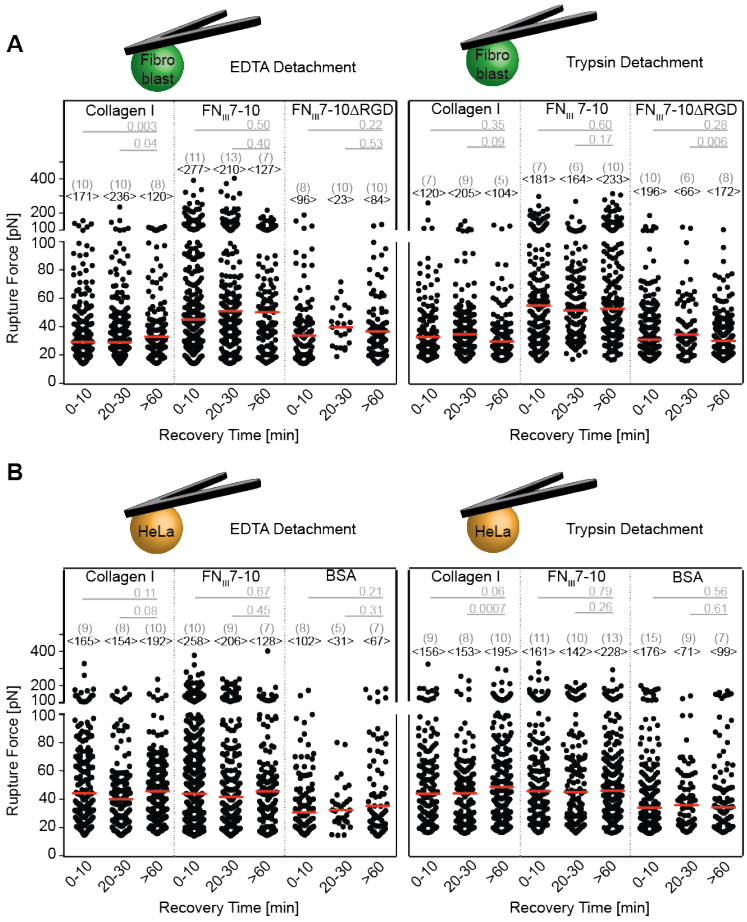

Figure 3-5 Forces of single rupture events recorded for (A) mouse kidney fibroblasts and (B) HeLa cells after different recovery in times from EDTA or trypsin treatment. Rupture forces were recorded upon detaching single fibroblasts adhering to Petri dishes coated with collagen I, $FN_{III}7$-10, or $FN_{III}7$-10ΔRGD and upon detaching HeLa cells adhering to Petri dishes coated with collagen I, $FN_{III}7$-10, or BSA. Cells were pressed onto the substrates with a 1 nN contact force and were allowed to establish adhesion for 60 seconds. Subsequently, the cantilever was retracted at 5 µm/s for at least 90 µm. The recovery time denotes the time cells were allowed to recover after detachment from culture flasks using either EDTA or trypsin. After the recovery time passed, adhesion of the cells to the different substrates was characterized using SCFS. Each dot represents one rupture event with the red bars indicating median values. <n> gives the number of rupture events and (n) the number curves analyzed for each condition. Mann-Whitney P-values indicating the significance of the measurements compared to those made after a recovery time of >60 min are given in gray. Distribution of rupture forces are shown in Supplementary Fig. S2

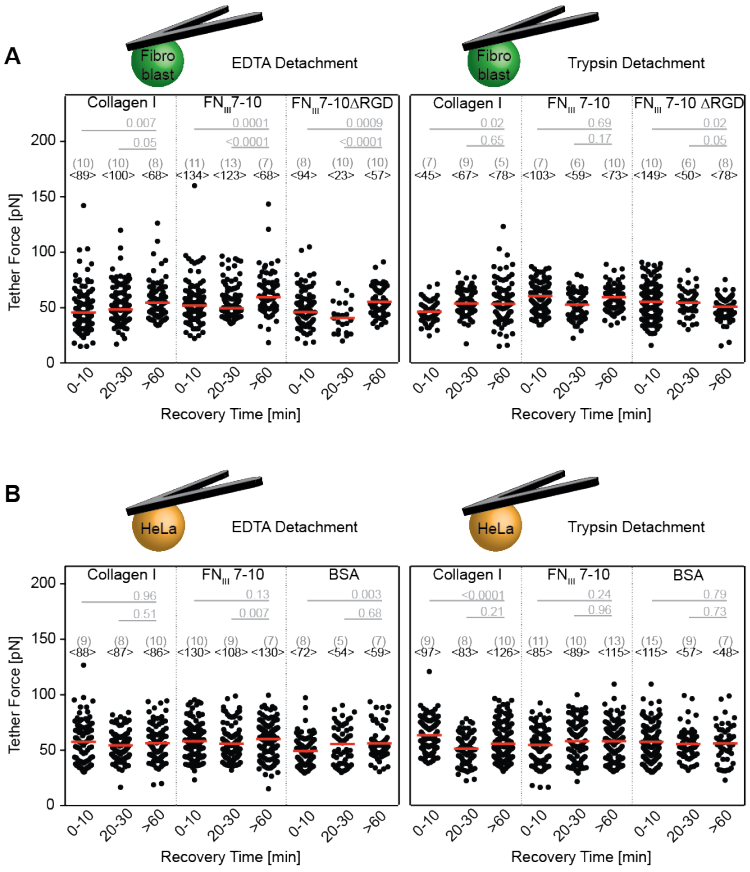

Figure 3-6 Forces required to mechanically extract single tethers from (A) fibroblasts and (B) HeLa cells after different recovery in times from EDTA or trypsin treatment. Tether forces were recorded upon detaching single fibroblasts adhering to Petri dishes coated with collagen I, $FN_{III}7$-10, or $FN_{III}7$-10ΔRGD or upon detaching HeLa cells adhering to Petri dishes coated with collagen I, $FN_{III}7$-10, or BSA. Cells were pushed onto the substrates with a contact force of 1 nN and were allowed to establish adhesion for 60 seconds. Subsequently, the cantilever was retracted at 5 µm/s for at least 90 µm. The recovery time denotes the time cells were allowed to recover after detachment from culture flasks using either EDTA or trypsin. After this recovery time passed the adhesion of the cells to the different substrates was characterized using SCFS. Each dot represents one tether event with the red bars indicating median values. <n> gives the number of tether events and (n) the number curves analyzed for each condition. Mann-Whitney P-values indicating the significance of the measurements compared to those made after >60 min recovery time are given in gray. Distribution of tether forces are shown in Supplementary Fig. S2

3.5. Discussion

We investigated the recovery of mechanical and adhesive properties of eukaryotic cell lines, which, prior to measuring these properties by AFM-based SCFS, have been detached from

culture flasks using either EDTA or trypsin. Therefore, we quantified mechanical stiffness and adhesion forces of mouse embryonic kidney fibroblasts and HeLa cells at different recovery times after detachment from culture flasks. The mechanical stiffness of a cell determines the contact area of the cell pressed onto the substrate and thus has a direct influence on the adhesion formed. Interestingly, the contact stiffness determined for fibroblasts and HeLa cells did not reveal any significant dependency on the detachment method applied or on the recovery time investigated. One reason may be that the low contact force of ≈1 nN applied by the cantilever on single cells while pressing them to the substrate only weakly deforms the cells and, thus, hardly stresses their actomyosin cortex. However, we applied only very little contact force to the cells in our SCFS measurements and applying much higher forces of 50-100 nN through the cantilever severely deforms pre-rounded interphase cells[74,75]. At such high forces the AFM cantilever probes different mechanical properties of the cell, which may depend on pretreatment using trypsin and/or EDTA. Such dependency would change the contact area between cell and substrate and, thus, the adhesion probed by SCFS.

There was also no significant influence on adhesive properties when detaching either cell types from culture flasks using EDTA. EDTA chelation of divalent ions inhibits CAMs that require divalent ions for establishing adhesive interactions[76]. Since the detached cells are transferred to EDTA-free buffer solutions this result suggests that CAMs recover quickly from EDTA treatment and can readily re-establish adhesion[33]. However, we can only make conclusions concerning mouse embryonic kidney fibroblasts and HeLa cells, and for CAMs facilitating adhesion to collagen I and fibronectin, and recovery from EDTA exposure may be need to be characterized for every cell line and CAM to be investigated by SCFS.

Trypsin severely affected the adhesive properties of fibroblasts. Shortly after trypsin-induced detachment of fibroblasts from cell culture flasks the adhesion force of these cells to the fibronectin constructs increased considerably. Fibroblasts needed >60 min to recover adhesive properties from trypsin treatment. In contrast the adhesion force of fibroblasts to collagen I was not increased by trypsin pre-treatment. Although the adhesion of fibroblasts was just above background level, we also did not observe a decrease in adhesion. This latter finding is in agreement with previous investigations showing that pre-treating CHO-A2 cells with trypsin does not cleave collagen I binding $\alpha_2\beta_1$ integrins and does not affect cell adhesion to collagen I matrices[22]. Thus, pre-treating fibroblasts using trypsin specifically upregulated CAMs binding to fibronectin. Indeed, trypsin cleaves and activates human PAR2, which stimulates $\alpha_5\beta_1$ integrin but not $\alpha_V\beta_3$ integrin dependent cell adhesion[77]. $\alpha_5\beta_1$ integrins bind to the RGD site located in the $FN_{III}7\text{-}10$ fragment of fibronectin [69] and besides $\alpha_V\beta_3$ integrins are the main CAMs for fibronectin in mouse kidney fibroblasts[68]. These results highlight that only certain CAMs may be affected by the procedure used to detach cells from culture flasks whereas other CAMs remain unaffected. Our results furthermore show that cell detachment does not alter the affinity of fibronectin binding

CAMs (e.g., binding strength remains unchanged), but that it may upregulate adhesion forces by increasing the avidity of these receptors (e.g., number of binding events).

To our surprise fibroblast adhesion to the $FN_{III}7\text{-}10\Delta RGD$ covered substrate increased after trypsin cleavage. Fibroblasts needed >60 min to recover this enhanced unspecific adhesion to $FN_{III}7\text{-}10\Delta RGD$. Because mouse kidney fibroblasts have no CAMs to specifically adhere to $FN_{III}7\text{-}10\Delta RGD$[68], we assume that this increased adhesion is due to an increased number of CAMs, which may interact unspecific (*e.g.* via sugar residues on $\alpha_5\beta_1$ integrins or other membrane proteins which are affected by either PAR or trypsin directly) with the substrate. However, the unspecific interactions may be different for different substrates. Such substrate dependent unspecific adhesion could explain, why the adhesion of fibroblasts to collagen I stays similar in all recovery times after trypsin treatment.

In contrast to fibroblasts the adhesion of HeLa cells was apparently not affected by trypsin treatment within the recovery times tested and force sensitivity of our SCFS-based assay. This shows that cell lines can react differently to the detachment methods used and that the recovery of each cell line must be carefully studied before characterizing its mechanical and adhesive properties by SCFS. Importantly, these results further demonstrate that the quantification of cell adhesion by SCFS and probably by other cell adhesion assays requires careful investigation whether the CAMs addressed in cell adhesion studies are affected by the detachment procedure and whether the cells characterized have sufficient time to recover from this detachment.

To date in most SCFS studies the cells were explicitly left to recover for a certain time from their detachment from the cell culture flask before being characterized by SCFS. Thus, SCFS users have already allocated a certain time span to enable detached cells to recover. However, so far a quantitative approach to characterize this recovery has not been presented. Our approach can be applied to characterize the recovery time of any adherent cell after detachment from cell culture flasks. Our approach can also be used to optimize the detachment procedure for specific cell types. For example, our measurements show that mouse kidney fibroblasts and HeLa cells, detached from culture flasks by EDTA, do not need recovery times of more than 10 min, whereas cells detached using trypsin need to recover for up to 60 min. Thus, EDTA may be more suitable to detach the cell lines investigated here from culture flasks and to investigate their mechanical and adhesive properties.

3.6. Authors Contribution

R.S., N.S. and D.J.M. designed the experiments and wrote the paper. R.S. and N.S. performed most experiments and analyzed and interpreted the data. S.P.R. performed fluorescence microcopy experiments. M.B. expressed, purified and characterized the fibronectin fragments. All authors discussed the experiments, read and approved the manuscript.

3.7. Acknowledgements

We thank Martin Stewart, Johannes Thoma and Jonne Helenius for critical discussion and assistance. Mouse embryonic kidney fibroblasts and plasmids for fibronectin fragments were kindly provided by Reinhard Fässler. This work was supported by the Swiss National Science Foundation.

3.8. References

1. Gumbiner, B. M. *Cell adhesion: the molecular basis of tissue architecture and morphogenesis*. (Cell, 1996).
2. Kreidberg, J. A. & Symons, J. M. Integrins in kidney development, function, and disease. *American Journal of Physiology - Renal Physiology* **279,** F233–F242 (2000).
3. Halbleib, J. M. & Nelson, W. J. Cadherins in development: cell adhesion, sorting, and tissue morphogenesis. *Genes & Development* **20,** 3199–3214 (2006).
4. Barone, V. & Heisenberg, C.-P. Cell adhesion in embryo morphogenesis. *Current Opinion in Cell Biology* **24,** 148–153 (2012).
5. Pokutta, S. & Weis, W. I. Structure and Mechanism of Cadherins and Catenins in Cell-Cell Contacts. *Annu. Rev. Cell Dev. Biol.* **23,** 237–261 (2007).
6. McEver, R. P. & Zhu, C. Rolling Cell Adhesion. *http://dx.doi.org/10.1146/annurev.cellbio.042308.113238* **26,** 363–396 (2010).
7. Zaidel-Bar, R. Cadherin adhesome at a glance. *Journal of Cell Science* **126,** 373–378 (2013).
8. Winograd-Katz, S. E., Fässler, R., Geiger, B. & Legate, K. R. The integrin adhesome: from genes and proteins to human disease. *Nat Rev Mol Cell Biol* **15,** 273–288 (2014).
9. Moser, M., Legate, K. R., Zent, R. & Fässler, R. The tail of integrins, talin, and kindlins. *Science* **324,** 895–899 (2009).
10. Steinberg, M. S. & McNutt, P. M. Cadherins and their connections: adhesion junctions have broader functions. *Current Opinion in Cell Biology* **11,** 554–560 (1999).
11. Brakebusch, C. & Fässler, R. The integrin–actin connection, an eternal love affair. *The EMBO Journal* **22,** 2324–2333 (2003).
12. Huveneers, S. & de Rooij, J. Mechanosensitive systems at the cadherin–F-actin interface. *Journal of Cell Science* **126,** jcs.109447–413 (2013).
13. García, A. J. & Gallant, N. D. Stick and grip: measurement systems and quantitative analyses of integrin-mediated cell adhesion strength. *Cell Biochem Biophys* **39,** 61–73 (2003).
14. Taubenberger, A. V., Hutmacher, D. W. & Müller, D. J. Single-Cell Force Spectroscopy, an Emerging Tool to Quantify Cell Adhesion to Biomaterials. *Tissue Engineering Part B: Reviews* **20,** 40–55 (2014).
15. Benoit, M., Gabriel, D., Gerisch, G. & Gaub, H. E. Discrete interactions in cell adhesion measured by single-molecule force spectroscopy. *Nat Cell Biol* **2,** 313–317 (2000).
16. Helenius, J., Heisenberg, C.-P., Gaub, H. E. & Müller, D. J. Single-cell force spectroscopy. *Journal of Cell Science* **121,** 1785–1791 (2008).
17. Neuman, K. C. & Nagy, A. Single-molecule force spectroscopy: optical tweezers, magnetic tweezers and atomic force microscopy. *Nature Methods* **5,** 491–505 (2008).
18. Friedrichs, J. *et al.* A practical guide to quantify cell adhesion using single-cell force spectroscopy. *Methods* **60,** 169–178 (2013).
19. Müller, D. J., Helenius, J., Alsteens, D. & Dufrêne, Y. F. Force probing surfaces of living cells to molecular resolution. *Nat Chem Biol* **5,** 383–390 (2009).
20. Force and compliance measurements on living cells using atomic force microscopy (AFM). **6,** 1–9 (2004).
21. Puech, P.-H. *et al.* Measuring cell adhesion forces of primary gastrulating cells from zebrafish using atomic force microscopy. *Journal of Cell Science* **118,** 4199–4206 (2005).
22. Taubenberger, A., Cisneros, D. A., Puech, P.-H., Müller, D. J. & Franz, C. M. Revealing early steps of alpha2beta1 integrin-mediated adhesion to collagen type I by using single-cell force spectroscopy. *Mol. Biol. Cell* **18,** 1634–1644 (2007).
23. Hsiao, S. C. *et al.* DNA-Coated AFM Cantilevers for the Investigation of Cell Adhesion

and the Patterning of Live Cells. *Angew. Chem. Int. Ed.* **47,** 8473–8477 (2008).
24. Ng, G. *et al.* Receptor-Independent, Direct Membrane Binding Leads to Cell-Surface Lipid Sorting and Syk Kinase Activation in Dendritic Cells. *Immunity* **29,** 807–818 (2008).
25. Selhuber-Unkel, C., López-García, M., Kessler, H. & Spatz, J. P. Cooperativity in Adhesion Cluster Formation during Initial Cell Adhesion. *Biophysical Journal* **95,** 5424–5431 (2008).
26. Friedrichs, J., Helenius, J. & Müller, D. J. Stimulated single-cell force spectroscopy to quantify cell adhesion receptor crosstalk. *Proteomics* **10,** 1455–1462 (2010).
27. Friedrichs, J., Helenius, J. & Muller, D. J. Quantifying cellular adhesion to extracellular matrix components by single-cell force spectroscopy. *Nature Protocols* **5,** 1353–1361 (2010).
28. Friedrichs, J., Werner, C. & Müller, D. J. in *Adhesion Protein Protocols* **1046,** 19–37 (Humana Press, 2013).
29. Dao, L., Gonnermann, C. & Franz, C. M. Investigating differential cell-matrix adhesion by directly comparative single-cell force spectroscopy. *J. Mol. Recognit.* **26,** 578–589 (2013).
30. Riet, Te, J. *et al.* Distinct kinetic and mechanical properties govern ALCAM-mediated interactions as shown by single-molecule force spectroscopy. *Journal of Cell Science* **120,** 3965–3976 (2007).
31. Riet, Te, J. *et al.* Dynamic coupling of ALCAM to the actin cortex strengthens cell adhesion to CD6. *Journal of Cell Science* **127,** 1595–1606 (2014).
32. Fichtner, D. *et al.* Covalent and Density-Controlled Surface Immobilization of E-Cadherin for Adhesion Force Spectroscopy. *PLoS ONE* **9,** e93123 (2014).
33. Krieg, M. *et al.* Tensile forces govern germ-layer organization in zebrafish. *Nat Cell Biol* **10,** 429–436 (2008).
34. Beckmann, J., Schubert, R., Chiquet-Ehrismann, R. & Müller, D. J. Deciphering teneurin domains that facilitate cellular recognition, cell-cell adhesion, and neurite outgrowth using atomic force microscopy-based single-cell force spectroscopy. *Nano Lett.* **13,** 2937–2946 (2013).
35. Dufrêne, Y. F., Martínez-Martín, D., Medalsy, I., Alsteens, D. & Müller, D. J. Multiparametric imaging of biological systems by force-distance curve-based AFM. *Nature Methods* **10,** 847–854 (2013).
36. Chu, C., Celik, E., Rico, F. & Moy, V. T. Elongated Membrane Tethers, Individually Anchored by High Affinity α4β1/VCAM-1 Complexes, Are the Quantal Units of Monocyte Arrests. *PLoS ONE* **8,** e64187 (2013).
37. Krieg, M., Helenius, J., Heisenberg, C.-P. & Müller, D. J. A Bond for a Lifetime: Employing Membrane Nanotubes from Living Cells to Determine Receptor-Ligand Kinetics. *Angew. Chem. Int. Ed.* **47,** 9775–9777 (2008).
38. Siamantouras, E., Hills, C. E., Younis, M. Y. G., Squires, P. E. & Liu, K.-K. Quantitative investigation of calcimimetic R568 on beta cell adhesion and mechanics using AFM single-cell force spectroscopy. *FEBS Letters* **588,** 1178–1183 (2014).
39. Benoit, M. & Gaub, H. E. Measuring cell adhesion forces with the atomic force microscope at the molecular level. *Cells Tissues Organs* **172,** 174–189 (2002).
40. Sheetz, M. P. Cell control by membrane–cytoskeleton adhesion. *Nat Rev Mol Cell Biol* **2,** 392–396 (2001).
41. Evans, E. A. & Calderwood, D. A. Forces and bond dynamics in cell adhesion. *Science* **316,** 1148–1153 (2007).
42. Marshall, B. T. *et al.* Direct observation of catch bonds involving cell-adhesion molecules. *Nature* **423,** 190–193 (2003).
43. Sun, M. *et al.* Multiple Membrane Tethers Probed by Atomic Force Microscopy. *Biophysical Journal* **89,** 4320–4329 (2005).
44. Krieg, M., Dunn, A. R. & Goodman, M. B. Mechanical control of the sense of touch by β-spectrin. *Nat Cell Biol* **16,** 224–233 (2014).
45. Vásquez, V., Krieg, M., Lockhead, D. & Goodman, M. B. Phospholipids that Contain Polyunsaturated Fatty Acids Enhance Neuronal Cell Mechanics and Touch Sensation. *Cell Reports* **6,** 70–80 (2014).
46. Rous, P. & Jones, F. S. A method for obtaining suspension of living cells from fixed tissues, and for the plating out of individual cells. *J. Exp. Med.* **23,** 549–555 (1916).

47. Franken, N. A. P., Rodermond, H. M., Stap, J., Haveman, J. & van Bree, C. Clonogenic assay of cells in vitro. *Nature Protocols* **1,** 2315–2319 (2006).
48. Lampugnani, M. G. *et al.* A novel endothelial-specific membrane protein is a marker of cell-cell contacts. *The Journal of Cell Biology* **118,** 1511–1522 (1992).
49. Coughlin, S. R. Thrombin signalling and protease-activated receptors : Article : Nature. *Nature* **407,** 258–264 (2000).
50. O'Brien, P. J., Molino, M., Kahn, M. & Brass, L. F. Protease activated receptors: theme and variations. *Oncogene* **20,** 1570–1581 (2001).
51. Adams, M. N. *et al.* Structure, function and pathophysiology of protease activated receptors. *Pharmacology & Therapeutics* **130,** 248–282 (2011).
52. Edwards, I. J. Proteoglycans in prostate cancer. *Nature Reviews Urology* **9,** 196–206 (2012).
53. Clapham, D. E. Calcium Signaling. *Cell* **131,** 1047–1058 (2007).
54. Howe, A. K. Cross-talk between calcium and protein kinase A in the regulation of cell migration. *Current Opinion in Cell Biology* **23,** 554–561 (2011).
55. Friedrichs, J. *et al.* Contributions of galectin-3 and -9 to epithelial cell adhesion analyzed by single cell force spectroscopy. *Journal of Biological Chemistry* **282,** 29375–29383 (2007).
56. Manninen, A., Müller, D. J. & Helenius, J. Galectin-3 regulates integrin alpha2beta1-mediated adhesion to collagen-I and -IV. *Journal of Biological Chemistry* **283,** 32264–32272 (2008).
57. Tulla, M. *et al.* TPA primes α2β1 integrins for cell adhesion. *FEBS Letters* **582,** 3520–3524 (2008).
58. Takahashi, S. *et al.* The RGD motif in fibronectin is essential for development but dispensable for fibril assembly. *The Journal of Cell Biology* **178,** 167–178 (2007).
59. Puech, P.-H., Poole, K., Knebel, D. & Müller, D. J. A new technical approach to quantify cell–cell adhesion forces by AFM. *Ultramicroscopy* **106,** 637–644 (2006).
60. Hutter, J. L. & Bechhoefer, J. Calibration of atomic-force microscope tips. *Review of Scientific Instruments* **64,** 1868 (1993).
61. Riet, Te, J. *et al.* Interlaboratory round robin on cantilever calibration for AFM force spectroscopy. *Ultramicroscopy* **111,** 1659–1669 (2011).
62. Kelly, S. M. & Macklem, P. T. Direct measurement of intracellular pressure. *American Journal of Physiology - Cell Physiology* **260,** C652–C657 (1991).
63. Gao, J. *et al.* Lens intracellular hydrostatic pressure is generated by the circulation of sodium and modulated by gap junction coupling. *The Journal of General Physiology* **137,** 507–520 (2011).
64. Stewart, M. P. *et al.* Hydrostatic pressure and the actomyosin cortex drive mitotic cell rounding. *Nature* **469,** 226–230 (2012).
65. Maddox, A. S. & Burridge, K. RhoA is required for cortical retraction and rigidity during mitotic cell rounding. *The Journal of Cell Biology* **160,** 255–265 (2003).
66. Tinevez, J.-Y. *et al.* Role of cortical tension in bleb growth. *Proc. Natl. Acad. Sci. U.S.A.* **106,** 18581–18586 (2009).
67. MacQueen, L. A., Thibault, M., Buschmann, M. D. & Wertheimer, M. R. Electromechanical deformation of mammalian cells in suspension depends on their cortical actin thicknesses. *Journal of Biomechanics* **45,** 2797–2803 (2012).
68. Schiller, H. B. *et al.* beta1- and alphav-class integrins cooperate to regulate myosin II during rigidity sensing of fibronectin-based microenvironments. *Nature Publishing Group* **15,** 625–636 (2013).
69. Ruoslahti, E. RGD and other recognition sequences for integrins. *Annu. Rev. Cell Dev. Biol.* **12,** 697–715 (1996).
70. Albigès-Rizo, C., Frachet, P. & Block, M. R. Down regulation of talin alters cell adhesion and the processing of the alpha 5 beta 1 integrin. *Journal of Cell Science* **108 (Pt 10),** 3317–3329 (1995).
71. Oba, M. *et al.* Cyclic RGD Peptide-Conjugated Polyplex Micelles as a Targetable Gene Delivery System Directed to Cells Possessing α vβ 3and αvβ 5Integrins. *Bioconjugate Chem.* **18,** 1415–1423 (2007).
72. Faull, R. J., Kovach, N. L., Harlan, J. M. & Ginsberg, M. H. Affinity modulation of integrin alpha 5 beta 1: regulation of the functional response by soluble fibronectin. *The*

Journal of Cell Biology **121,** 155–162 (1993).
73. Lee, M. H., Brass, D. A., Morris, R., Composto, R. J. & Ducheyne, P. The effect of non-specific interactions on cellular adhesion using model surfaces. *Biomaterials* **26,** 1721–1730 (2005).
74. Stewart, M. P. *et al.* Wedged AFM-cantilevers for parallel plate cell mechanics. *Methods* **60,** 186–194 (2013).
75. Stewart, M. P., Toyoda, Y., Hyman, A. A. & Müller, D. J. Force probing cell shape changes to molecular resolution. *Trends in Biochemical Sciences* **36,** 444–450 (2011).
76. Humphries, M. J. Integrin Structure. 1–30 (2009).
77. Miyata, S., Koshikawa, N., Yasumitsu, H. & Miyazaki, K. Trypsin stimulates integrin alpha(5)beta(1)-dependent adhesion to fibronectin and proliferation of human gastric carcinoma cells through activation of proteinase-activated receptor-2. *Journal of Biological Chemistry* **275,** 4592–4598 (2000).

3.9. Supplementary Data

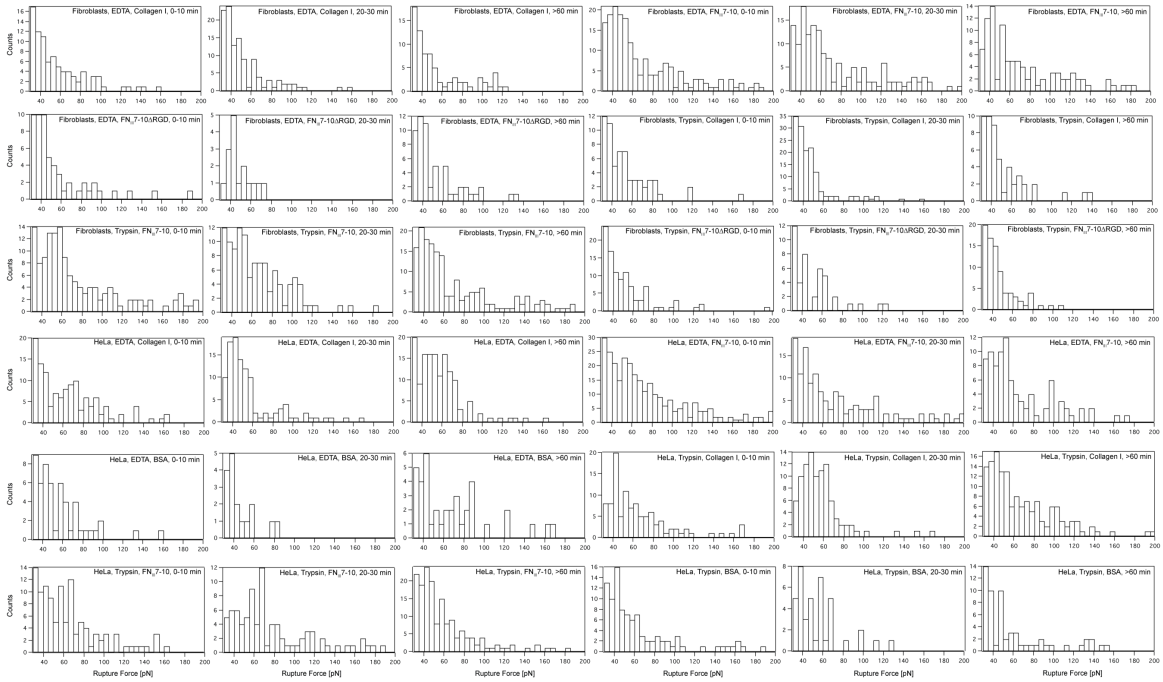

Suppl. Fig. 1. Histograms of forces of single rupture events recorded for mouse kidney fibroblasts and HeLa cells after different recovery in times from EDTA or trypsin treatment. Histograms belong to data shown in Figure 5.

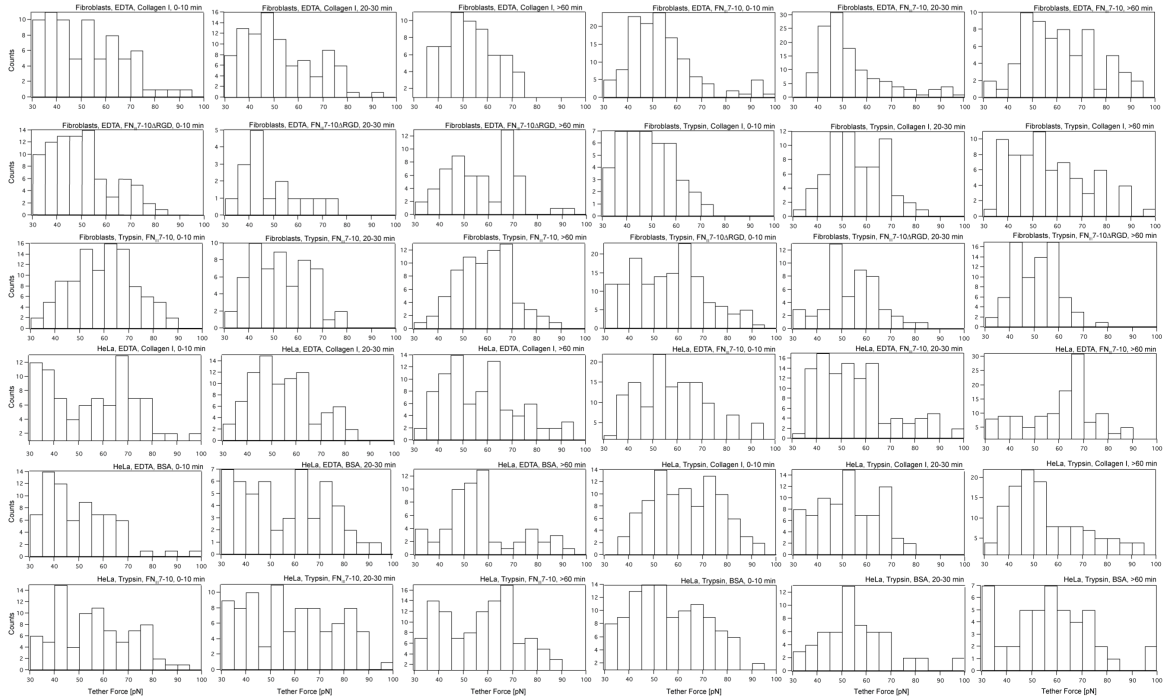

Suppl. Fig. 2. Histograms of forces of single tether events recorded for mouse kidney fibroblasts and HeLa cells after different recovery in times from EDTA or trypsin treatment. Histograms belong to data shown in Figure 6.

4. αV-class integrins exert dual roles on α5β1 integrins to strengthen adhesion to fibronectin

Mitasha Bharadwaj[1], Nico Strohmeyer[1], Georgina P. Colo[2], Jonne Helenius[1], Niko Beerenwinkel[1], Herbert B. Schiller[2,3], Reinhard Fässler[2] & Daniel J. Müller[1]

1. Department of Biosystems Science and Engineering, ETH Zurich, Mattenstrasse 26, 4058 Basel, Switzerland

2. Max Planck Institute of Biochemistry, Department of Molecular Medicine, 82152 Martinsried, Germany.

3. Comprehensive Pneumology Center, Institute of Lung Biology and Disease, Helmholtz Zentrum München, Oberschlei heim 85764, Germany

Correspondence: Daniel J. Müller, daniel.mueller@bsse.ethz.ch

Published in *Nat. Commun.* **8,** 14348 (2017).

4.1. Abstract

Upon binding to the extracellular matrix protein, fibronectin, αV-class and α5β1 integrins trigger the recruitment of large protein assemblies and strengthen cell adhesion. Both integrin classes have been functionally specified, however their specific roles in immediate phases of cell attachment remain uncharacterized. Here, we quantify the adhesion of αV-class and/or α5β1 integrins expressing fibroblasts initiating attachment to fibronectin (≤120 s) by single-cell force spectroscopy. Our data reveals that αV-class integrins outcompete α5β1 integrins. Once engaged, αV-class integrins signal to α5β1 integrins to establish additional adhesion sites to fibronectin, away from those formed by αV-class integrins. This crosstalk, which strengthens cell adhesion, induces α5β1 integrin clustering by RhoA/ROCK/myosin-II and Arp2/3-mediated signalling, whereas overall cell adhesion depends on formins. The dual role of both fibronectin-binding integrin classes commencing with an initial competition followed by a cooperative crosstalk appears to be a basic cellular mechanism in assembling focal adhesions to the extracellular matrix.

4.2. Introduction

Integrins are transmembrane receptors composed of α/β heterodimers that facilitate cell adhesion and regulate basic cellular processes such as migration, proliferation, survival and differentiation[1,2,3]. Mammals harbor eighteen α and eight β genes. Through different combinations of α and β subunits, 24 integrins can be generated that bind counter receptors such as vascular cell adhesion molecules (VCAM) and intracellular cell adhesion molecules (ICAM), or extracellular matrix (ECM) proteins such as fibronectin (FN), vitronectin (VN), collagen, and laminin[4]. Individual adhesion mechanisms of integrin heterodimers with ECMs substrates have been extensively studied over the past few years. However, the regulatory mechanisms through which different integrins crosstalk with each other to initiate cell adhesion are still poorly understood.

Early integrin-mediated cell adhesion is believed to follow a cascade of events that starts with integrin activation through talin and kindlin (also called integrin-inside-out signaling), followed by integrin clustering and the assembly of a large protein network at the clustered integrin cytoplasmic domain collectively called the adhesome[2,5]. The adhesome comprises hundreds of proteins including talin and kindlin, which together with several adaptor and signaling molecules transduce signals from ligand-bound integrins to the cell inside (also called integrin-outside-in signaling)[5]. An important consequence of outside-in signaling is the activation of actomyosin including Rho-like GTPases and their effectors such as Rho kinase (ROCK), cortical F-actin nucleators such as formins, the Arp2/3 complex and the non-muscle myosin-II.

FN consists of an array of type I, II and III modules and is one of the most abundant ECM proteins to which α5β1 and αV-class integrins adhere. Cell adhesion mediated by FN-binding integrins leads to the formation of nascent adhesions that eventually mature into large focal adhesions and then convert into central or fibrillar adhesions[5,6]. While both integrin classes bind the tripeptide sequence Arg-Gly-Asp (RGD) in the 10th type III module of FN (FNIII10)[7,8], α5β1 integrins also require the Pro-His-Ser-Arg-Asn (PHSRN) synergy site in the FNIII9 module, which is in close proximity to the RGD motif, to establish cell adhesion[9]. It is not clear, whether α5β1 and αV-class integrins function individually and/or cooperate with each other during the first few seconds and minutes of adhesion initiation. Furthermore, it is also unclear whether and how the two FN-binding integrin classes signal to each other to induce and orchestrate their assembly and to strengthen adhesion to FN before nascent adhesions have formed. Interestingly, crosstalk between both integrin classes has been reported to occur at later stages (>90 min) of cell adhesion[9,10-12]. For example, it has been demonstrated that both integrins compete for the cytoplasmic talin pool leading to negative, trans-dominant effects[13,14], while they also strengthen adhesion to the ECM and trigger the formation of large focal adhesions[15].

To provide quantitative insights into the mechanisms regulating early (≤ 120 s) fibroblast adhesion established by α5β1 and αV-class integrins to FN, we employed atomic force microscopy (AFM)-based single-cell force spectroscopy (SCFS)[16]. SCFS is well suited to characterize

specific adhesion mechanisms of cells to the ECM[17,18]. Compared to other methods allowing the qualitative or/and quantitative characterization of cell adhesion, SCFS offers the particular advantage to decipher early adhesion mechanisms occurring within the first few seconds to minutes of cell-ECM attachment[17]. Therefore, we employed SCFS together with confocal microscopy to study the adhesion kinetics of α5β1 and αV-class integrins in mouse kidney fibroblasts to FN. Our results reveal a dual role of the two integrin classes upon contacting FN. First, they compete for FN binding, to which αV-class integrins bind faster, thereby preventing the engagement of α5β1 integrins. In the second phase, αV-class integrins, engaged with the substrate, signal to α5β1 integrins to establish binding to FN and to strengthen adhesion. By combining SCFS with total internal reflection fluorescence (TIRF) microscopy, we characterized that this crosstalk triggers the clustering of α5β1 integrins and recruitment of adhesome proteins. Specific perturbation experiments identified signaling pathways involved in the early crosstalk between both FN-binding integrin classes.

4.3. Results

4.3.1. Differential contributions of α5β1 and αV-class integrins

To determine how α5β1 and αV-class integrins contribute to the initiation of cell adhesion, we quantified the adhesion forces of α5β1 and/or αV-class integrin-expressing mouse kidney fibroblasts to FN by SCFS (Figure 4-1a). The cell lines were derived from pan-integrin deficient fibroblasts (pKO) reconstituted with either αV-class (pKO-αV), or β1 (pKO-β1), or both classes of integrins (pKO-αV/β1)[6]. To minimize the binding of FN by receptors other than α5β1 and αV-class integrins, i.e. syndecans[19], we used the FN fragment FNIII7–10, which contains the RGD- and PHSRN-motifs. For SCFS, a single fibroblast was attached to concanavalin A (ConA)-functionalized AFM cantilever and incubated for 7-10 minutes to ensure firm adhesion of the fibroblast to the cantilever. The rounded fibroblast bound to the cantilever was then brought into contact with the FNIII7–10 substrate for contact times ranging from 5 to 120 s. Subsequently, the fibroblast was separated from the substrate to measure the fibroblast-substrate adhesion force at maximum cantilever deflection (Supplementary Figure 4-1a). To obtain statistically firm results, the single-cell experiments were repeated multiple times using different cantilevers, fibroblasts and FNIII7–10-coated substrates. Our measurements revealed that the three reconstituted pKO fibroblast lines showed characteristic integrin-specific adhesion profiles to FNIII7–10, whereas non-reconstituted pKO fibroblasts displayed negligible adhesion (Figure 4-1a). pKO-αV/β1, pKO-αV and pKO-β1 fibroblasts significantly strengthened adhesion with increasing contact times to FNIII7–10. Interestingly, while the adhesion strength of pKO-αV/β1 and pKO-αV fibroblasts was similar, pKO-β1 fibroblasts established much stronger adhesion to FNIII7–10, which doubled at 120 s contact time compared to pKO-αV and pKO-αV/β1 fibroblasts. Importantly, the stronger adhesion of pKO-β1 fibroblasts was also observed with full-length FN (Supplementary Figure 4-1b). Furthermore, pKO-αV/β1, pKO-αV and pKO-β1

fibroblasts reduced adhesion to RGD-deleted FN fragments (FNIII7-10ΔRGD) to integrin-unspecific levels confirming that the adhesion strengthening was integrin-dependent (Supplementary Figure 4-1c). In summary, our results showed that pKO-β1 fibroblasts established much stronger adhesion and strengthened adhesion much faster to FN compared to pKO-αV/β1 fibroblasts, indicating that the presence of αV-class integrins prevented adhesion strengthening to FN *via* α5β1 integrins.

Next, we tested whether blocking α5β1 integrins with an α5β1 integrin-blocking antibody (β1AB) or αV-class integrins with cyclic RGD (cilengitide, CiL)[20] alters adhesion of pKO-αV/β1 fibroblasts to FNIII7–10 (Figure 4-1b). We found that blocking α5β1 integrins did not alter the adhesion of fibroblasts to FNIII7-10, while blocking αV-class integrins, increased the adhesion of pKO-αV/β1 fibroblasts to levels observed for pKO-β1 fibroblasts (Figure 4-1b). One hypothesis for αV-class integrins hindering adhesion strengthening of α5β1 integrins, could be the preferential binding of talin and kindlin to the β-tail of αV-class integrins. Hence, upon blocking αV-class integrins, talin and kindlin became available to bind and activate α5β1 integrins[21,22]. Thus, we performed cytoplasmic β-tail pull-down assays (Supplementary Figure 4-1d), which in line with a recent study[23], confirmed that talin equivalently bound to both β3 and β1 subunits, while kindlin-2 preferentially associated with the cytoplasmic domain of the β1 subunit. A second hypothesis could be that αV-class integrins have higher binding rates and therefore, compete with α5β1 integrins for substrate binding. Thereto, we performed SCFS with single molecule sensitivity[24] (Supplementary Figure 4-1e) to determine the binding probability of both αV-class and α5β1 integrins with FN. This binding probability allowed estimating if one or both FN-binding integrins bind RGD in pKO-αV/β1 fibroblasts, upon initial contact. Therefore, the contact time of the fibroblasts to FNIII7–10 was reduced to ≈ 100 ms and the probability of single-integrin binding events, in the presence of either β1AB or CiL (Figure 4-1c), was determined. The experiments revealed an integrin binding probability of 0.25 ± 0.07 (mean ± SD, n = 3,529) per unperturbed pKO-αV/β1 fibroblast as compared to an unspecific binding probability of 0.10 ± 0.05 (n = 1,636) per pKO fibroblast. In the presence of β1AB, the binding probability increased to 0.40 ± 0.21 (n = 2,244), while in the presence of CiL, the binding probability decreased to 0.12 ± 0.06 (n = 3,218), comparable to that of pKO fibroblasts lacking FN-binding integrins.

Despite of equivalent binding of talin with β3 and β1 subunits, α5β1 integrins exhibited lower on-rates compared to αV-class integrins. This suggested for a role of integrin-inhibitory adapter proteins, such as the integrin cytoplasmic associated protein 1 (ICAP-1)[25,26], which delays the activation of α5β1 integrins and confers them lower on-rates. Hence, we performed SCFS experiments with ICAP-1-deficient mouse embryonic fibroblasts[25] (ICAP-1 KO MEFs, Supplementary Figure 4-1f). Indeed, while control WT MEFs showed similar adhesion to FN as that of pKO-αV/β1 fibroblasts, ICAP1-deficient MEFs adhered stronger to FN at all contact times, with adhesion forces comparable to those observed for pKO-β1 fibroblasts. These findings suggest

that ICAP-1 curbs FN-binding of α5β1 integrins and hence available talin/kindlin readily binds αV-class integrins instead, during adhesion initiation.

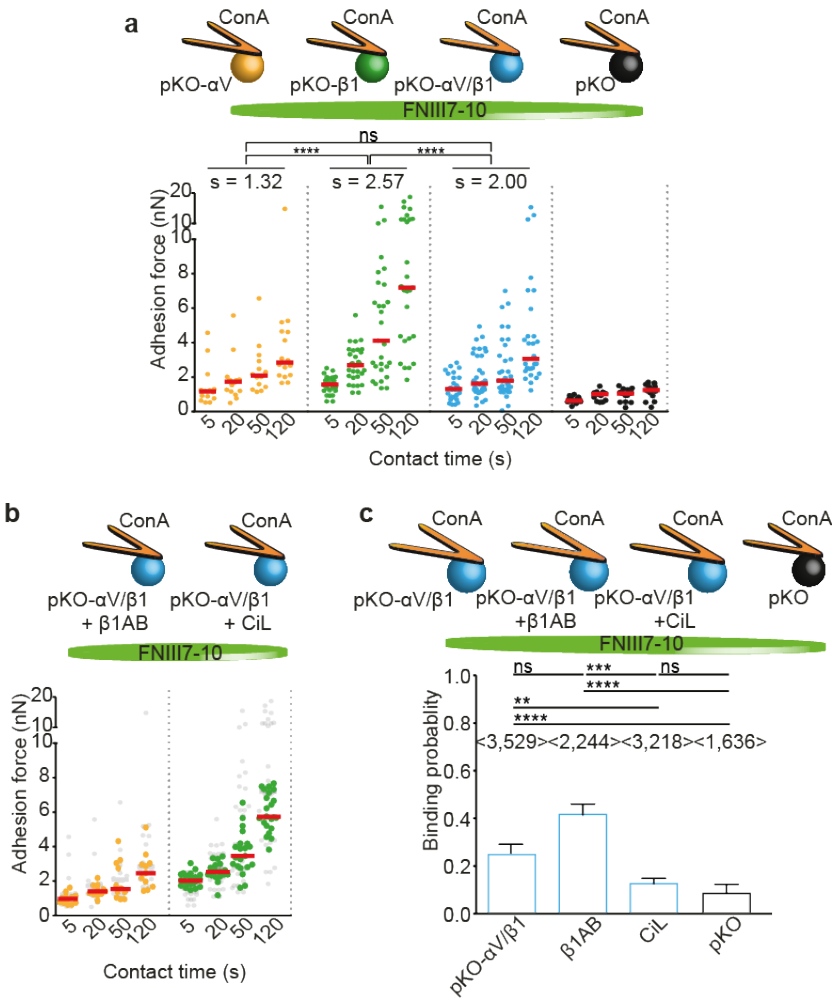

Figure 4-1 Fibronectin (FN) engagement of α5β1 and αV-class integrins on mouse fibroblasts. (a) Adhesion forces of pan-integrin knockout (pKO, black) fibroblasts rescued with either αV-class integrins (pKO-αV, yellow), or α5β1 (pKO-β1, green), or α5β1 and αV-class integrins (pKO-αV/β1, blue). For statistical analysis, average slopes of the adhesion force over all time points were defined as adhesion strengthening and determined using a dedicated R-code (Methods and Supplementary Note 1). Statistical significant differences between the slopes (n = 100) were determined by applying two-tailed Wilcoxon tests. (b) Adhesion force of pKO-αV/β1 fibroblasts to FNIII7–10 in presence of a β1 integrin-blocking antibody (β1AB) (yellow) and the specific αV-class integrin inhibitor cilengitide (CiL) (green). Adhesion forces of pKO-αV and pKO-β1 fibroblasts (data taken from (a)) are shown in light grey as reference for β1AB and CiL experiments, respectively. Dots in (a,b) show adhesion forces of single fibroblasts (n ≥ 10 for each condition) and red bars their median. (c) Binding probability of single α5β1 and αV-class integrins to FNIII7–10. The binding probabilities of unperturbed pKO-αV/β1 fibroblasts, in the presence of β1AB, CiL and pKO fibroblasts are shown. <n> equivalent to total number of force curves analyzed to detect single binding event. Bars show mean and error bars the s.d. Statistical significances were calculated with two-tailed Mann-Whitney U-tests. ****, P<0.0001; ***, P<0.001; **, P<0.01; * P<0.05; ns, P≥0.05.

Thus, the higher binding rates of αV-class *versus* α5β1 integrins, the negligible expression and undetectable functional role of αVβ1 integrins for early adhesion to FN (Supplementary Figure 4-2 andSupplementary Figure 4-3), together with the similar surface expression of α5β1 integrins on pKO-β1 and pKO-αV/β1 fibroblasts[6] demonstrate that αV-class integrins outcompete

α5β1 integrins likely due to inactivity of α5β1 integrins and thereby prevent pKO-αV/β1 fibroblasts to fully strengthen adhesion to FN.

4.3.2. αV-class integrins stimulate fibroblast adhesion to FN

Although we report an outcompeting of α5β1 integrins by αV-class integrins during early FN adhesion, cooperation of both integrin classes during late FN adhesion (> 45 minutes) was reported[6]. To test the possibility whether engaged αV-class integrins crosstalk with non-outcompeted FN-binding α5β1 integrins *via* signaling to regulate early fibroblast adhesion, we coated the cantilever with VN, which enabled adhesion, integrin clustering and phospho-tyrosine induction of αV-class integrins in pKO-αV and pKO-αV/β1 fibroblasts (Figure 4-2a and Supplementary Figure 4-4a,b). To pertain the high adhesion strength of fibroblast to FNIII7-10, we functionalized the cantilever with 5 μg ml^{-1} VN diluted in ConA. Control experiments excluded ConA as co-signaling receptor to VN (Figure 4-2a). After 20 s of contact time, pKO-αV/β1 fibroblasts attached to VN-coated cantilevers established faster and stronger adhesion to FNIII7–10 compared to pKO-αV/β1 fibroblasts attached to ConA only. After a contact time of 120 s to FNIII7–10, VN-stimulated fibroblasts further increased the adhesion compared to non-stimulated pKO-αV/β1 (Figure 4-2b) and non-stimulated pKO-β1 (Supplementary Figure 4-5) fibroblasts, which indicates that VN-engaged αV-class integrins promotes fibroblast adhesion to FN. Furthermore, the concomitant decrease in sequestering of αV-class integrins, by reducing the concentration of VN on the cantilever, increased adhesion to FNIII7-10 (Supplementary Figure 4-4c). These results suggest that unoccupied αV-class integrins on VN-stimulated pKO-αV/β1 fibroblasts also bind to FN to strengthen adhesion (Figure 4-2c). Moreover, the reduced adhesion of VN-stimulated pKO-αV/β1 fibroblasts to FN, in the presence of α5β1 integrin-blocking antibody (Figure 4-2d), indicates that the increased adhesion of pKO-αV/β1 fibroblasts was primarily mediated by α5β1 integrins and to a lesser extent by αV-class integrins.

To evaluate, whether FN-engaged αV-class integrins also signal and enforce adhesion of α5β1 integrins to FN, we attached pKO-αV/β1 fibroblasts to a cantilever coated with FNIII7–10 carrying a mutation in the synergy site (FNIII7–10-mSyn), to which α5β1 integrins poorly bind[9]. FNIII7–10-mSyn-stimulated pKO-αV/β1 fibroblasts strengthened adhesion to FNIII7–10 substrates similar to VN-stimulated pKO-αV/β1 fibroblasts (Figure 4-2c and Supplementary Figure 4-6a) or pKO-αV/β1 fibroblasts attached to FN-coated cantilevers (Supplementary Figure 4-6b) indicating that αV-class integrins, stimulated either by VN or FN, induced α5β1 integrin-mediated cell adhesion to FN.

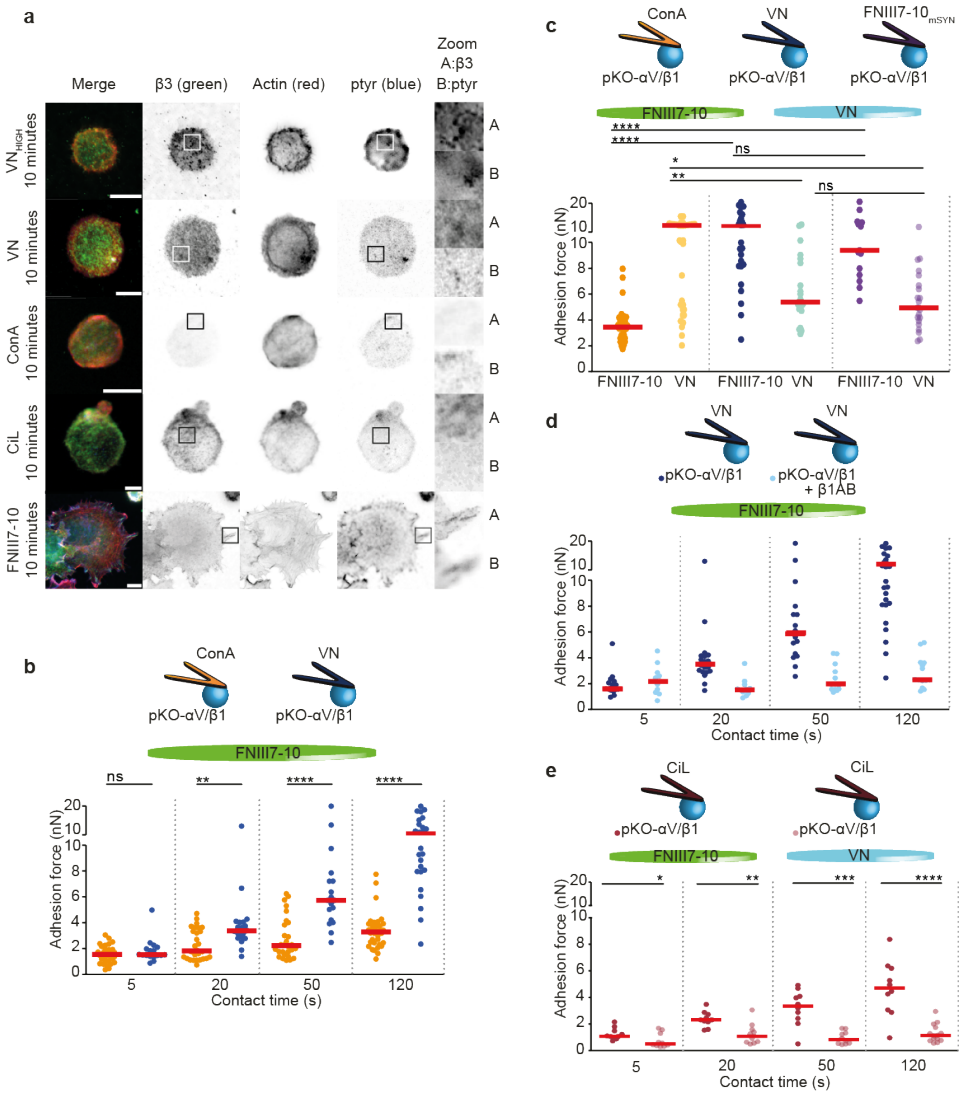

Figure 4-2 Engagement of αV-class integrins reinforces adhesion of α5β1 integrins to FN. (a) Immunofluorescence of pKO-αV/β1 fibroblasts seeded on VN-, ConA-, or FNIII7–10-functionalized substrates. Fibroblasts adhering to 50 µg ml^{-1} VN (VN$_{HIGH}$), 5 µg ml^{-1} VN diluted in ConA (VN), ConA, CiL and FNIII7–10 for 10 minutes were stained for αV-class integrin (green), actin (red) and phospho-tyrosine (ptyr, blue) using β3 integrin specific antibodies for the detection of αVβ3 integrins, phalloidin and ptyr antibody, respectively (Methods). Immunostaining of αV-class integrins and phospho-tyrosine in pKO-αV/β1 fibroblasts adhering to FNIII7-10-coated substrates is used as a positive control. Scale bars, 10 µm. (b) αV-class integrins engaged to VN augment fibroblasts adhesion to FNIII7–10. pKO-αV/β1 fibroblasts were either attached to ConA (yellow)- or to VN (blue)-coated cantilevers for 7–10 minutes, then approached to the FNIII7–10-coated substrate for defined contact time and finally retracted to measure the adhesion force. (c) αV-class integrins engaged to FNIII7–10 could also strengthen fibroblast adhesion to FNIII7-10 *via* α5β1 integrins. pKO-αV/β1 fibroblasts attached either to cantilevers coated with VN (blue) or FNIII7-10 having a mutated synergy site (FNIII7-10$_{mSYN}$, violet) enhanced adhesion to FNIII7-10. (d) VN-stimulated fibroblasts enhance adhesion to FNIII7–10 *via* α5β1 integrins. pKO-αV/β1 fibroblasts were incubated with a α5β1 integrin-blocking antibody (β1AB) for 30 minutes, then attached to VN-coated cantilevers and finally approached to FNIII7–10 for defined contact time (5–120 s). For VN-stimulation, (b-d) cantilevers were coated by 5 µg ml^{-1} VN diluted in ConA. (e) αV-class integrins must be engaged to stimulate pKO-αV/β1 fibroblasts to strengthen adhesion to FN. Adhesion of pKO-αV/β1 fibroblasts attached to CiL-coated cantilevers measured to FNIII7–10 and VN. Dots show adhesion forces of single fibroblasts (n ≥ 10 for each condition) and red bars their median. Statistical significances were calculated with two-tailed Mann-Whitney U-tests (****, P<0.0001; ***, P<0.001; **, P<0.01; * P<0.05; *ns*, P≥0.05).

Next, we tested whether signaling by and/or the fast binding rates of αV-class integrins on pKO-αV/β1 fibroblasts induced the strong adhesion of α5β1 integrins to FN-coated substrates.

To this end, we attached pKO-αV/β1 fibroblasts to cantilevers coated with CiL, to which αV-class integrins bind but elicit relatively less signaling response, if any, compared to VN-bound αV-class integrins[20] (Figure 4-2a). The experiments revealed that CiL-attached pKO-αV/β1 fibroblasts failed to adhere to VN-coated substrates (Figure 4-2e), suggesting that efficient sequestering of αV-class integrins prevented adhesion to VN at the opposite side of the fibroblast. However, CiL-attached pKO-αV/β1 fibroblasts adhered to FN-coated substrates at similar strengths (Figure 4-2e) as CiL-treated ConA-attached pKO-αV/β1 fibroblasts (Figure 4-1b) but at lower strength compared to VN-attached pKO-αV/β1 fibroblasts (Figure 4-2b). These results suggest that the functional state of αV-class integrins, upon sequestration to the cantilever, governs cell adhesion to FN and that αV-class integrin-mediated outcompeting of α5β1 integrins and αV-class integrin-mediated signaling act together to orchestrate α5β1 integrin-mediated adhesion strengthening.

4.3.3. αV-class integrins crosstalk with α5β1 integrins

Our data indicates that αV-class integrin engagement influences α5β1 integrin-mediated cell adhesion strengthening to FN. To test whether the engagement of αV-class integrins promoted activation of α5β1 integrins, we attached ICAP-1 KO MEFs to VN-coated cantilevers and characterized their adhesion to FN (Supplementary Figure 4-7a). Although these fibroblasts had constitutively active α5β1 integrins[27], adhesion of VN-stimulated ICAP-1 KO MEFs was still enhanced compared to non-stimulated ICAP-1 KO MEFs and WT MEFs. Thus, this result suggests that the crosstalk between αV-class and α5β1 integrins involves integrin-mediated signaling pathways. To identify the key signaling molecules/pathways involved in this crosstalk, we interfered with the functions of (i) integrin-associated molecules including talin, kindlin and integrin linked kinase (ILK), (ii) actomyosin system including RhoA, Rho associated protein kinase (ROCK) and myosin-II, and (iii) actin nucleators including formins and Arp2/3, and measured the consequences on fibroblast adhesion to FN (Figure 4-3). Talin1/2-, kindlin1/2-, ILK-deficient fibroblasts and SMIFH2-treated (to inhibit formins) pKO-αV/β1 fibroblasts showed negligible adhesion to FNIII7–10, irrespective whether they were attached to VN- or ConA-coated cantilevers. Treatment of pKO-αV/β1 fibroblasts with C3 toxin to inhibit RhoA, Y27632 to inhibit ROCK, CK666 to inhibit Arp2/3, or blebbistatin to inhibit myosin-II had no effect on adhesion of ConA-attached pKO-αV/β1 fibroblasts. However, each of these treatments diminished adhesion of VN-stimulated pKO-αV/β1 fibroblasts to FNIII7–10 to the level of non-stimulated pKO-αV/β1 fibroblasts attached to ConA-coated cantilevers (Figure 4-3). Moreover, the treatments with Y16 to block RhoA, H1152P to block ROCK, and CK869 to block Arp2/3 produced a similar reduced adhesion strength of VN-stimulated but not of non-stimulated ConA-attached pKO-αV/β1 fibroblasts to FNIII7-10 (Supplementary Fig. 7b), supporting a role of RhoA/ROCK and Arp2/3 in VN-stimulated enhancement of fibroblast adhesion. Interestingly, treatment of VN-stimulated or non-stimulated pKO-αV/β1 fibroblasts with either ML-7 to inhibit MLC kinase,

S-trity-L-cysteine (STC) to inhibit kinesin Eg5[28], glycerol (Gly) or DMSO did not effect adhesion to FNIII7–10 (Fig. 3). In summary, these results suggest that RhoA/ROCK driven myosin-II activity and Arp2/3 take important roles in facilitating the crosstalk from αV-class integrins to α5β1 integrins.

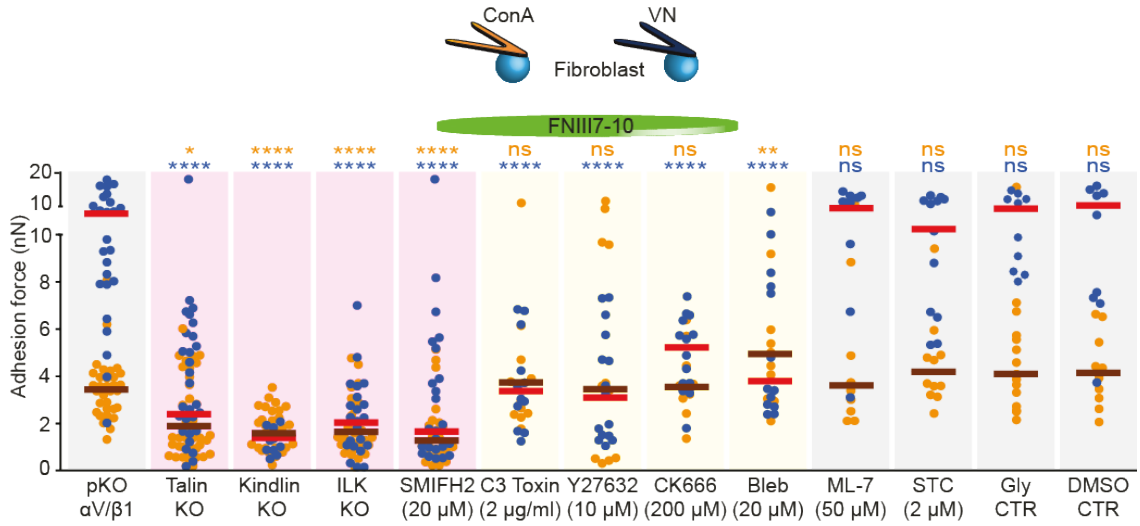

Figure 4-3 Role of signaling molecules for the development of α5β1 and αV-class integrin-mediated adhesion forces. Adhesion forces of knockout (KO) or pKO-αV/β1 fibroblasts to FNIII7–10 were determined both in the absence and presence of specific chemical inhibitors. pKO-αV/β1, talin KO, kindlin KO, ILK KO fibroblasts and pKO-αV/β1 fibroblasts treated with chemical inhibitors were attached to either ConA (yellow)- or VN (blue)-coated cantilevers. If not stated pKO-αV/β1 fibroblasts were used for experiments. Fibroblasts were adhered to FNIII7–10-coated substrates for 120 s. Chemical inhibitors were added at indicated concentrations to pKO-αV/β1 fibroblasts starting 30 minutes prior to experiments, with the exception of C3 toxin, which was added 3 h before. S-trityl-L-cysteine (STC), glycerol (Gly) and DMSO were used as negative controls (CTR) to measure the adhesion of pKO-αV/β1 fibroblasts. For VN-stimulating fibroblasts, cantilevers were coated by 5 μg ml–1 VN diluted in ConA. Dots show adhesion forces of single fibroblasts (n ≥ 10 for each condition) and red bars their median. Statistical significance was determined to compare unperturbed and perturbed adhesion for each (non-stimulated and VN-stimulated) condition by two-tailed Mann-Whitney U-tests (****, P<0.0001; ***, P<0.001; **, P<0.01; * P<0.05; ns, P≥0.05).

4.3.4. Engagement of αV-class integrins clusters α5β1 integrins

We have observed that αV-class integrin signaling contributed to α5β1 integrin-mediated fibroblast adhesion to FN. Next, we tested whether αV-class integrin engagement induces clustering of α5β1 integrins, by combining SCFS with TIRF microscopy to visualize GFP-tagged paxillin clusters in fibroblasts adhering to FNIII7–10 substrates, for contact times ranging from 5 to 500 s (Figure 4-4)[29]. Irrespective, whether pKO-αV, pKO-β1 andpKO-αV/β1 were attached on VN- or ConA–coated cantilevers, the size and occurrence of the paxillin-positive clusters increased for the first ≈ 40 s of contact time and remained constant thereafter. Strikingly, the intensity/size of paxillin-positive clusters in VN-stimulated pKO-αV/β1 fibroblasts adhering to FNIII7–10 was higher compared to any other condition, indicating that VN-binding of αV-class integrins at the cantilever triggered robust α5β1 integrin clustering at the opposing FNIII7–10 substrate (Figure 4-4 and Supplementary Table 4-1).Interestingly, ConA-attached pKO-αV and ConA-attached pKO-αV/β1 fibroblasts showed comparable intensities of paxillin clusters, further supporting that αV-class integrins dominate early fibroblast adhesion to FN. Surprisingly,

although ConA-attached pKO-β1 fibroblasts exhibited higher adhesion to FNIII7–10, compared to pKO-αV and pKO-αV/β1 fibroblasts (Figure 4-1a), they assembled paxillin-positive adhesion clusters with lowest intensities (Figure 4-4), suggesting that the affinity of α5β1 integrin for FN is influenced by the absence of αV-class integrins.

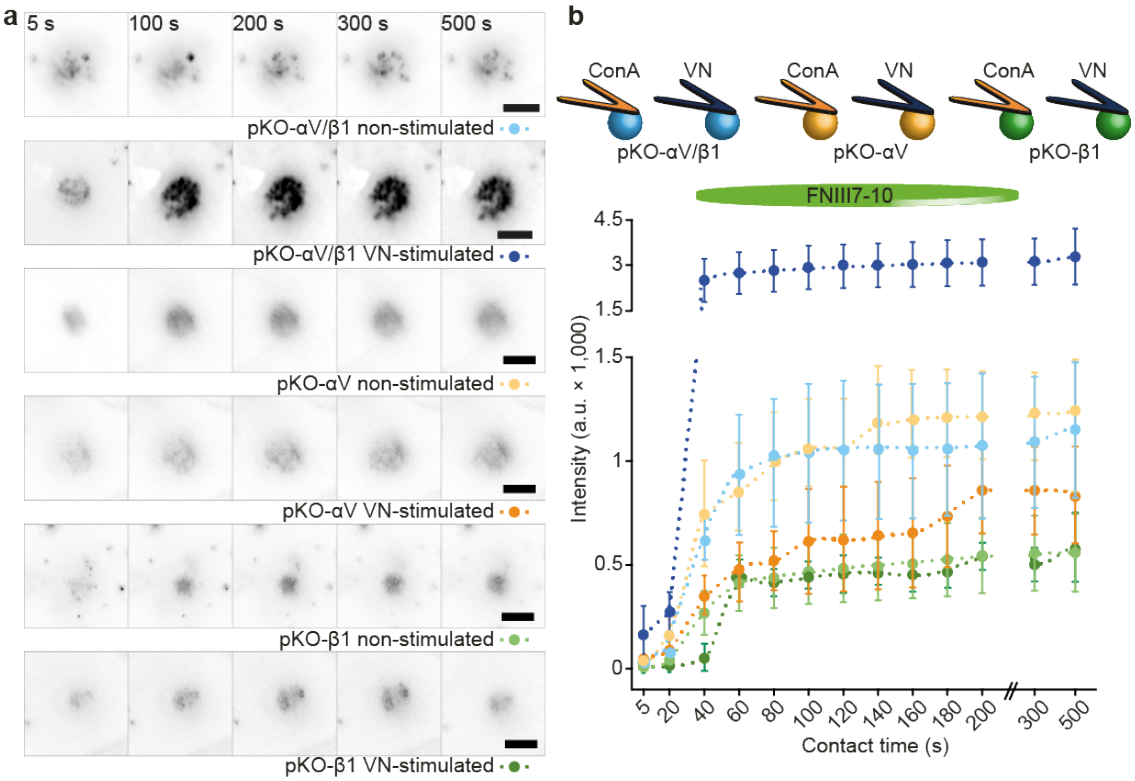

Figure 4-4 Engagement of αV-class integrins induces α5β1 integrin clustering. (a) Time series of TIRF images of GFP-labeled paxillin expressed in pKO-αV/β1 (blue), pKO-αV (yellow) and pKO-β1 (green) fibroblasts adhering to FNIII7-10-coated substrates. To record the images, single fibroblasts were attached to ConA- (non-stimulated) or VN-coated (stimulated) cantilevers, incubated for 7-10 min and then approached to the FNIII7–10-coated substrate. Paxillin-GFP-intensity was detected by TIRF microscopy after 5 s and then after every 20 s for up to 500 s contact time with the substrate. To stimulate fibroblasts by VN, cantilevers were coated using 5 µg ml^{-1} VN diluted in ConA. Scale bars, 10 µm. (b) Paxillin-GFP-intensity over contact time. The data was taken from TIRF images such as shown here and the statistical analysis of the data is given in Supplementary Table 1. Dots show mean fluorescence intensities of fibroblasts and error bars show s.e.m (n ≥ 10 for each condition).

4.4. Discussion

The establishment of cell adhesion is a tightly regulated process, which is governed by the binding of integrins to the ECM. Here, we report that different FN-binding integrin classes establish distinct adhesion profiles during the initiation of cell adhesion to FN. In the early phase of adhesion formation (< 2 min), fibroblasts expressing only α5β1 integrins establish stronger adhesion to FN compared to αV-class integrins, which is in line with previous reports reporting stronger adhesion promoting function of α5β1 integrins compared to αV-class integrins[30]. However, we also observe that fibroblasts expressing both FN-binding integrin classes establish considerably lower adhesion strengths compared to fibroblasts expressing only α5β1 integrins. This

finding of a 'differential integrin-dependent adhesion' was surprising since both fibroblast lines express comparable numbers of αV-class and α5β1 integrins on their cell surface and expression of both integrins was shown to establish strongest adhesion after a contact time of more than an hour[6].

Integrins crosstalk among each other and other cell adhesion molecules, such as ephrins and cadherins[31,32,30], to perfectly adjust cell adhesion to the ECM. Our experiments identify a novel crosstalk between αV-class and α5β1 integrins to establish and strengthen early cell adhesion to FN. When initiating cell adhesion to FN, αV-class integrins compete with α5β1 integrins for substrate binding. We observe that αV-class integrins show a higher binding rate ("on-rate") to FN, which initially prevents α5β1 integrins from binding. In line with our results, earlier studies reported that αVβ3 integrins prevent the recruitment of α5β1 integrins to adhesion sites at early cell spreading[14]. This competition for FN-binding could be due to differences in extracellular ligand binding and/or interactions of integrin β-tails with cytoplasmic proteins such as talin[13], kindlin[26] and/or inhibitory adapter proteins[33]. It has been demonstrated that despite the presence of αVβ3 integrins, mutation in the talin binding site in β3-integrin leads to the predominant engagement α5β1 integrins to FN[14]. In our results β1- and β3-tails showed equivalent binding to talin and the adhesion of ICAP-1 deficient fibroblasts to FNIII7-10 was higher than that of wild-type fibroblasts. This finding suggests that ICAP-1 hinders the binding of talin or kindlin to β1-tail during adhesion initiation[26] and thereby increases the available pool of talin/kindlin for αV-class integrins to bind and to initiate adhesion. After initiating adhesion and engaging the substrate, αV-class integrins signal to α5β1 integrins to induce their clustering and to establish adhesion to FN, which is much stronger and faster than the adhesion established by both integrin classes in the absence of the crosstalk (Supplementary Figure 4-5). Eventually, the adhesion strengthens with time and develops into adhesion sites, in which α5β1 and αV-class integrins separate into different compartments[8]. Although, the distinct roles of and the cooperativity among β1- and αV-class integrins have been extensively studied during adhesion maturation[11,6,12,14] and in response to force[34], here, we show that both FN-binding integrins interplay from the early onset of adhesion.

Our data demonstrates that already within the first two minutes of early fibroblast adhesion, FN-binding integrins critically depend on integrin-associated proteins such as talin, kindlin and ILK[35,36]. However, it was surprising to observe that formin inhibition also affected early cell adhesion. A recent report showing that the formin homology 2 domain containing 1 (FHOD1) is required for the formation of early integrin clusters during cell spreading and migration[37] is in line with our finding. We also found that RhoA, ROCK and Arp2/3 are primarily required for the crosstalk between both FN-binding integrins. Interestingly, myosin-II is also involved in the crosstalk, although it appears to be regulated not *via* myosin light chain kinase (MLCK). The crosstalk αV-class and α5β1 integrins was further augmented in the absence of ICAP-1 suggesting that constitutively active β1 integrins[27] bind FN even much more stronger in response to

signaling originating from engaged αV-class integrins. This observation suggests that interactions at the cytoplasmic domains might play a pivotal role in the crosstalk.

We also observed that Arp2/3, a key component stimulating actin nucleation and polymerization[38], is required for the crosstalk between αV-class and α5β1 integrins. During adhesion, Arp2/3 is recruited to vinculin[39], and therefore perturbation of Arp2/3 could affect this interaction and impair adhesion of fibroblasts to FN. Interestingly, Arp2/3 inhibition specifically reduced VN-stimulated fibroblast adhesion to FN, suggesting that Arp2/3 in the Rac1/Wave/Arp2/3 pathway[6] affects the crosstalk from αV-class to α5β1 integrins. Our results do not allow to distinguish whether the RhoA/ROCK pathway[6] and Rac1/Wave/Arp2/3 pathway[6] regulate the crosstalk by affecting αV-class integrins and/or α5β1 integrins. Previous reports suggested that the RhoA/ROCK pathway is dominated by α5β1 integrins[6] suggesting that RhoA inhibition operates upstream and/or downstream of FN-bound α5β1 integrins. Thus, these pathways not only control established adhesion but also influence adhesion initiation (i.e. the binding probability of αV-class and/or α5β1 integrins) and hence the integrin crosstalk.

Our data also implies that myosin-II activity is required for the crosstalk between both FN-binding integrins. Myosin-II triggers mechanical signals required to promote adhesion maturation[40]. The myosin-II requirement argues that αV-class integrin signaling can regulate α5β1 integrin clustering. SCFS combined with TIRF microscopy provided insight into the formation of adhesion clusters by integrins. In response to αV-class integrin engagement, α5β1 integrins enhanced binding to FN and formed adhesion clusters that considerably strengthened early fibroblast adhesion within ≤ 120 s. Although, we clearly observed the formation of paxillin clusters in VN-stimulated fibroblast adhering to FN, the lateral resolution limit of TIRF does not allow us to determine their sizes. Hence, SCFS combined with super resolution microscopy will be necessary to further characterize the assembly of adhesion clusters[41,42].

In summary, our study provides direct evidence that αV-class integrins adhering to VN- or FN-coated cantilevers signal to α5β1 integrins to bind FN at the opposite side of the fibroblast and to form adhesion clusters. Hence, we deduced a model to depict the two-step process by which αV-class integrins crosstalk with α5β1 integrins to establish and to strengthen cell adhesion to FN (Figure 4-5). In the first step, αV-class integrins initiate cell adhesion by binding FN quicker than α5β1 integrins. The engagement of αV-class integrins to VN (or FN) clusters, recruits and activates adhesion-specific proteins including talin, kindlin, ILK and formins to mediate the link to the actin cytoskeleton (Figure 4-5). In a second step, the engaged αV-class integrins activate signaling involving the RhoA/Rock and the Rac1/Wave/Arp2/3 pathways that finally promote α5β1 integrins binding to FN. Gradually, the adhesion strengthens and matures by clustering and separating α5β1 integrins *via* myosin-II into different FA compartments (Figure 4-5).

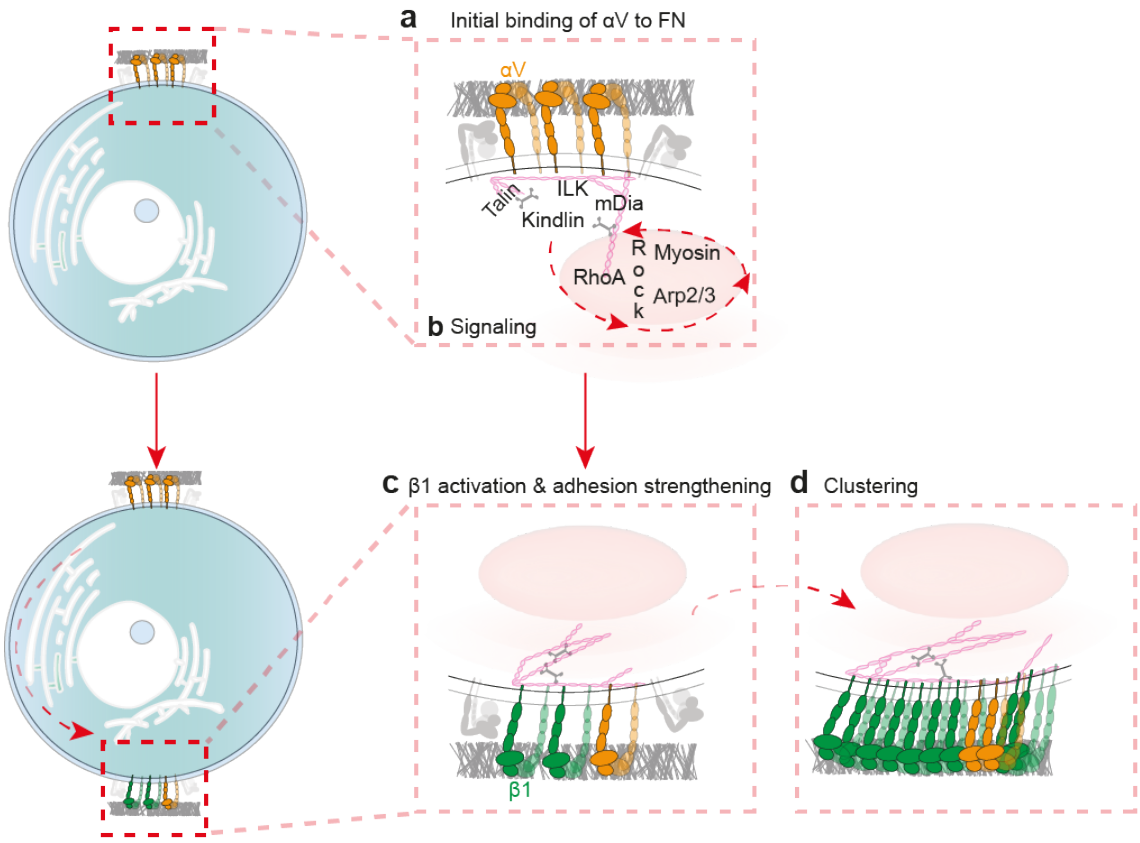

Figure 4-5 αV-class integrins compete with α5β1 integrins for the binding of FN and after engagement, crosstalk to α5β1 integrins to strengthen adhesion to FN. (a) As fibroblasts initiate contact with FN, αV-class integrins successfully compete with α5β1 integrins to bind the substrate. (b) This binding engages αV-class integrins and recruits integrin-associated proteins such as talin, kindlin, ILK and formins to the adhesion site. Upon recruitment, the integrin-associated proteins mediate and strengthen the attachment of integrins to the actomyosin cortex. To strengthen fibroblast adhesion, activated αV-class integrins *via* the RhoA/ROCK/myosin-II and Arp2/3 pathway signal to (c) α5β1 integrins to bind FN thereby forming new adhesion sites. (d) Consequently, α5β1 integrins cluster to strengthen adhesion. This crosstalk eventually leads to the formation of nascent adhesions. Recent structural investigations suggested that inactive α5β1 integrins can co-exist in bent and unbent conformations, while inactive αV-class integrins have shown to be bent[51]. Thus, for simplicity we here illustrate inactive integrins in the bent confirmations (grey) and active/engaged integrins in the extended conformation (colored).

4.5. Methods

4.5.1. Cell Culture.

pKO, pKO-αV/β1, pKO-αV/β1 lifeact-mCherry paxillin-GFP, pKO-αV, pKO-αV lifeact-mCherry paxillin-GFP, pKO-β1, pKO-β1 lifeact-mCherry paxillin-GFP[6], talin KO, kindlin KO[41] and ILK KO[44] mouse kidney fibroblasts and ICAP-1 KO, ICAP-1 WT[27] mouse embryonic fibroblast cell lines were maintained in DMEM (Gibco-Life technologies, NY, USA), supplemented with 10% (v/v) fetal calf serum (FCS, Sigma, Steinheim, Germany), 100 units ml^{-1} penicillin and

100 µg ml^{-1} streptomycin (both Gibco-Life technologies). Fibroblasts were grown on fibronectin (FN, Calbiochem-Merck, Darmstadt, Germany) coated tissue culture flasks (Jet BioFil, Guangzhou, China) in a humidifying incubator with 5% CO_2 at 37°C. For SCFS, fibroblasts were grown on 24 well plates (Thermo Scientific, Roskilde, Denmark) and serum-starved overnight before measurements. The fibroblasts were regularly tested for mycoplasma contamination.

4.5.2. Expression and purification of fibronectin (FN) fragments.

FN fragment FNIII7-10, RGD-deleted FN fragment FNIII7-10ΔRGD and synergy site mutated FN fragment FNIII7–10-mSYN were expressed from plasmid pET15b-FNIII7–10 and pET15b-FNIII7–10ΔRGD[45] in *E.coli* BL21 (DE3) pLysS[45]. Briefly, cells were grown in Lennox L broth (Invitrogen, Carlsbad, USA) supplemented with 100 µg ml^{-1} ampicillin (Sigma-Aldrich, Buchs, Switzerland) at 37°C. Expression was induced with 1 mM isopropyl thiogalactose (IPTG, Sigma) at optical density $(OD)_{600}$ = 0.6. Cells were harvested after 4 h, re-suspended in buffer (20 mM Tris-HCl, 150 mM NaCl, pH 8.0), and broken by sonication. Cell debris was removed by ultracentrifugation at 40'000x g for 45 minutes. The soluble protein fraction was bound to nickel-nitrilotriacetic acid resin (Protino® Ni-NTA Agarose, MACHEREY-NAGEL, Düren, Germany) for 1 h at 4°C. The resin was then loaded onto a column and washed with buffer (20 mM Tris-HCl, 150 mM NaCl, 10 mM imidazole, pH 8.0). FN fragments were eluted with elution buffer (20 mM Tris-HCl, 150 mM NaCl, 500 mM imidazole, pH 8.0). Peak fractions were pooled and dialyzed against washing buffer (20 mM Tris-HCl, 150 mM NaCl, pH 8.0). The protein concentration was adjusted to 1.0 mg ml^{-1} with dialyzing buffer and aliquots were stored at –20°C.

4.5.3. Cantilever and substrate functionalization.

For fibroblast attachment, cantilevers were plasma cleaned (PDC-32G, Harrick Plasma) and then incubated overnight at 4°C in PBS containing ConA (2 mg ml^{-1}, Sigma-Aldrich), VN (50 µg ml^{-1}, Calbiochem-Merck) or full-length FN (50 µg ml^{-1}, Calbiochem-Merck)[41]. For further dilutions, VN or FN stock solutions (50 µg ml^{-1}) were diluted to 0.05, 0.5 or 5 µg ml^{-1} with 2 mg ml^{-1} ConA in PBS. For substrate coatings, 200µm thick four-segmented polydimethylsilane (PDMS) mask fused to the surface of glass bottom Petri dishes (WPI) was used[46]. Each of the four PDMS framed glass surfaces were incubated overnight at 4°C either with the FN fragment $FN_{III}7–10$ (50 µg ml^{-1}), or RGD deleted FN fragment $FN_{III}7–10\Delta RGD$ (50 µg ml^{-1}), or VN (50 µg ml^{-1}) or full-length FN (50 µg ml^{-1}) all in PBS.

SCFS. For SCFS, we mounted an AFM (Nanowizard II equipped with CellHesion Module, JPK Instruments, Berlin, Germany) on an inverted fluorescence microscope[47] (Observer.Z1/A1, Zeiss, Germany). The temperature was kept at 37°C throughout the experiment by a Petri dish heater (JPK Instruments). 200 µm long tip-less V-shaped silicon nitride cantilevers having nominal spring constants of 0.06 N m^{-1} (NP-0, Bruker, USA) were used. Each cantilever was calibrated prior the measurement by determining its sensitivity and spring constant using the

thermal noise analysis of the AFM[48]. To adhere a single fibroblast to the AFM cantilever, overnight serum-starved fibroblasts with confluency up to ≈ 80% were washed with PBS and detached from the culture flask with 0.25% (w/v) trypsin (Sigma-Aldrich), for up to two minutes. Trypsinized fibroblasts were suspended in SCFS media (DMEM supplemented with 20 mM HEPES) containing 1% (v/v) FCS, pelleted and resuspended in serum free SCFS media[49]. Fibroblasts were allowed to recover for at least 30 minutes from trypsin treatment[50]. Functionalized Petri dishes were washed with SCFS media to remove unbound proteins. Adhesion of a single fibroblast to the free cantilever end was achieved by pipetting the fibroblast suspension onto the functionalized Petri dishes. The functionalized cantilever was lowered onto a fibroblast with a speed of 10 μm s^{-1} until a force of 5 nN was recorded. After ≈ 5 s contact, the cantilever was retracted with 10 μm s^{-1} for 50 μm and cantilever bound fibroblast was incubated for 7–10 minutes to assure firm binding to the cantilever. Using optical microscopy (DIC and phase contrast), the morphological state of the fibroblast was monitored. Adhesion measurements were only conducted using rounded fibroblast before they spread on the cantilever. For adhesion force experiments, the rounded fibroblast bound to the cantilever was lowered onto the coated substrate with a speed of 5 μm s^{-1} until a contact force of 2 nN was recorded. For contact times of 5, 20, 50 or 120 s, the cantilever height was maintained constant. Subsequently, the cantilever was retracted at 5 μm s^{-1} and for > 90 μm until the fibroblast and substrate were fully separated. After the experimental cycle, the fibroblast was allowed to recover for a time period equal to contact time before measuring the adhesion force for a different contact time. A single fibroblast was used to probe the adhesion force for all contact times or until morphological changes (i.e. spreading) was observed. The sequence of contact time measurements and area of the substrate were varied. The adhesion of at least 10 fibroblasts was measured per condition to obtain statistically firm results. Adhesion forces were determined after baseline correction of force-distance curves with JPK software (JPK Instruments). For single molecule sensitivity, we modified SCFS with low contact force (200 pN) and zero contact time. Force-distance curves were analyzed to determine binding probability using JPK software.

4.5.4. Statistical tests comparing the adhesion forces and slopes.

Unpaired t-tests: two-tailed Mann-Whitney tests were applied to determine significant differences between the median adhesion forces at the given contact times among different conditions. Tests were done using Prism (GraphPad, La Jolla, USA). To compare adhesion strengthening among different fibroblast lines, we determined the differences in their slopes describing the adhesion force over time. We defined the (discrete) slope between contact times t_1 and t_2 with corresponding adhesion force measurements F_1 and F_2 as $s_{2\text{-}1} = (F_2 - F_1) / (t_2 - t_1)$. For each fibroblast cell line, we defined the slope of the adhesion force-time data as the average slope of all adjacent time points. We generated 100 bootstrap samples from the original data in order to

obtain samples of equal size and tested for differences in slope between fibroblast cell lines using two-tailed Wilcoxon's test.

4.5.5. Analysis of statistical interactions between integrins.

For each time point, the statistical interaction strength between the αV-class and α5β1 integrins with respect to adhesion force is defined as $\varepsilon = F_{\text{pKO-}\alpha\text{V}/\beta1} + F_{\text{pKO}} - F_{\text{pKO-}\alpha\text{V}} - F_{\text{pKO-}\beta1}$, where F denotes the adhesion force. The quantity ε is the deviation of the expected effect of both integrins under an additive null model, namely $F_{\text{pKO-}\alpha\text{V}} + F_{\text{pKO-}\beta1}$, from the observed effect, namely $F_{\text{pKO-}\alpha\text{V}/\beta1} + F_{\text{pKO}}$. If $\varepsilon > 0$, then there is a positive, whereas if $\varepsilon < 0$, then there is a negative interaction between αV-class and α5β1 integrins. Statistical testing of the null hypothesis of no interaction ($\varepsilon = 0$) was performed on 100 bootstrap samples using two-tailed Wilcoxon's test.

4.5.6. Immunoprecipitation of integrins.

For immunoprecipitation of β1 integrin, pKO-fibroblasts were washed twice with PBS and incubated with fresh crosslinking solution - 0.5 mM dithiobis-(succinimidyl proprionate) (DSP, Thermo scientific, USA) for 30 minutes at room temperature. DSP was quenched with 50 mM Tris-HCl pH 7.5 for 10 minutes. Fibroblasts were lysed in lysis buffer (50 mM Tris-HCl pH 8, 150 mM NaCl, 1% Triton X-100, 0,05% sodium deoxycholate) with protease and phosphatase inhibitors and sonicated. The samples were pre-cleaned with A/G Plus Agarose (Santa Cruz, Germany) protein for 15 minutes at 4°C. After centrifugation, 30 µg of protein was used as an input and 1 mg of cell lysate was incubated with 3 µl of anti-β1 integrin antibody[6] (rabbit-polyclonal, homemade) for 1 h at 4°C, followed by the addition of 50 µl A/G agarose protein for another hour, in an end-over-end rocker. After three washes with lysis buffer, the crosslink was reversed with 50 µl of 2X Laemmli sample buffer (homemade) containing 50 mM DTT (Sigma, Germany) for 30 minutes at 37°C. After this, 1 µl of beta-mercaptoethanol (Sigma) was added and samples were incubated for 5 minutes at 95°C. Samples were subjected to SDS-PAGE and western blot analysis against integrins using specific αV integrin (AB1930, Millipore, Germany), α5 integrin (#4705, Cell Signaling Technology, Germany) and β1 integrin (homemade[6]) antibodies with the dilution of 1:1000.

4.5.7. Integrin β-tail peptide pull downs.

Pull downs were performed with the following peptides: β1 wild-type cytoplasmic tail peptide (HDRREFAKFEKEKMNAKWDTGENPIYKSAVTTVVNPKYEGK-OH), β1 scrambled peptide (NYEEKKHDEYATKNNKAVKGPMESGIRFTWRVVKEPFKATD-OH), β3 wild-type cytoplasmic tail peptide (HDRKEFAKFEEERARAKWDTANNPLYKEATSTFTNITYRGT-OH), β3 scrambled (RRIESFNAGKTEEDRANTYWLAFPEETKYRAHKTTDTFNAK-OH). All peptides were desthiobiotinylated. Prior to use, peptides were immobilized on Dynabeads MyOne Streptavidin C1 (10 mg ml^{-1}, Invitrogen) for 3 h at 4 °C. pKO-αVβ1 fibroblasts were lysed on ice in

mammalian protein extraction reagent (Thermo Scientific, USA) and 1 mg of cell lysate was incubated with the indicated peptides overnight at 4 °C. After three washing steps with lysis buffer, we boiled the beads in SDS-PAGE sample buffer and loaded the supernatant on a 4–20% SDS-PAGE gel. Samples were analyzed by Western blot using specific antibodies against talin (T3287, Sigma, Germany) and kindlin-2 (MAB2617, Millipore, Germany) with the dilution of 1:1000. Uncropped scans of the Western blots are provided in Supplementary Fig. 8.

4.5.8. SCFS with inhibitors and antibodies.

For chemical perturbations, suspended fibroblasts were pre-incubated with the inhibitors: SMIFH2 (20 µM, Merck Millipore, Billerica, MA), Y27632 (10 µM, Sigma-Aldrich), H1152 (1.6 nM, Merck Millipore), CK666 (200 µM, Tocris Bioscience, Bristol, UK), CK869 (200 µM, Tocris Bioscience, Bristol, UK), C8 inhibitor[51] (1 µM, kind gift of William deGrado, UCSF), blebbistatin (20 µM, Sigma-Aldrich), ML-7 (50 µM, Tocris Bioscience, Bristol, UK) and STC (2 µM, Sigma-Aldrich) for 30 minutes in SCFS media at 37°C. To inhibit RhoA, fibroblasts were incubated with C3 toxin (2 µg ml^{-1}, Cytoskeleton, Denver, USA) or Y12 (30 µM, Merck Millipore) for 2 or 3 h, respectively, before the experiments. All reagents were dissolved in dimethylsulphoxide (DMSO) except cell permeable C3 toxin, which was dissolved in 50% (v/v) glycerol. As control we used 0.1% (v/v) DMSO. To block β1-integrins, trypsinised fibroblasts were incubated with α5β1 blocking antibody MAB2575 (Millipore, USA) for 30 minutes, prior to the experiments. To block β3-integrins, trypsinised fibroblasts were incubated with 1 µM cilengitide (Selleck Chemicals, Houston, TX, USA) for 30 minutes, prior to the experiments. SCFS was conducted in the presence of the respective drug/antibody in the stated concentrations.

4.5.9. Combined TIRF and SCFS.

TIRF microscopy was combined with an AFM-based SCFS (CellHesion200) mounted on an inverted microscope (Observer.Z1, Zeiss, Germany) with a 100X/1.45 a Plan-FLUOR objective (Zeiss). TIRF illumination was achieved by coupling a beam emitted by a solid-state laser (Sapphire 488 LP, 50 mW, Coherent) into a single mode fiber (coupler: HPUC-2-488-4.5AS-11, fiber: QPMJ-A3A, 3S-488-3.5/125-SAS-4, OZ Optics) connected to a slider TIRF condenser (Laser TIRF, Zeiss). An optimized GFP filter set (Chroma Technology Corp.) and 10% laser power using quantum dots (Crystalplex, USA) was used for TIRF. Images were recorded using a camera (Evolve, Photometrics) and imaging software (Axiovision, Zeiss). The experimental setup for TIRF combined SCFS using paxillin-GFP, lifeact-mCherry expressing pKO-αVβ1, pKO-αV and pKO-β1 fibroblasts was as described above except for an extended contact time of 500 s. TIRF images were acquired at initial 5 s and thereafter at 20 s intervals for the fibroblast attached to the cantilever, brought in contact with FNIII7-10.

4.5.10. Confocal laser scanning microscopy.

To determine localization of integrins, 24-well glass bottom plates (MatTek corporation, USA) were functionalized with 2 mg ml^{-1} ConA, or 50 μg ml^{-1} FN, or 5 μg ml^{-1} VN diluted in ConA or 50 μg ml^{-1} VN or 1 μM cilengitide (CiL). Overnight serum-starved fibroblasts were trypsinized and cell suspension in DMEM supplemented with 20 mM HEPES was pipetted onto functionalized 24-well glass bottom plates and allowed to spread for 10 or 90 minutes. The fibroblasts were rinsed thrice with PBS and fixed using 4% paraformaldehyde in PBS (Sigma-Aldrich) for 20 minutes at room temperature (RT). Fixed fibroblasts were permeabilized using PBS-T (0.1% Triton X-100 (Sigma-Aldrich) in PBS) for 30 minutes at RT and blocked using blocking buffer (2% bovine serum albumin (BSA, Sigma-Aldrich) in PBS-T) for 1 h at 37°C. Fibroblasts were incubated with anti-integrin β3 antibody (M031-0, emfret, Germany) and AlexaFluor 647-preconjugated anti-integrin β1 antibody (102214, BioLegend, USA) with the dilution of 1:25 in blocking buffer or with ptyr antibody (PY99, sc-7020, Santa Cruz, USA) with the dilution of 1:50 in blocking buffer overnight at 4°C. Secondary antibodies used for integrin β3 and phosphotyrosine were anti-rat AlexaFluor 488 (A11006, Life Technologies, USA) and anti-mouse AlexaFluor 647 (AB150115, Life Technologies, USA), respectively, diluted 1:100 in blocking buffer for 1 h at RT. Actin was stained using rhodamine-phalloidin (Life Technologies, USA) in dilution of 1:500 in blocking buffer for 1 h at RT. Fibroblasts were washed thrice with PBS after every step. Stained fibroblasts were treated with Prolong gold anti-fade reagent (Invitrogen AG, Switzerland) for 24 h at RT and analyzed with inverted confocal microscope (Nikon TiE) equipped with an A1R confocal laser scan head (Nikon, Switzerland) using a 63×/1.40 oil objective. Signals were collected sequentially and images were analyzed with NIS software (Nikon).

4.5.11. Code availability.

The procedures for comparing adhesion slopes and for assessing interactions were implemented in a code in the statistical programming language R, which is included in Supplementary Note 1.

4.5.12. Data availability.

The data that support the findings of this study are available from the corresponding author upon reasonable request.

4.6. Author Contribution

M.B., N.S., R.F. and D.J.M designed the experiments and wrote the paper. M.B. performed and analyzed most experiments. N.S. contributed to TIRF experiments. J.H. helped with experimental set-up and data analysis. H.B.S. and R.F. provided important reagents and/or analytical tools. G.P.C. performed immunoprecipitation experiments. N.B. wrote the R-code for statistical analysis. All authors discussed the experiments, read and approved the manuscript.

4.7. Acknowledgements

We thank J. Thoma and S. Weiser assisting in purification of fibronectin fragment cloning, expression and purification, V. Jäggin for FACS analysis and T. Horn for help with confocal microscopy. The work was supported by the Swiss National Science Foundation (Grants 31003A_138063 and 310030B_160225 to D.J.M.), and the ERC, DFG and Max Planck Society (to R.F.).

4.8. References

1. Campbell, I. D., Campbell, I. D., Humphries, M. J. & Humphries, M. J. Integrin Structure, Activation, and Interactions. *Cold Spring Harb Perspect Biol* **3,** a004994–a004994 (2011).
2. Winograd-Katz, S. E., Fässler, R., Geiger, B. & Legate, K. R. The integrin adhesome: from genes and proteins to human disease. *Nat. Rev. Mol. Cell Biol.* **15,** 273–288 (2014).
3. Cox, D., Brennan, M. & Moran, N. Integrins as therapeutic targets: lessons and opportunities. *Nat Rev Drug Discov* **9,** 804–820 (2010).
4. Hynes, R. O. Integrins: bidirectional, allosteric signaling machines. *Cell* **110,** 673–687 (2002).
5. Iwamoto, D. V. & Calderwood, D. A. Regulation of integrin-mediated adhesions. *Curr. Opin. Cell. Biol.* **36,** 41–47 (2015).
6. Schiller, H. B. *et al.* β1- and αv-class integrins cooperate to regulate myosin II during rigidity sensing of fibronectin-based microenvironments. *Nat. Cell Biol.* **15,** 625–636 (2013).
7. Pierschbacher, M. D., Hayman, E. G. & Ruoslahti, E. The cell attachment determinant in fibronectin. *Journal of Cellular Biochemistry* **28,** 115–126 (1985).
8. Morgan, M. R., Byron, A., Humphries, M. J. & Bass, M. D. Giving off mixed signals-Distinct functions of α 5β 1and α vβ 3integrins in regulating cell behaviour. *IUBMB Life* **61,** 731–738 (2009).
9. Blystone, S. D., Slater, S. E., Williams, M. P., Crow, M. T. & Brown, E. J. A molecular mechanism of integrin crosstalk: alphavbeta3 suppression of calcium/calmodulin-dependent protein kinase II regulates alpha5beta1 function. *J. Cell Biol.* **145,** 889–897 (1999).
10. Retta, S. F. *et al.* Cross talk between beta(1) and alpha(V) integrins: beta(1) affects beta(3) mRNA stability. *Mol. Biol. Cell* **12,** 3126–3138 (2001).
11. Balcioglu, H. E., van Hoorn, H., Donato, D. M., Schmidt, T. & Danen, E. H. J. The integrin expression profile modulates orientation and dynamics of force transmission at cell-matrix adhesions. *J. Cell Sci.* **128,** 1316–1326 (2015).
12. Missirlis, D. *et al.* Substrate engagement of integrins α5β1 and αvβ3 is necessary, but not sufficient, for high directional persistence in migration on fibronectin. *Scientific Reports* **6,** 23258 (2016).
13. Calderwood, D. A. *et al.* Competition for Talin Results in Trans-dominant Inhibition of Integrin Activation. *Journal of Biological Chemistry* **279,** 28889–28895 (2004).
14. Pinon, P. *et al.* Talin-bound NPLY motif recruits integrin-signaling adapters to regulate cell spreading and mechanosensing. *J. Cell Biol.* **205,** 265–281 (2014).
15. Harburger, D. S. & Calderwood, D. A. Integrin signalling at a glance. *J. Cell Sci.* **122,** 159–163 (2009).
16. Helenius, J., Heisenberg, C.-P., Gaub, H. E. & Müller, D. J. Single-cell force spectroscopy. *J. Cell Sci.* **121,** 1785–1791 (2008).
17. Taubenberger, A., Cisneros, D. A., Puech, P.-H., Müller, D. J. & Franz, C. M. Revealing early steps of alpha2beta1 integrin-mediated adhesion to collagen type I by using single-cell force spectroscopy. *Mol. Biol. Cell* **18,** 1634–1644 (2007).
18. Friedrichs, J., Helenius, J. & Müller, D. J. Stimulated single-cell force spectroscopy to quantify cell adhesion receptor crosstalk. *Proteomics* **10,** 1455–1462 (2010).
19. Orend, G., Huang, W., Olayioye, M. A., Hynes, N. E. & Chiquet-Ehrismann, R. Tenascin-C blocks cell-cycle progression of anchorage-dependent fibroblasts on fibronectin

through inhibition of syndecan-4. *Oncogene* **22,** 3917–3926 (2003).
20. Dechantsreiter, M. A. *et al.* N-Methylated Cyclic RGD Peptides as Highly Active and Selective α Vβ 3Integrin Antagonists. *J. Med. Chem.* **42,** 3033–3040 (1999).
21. Margadant, C., Kreft, M., de Groot, D.-J., Norman, J. C. & Sonnenberg, A. Distinct Roles of Talin and Kindlin in Regulating Integrin α5β1 Function and Trafficking. *Current Biology* **22,** 1554–1563 (2012).
22. Harburger, D. S. *et al.* Kindlin-1 and -2 Directly Bind the C-terminal Region of Integrin Cytoplasmic Tails and Exert Integrin-specific Activation Effects. *Journal of Biological Chemistry* **284,** 11485–11497 (2009).
23. Sun, Z. *et al.* Kank2 activates talin, reduces force transduction across integrins and induces central adhesion formation. *Nat. Cell Biol.* **18,** 941–953 (2016).
24. Müller, D. J., Helenius, J., Alsteens, D. & Dufrêne, Y. F. Force probing surfaces of living cells to molecular resolution. *Nat. Chem. Biol.* **5,** 383–390 (2009).
25. Bouvard, D. *et al.* Unraveling ICAP-1 function: Toward a new direction? *European Journal of Cell Biology* **85,** 275–282 (2006).
26. Brunner, M. *et al.* Osteoblast mineralization requires β1 integrin/ICAP-1–dependent fibronectin deposition. *J. Cell Biol.* **194,** 307–322 (2011).
27. Millon-Frémillon, A. *et al.* Cell adaptive response to extracellular matrix density is controlled by ICAP-1–dependent β1-integrin affinity. *J. Cell Biol.* **180,** 427–441 (2008).
28. Skoufias, D. A. *et al.* S-Trityl-L-cysteine Is a Reversible, Tight Binding Inhibitor of the Human Kinesin Eg5 That Specifically Blocks Mitotic Progression. *Journal of Biological Chemistry* **281,** 17559–17569 (2006).
29. Brown, M. C., Perrotta, J. A. & Turner, C. E. Identification of LIM3 as the principal determinant of paxillin focal adhesion localization and characterization of a novel motif on paxillin directing vinculin and focal adhesion kinase binding. *J. Cell Biol.* **135,** 1109–1123 (1996).
30. Roca-Cusachs, P., Gauthier, N. C., del Rio, A. & Sheetz, M. P. Clustering of α5β1 integrins determines adhesion strength whereas αvβ3 and talin enable mechanotransduction. *Proc. Natl. Acad. Sci. U.S.A.* **106,** 16245–16250 (2009).
31. Yu, M., Wang, J., Müller, D. J. & Helenius, J. In PC3 prostate cancer cells ephrin receptors crosstalk to [bgr]1-integrins to strengthen adhesion to collagen type I. *Scientific Reports* **5,** 8206 (2015).
32. Schwartz, M. A. & Ginsberg, M. H. Networks and crosstalk: integrin signalling spreads. *Nat. Cell Biol.* **4,** E65–E68 (2002).
33. Liu, W., Draheim, K. M., Zhang, R., Calderwood, D. A. & Boggon, T. J. Mechanism for KRIT1 Release of ICAP1-Mediated Suppression of Integrin Activation. *Mol. Cell* **49,** 719–729 (2013).
34. Elosegui-Artola, A. *et al.* Rigidity sensing and adaptation through regulation of integrin types. *Nat. Mater.* **13,** 631–637 (2014).
35. Calderwood, D. A., Campbell, I. D. & Critchley, D. R. Talins and kindlins: partners in integrin-mediated adhesion. *Nat. Rev. Mol. Cell Biol.* **14,** 503–517 (2013).
36. Widmaier, M., Rognoni, E., Radovanac, K., Azimifar, S. B. & Fässler, R. Integrin-linked kinase at a glance. *J. Cell Sci.* **125,** 1839–1843 (2012).
37. Iskratsch, T. *et al.* FHOD1 Is Needed for Directed Forces and Adhesion Maturation during Cell Spreading and Migration. *Dev. Cell* **27,** 545–559 (2013).
38. Welch, M. D., DePace, A. H., Verma, S., Iwamatsu, A. & Mitchison, T. J. The human Arp2/3 complex is composed of evolutionarily conserved subunits and is localized to cellular regions of dynamic actin filament assembly. *J. Cell Biol.* **138,** 375–384 (1997).
39. DeMali, K. A., Barlow, C. A. & Burridge, K. Recruitment of the Arp2/3 complex to vinculin: coupling membrane protrusion to matrix adhesion. *J. Cell Biol.* **159,** 881–891 (2002).
40. Geiger, B., Spatz, J. P. & Bershadsky, A. D. Environmental sensing through focal adhesions. *Nat. Rev. Mol. Cell Biol.* **10,** 21–33 (2009).
41. Theodosiou, M. *et al.* Kindlin-2 cooperates with talin to activate integrins and induces cell spreading by directly binding paxillin. *eLIFE* **5,** e10130 (2016).
42. Changede, R., Xu, X., Margadant, F. & Sheetz, M. P. Nascent Integrin Adhesions Form on All Matrix Rigidities after Integrin Activation. *Dev. Cell* **35,** 614–621 (2015).
43. Böttcher, R. T., Lange, A. & Fässler, R. How ILK and kindlins cooperate to orchestrate

integrin signaling. *Curr. Opin. Cell. Biol.* **21,** 670–675 (2009).
44. Takahashi, S. *et al.* The RGD motif in fibronectin is essential for development but dispensable for fibril assembly. *J. Cell Biol.* **178,** 167–178 (2007).
45. Yu, M., Strohmeyer, N., Wang, J., Müller, D. J. & Helenius, J. Increasing throughput of AFM-based single cell adhesion measurements through multisubstrate surfaces. *Beilstein J. Nanotechnol.* **6,** 157–166 (2015).
46. Puech, P.-H., Poole, K., Knebel, D. & Müller, D. J. A new technical approach to quantify cell–cell adhesion forces by AFM. *Ultramicroscopy* **106,** 637–644 (2006).
47. Hutter, J. L. & Bechhoefer, J. Calibration of atomic-force microscope tips. *Rev. Sci. Instrum.* **64,** 1868 (1993).
48. Friedrichs, J., Helenius, J. & Müller, D. J. Quantifying cellular adhesion to extracellular matrix components by single-cell force spectroscopy. *Nat. Protoc.* **5,** 1353–1361 (2010).
49. Schubert, R. *et al.* Assay for characterizing the recovery of vertebrate cells for adhesion measurements by single-cell force spectroscopy. *FEBS Lett.* 1–10 (2014). doi:10.1016/j.febslet.2014.06.012
50. Reed, N. I. *et al.* The αvβ1 integrin plays a critical in vivo role in tissue fibrosis. *Sci Transl Med* **7,** 288ra79–288ra79 (2015).
51. Su, Y. *et al.* Relating conformation to function in integrin α5β1. *Proc. Natl. Acad. Sci. U.S.A.* **113,** 201605074–E3881 (2016).

4.9. Supplementary Information

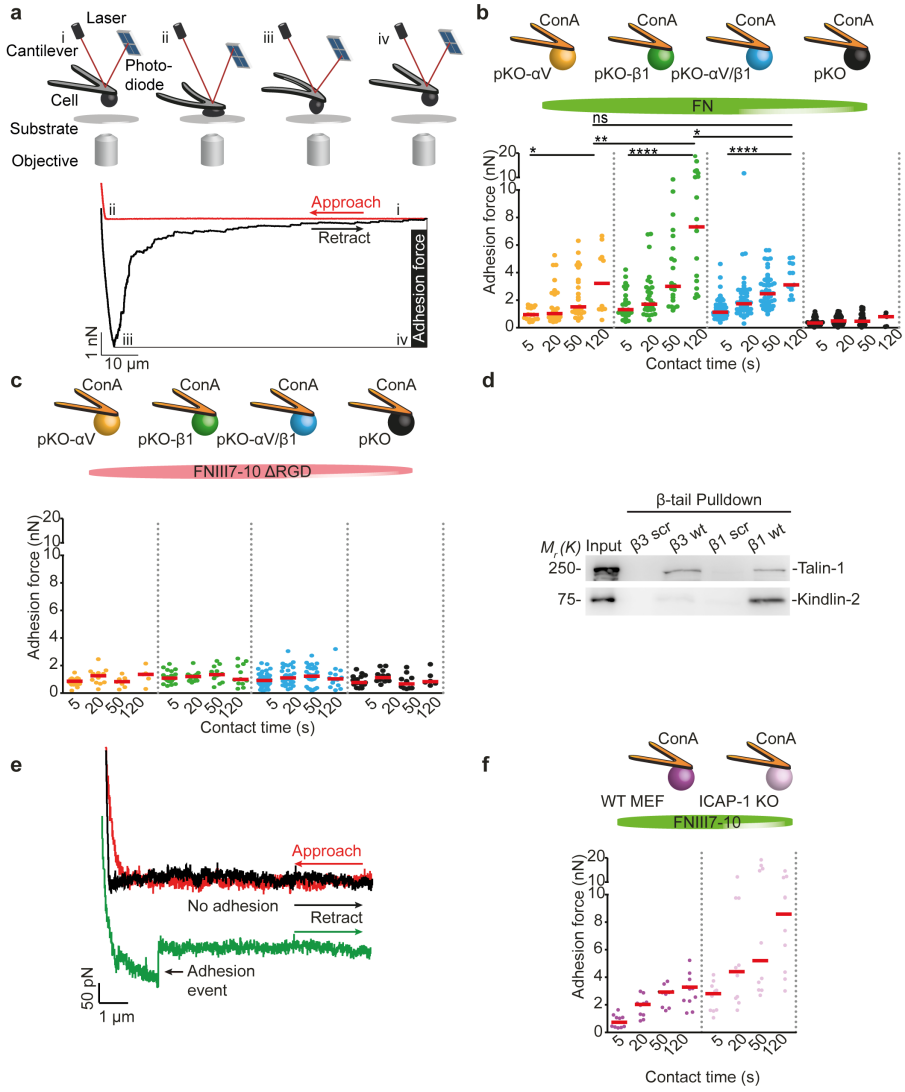

Supplementary Figure 4-1 Differential contribution α5β1 and αV-class integrins to the early adhesion of mouse kidney fibroblasts. (a) AFM-based single-cell force spectroscopy (SCFS) to characterize the adhesion of fibroblasts. (i) A single fibroblast is immobilized on a concanavalin A (ConA)-functionalized cantilever for 7-10 minutes. (ii) The cantilever-attached fibroblast is approached to a functionalized substrate until reaching a preset contact force (≈ 2 nN). Then, the cantilever height is maintained for a defined contact time. (iii-iv) Subsequently, the cantilever is retracted to separate fibroblast and substrate. The force deflecting the cantilever and the distance travelled by the cantilever is displayed in a force-distance curve. During retracting the cantilever, the adhesion force is measured. (b,c) Adhesion force of four different fibroblast lines, expressing either αV-class integrins (pKO-αV, yellow), or α5β1 integrins (pKO-β1, green), or α5β1 and αV-class integrins (pKO-αV/β1, blue), or pan-integrin knockout (pKO, black) was characterized by SCFS. The adhesion of fibroblasts bound to ConA-functionalized cantilevers was measured to substrates coated by (b) full-length FN and (c) RGD-deleted FN fragments FNIII7–10ΔRGD for contact times ranging from 5–120 s. Dots show adhesion forces of single fibroblasts (n ≥ 10 for each condition) and red bars their median. Statistical significances were analyzed by two-tailed Mann-Whitney U-tests (****, $P < 0.0001$; ***, $P < 0.001$; **, $P < 0.01$; *, $P < 0.05$; *ns*, $P \geq 0.05$). (d) Western blot showing talin-1 and kindlin-2, binding to biotinylated β1- and β3-integrin tail peptides. Peptides with scrambled amino-acid sequences (β1 scr tail; β3 scr tail) were used as negative controls. WT, wild-type. Input, whole wild-type (WT) pKO-αV/β1 fibroblast lysate. (e) Force-distance curves representing the binding of single integrins of pKO-αV/β1 fibroblasts to a FN-coated substrate. To record single integrin binding events with SCFS, fibroblasts were approached to the substrate (red curve) at minimal contact force (200 pN) and contact

time (≈ 100ms) and then retracted (black/green curve). The green force-distance curve shows a single adhesion event while the black curve shows no adhesion event. (f) Adhesion forces of WT mouse embryonic fibroblasts (WT MEF, left panel) and ICAP-1 deficient MEF (ICAP-1 KO, right panel) to FNIII7-10-coated substrates are shown. Fibroblasts were attached to ConA-coated cantilevers. Dots show adhesion forces of single fibroblasts (n ≥ 10 for each condition) and red bars their median.

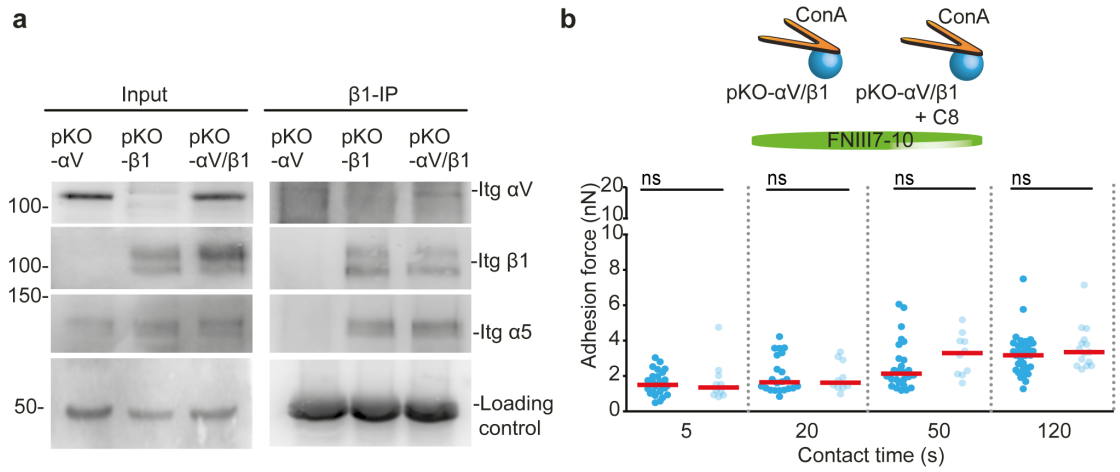

Supplementary Figure 4-2 αVβ1 integrins do not contribute to fibroblast adhesion to FN. (a) Total cell lysates (Input panel) and immunoprecipitated β1 integrin (β1-IP panel) were immunoblotted for αV, α5 and β1 integrins. We observed comparable amounts of αV-class and α5β1 integrins in all fibroblasts lines. The αVβ1 heterodimer was also detected but at considerably lower amounts compared to αV-class and α5β1 integrins in pKO-αV/β1 fibroblasts. (b) αVβ1 integrins do not play vital roles in early fibroblast adhesion to FNIII7–10. pKO-αV/β1 fibroblasts were incubated with C8 inhibitor for 30 minutes, then attached to ConA-coated cantilevers and finally approached to FNIII7–10 for contact times ranging from 5–120 s. The adhesion of C8 inhibitor treated fibroblasts was comparable to untreated. Dots show adhesion forces of single fibroblasts (n ≥ 10 for each condition) and red bars their median. Statistical significances were analyzed with two-tailed Mann-Whitney U-tests (****, $P < 0.0001$; ***, $P < 0.001$; **, $P < 0.01$; *, $P < 0.05$; *ns*, $P \geq 0.05$).

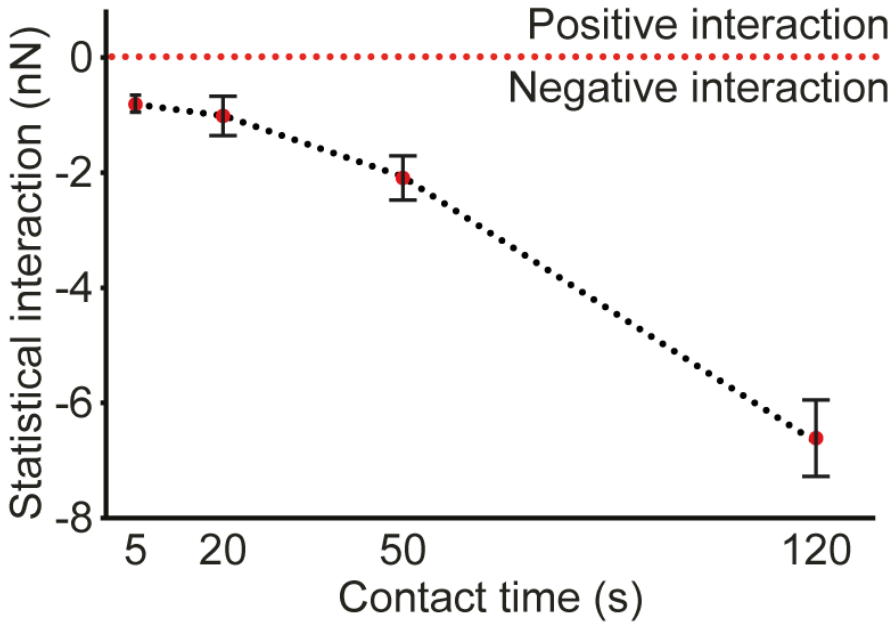

Supplementary Figure 4-3 Statistical interaction reveals that αV-class integrins suppress α5β1 integrins from binding to FN. Displayed is the statistical interaction measured as the deviation of the adhesion force from the expected additive effect of αV-class and α5β1 integrins when present together relative to the knockout pKO fibroblasts, for each contact time. The statistical interactions determined (see Methods) are significantly different from zero (and negative) at all four contact times, clearly showing a negative relationship with respect to adhesion force between αV-class and α5β1 integrins when present together. Red circles show mean values and error the s.e.m. (n = 100) The R-code used for the statistical analysis is shown in the Supplementary data.

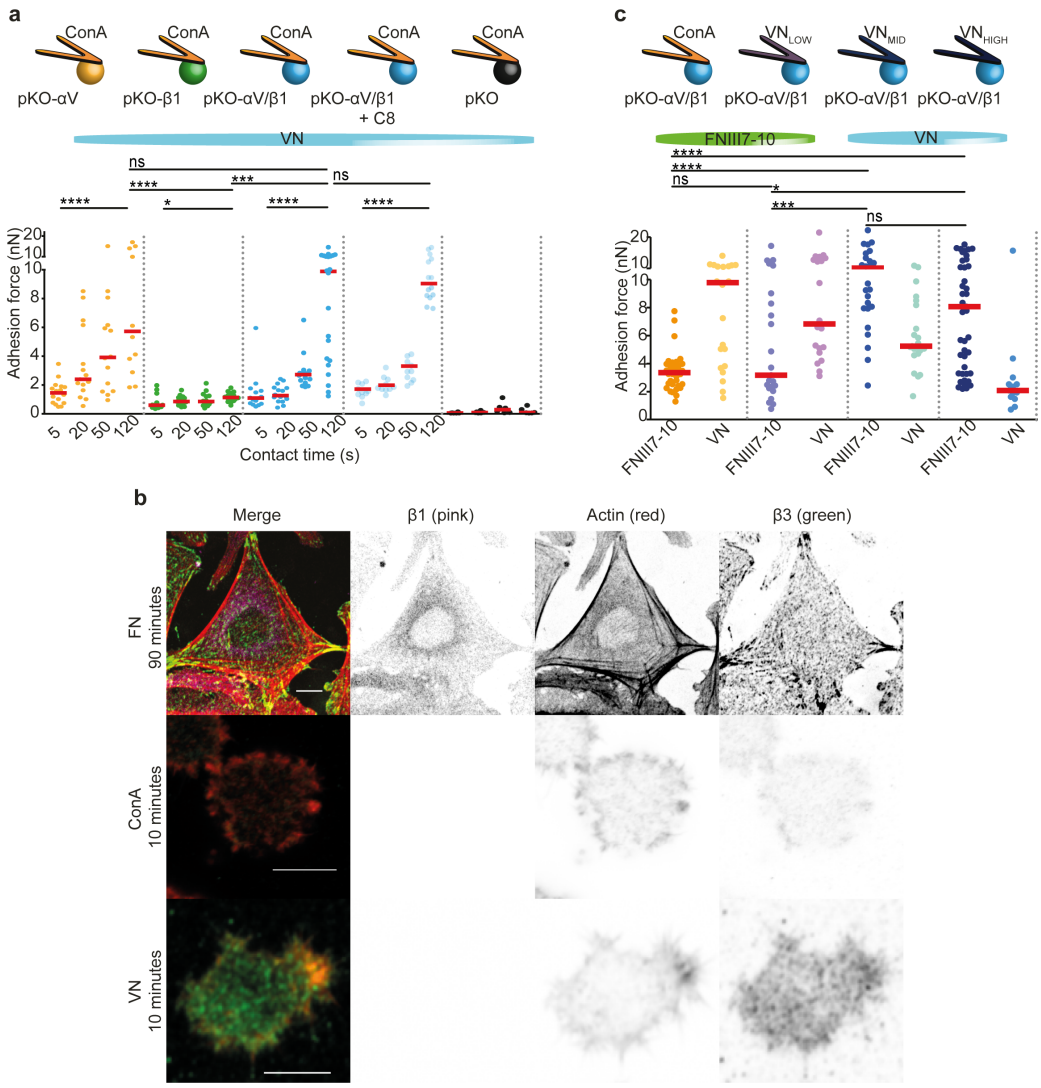

Supplementary Figure 4-4 αV-class integrins bind and cluster on VN. (a) Adhesion force of fibroblast lines expressing either αV-class integrins (pKO-αV, yellow), or α5β1 integrins (pKO-β1, green), or α5β1 and αV-class integrins (pKO-αV/β1, blue untreated and light blue C8 inhibitor treated) or pan-integrin knockout (pKO, black) contacted to VN-substrate for times ranging from 5–120 s. All fibroblasts were attached to ConA-functionalized cantilevers. (b) Immunofluorescence of pKO-αV/β1 fibroblasts seeded on VN (5 µg ml^{-1} VN diluted in ConA)-, ConA-, or FN-functionalized substrates. Fibroblasts adhering to VN, ConA for 10 minutes and to FN for 90 minutes were stained for αV-class integrin (green), actin (red) and β1 integrin (pink) using β3 integrin specific antibodies for the detection of αVβ3 integrins, β1 integrin antibody (Methods) and phalloidin. pKO-αV/β1 fibroblasts adhering to VN for 10 minutes mimic the condition of VN-stimulated fibroblasts, wherein fibroblast adhere for 7–10 minutes to VN-functionalized cantilevers. Clustered αV-class and α5β1 integrins on FN for 90 minutes were referred to as a positive control. Scale bars, 10 µm. (c) Fibroblasts enhance adhesion to FN upon VN-stimulation in a concentration-dependent manner. pKO-αV/β1 fibroblasts were attached to cantilevers coated either with ConA only or with VN concentrations of 0.5 µg ml^{-1} (VN_{LOW}), 5 µg ml^{-1} (VN_{MID}, used in experiments above), both diluted in ConA, or 50 µg ml^{-1} (VN_{HIGH}). Single fibroblasts were attached to the cantilever for 7–10 minutes, then approached to the FNIII7–10-coated substrate for 120 s and finally retracted to measure the adhesion force. At 120 s contact time to FNIII7–10-coated substrates, VN_{LOW}-stimulated pKO-αV/β1 fibroblasts established adhesion forces comparable to fibroblasts attached to ConA-coated cantilevers, whereas VN_{MID}- and VN_{HIGH}-stimulated pKO-αV/β1 fibroblasts considerably strengthened adhesion to FNIII7–10. These experiments show that increasing the VN-density/coating on the cantilever more αV-class integrins were recruited, which were thus unavailable for establishing adhesion to the VN-coated substrate located at the opposite side of the cell. Dots show adhesion forces of single fibroblasts (n ≥ 10 for each condition) and red bars their median. Statistical significances were calculated with two-tailed Mann-Whitney U-tests (****, $P < 0.0001$; ***, $P < 0.001$; **, $P < 0.01$; *, $P < 0.05$; *ns*, $P \geq 0.05$).

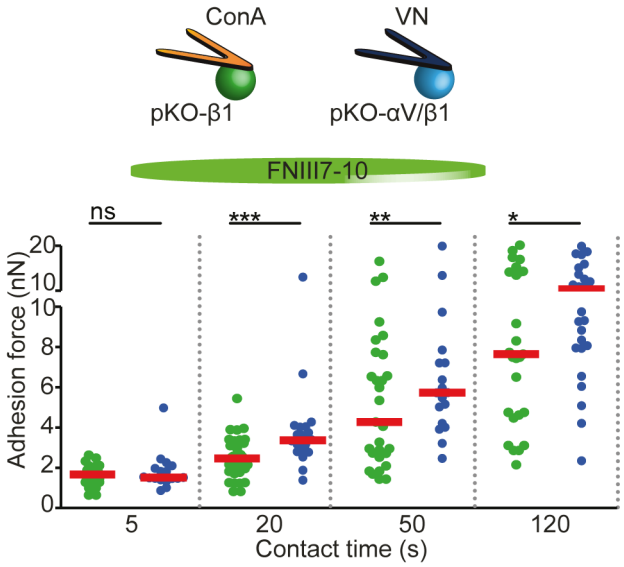

Supplementary Figure 4-5 αV-class integrins signal to regulate fibroblast adhesion to FN *via* β1 integrins. Adhesion forces of pan-integrin knockout (pKO) fibroblasts rescued with α5β1 integrins attached to ConA-coated cantilevers (pKO-β1, green) and α5β1 and αV-class integrins attached to VN-coated cantilevers (pKO-αV/β1, blue). VN-coated cantilevers were coated by 5 µg ml^{-1} VN diluted in ConA. Dots show adhesion forces of single fibroblasts (n ≥ 10 for each condition) and red bars their median. Statistical significances were calculated with two-tailed Mann-Whitney U-tests. ****, $P < 0.0001$; ***, $P < 0.001$; **, $P < 0.01$; *, $P < 0.05$; ns, $P \geq 0.05$.

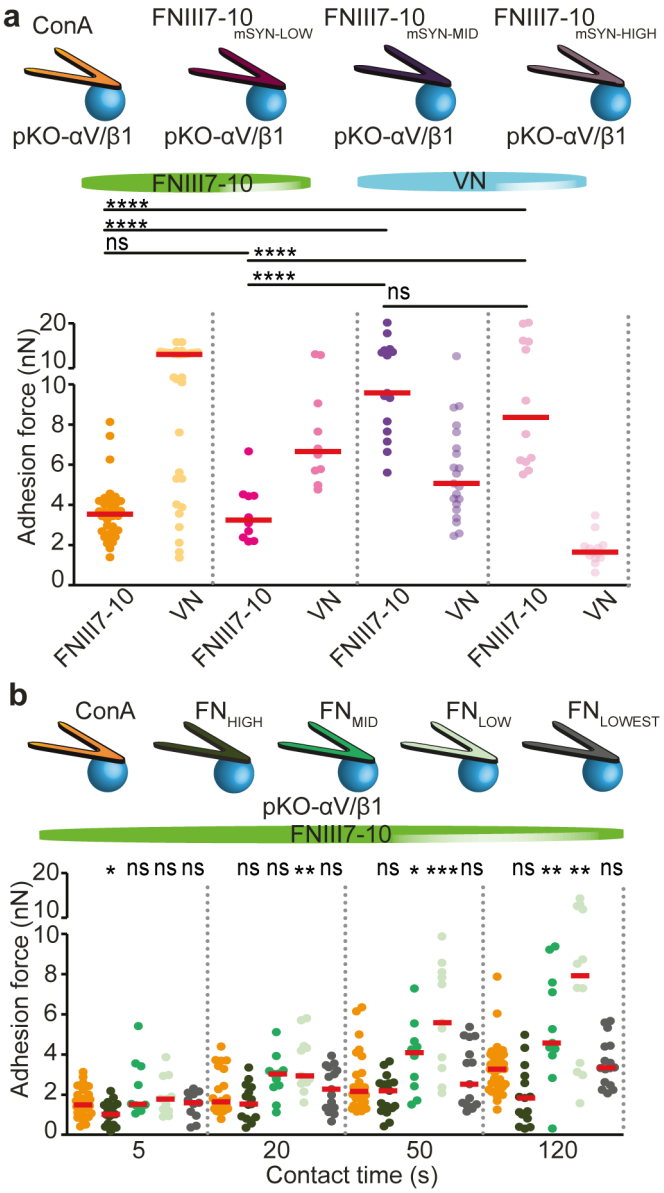

Supplementary Figure 4-6 FN can activate αV-class integrins to stimulate fibroblasts for strengthening adhesion to FN. FNIII7–10-mediated adhesion forces of pKO-αV/β1 fibroblasts attached either to (a) FN-fragment FNIII7–10 with mutated synergy site (FNIII7–10_{mSYN}) (b) or full length FN. pKO-αV/β1 fibroblasts either attached to a ConA-functionalized cantilever or to cantilevers functionalized with different FNIII7–10_{mSYN} or FN concentrations (FNIII7-$10_{mSYN\text{-}HIGH}$/ FN_{HIGH} 50 µg ml^{-1}, FNIII7-$10_{mSYN\text{-}MID}$/ FN_{MID} 5 µg ml^{-1}, FNIII7-$10_{mSYN\text{-}LOW}$/ FN_{LOW} 0.5 µg ml^{-1}, FN_{LOWEST} 0.05 µg ml^{-1}). Prior to adhesion measurements, single fibroblasts were incubated on the cantilever for 7–10 minutes and then approached to the FNIII7-10-coated substrate for 120 s in (a) and for contact times as indicated in (b). Finally, single fibroblasts were retracted to measure the adhesion force. Dots show adhesion forces of single fibroblasts (n ≥ 10 for each condition) and red bars their median. Statistical significances were analyzed with two-tailed Mann-Whitney U-tests (****, $P < 0.0001$; ***, $P < 0.001$; **, $P < 0.01$; *, $P < 0.05$; *ns*, $P \geq 0.05$).

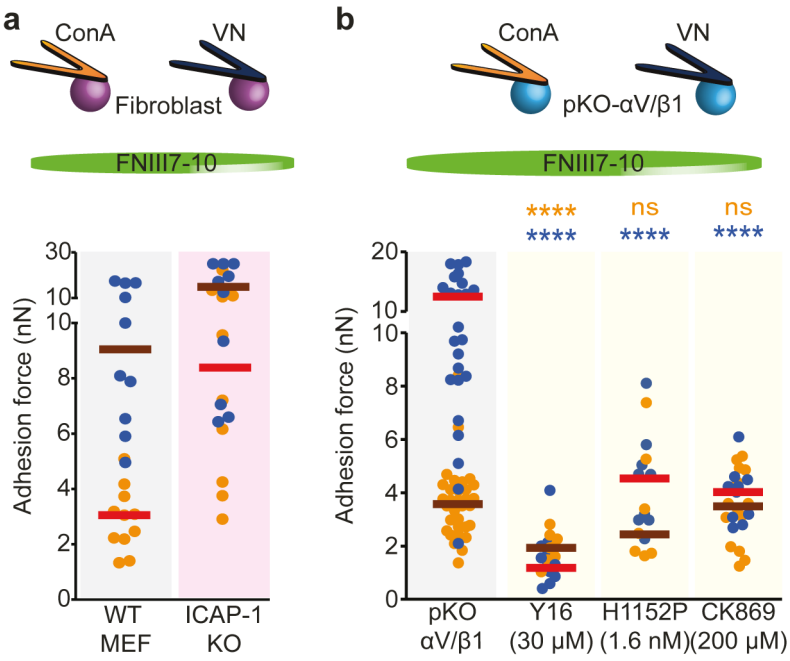

Supplementary Figure 4-7 Contribution of integrin associated proteins to the crosstalk between α5β1 and αV-class integrins. (a) Adhesion forces of ConA-attached (yellow) and VN-stimulated (blue) WT mouse embryonic fibroblasts (WT MEF, first panel) and ConA- and VN-attached ICAP-1 deficient MEFs (ICAP-1 KO, second panel) to FNIII7-10 after 120 s are shown. For VN-stimulating fibroblasts, cantilevers were coated by 5 μg ml^{-1} VN diluted in ConA. (b) After incubating single pKO-αV/β1 fibroblasts to either ConA (yellow)- of VN (blue)-coated cantilevers, their adhesion forces after 120 s contact time to FNIII7–10 were measured. 30 minutes prior to the experiments, the pKO-αV/β1 fibroblasts were incubated with the chemical inhibitors at given concentrations. For VN-stimulating fibroblasts, cantilevers were coated by 5 μg ml^{-1} VN diluted in ConA. Dots show adhesion forces of single fibroblasts (n ≥ 10 for each condition) and red bars their median. Statistical significance was determined to compare non-stimulated and stimulated adhesion for each condition by with two-tailed Mann-Whitney U-tests (****, $P < 0.0001$; ***, $P < 0.001$; **, $P < 0.01$; *, $P < 0.05$; *ns*, $P \geq 0.05$).

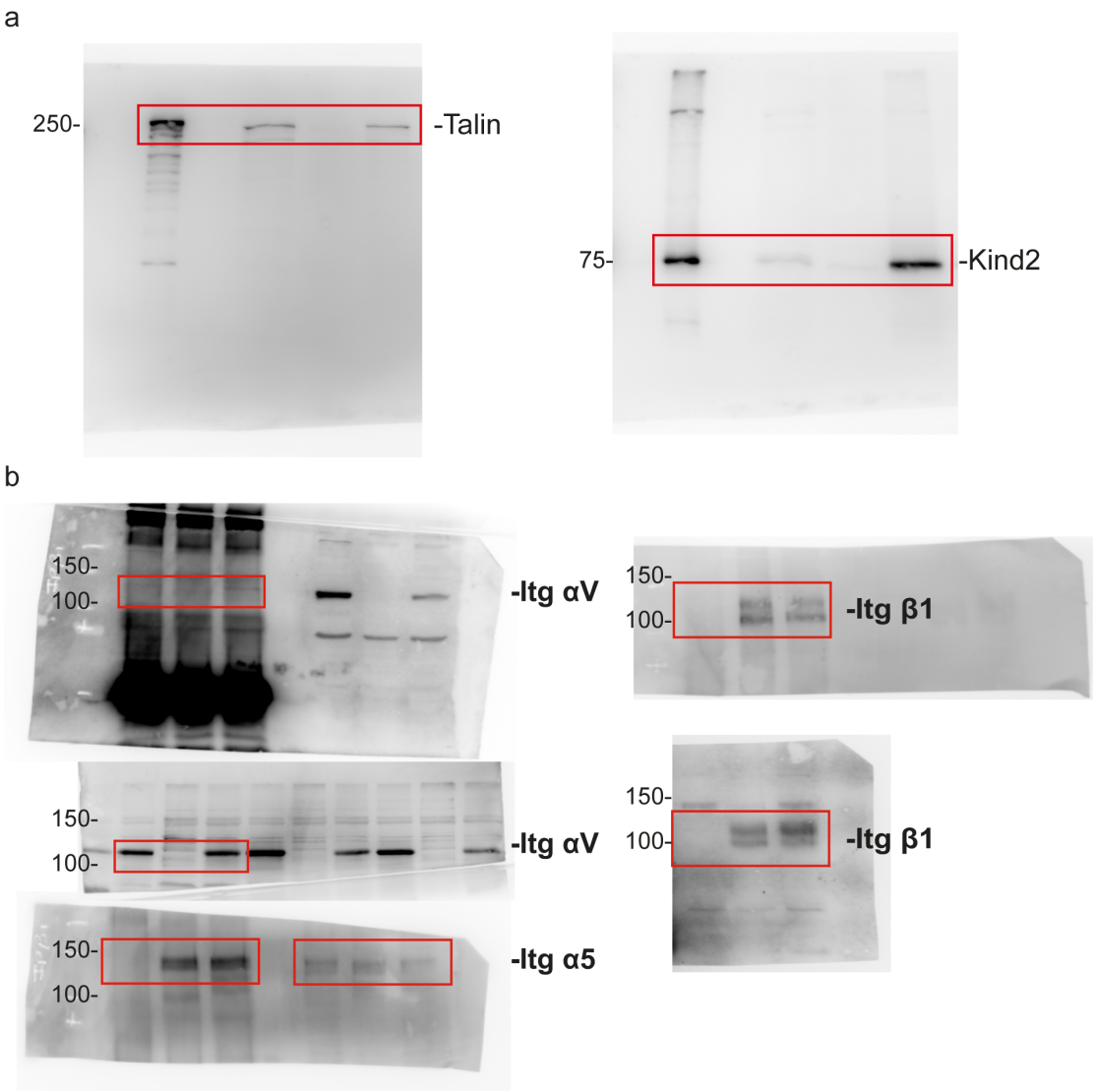

Supplementary Figure 4-8 Uncropped images of western blots shown in Supplementary Figure 4d. and Supplementary Fig. 2a. (a) Western blots showing talin-1 and kindlin-2, binding to biotinylated β1- and β3-integrin tail peptides. Peptides with scrambled amino-acid sequences (β1 scr tail; β3 scr tail) were used as negative controls. WT, wild-type. Input, whole wild-type (WT) pKO-αV/β1 fibroblast lysate. (b) Total cell lysates (Input panel) and immunoprecipitated β1 integrin (β1-IP panel) were immunoblotted for αV, α5 and β1 integrins. We observed comparable amounts of αV-class and α5β1 integrins in all fibroblasts lines. The αVβ1 heterodimer was detected at considerably lower amounts compared to αV-class and α5β1 integrins in pKO-αV/β1 fibroblasts.

	pKO-αVβ1 non-stimu-lated	pKO-αVβ1 VN-stimu-lated	pKO-αV non-stimu-lated	pKO-αV VN-stimu-lated	pKO-β1 non-stimu-lated	pKO-β1 VN-stimu-lated
pKO-αVβ1 non-stimu-lated	ns	***	ns	**	***	***
pKO-αVβ1 VN-stimulated	***	ns	***	***	***	***
pKO-αV non-stimu-lated	ns	***	ns	**	***	***
pKO-αV VN-stimulated	**	***	**	ns	*	*
pKO-β1 non-stimu-lated	***	***	***	*	ns	ns
pKO-β1 VN-stimulated	***	***	***	*	ns	ns

Supplementary Table 4-1 Statistical analysis comparing the paxillin-GFP-intensity detected by TIRF microscopy in Fig. 4. Two-tailed Mann-Whitney tests were applied to determine significant differences between the paxillin-GFP-intensity among different conditions (n≥10 for each condition) as shown in Fig. 4. ****, $P < 0.0001$; ***, $P < 0.001$; **, $P < 0.01$; *, $P < 0.05$; *ns*, $P \geq 0.05$.

Supplementary Note 1

R-code for statistical analysis in Supplementary Fig. 3

```
# load data:
D  <- read.table(
 "FN.csv",
 header=T,
 sep=","
);
colnames(D) <- c(
 "a5", "a20", "a50", "a120",
 "b5", "b20", "b50", "b120",
 "ab5", "ab20", "ab50", "ab120",
 "null5", "null20", "null50", "null120"
);
a5 <- D[is.na(D[1]) == FALSE, 1];
a20 <- D[is.na(D[2]) == FALSE, 2];
a50 <- D[is.na(D[3]) == FALSE, 3];
a120 <- D[is.na(D[4]) == FALSE, 4];
b5 <- D[is.na(D[5]) == FALSE, 5];
b20 <- D[is.na(D[6]) == FALSE, 6];
b50 <- D[is.na(D[7]) == FALSE, 7];
b120 <- D[is.na(D[8]) == FALSE, 8];
ab5 <- D[is.na(D[9]) == FALSE, 9];
ab20 <- D[is.na(D[10]) == FALSE, 10];
ab50 <- D[is.na(D[11]) == FALSE, 11];
ab120 <- D[is.na(D[12]) == FALSE, 12];
null5 <- D[is.na(D[13]) == FALSE, 13];
null20 <- D[is.na(D[14]) == FALSE, 14];
null50 <- D[is.na(D[15]) == FALSE, 15];
null120 <- D[is.na(D[16]) == FALSE, 16];

# bootstrap samples:
n = 100;
null <- matrix(ncol = 4, nrow = n);
null[,1] <- sample(null5, n, replace = TRUE);
null[,2] <- sample(null20, n, replace = TRUE);
null[,3] <- sample(null50, n, replace = TRUE);
null[,4] <- sample(null120, n, replace = TRUE);
a <- matrix(ncol = 4, nrow = n);
a[,1] <- sample(a5, n, replace = TRUE);
a[,2] <- sample(a20, n, replace = TRUE);
a[,3] <- sample(a50, n, replace = TRUE);
a[,4] <- sample(a120, n, replace = TRUE);
b <- matrix(ncol = 4, nrow = n);
b[,1] <- sample(b5, n, replace = TRUE);
b[,2] <- sample(b20, n, replace = TRUE);
b[,3] <- sample(b50, n, replace = TRUE);
b[,4] <- sample(b120, n, replace = TRUE);
ab <- matrix(ncol = 4, nrow = n);
ab[,1] <- sample(ab5, n, replace = TRUE);
ab[,2] <- sample(ab20, n, replace = TRUE);
ab[,3] <- sample(ab50, n, replace = TRUE);
ab[,4] <- sample(ab120, n, replace = TRUE);

# slope:
slope <- function(x) {
        ((x[2]-x[1])/15 + (x[3]-x[2])/30 + (x[4]-x[3])/70) / 3  # average slope along x
}
null_slope <- apply(null, 1, slope);
a_slope <- apply(a, 1, slope);
b_slope <- apply(b, 1, slope);
ab_slope <- apply(ab, 1, slope);
print(c("median slope of null = ", median(null)));
print(c("median slope of a = ", median(a)));
print(c("median slope of b = ", median(b)));
print(c("median slope of ab = ", median(ab)));
print(wilcox.test(a_slope, b_slope));
print(wilcox.test(a_slope, ab_slope));
print(wilcox.test(b_slope, ab_slope));
# statistical interaction:
i5 <- null[,1] - a[,1] - b[,1] + ab[,1];
print(c("median interaction between a and b at t=5: ", median(i5)));
```

```
print(wilcox.test(i5));

i20 <- null[,2] - a[,2] - b[,2] + ab[,2];
print(c("median interaction between a and b at t=20: ", median(i20)));
print(wilcox.test(i20));

i50 <- null[,3] - a[,3] - b[,3] + ab[,3];
print(c("median interaction between a and b at t=50: ", median(i50)));
print(wilcox.test(i50));

i120 <- null[,4] - a[,4] - b[,4] + ab[,4];
print(c("median interaction between a and b at t=120: ", median(i120)));
print(wilcox.test(i120));
```

5. Fibronectin-bound α5β1 integrins sense load and signal to reinforce adhesion in less than a second

Nico Strohmeyer[1], Mitasha Bharadwaj[1], Mercedes Costell[3], Reinhard Fässler[2] and Daniel J. Müller[1,*]

1. Department of Biosystems Science and Engineering, ETH Zurich, Mattenstrasse 26, 4058 Basel, Switzerland

2. Max Planck Institute of Biochemistry, Department of Molecular Medicine, 82152 Martinsried, Germany.

3. Department of Biochemistry and Molecular Biology, Estructura de Reserca Interdisciplinar en Biotechnologia i Biomedicina, Universitat de València, Spain.

Correspondence: Daniel J. Müller, daniel.mueller@bsse.ethz.ch

Published in *Nat. Mater.* **16**, 1262–1270 (2017).

Integrin-mediated mechanosensing of the extracellular environment allows cells to control adhesion and signalling. Whether cells sense and respond to force immediately upon ligand-binding is unknown. Here, we report that during adhesion initiation, fibroblasts respond to mechanical load by strengthening integrin-mediated adhesion to fibronectin (FN) in a biphasic manner. In the first phase, which depends on talin and kindlin as well as the actin nucleators Arp2/3 and mDia, FN-engaged α5β1 integrins activate focal adhesion kinase (FAK) and c-Src in less than 0.5 s to steeply strengthen α5β1- and αV-class integrin-mediated adhesion. When the mechanical load exceeds a certain threshold, fibroblasts decrease adhesion and initiate the second phase, which is characterized by less steep adhesion strengthening. This unique, biphasic cellular adhesion response is mediated by α5β1 integrins, which form catch bonds with FN and signal to FN-binding integrins to reinforce cell adhesion much before visible adhesion clusters are formed.

Shear stress, compression, tension, and the rigidity of the extracellular matrix (ECM) guide function and form of cells and tissues[1,2]. Integrins are main mediators of cell adhesion to the ECM where they sense mechanical properties and translate them into biochemical signals to regulate cellular processes that are crucial for development, tissue homeostasis and pathology[3-5]. In mammals, 24 integrin heterodimers are formed from 18 α- and 8 β-subunits[6]. Usually cells co-express several integrins that bind to specific, small amino acid sequences of ECM proteins. The Arg-Gly-Asp (RGD) sequence is found in different ECM proteins, including fibronectin (FN), where it associates with α5β1 and αV-class integrins[6-8]. α5β1 integrins can additionally bind the Pro-His-Ser-Arg-Asn (PHSRN) synergy site of the 9th type III repeat of FN in order to establish firm adhesion[9]. After ligand-binding, integrins cluster in ≥ 60 seconds[10,11], and assemble an increasing number of intracellular proteins at their cytoplasmic tails, collectively called adhesome. The adhesome stabilizes the binding of the integrin ectodomain to the ligand, connects integrins to the actin cytoskeleton and initiates signalling. The composition of the adhesome depends on the engaged integrin and the extent of coupling to the actomyosin-mediated pulling forces[12-14]. These forces induce conformational changes in adhesome proteins including talin, vinculin, tyrosine-protein kinase Src, focal adhesion kinase (FAK) and p130Cas that expose cryptic protein binding sites and/or induce catalytic activities[15-18]. Together, intracellular tension and conformational changes of adhesome proteins are required to mature short-lived nascent adhesions into focal adhesions[5,19].

Integrins withstand strong extra- and intracellularly generated forces. α5β1 integrins accomplish this task by switching from a relaxed, low affinity state for ligand binding to a tensioned, high affinity state[20] with prolonged integrin-ligand bond lifetime[21]. This catch bond behavior[22] was demonstrated with recombinant integrin ectodomains *in vitro*[21]. However, it remains unclear if other integrins form catch bonds, catch bonds occur in the native cellular

environment and in which time range integrins strengthen cell adhesion in response to mechanical cues.

We addressed these questions by studying fibroblasts initiating adhesion to FN. Using atomic force microscopy (AFM)-based single-cell force spectroscopy (SCFS), we characterized the adhesion force at which fibroblasts start detaching from FN and rupture forces at which single integrins unbind ligand[23,24]. We found that already at the onset of adhesion ($\gtrapprox$ 2 s), fibroblasts respond to mechanical load by strengthening adhesion in two distinct phases using different mechanisms.

5.1. FN-ligated integrins respond to mechanical load

The mechanical environment influences the initiation, maturation and function of integrin-mediated adhesion sites in cells[14,25,26]. We used AFM-based SCFS (Supplementary Figure 5-1) to determine the impact of mechanical load on FN adherent mouse fibroblasts lacking the expression of all integrins (pan integrin knock-out; pKO), and reconstituted with FN-binding αV-class integrins (pKO-αV), α5β1 integrins (pKO-β1), or both integrin classes (pKO-αV/β1)[14]. The cell surface levels of integrins and the cell size of the fibroblast lines were comparable to those of parental wild-type (WT) fibroblasts[14] (Supplementary Figure 5-2). For SCFS, a single fibroblast was attached to a concanavalin A (ConA)-coated tip-less cantilever and optically monitored to assure a round morphology throughout the experiments. The fibroblast was lowered onto a FN fragment (FNIII7-10)-coated substrate to initiate adhesion for 5 s. While separating the fibroblast and substrate, the maximum deflection of the cantilever measured the adhesion force the fibroblast withstood before detaching from the substrate (Supplementary Figure 5-1b). To increase the mechanical load to the substrate-adhering fibroblast, the retraction speed of the cantilever was increased. pKO-αV/β1 and WT fibroblasts markedly strengthened adhesion force to FNIII7-10 in response to the retraction speed increasing from 1 to 5 μm s^{-1}. This strengthening was defined by the slope of adhesion forces (Figure 5-1a and Supplementary Figure 5-3). At 6 μm s^{-1}, the adhesion force decreased, while further elevating the retraction speed increased adhesion forces with a smaller slope. Since biphasic adhesion strengthening occurred with single fibroblasts irrespective of repeated retractions at randomized or fixed speeds (Figure 5-1a and Supplementary Figure 5-4), we excluded an involvement of mechanical memory for this effect.

Importantly, we observed very low adhesion force and no biphasic adhesion response of pKO fibroblasts to FN, pKO-αV/β1 fibroblasts to FN lacking the RGD motif (FNIII7-10ΔRGD) and pKO-αV/β1 fibroblasts treated with EDTA (Figure 5-1b and Supplementary Figure 5-5a). To investigate the contribution of αV-class and α5β1 integrins to the biphasic adhesion response, we quantified the adhesion force of pKO-αV and pKO-β1 fibroblasts to FN (Figure 5-1c). The adhesion of both, pKO-αV and pKO-β1 fibroblasts, was lower than of pKO-αV/β1 fibroblasts.

Importantly, only pKO-β1 fibroblasts showed a biphasic adhesion response, although much less pronounced.

Taken together, fibroblasts adhering to FN for only 5 s use α5β1 integrins to biphasically strengthen adhesion in response to mechanical load, and co-expression of αV-class integrins amplifies this effect.

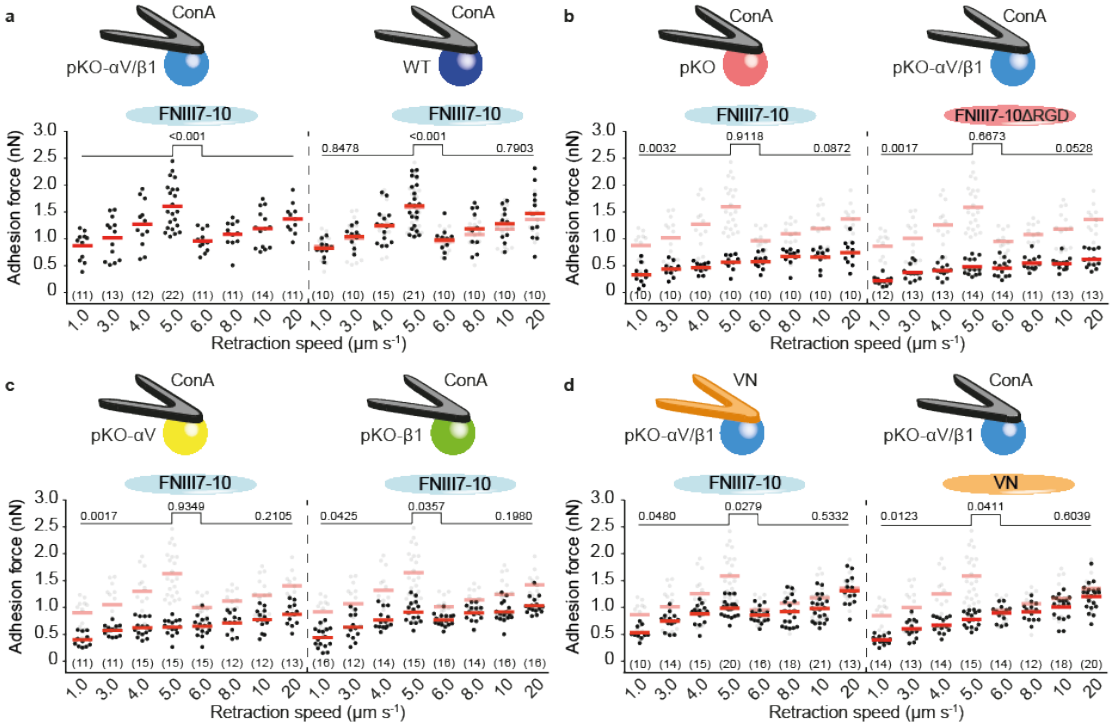

Figure 5-1 Fibroblast adhesion to fibronectin (FN) increases biphasically with the retraction speed applied to separate cell and substrate. a-d, Speed-dependent adhesion profiles of pan-integrin-null (pKO) mouse fibroblasts, pKO fibroblasts reconstituted with αV (pKO-αV), β1 (pKO-β1), or both integrin subunits (pKO-αV/β1), and wild-type (WT) fibroblasts adhering to supports coated with the FNIII7-10 fragment, RGD-deleted FNIII7-10 (FNIII7-10ΔRGD) or vitronectin (VN). Single fibroblasts were attached to a ConA- or VN-coated (50 μg ml^{-1} VN) cantilever, approached to the substrate-coated support, and after 5 s contact time retracted vertically to measure the adhesion force between fibroblast and support. Adhesion forces of individual fibroblasts (dots) and their mean (red bar) are given for each retraction speed. Adhesion forces at different retraction speeds are referred to as speed-dependent adhesion profiles. (*n*) denotes the number of fibroblasts probed for each condition. The adhesion profile of pKO-αV/β1 fibroblasts adhering to FNIII7-10 substrates a, is displayed in grey as reference. For statistical analysis, the slopes of adhesion forces (e.g. adhesion strengthening) in the first (1–5 μm s^{-1}) and second (6–20 μm s^{-1}) phase were compared with the respective slopes of pKO-αV/β1 fibroblasts attached to ConA-coated cantilevers. Slopes were compared based on difference in differences. Differences of adhesion forces between 5 μm s^{-1} and 6 μm s^{-1} were evaluated applying the Mann-Whitney test. P-values are given above graphs.

5.2. FN-bound α5β1 and αV-class integrins work in proximity

To test whether non-ligated α5β1 integrins can induce the biphasic adhesion response, we adhered ConA-bound pKO-αV/β1 fibroblasts to VN-coated substrates (Figure 5-1d) and found a monophasic response similar to that of pKO-αV fibroblasts adhering to FN (Figure 5-1c). We also tested whether both FN-binding integrin classes cooperate across the cell or require

proximity to amplify the biphasic adhesion strengthening of α5β1 integrins. Sequestering αV-class integrins of pKO-αV/β1 fibroblasts to VN-coated cantilevers prevented them from binding to VN-coated substrates at the opposite fibroblast surface (Supplementary Figure 5-5b), and resulted in an adhesion behavior, resembling ConA-bound pKO-β1 fibroblasts adhering to FN (Figure 5-1c,d). These data show that α5β1 integrins must bind FN to biphasically strengthen adhesion in response to mechanical load and that αV-class integrins amplify this response when they are close to α5β1 integrins.

5.3. α5β1 integrins transition from catch to slip bonds

To investigate how integrins unbind from FN in response to mechanical load, we analysed their single rupture events (Supplementary Figure 5-1b)[23,24] in force-distance curves recorded upon detaching fibroblasts from FNIII7-10 (Figure 5-2). The rupture forces of αV-class integrins continuously increased with increasing the retraction speed from 1 to 20 µm s^{-1}. In contrast, the median rupture forces of α5β1 integrins increased at retraction speeds from 1 to 5 µm s^{-1}, dropped from 6 to 8 µm s^{-1} and increased again from 10 to 20 µm s^{-1}. The median rupture forces of pKO-αV/β1 fibroblasts, expressing αV-class and α5β1 integrins, closely followed the combination of rupture forces of the two integrin classes (Supplementary Figure **5-6**). This biphasic strengthening of the α5β1 integrin-FNIII7-10 bond supports recent findings reporting that recombinant α5β1 integrins bound to FN transition from catch to slip bond behaviour[21,27].

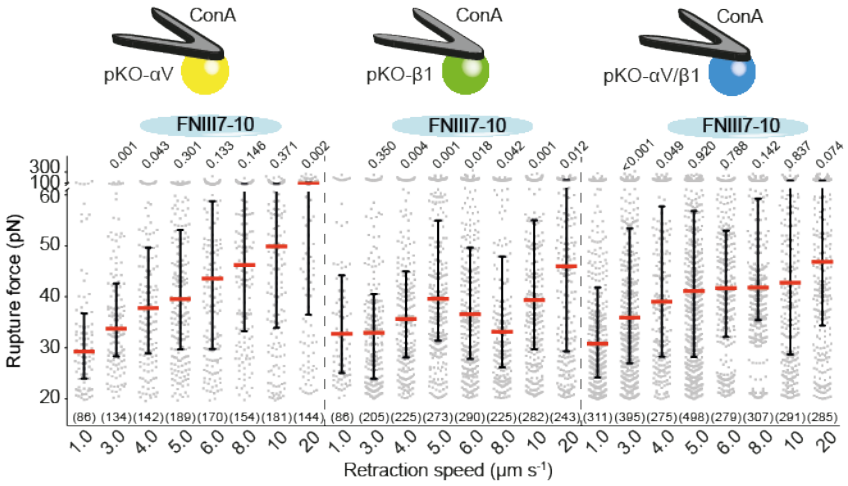

Figure 5-2 Speed-dependent rupture forces required to separating single αV-class and α5β1 integrins bound to fibronectin. pKO-αV/β1, pKO-αV or pKO-β1 fibroblasts were approached to FNIII7-10-coated supports, allowed to adhere for 5 s and separated at indicated retraction speeds. Rupture forces required to separating single integrin-FN bonds were taken from single rupture events detected in force-distance curves acquired for Figure 5-1. The analysis of such events, which describe the force required to rupture individual bonds formed between actin bound integrins and FN[23,24], has been exemplified in Supplementary Figure 5-1. Rupture forces of single integrin-FN bonds (grey dots), their median (red bars) and the interquartile range are given. (*n*) denotes the number of single unbinding events analysed. Statistical significance of median differences to the slower retraction speed was tested using the Mann-Whitney-Test. P-values are given above graphs.

5.4. Integrin activation alters adhesion response

To test whether the integrin activation state influences the biphasic adhesion behavior of fibroblasts, we activated all integrins at the cell surface using Mn^{2+}. Whereas the Mn^{2+}-treatment increased the adhesion force in the first phase (≤ 5 µm s^{-1}) of pKO-β1 and pKO-αV fibroblasts to FNIII7-10, the adhesion forces of pKO-αV/β1 remained unaffected (Figure 5-3a). Mn^{2+}-treated pKO-β1 and pKO-αV but not pKO-αV/β1 fibroblasts increased adhesion force more steeply with increasing mechanical load. Furthermore, Mn^{2+}-activated pKO-αV/β1 and pKO-β1 fibroblasts lacked the characteristic drop of adhesion force at the transition between both phases. All three fibroblasts lines did not further increase the adhesion that was reached at the end of first phase. The ability of Mn^{2+} to affect adhesion forces of pKO-αV/β1 fibroblasts in the second but not in the first phase indicates that in the absence of Mn^{2+} fibroblasts respond to mechanical load by engaging additional integrins in the first phase, which does not occur in the second phase.

To further test whether ligand-induced integrin activation modulates adhesion strengthening, we shortened the contact time of pKO-αV/β1 fibroblasts with FN from 5 to 3, 2 and 1 s and measured their adhesion force depending on the mechanical load (Figure 5-3b). At 3 s contact time, adhesion forces and biphasic adhesion response were similar to those observed at 5 s. At 2 s, adhesion forces reduced with a biphasic adhesion response being still observable. However, at 1 s the characteristic drop of the biphasic adhesion response was lost indicating that mechanical stimulation regulates very early stages of integrin-mediated adhesion formation of fibroblasts.

Next, we extended the contact times of pKO-αV/β1 fibroblasts with FN to 20, 35 and 50 s and measured their adhesion force depending on the mechanical load (Figure 5-3c). With increasing contact time, adhesion force and slope increased in the first phase. However, at the transition of both phases, the adhesion dropped with different magnitudes. After 20 s, the drop of adhesion force was augmented compared to fibroblasts adhering for 5 s (Figure 5-3c) and the slope of adhesion forces in the second phase was less steep compared to the first phase. After 35 s, the adhesion drop was still apparent, but less pronounced than after 20 s (Figure 5-3c), whereas after 50 s the characteristic adhesion drop was barely visible and the fibroblasts entered an enhanced adhesion force plateau in the second phase. The drop of adhesion force at the transition from the first to the second phase decreases with increasing contact time, which is due to integrin engagement rather than clustering, since integrins cluster at extended contact times ≥ 60 s (ref. 10).

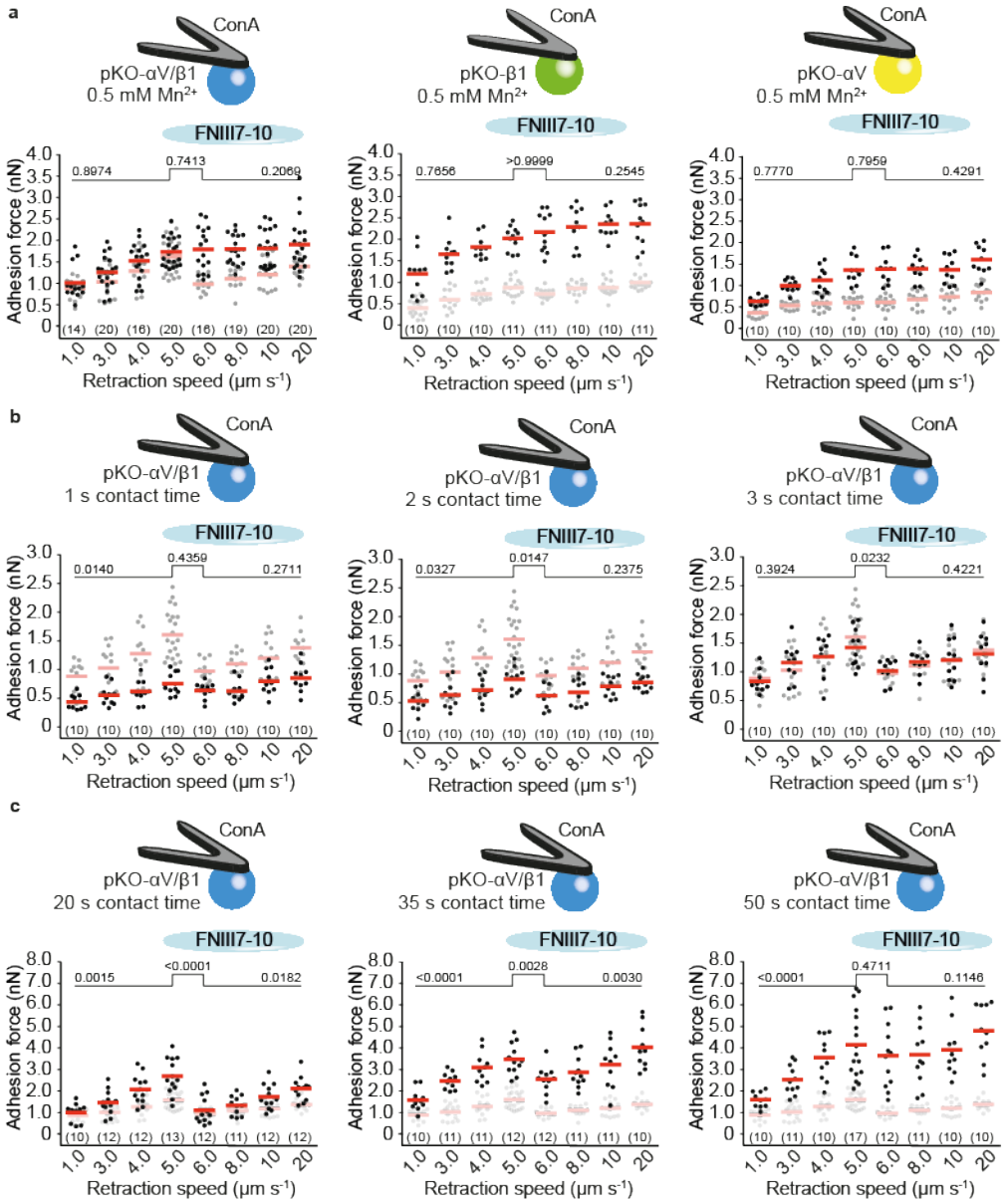

Figure 5-3 How fibroblast strengthen adhesion in response to mechanical load depends on integrin activity and contact time with the substrate. a, Adhesion strengthening of pKO-αV/β1, pKO-β1 or pKO-αV fibroblasts treated with 0.5 mM Mn^{2+} 30 min before adhering to FNIII7-10-coated supports and during SCFS to activate integrins. b and c, Adhesion strengthening of untreated pKO-αV/β1 fibroblasts adhering to FNIII7-10-coated supports for (b) 1, 2 or 3 and (c) 20, 35 or 50 s. For each retraction speed, adhesion forces of individual fibroblasts (dots) and their mean (red bar) are given. (n) denotes the number of fibroblasts probed for each condition. Speed-dependent adhesion profile of (a, left, b and c) untreated pKO-αV/β1, (a, middle) pKO-β1 or (a, right) pKO-αV fibroblasts attached to ConA-coated cantilevers and adhering to FNIII7-10 substrates for a contact time of 5 s are displayed in gray as reference (data taken from Figure 5-1). For statistical analysis the slopes of adhesion forces in the first (1–5 µm s^{-1}) and second (6–20 µm s^{-1}) phase were compared with the respective slopes of the given references. Slopes were compared based on difference in differences. Differences of adhesion forces between 5 µm s–1 and 6 µm s–1 were evaluated applying the Mann-Whitney test. P-values are given above graphs.

Finally, we determined the contribution of α5β1 and αV-class integrins to the mechanical load-dependent adhesion strengthening at higher contact times to FN-coated substrates (Supplementary Figure 5-7), where pKO-β1 fibroblasts developed higher adhesion forces compared to pKO-αV fibroblasts. Furthermore, pKO-β1 fibroblasts strengthened adhesion biphasically in

response to load, which was not the case for pKO-αV fibroblasts. The load-dependent biphasic adhesion strengthening of pKO-β1 fibroblasts at 20 and 35 s contact time was similar to pKO-αV/β1 fibroblasts and exceeded adhesion forces of pKO-αV/β1 fibroblasts at 50 s.

These results show that within the contact times tested, α5β1 integrins but not αV-class trigger the engagement of additional integrins to the substrate. The similarity of the biphasic responses of pKO-β1 fibroblasts at higher contact times and of pKO-αV/β1 fibroblasts at 5 s contact time suggest that FN-bound α5β1 integrins respond to mechanical load by triggering the engagement of additional integrins.

5.5. Biphasic response requires integrins coupling to actin

Talin and kindlin binding to integrins is required to maintain the active state of integrins[28]. We probed the adhesion of talin-1- and -2-deficient (talin KO) and kindlin-1- and -2-deficient (kindlin KO) fibroblasts[28] to FNIII7-10 in response to mechanical load after 5 s contact time (Fig. 4a). Compared to pKO-αV/β1 fibroblasts, both fibroblast lines expressed similar levels of FN-binding integrins on their surface (Supplementary Figure 5-2). However, individual fibroblasts were smaller, which could influence the contact area between fibroblasts and substrate and consequently the magnitude of the biphasic response. Talin KO fibroblasts lacked the biphasic adhesion behaviour. While the adhesion forces of talin KO fibroblasts were lower in the first phase, in the second phase they were similar to those of pKO-αV/β1 (Figure 5-4a) and talin control fibroblasts[28] (Supplementary Figure 5-8a). Mn^{2+} was unable to induce biphasic adhesion behaviour of talin KO fibroblasts (Figure 5-4a), indicating that talin is required for the first and not for the second phase of the biphasic adhesion strengthening.

Kindlin KO fibroblasts strengthened adhesion biphasically, although the adhesion forces were generally lower compared to pKO-αV/β1 fibroblasts (Figure 5-4b). Upon addition of Mn^{2+}, kindlin KO fibroblasts increased adhesion at low retraction speeds < 5 μm s^{-1} to the levels of pKO-αV/β1 fibroblasts and at higher retraction speeds strengthened the adhesion forces to values observed for Mn^{2+}-treated pKO-αV/β1 fibroblasts. These results indicate that kindlin is not involved in the biphasic adhesion response of fibroblasts but required to strengthen adhesion by stabilizing the active conformation of integrins[28,29].

The requirement of talin for the first phase of the adhesion response suggests that F-actin and myosin II-mediated contractile forces are involved in adhesion strengthening. To test their roles, we chemically interfered with F-actin formation and myosin II activity (Figure 5-4c). Depolymerizing actin filaments in pKO-αV/β1 fibroblasts lowered the adhesion force of the first and marginally of the second phase, thereby abrogating the biphasic adhesion strengthening. Inhibition of mDia lowered the adhesion of pKO-αV/β1 fibroblasts to FN for all retraction speeds and attenuated the biphasic adhesion response. Inhibition of Arp2/3 lowered

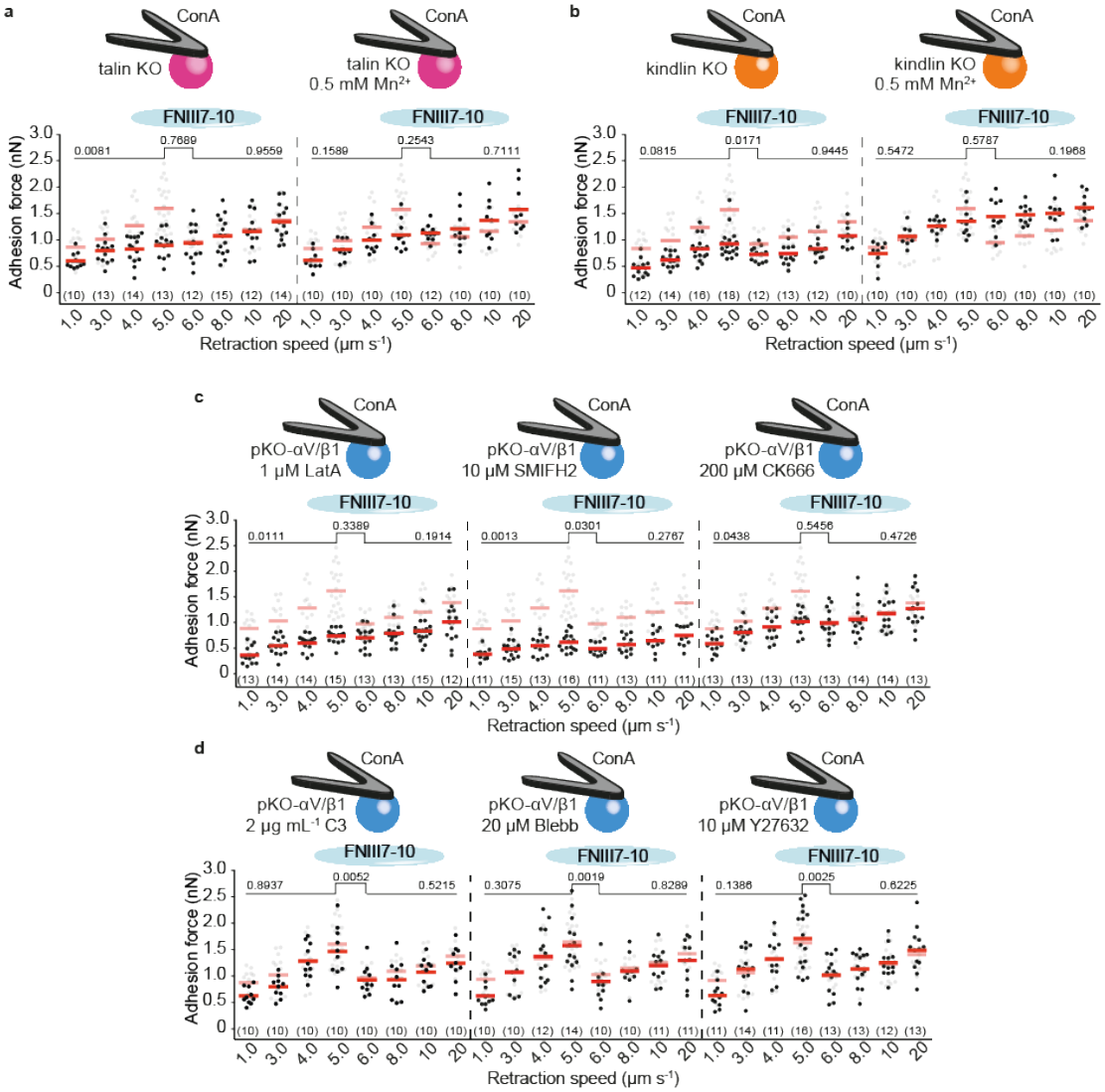

Figure 5-4 Fibroblasts require talin, F-actin polymerization to strengthen adhesion in response to mechanical load. To quantify cell adhesion **a,** talin-1- and -2-deficient (talin KO) mouse fibroblasts, **b,** kindlin-1- and -2-deficient (kindlin KO) mouse fibroblasts or **c**, chemically perturbed pKO-αV/β1 fibroblasts were attached to ConA-coated cantilevers, brought into contact with a FNIII7-10-coated support for 5 s and then vertically separated at the given speeds. **a**,**b**, to activate integrins, fibroblasts were incubated with 0.5 mM Mn^{2+} 30 min before and during measurements. **c and d**, pKO-αV/β1 fibroblasts were incubated with latrunculin A (LatA) to depolymerize actin, SMIFH2 to block mDia or CK666 to inhibit the Arp2/3 complex, C3 toxin to inhibit RhoA, blebbistatin (Blebb) to inhibit myosin II or with Y27632 to inhibit ROCK. Fibroblasts were treated with chemical inhibitors at the indicated concentrations 30 min (3 h for C3 toxin) before and during SCFS experiments and all fibroblasts were attached to ConA-coated cantilevers. **a-d**, For each retraction speed, the adhesion forces of individual fibroblasts (dots) and their mean (red bar) are given. (*n*) denotes the number of fibroblasts probed for each condition. The speed-dependent adhesion profile of pKO-αV/β1 fibroblasts attached to ConA-coated cantilevers and adhering to FNIII7-10 substrates (**Figure 5-1a**) is displayed in gray as reference. For statistical analysis the slopes of adhesion forces in the first (1–5 µm s^{-1}) and second (6–20 µm s^{-1}) phase were compared with the respective slopes of pKO-αV/β1 fibroblasts on ConA-coated cantilevers. Slopes were compared based on difference in differences. Differences of adhesion forces between 5 µm s^{-1} and 6 µm s^{-1} were evaluated applying the Mann-Whitney test. P-values are given above graphs.

adhesion in the first but not in the second phase of adhesion strengthening. Inhibition of RhoA, regulating the myosin II-mediated contractility of the actomyosin cortex, as well as inhibition of this contractility with blebbistatin or Y27632 retained the characteristic biphasic adhesion response (Figure 5-4d).

These results indicate that the biphasic adhesion response of fibroblasts to mechanical load requires talin-mediated integrin linkage to Arp2/3 assembled F-actin but not actomyosin contractility.

5.6. Adhesion strengthening requires FAK, Src and synergy site

In shear stress-dependent integrin activation, PI3 kinase and c-Src rapidly (10 and 0.3 s, respectively) phosphorylate[30,31]. Therefore, we tested their role as well as other proteins participating in integrin-activation, including Rap1 and FAK, in the biphasic adhesion response of pKO-αV/β1 fibroblasts. Using chemical perturbations, we found that FAK and Src activities are necessary to establish adhesion force of the first phase and the biphasic adhesion response (Figure 5-5a,b and Supplementary Figure 5-8b). However, perturbing either kinase did not interfere with the second phase of adhesion strengthening. Inhibition of PI3 kinase decreased the adhesion force for all retraction speeds, while the biphasic adhesion response remained (Figure 5-5c). Interestingly, inhibition of the talin-activating small GTPase Rap1 (ref. 32) neither influenced the adhesion force nor the biphasic adhesion strengthening (Fig. 5d). While the biphasic adhesion response of pKO-β1 fibroblasts remained unchanged upon Src inhibition, perturbation of FAK decreased adhesion forces and abolished the biphasic adhesion response (Figure 5-5e,f).

The synergy site of FN is required for α5β1 integrins to mechanically activate FAK[20]. Thus, we characterized the response of pKO-αV/β1 and pKO-β1 fibroblasts adhering to a synergy site-mutated FN fragment (FNIII7-10mSyn) to mechanical load. The adhesion strength of both fibroblast lines as well as rupture forces of single α5β1 integrins in the first phase reduced and the biphasic adhesion strengthening disappeared (Figure 5-5g and Supplementary Figure 5-9).

These experiments indicate that α5β1 integrins must bind the FN synergy site to form catch bonds and to engage additional integrins. Whereas, FAK and Src are critically involved in the first phase of the biphasic adhesion strengthening, PI3K plays a general role in adhesion strengthening.

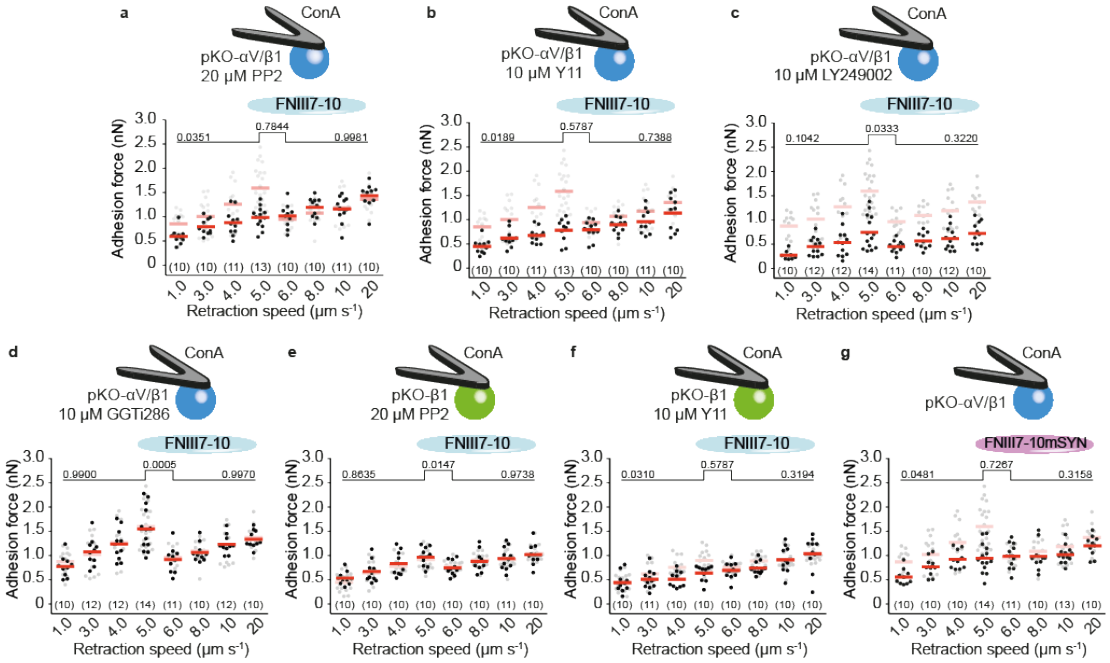

Figure 5-5 Integrin activation in response to mechanical load depends on FAK and c-Src signalling. a-g, Speed-dependent adhesion response of chemically perturbed pKO-αV/β1 pKO-αV/β1 or pKO-β1 fibroblasts separated from a-f FNIII7-10- or g, FNIII7-10mSYN-coated to which they adhered for 5 s. pKO-αV/β1 fibroblasts were treated with (a) PP2 to inhibit the Src-kinase family, b, Y11 to inhibit FAK, (c) LY249002 to inhibit PI3K, or d, GGTi286 to inhibit Rap1. pKO-β1 fibroblasts were treated with e, PP2 to inhibit the Src-kinase family or f Y11 to inhibit FAK. Inhibitors were added for 30 min before and were present during SCFS and all fibroblasts were attached to ConA-coated cantilevers. For each retraction speed, adhesion forces of individual fibroblasts (dots) and their mean (red bar) are given. (*n*) denotes the number of fibroblasts probed for each condition. The speed-dependent adhesion profiles of untreated pKO-αV/β1 (a-d, g) or pKO-β1 (f, g) fibroblasts attached to ConA-coated cantilevers and adhering to FNIII7-10 substrates (**Figure 5-1**) are displayed in gray as reference. For statistical analysis the slopes of adhesion forces in the first (1–5 μm s^{-1}) and second (6–20 μm s^{-1}) phase were compared with the respective slopes of untreated pKO-αV/β1 (a-d, g) or pKO-β1 (e,f) fibroblasts attached to ConA-coated cantilevers and adhering to FNIII7-10 substrates. Slopes were compared based on difference in differences. Differences of adhesion forces between 5 μm s^{-1} and 6 μm s^{-1} were evaluated applying the Mann-Whitney test. P-values are given above graphs.

5.7. Discussion

FN-binding α5β1 and αV-class integrins assemble mixed adhesion sites where they cooperate to probe extracellular properties and regulate cell adhesion[14,25,33]. However, it is not known whether and how the two integrin-classes respond to mechanical load before they assemble adhesion plaques. We found that during adhesion initiation, fibroblasts adhere biphasically in response to mechanical load. In the first phase, at cantilever retraction speeds ≤ 5 μm s^{-1}, fibroblasts expressing both α5β1 and αV-class integrins steeply strengthen adhesion with increasing mechanical load. At a retraction speed of 6 μm s^{-1}, adhesion markedly drops and fibroblasts initiate the second phase to increase adhesion again with rising mechanical load, but less steep compared to the first phase. Mn^{2+}-activation of integrins does not affect the first phase of adhesion strengthening, but plateaus the second phase at high adhesion forces. This indicates that in the first phase fibroblasts engage additional integrins in response to mechanical load and above a certain threshold, in the second phase, this 'mechanoactivation' of integrins fails.

Our experiments show that α5β1 integrins actively respond to mechanical load by regulating fibroblast adhesion and engaging additional integrins binding to FN. In fibroblasts, single α5β1 integrins binding to FN transition from catch to slip bond behaviour at ≈ 39 pN, which corresponds to values (> 30 pN) found for recombinant α5β1 integrin ectodomains[21]. To establish catch bonds, α5β1 integrins are believed to simultaneously bind RGD and synergy sites of FN[9,20]. Indeed, disruption of the synergy site abolishes the biphasic response of pKO-αV/β1 and pKO-β1 fibroblasts. We hence speculate that the load-dependent integrin crosstalk initiated by α5β1 integrins correlates with their catch bond behavior.

In our experiments αV-class integrins do not actively regulate initial fibroblast adhesion when loaded. However, FN-bound αV-class integrins withstand higher forces before unbinding than α5β1 integrins, indicating that bearing a higher load retains them longer in mechanically stressed adhesion sites[14,34,35]. It has been speculated that αV-class integrins may form stronger catch bonds than α5β1 integrins[14]. We did not observe a transition of bond properties within the range of retraction speeds investigated and hence cannot exclude catch bond behavior. It is conceivable that upon extension of the contact times, which allow integrin clustering and assembly of adhesomes, αV-class integrins may modulate their bond properties differently.

We recently showed that αV-class integrins have higher binding rates than α5β1 integrins and successfully compete with α5β1 integrins to bind FN[29]. Our findings suggest that few α5β1 integrins engaging to FN are sufficient to respond to mechanical load and to reinforce fibroblast adhesion by engaging additional FN-binding integrins of both classes. Although αV-class integrins show higher unbinding forces than α5β1 integrins, pKO-αV fibroblasts adhere less strongly compared to pKO-β1 fibroblasts[29]. This observation suggests that in the absence of αV-class integrins, α5β1 integrins either are faster recruited to bind ligand, or their F-actin linkage stabilizes integrin-ligand bonds. However, the exact mechanistic basis of this observation remains to be elucidated.

We estimate that fibroblasts regulate adhesion in response to mechanical load within 0.5 s (Supplementary Figure 5-10). Fibroblasts establish the biphasic adhesion response at the onset of initiating adhesion to FN ($\gtrapprox$ 2 s). Hence, the load-dependent adhesion reinforcement relies on rapid signalling of mechanically loaded α5β1 integrins to engage additional FN-binding integrins. In line with previous reports, we identify talin as mechanosensor in the biphasic adhesion response, which is required for integrin engagement and subsequent adhesion maturation[28,32,36-39]. Although fibroblast adhesion reduced in the absence of kindlin, the biphasic adhesion response remained evident. These findings suggest that fibroblasts require talin to respond to mechanical load and kindlin to strengthen adhesion in response to mechanical cues[28,40]. In line with a role of kindlin to recruit the Arp2/3 complex to early adhesion sites, Arp2/3 was found to be essential to strengthen adhesion in response to mechanical load, whereas mDia was of general importance for early adhesion formation[29]. Our results also suggest a central role for the catalytic

function of FAK, which can be activated by mechanical load[20,27]. Additionally, FAK was shown to recruit talin to nascent integrin-containing adhesion sites, which in turn promotes integrin-ligand engagement[41]. Similarly, c-Src is also involved in integrin-ligand engagement in response to mechanical stimulation, probably by transducing signals from α5β1 to αVβ3 integrins.

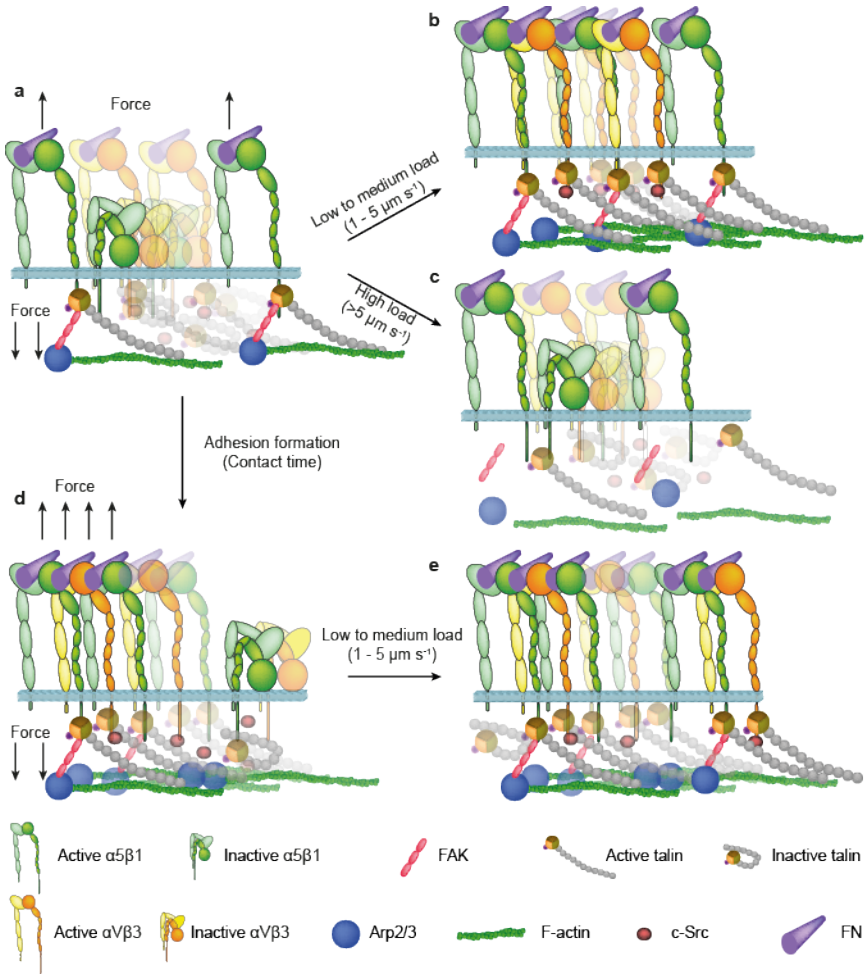

Figure 5-6 Instant strengthening of fibroblast adhesion to FN in response to mechanical load. a, In the initial phase of adhesion formation of fibroblasts, α5β1 and αV-class integrins bind FN and recruit talin and associate with F-actin within 5 s. b, Tensioned either by extra- or by intracellular forces α5β1 integrins activate other FN-binding integrins *via* FAK and c-Src to reinforce adhesion, which depends further on Arp2/3 and talin. c, If the force applied to integrins exceeds a certain threshold, fibroblasts fail to stabilize FN-integrin bonds, likely because the mechanical stimuli cannot be transmitted to activate integrins. d, With increasing contact time to FN adhesion maturates and the number of FN-bound integrins increases, consequently e, the ratio of integrins activated by mechanical load and integrins already bound to FN decreases.

The adhesion modulation in response to mechanical load at the onset of adhesion may be important at the leading edge of migrating fibroblasts, where ligand-bound integrins anchor membrane protrusions to ECM proteins. Interestingly, active α5β1 integrins complexing with FAK, Src and talin are internalized from stable adhesions and then recycled back to the leading edge of migrating fibroblasts[42], where newly formed adhesion sites quickly reinforce in response

to mechanical load. Similar processes may operate in other systems such as platelets, which adhere with different integrin classes to ECM proteins, including FN, fibrinogen, or the von-Willebrand factor, during clotting.

5.8. Methods

5.8.1. Cell culture

Parental (WT)[14], pKO-αV/β1[14], pKO-αV[14], pKO-β1[14], pKO[14], talin KO[28], talin crtl[28] and kindlin KO[28] fibroblasts were maintained in DMEM GlutaMAX (Gibco-Life technologies, NY, USA), supplemented with 10% (v/v) fetal calf serum (FCS, Sigma, Steinheim, Germany), 100 units mL^{-1} penicillin (Gibco-Life technologies) and 100 µg mL^{-1} streptomycin (Gibco-Life technologies). All fibroblasts were grown on fibronectin (Calbiochem-Merck, Darmstadt, Germany) coated tissue culture flasks (Jet BioFil, Guangzhou, China). All fibroblasts lines were tested for mycoplasma

5.8.2. Fibronectin fragment expression and purification

We expressed fibronectin fragment FNIII7-10 and RGD-deleted FNIII7-10 (FNIII7-10 RGD) from plasmid pET15b-FNIII7-10 in Escherichia coli BL21 (DE3) pLysS as described[43]. Briefly, cells were grown at 37°C in Lennox L broth (Invitrogen) with 100 µg ml−1 ampicillin (Sigma). At optical density (OD)600 = 0.6, 1 mM isopropyl thiogalactose (IPTG, Sigma) was used to induce protein expression. After 4 h, cells were pelleted, resuspended in buffer (20 mM Tris-HCl, 150 mM NaCl, pH 8.0), and later broken by sonication. Ultracentrifugation at 40,000g was applied for 45 min to remove cell debris. Soluble protein fractions were bound to nickel-nitrilotriacetic acid resin (Protino Ni-NTA Agarose, MACHEREY-NAGEL) for 1 h at 4°C. Then, the resin was loaded onto a column and washed with buffer (20 mM Tris-HCl, 150 mM NaCl, 10 mM imidazole, pH 8.0). Fibronectin fragments were eluted with elution buffer (20 mM Tris-HCl, 150 mM NaCl, 500 mM imidazole, pH 8.0). Thereafter, we pooled the peak fractions and dialysed them against imidazole free buffer (20 mM Tris-HCl, 150 mM NaCl, pH 8.0). Using dialysing buffer, the protein concentration was adjusted to 1.0 mg ml^{-1}, the purified protein was aliquoted and stored at −20°C.

5.8.3. Expression and purification of fibronectin fragments

Fibronectin fragment FNIII7-10 and RGD-deleted FNIII7-10 (FNIII7-10ΔRGD) were expressed from plasmid pET15b-FNIII7-10 in *E.coli* BL21 (DE3) pLysS[41]. Briefly, cells were grown in Lennox L broth (Invitrogen, Carlsbad, USA) supplemented with 100 µg mL^{-1} ampicillin (Sigma, Buchs, Switzerland) at 37°C. Expression was induced with 1 mM isopropyl thiogalactose (IPTG, Sigma) at optical density $(OD)_{600}$ = 0.6. Cells were harvested after 4 h, re-suspended in buffer (20 mM Tris-HCl, 150 mM NaCl, pH 8.0), and broken by sonication. Cell debris was removed

by ultracentrifugation at 40'000xg for 45 min. The soluble protein fraction was bound to nickel-nitrilotriacetic acid resin (Protino® Ni-NTA Agarose, MACHEREY-NAGEL, Düren, Germany) for 1 h at 4°C. The resin was then loaded onto a column and washed with buffer (20 mM Tris-HCl, 150 mM NaCl, 10 mM imidazole, pH 8.0). Fibronectin fragments were eluted with elution buffer (20 mM Tris-HCl, 150 mM NaCl, 500 mM imidazole, pH 8.0). Peak fractions were pooled and dialyzed against imidazole free buffer (20mM Tris-HCl, 150 mM NaCl, pH 8.0). The protein concentration was adjusted to 1.0 mg mL^{-1} with dialyzing buffer and aliquots were stored at −20°C.

5.8.4. Integrin surface expression level and cell size determination.

Overnight serum-starved (DMEM Glutamax, 100 units mL^{-1} penicillin and 100 µg mL^{-1} streptomycin) fibroblasts grown in 6 well plates (Thermo Scientific, Roskilde, Denmark) to confluency of ~ 80% were washed with PBS and detached with 200 µL of 0.25 % (w/v) trypsin/EDTA (Sigma) for 2 min. Detached fibroblasts were suspended in SCFS media (DMEM high glucose, supplemented with 20 mM HEPES) containing 1% (v/v) FCS, pelleted and resuspended in serum free SCFS media. 300'000 fibroblasts were incubated at 37°C for 30 min (ref. [43]). Thereafter, fibroblasts were washed twice with twice with flow cytometry buffer (PBS supplemented with 0.1% BSA (w/v) and 2 mM EDTA). Pelleted fibroblasts were resuspended in 60 µL flow cytometry buffer supplemented with 3 µL of phycoerythrin (PE)-labelled antibodies against integrin subunits αV (551187, Becton Dickinson (BD) AG, Switzerland), α5 (Cat.Nr. 557447, BD AG), β1 (Cat.Nr. 102207, BioLegend, UK) or β3 (Cat.Nr. 12-0611-81, Life Technologies, Switzerland). Fibroblasts were incubated for 30 min at 4°C before they were washed twice with 300 µl flow cytometry buffer. Fluorescence intensity was characterized using LSRFortessa (BD AG).

For cell size characterization, fibroblasts lines were serum starved overnight. Adherent fibroblasts were detached with 200 µL of 0.25 % (w/v) trypsin/EDTA (Sigma) for 2 min and suspended in SCFS media containing 1% (v/v) FCS. Fibroblasts lines were pelleted and resuspended in 100–300 µL SCFS media. Fibroblasts sizes were characterized using an automated cell counter (Countess II, Thermo Fisher Scientific) with standard protocols from the manufacturer.

5.8.5. Coating of AFM cantilever and Petri dishes

Cantilevers (NP-O, Bruker, USA) were plasma-cleaned prior to overnight incubation in ConA (2 mg mL^{-1}, Sigma) or vitronectin (50 µg mL^{-1}) in PBS at 4°C (ref. 44). For VN-dilution series, VN stock solutions (50 µg ml^{-1}) were diluted to final concentrations 0.05, 0.5 or 5 µg ml^{-1} in 2 mg ml^{-1} ConA in PBS. To allow the efficient characterization of cell adhesion to different substrates, a four-segmented PDMS mask was attached to the glass surface of a Petri dish (35 mm

FluoroDish, World Precision Instruments, US)[45]. The PDMS segmented glass surfaces were then incubated overnight either with FNIII7-10 (50 μg mL^{-1}), FNIII7-10ΔRGD (50 μg mL^{-1}), FNIII7-10Δsyn (50 μg mL^{-1}), or vitronectin (50 μg mL^{-1}) in PBS at 4°C.

5.8.6. SCFS

For SCFS, an AFM (NanoWizard II, JPK Instruments, Berlin, Germany) equipped with a CellHesion module (JPK Instruments) was mounted on an inverted microscope (Observer.Z, Zeiss, Jena, Germany). During SCFS fibroblasts were maintained at 37°C using a Petri dish heater (JPK Instruments). 200 μm long tip-less V-shaped silicon nitride cantilevers with a nominal spring constants of 0.06 N m^{-1} (NP-O, Bruker, USA) were used. The spring constant of every cantilever was determined prior the experiment using the thermal noise method[46].

Overnight serum-starved (DMEM Glutamax, 100 units mL^{-1} penicillin and 100 μg mL^{-1} streptomycin) fibroblasts grown in 24 well plates (Thermo Scientific) to confluency of ~ 80% were washed with PBS and detached with 200 μL of 0.25 % (w/v) trypsin/EDTA (Sigma) for 2 min. Detached fibroblasts were suspended in SCFS media (DMEM high glucose, supplemented with 20 mM HEPES) containing 1% (v/v) FCS, pelleted and resuspended in serum free SCFS media. Fibroblasts were allowed to recover from trypsin treatment for at least 30 min (ref. [43]). Petri dishes were washed with SCFS media. Fibroblast suspensions were pipetted into the Petri dishes containing the substrate-coated glass supports and allowed to settle. Rounded fibroblasts having similar size were optically selected for adhesion measurements. To attach single fibroblasts, the apex of a calibrated, ConA functionalized cantilever was lowered with a speed of 10 μm s^{-1} onto a fibroblast until a contact force of 3 nN was reached. After 5 s contact time, the cantilever was retracted by 50 μm to detach the fibroblast from the substrate. Fibroblasts were allowed to attach firmly to the cantilever for at least 5 min before adhesion experiments. For adhesion experiments, cantilever-bound fibroblasts were lowered onto a substrate-coated glass segment with a speed of 5 μm s^{-1} until reaching a contact force of 1 nN. The cantilever position was maintained stationary (constant height) for 1, 2, 3, 5, 20, 35 or 50 s and subsequently retracted at a set speed ranging from 1 to 20 μm s^{-1} for > 90 μm until the fibroblast fully detached from the substrate-coated support. After detachment from the substrate the fibroblast was allowed to recover for at least the contact time before probing the adhesion force of a different retraction speed. Retraction speeds were randomized for all experiments if not stated differently. Single fibroblasts were used to probe adhesion forces once for all retraction speeds or until morphological changes (i.e. spreading) were observed by optical microscopy (**Supplementary Fig. 1c**). After this, a new cantilever was taken to select a new fibroblast. To achieve statistically firm results, the adhesion of at least 10 fibroblasts were characterized per retraction speed.

5.8.7. Data analysis

Adhesion forces were extracted from force-distance curves using the JPK data processing software (JPK Instruments). Fibroblast stiffness and rupture forces were analysed using in-house build routines, which were based on Igor 6 (Wavemetric, Oregon, USA). For the analysis of single integrin bonds, force-distance curves, acquired after 5 s contact time as described in the 'SCFS' section, were condensed to 15'000 points for pKO-αV and pKO-β1 fibroblasts and to 30'000 points for pKO-αV/β1 fibroblasts. Rupture events were analysed to measure the forces rupturing single integrin-FN bonds[24,47]. Tether events were excluded from analysis, as they represent the force required to extract a tether from the cell membrane[48,49]. Rupture and tether events were distinguished by the slope prior to the unbinding event, where tether plateaus had a maximum angle of ~ 10° (Supplementary Fig. 5-1). The minimum rupture force analysed was set to 20 pN.

5.8.8. Statistical analysis

Statistical test were done in Prism (GraphPad, La Jolla, USA) or R (ref. 50). To statistically compare load-dependent adhesion strengthening in different conditions, linear regression analysis of recorded adhesion forces in the first (1–5 μm s^{-1}) and second phase (6–20 μm s^{-1}) was performed. Two-tailed P-values tested the null hypothesis that slopes are identical (parallel). Thereby, the P-values tested the chance that randomly selected data points from both conditions would have slopes at least as different than observed in the compared condition[51]. To compare differences in median adhesion forces, two-tailed Mann-Whitney test was performed. In all statistical analysis, P-values are given as not significant (ns) if $P > 0.05$, and gradually indicated as significant if $P < 0.05$ (*), $P < 0.01$ (**) and $P < 0.001$ (***).

5.8.9. Perturbation and Mn2+ assays

To perturb proteins suspended fibroblasts were incubated with 20 μM SMIFH2 (Merck Millipore), 10 μM Y27632 (Sigma), 200 μM CK666 (Tocris Bioscience), 20 μM blebbistatin (Sigma), 10 μM LY249002 (Cell Signaling Technology), 1 μM latrunculin A (Sigma), 5 mM EDTA (Sigma), 10 and 20 μM PP2 (Tocris), 20 μM PP1 (Tocris), 10 μM Y11 (Tocris), GGTi286 (Merck Millipore) and 20 μM PF573228 (Tocris) for 30 min in SCFS media at 37°C. Fibroblasts were incubated with 2 μM C3 toxin (Cytoskeleton) for 3 h before of the experiments. Perturbants were present during SCFS at the stated concentrations. All perturbants were stored at −20°C and dissolved in DMSO, except C3 Toxin which was dissolved in 50% (v/v) glycerol. For integrin activation, fibroblasts were incubated with 0.5 mM Mn^{2+} for 30 min prior to SCFS and Mn^{2+} was present in the same concentration during adhesion measurements.

5.9. References

1. Schwartz, M. A. & DeSimone, D. W. Cell adhesion receptors in mechanotransduction. *Curr. Opin. Cell. Biol.* **20,** 551–556 (2008).
2. Butcher, D. T., Alliston, T. & Weaver, V. M. A tense situation: forcing tumour progression. *Nat. Rev. Cancer* **9,** 108–122 (2009).
3. Ross, T. D. *et al.* Integrins in mechanotransduction. *Curr. Opin. Cell. Biol.* **25,** 613–618 (2013).
4. Humphrey, J. D., Dufresne, E. R. & Schwartz, M. A. Mechanotransduction and extracellular matrix homeostasis. *Nat. Rev. Mol. Cell Biol.* **15,** 802–812 (2014).
5. Iskratsch, T., Wolfenson, H. & Sheetz, M. P. Appreciating force and shape — the rise of mechanotransduction in cell biology. *Nat. Rev. Mol. Cell Biol.* **15,** 825–833 (2014).
6. Hynes, R. O. Integrins: bidirectional, allosteric signaling machines. *Cell* **110,** 673–687 (2002).
7. Humphries, J. D., Byron, A. & Humphries, M. J. Integrin ligands at a glance. *J. Cell Sci.* **119,** 3901–3903 (2006).
8. Leiss, M., Beckmann, K., Girós, A., Costell, M. & Fässler, R. The role of integrin binding sites in fibronectin matrix assembly in vivo. *Curr. Opin. Cell. Biol.* **20,** 502–507 (2008).
9. Benito-Jardón, M. *et al.* The fibronectin synergy site re-enforces cell adhesion and mediates a crosstalk between integrin classes. *eLIFE* **6,** e22264 (2017).
10. Taubenberger, A., Cisneros, D. A., Puech, P.-H., Müller, D. J. & Franz, C. M. Revealing early steps of alpha2beta1 integrin-mediated adhesion to collagen type I by using single-cell force spectroscopy. *Mol. Biol. Cell* **18,** 1634–1644 (2007).
11. Changede, R., Xu, X., Margadant, F. & Sheetz, M. P. Nascent Integrin Adhesions Form on All Matrix Rigidities after Integrin Activation. *Dev. Cell* **35,** 614–621 (2015).
12. Robertson, J. *et al.* Defining the phospho-adhesome through the phosphoproteomic analysis of integrin signalling. *Nat. Commun.* **6,** 6265 (2015).
13. Schiller, H. B., Friedel, C. C., Boulegue, C. & Fässler, R. Quantitative proteomics of the integrin adhesome show a myosin II-dependent recruitment of LIM domain proteins. *EMBO Rep.* **12,** 259–266 (2011).
14. Schiller, H. B. *et al.* β1- and αv-class integrins cooperate to regulate myosin II during rigidity sensing of fibronectin-based microenvironments. *Nat. Cell Biol.* **15,** 625–636 (2013).
15. Grashoff, C. *et al.* Measuring mechanical tension across vinculin reveals regulation of focal adhesion dynamics. *Nature* **466,** 263–266 (2010).
16. del Rio, A. *et al.* Stretching single talin rod molecules activates vinculin binding. *Science* **323,** 638–641 (2009).
17. Sawada, Y. *et al.* Force Sensing by Extension of the Src Family Kinase Substrate, p130Cas. *Cell* **127,** 1015–1026 (2006).
18. Wang, Y. *et al.* Visualizing the mechanical activation of Src. *Nature* **434,** 1040–1045 (2005).
19. Parsons, J. T., Horwitz, A. R. & Schwartz, M. A. Cell adhesion: integrating cytoskeletal dynamics and cellular tension. *Nat. Rev. Mol. Cell Biol.* **11,** 633–643 (2010).
20. Friedland, J. C., Lee, M. H. & Boettiger, D. Mechanically activated integrin switch controls alpha5beta1 function. *Science* **323,** 642–644 (2009).
21. Kong, F., García, A. J., Mould, A. P., Humphries, M. J. & Zhu, C. Demonstration of catch bonds between an integrin and its ligand. *J. Cell Biol.* **185,** 1275–1284 (2009).
22. Thomas, W. Catch Bonds in Adhesion. *Annu. Rev. Biomed. Eng.* **10,** 39–57 (2008).
23. Friedrichs, J. *et al.* A practical guide to quantify cell adhesion using single-cell force spectroscopy. *Methods* **60,** 169–178 (2013).
24. Helenius, J., Heisenberg, C.-P., Gaub, H. E. & Müller, D. J. Single-cell force spectroscopy. *J. Cell Sci.* **121,** 1785–1791 (2008).
25. Balcioglu, H. E., van Hoorn, H., Donato, D. M., Schmidt, T. & Danen, E. H. J. The integrin expression profile modulates orientation and dynamics of force transmission at cell–matrix adhesions. *J. Cell Sci.* **128,** 1316–1326 (2015).
26. Elosegui-Artola, A. *et al.* Rigidity sensing and adaptation through regulation of integrin types. *Nat. Mater.* **13,** 631–637 (2014).
27. Kong, F. *et al.* Cyclic mechanical reinforcement of integrin-ligand interactions. *Mol. Cell*

49, 1060–1068 (2013).
28. Theodosiou, M. *et al.* Kindlin-2 cooperates with talin to activate integrins and induces cell spreading by directly binding paxillin. *eLIFE* **5,** e10130 (2016).
29. Bharadwaj, M. *et al.* αV-class integrins exert dual roles on α5β1 integrins to strengthen adhesion to fibronectin. *Nat. Commun.* **8,** 14348 (2017).
30. Na, S. *et al.* Rapid signal transduction in living cells is a unique feature of mechanotransduction. *Proc. Natl. Acad. Sci. U.S.A.* **105,** 6626–6631 (2008).
31. Tzima, E. *et al.* A mechanosensory complex that mediates the endothelial cell response to fluid shear stress. *Nature* **437,** 426–431 (2005).
32. Shattil, S. J., Kim, C. & Ginsberg, M. H. The final steps of integrin activation: the end game. *Nat. Rev. Mol. Cell Biol.* **11,** 288–300 (2010).
33. Roca-Cusachs, P., Gauthier, N. C., del Rio, A. & Sheetz, M. P. Clustering of α5β1 integrins determines adhesion strength whereas αvβ3 and talin enable mechanotransduction. *Proc. Natl. Acad. Sci. U.S.A.* **106,** 16245–16250 (2009).
34. Rossier, O. *et al.* Integrins β1 and β3 exhibit distinct dynamic nanoscale organizations inside focal adhesions. *Nat. Cell Biol.* **14,** 1057–1067 (2012).
35. Sun, Z. *et al.* Kank2 activates talin, reduces force transduction across integrins and induces central adhesion formation. *Nat. Cell Biol.* **18,** 941–953 (2016).
36. Das, M., Subbayya Ithychanda, S., Qin, J. & Plow, E. F. Mechanisms of talin-dependent integrin signaling and crosstalk. *BBA-Biomembranes* **1838,** 579–588 (2014).
37. Calderwood, D. A., Campbell, I. D. & Critchley, D. R. Talins and kindlins: partners in integrin-mediated adhesion. *Nat. Rev. Mol. Cell Biol.* **14,** 503–517 (2013).
38. Priddle, H. *et al.* Disruption of the talin gene compromises focal adhesion assembly in undifferentiated but not differentiated embryonic stem cells. *J. Cell Biol.* **142,** 1121–1133 (1998).
39. Zhang, X. *et al.* Talin depletion reveals independence of initial cell spreading from integrin activation and traction. *Nat. Cell Biol.* **10,** 1062–1068 (2008).
40. Moser, M., Legate, K. R., Zent, R. & Fässler, R. The tail of integrins, talin, and kindlins. *Science* **324,** 895–899 (2009).
41. Lawson, C. *et al.* FAK promotes recruitment of talin to nascent adhesions to control cell motility. *J. Cell Biol.* **196,** 223–232 (2012).
42. Nader, G., Ezratty, E. J. & Gundersen, G. G. FAK, talin and PIPKIγ regulate endocytosed integrin activation to polarize focal adhesion assembly. *Nat. Cell Biol.* **18,** 491–503 (2016).
43. Schubert, R. *et al.* Assay for characterizing the recovery of vertebrate cells for adhesion measurements by single-cell force spectroscopy. *FEBS Lett.* **588,** 3639–3648 (2014).
44. Friedrichs, J., Helenius, J. & Müller, D. J. Quantifying cellular adhesion to extracellular matrix components by single-cell force spectroscopy. *Nat. Protoc.* **5,** 1353–1361 (2010).
45. Yu, M., Strohmeyer, N., Wang, J., Müller, D. J. & Helenius, J. Increasing throughput of AFM-based single cell adhesion measurements through multisubstrate surfaces. *Beilstein J. Nanotechnol.* **6,** 157–166 (2015).
46. Hutter, J. L. & Bechhoefer, J. Calibration of atomic-force microscope tips. *Rev. Sci. Instrum.* **64,** 1868 (1993).
47. Müller, D. J., Helenius, J., Alsteens, D. & Dufrêne, Y. F. Force probing surfaces of living cells to molecular resolution. *Nat. Chem. Biol.* **5,** 383–390 (2009).
48. Krieg, M., Helenius, J., Heisenberg, C.-P. & Müller, D. J. A Bond for a Lifetime: Employing Membrane Nanotubes from Living Cells to Determine Receptor-Ligand Kinetics. *Angew. Chem. Int. Ed.* **47,** 9775–9777 (2008).
49. Sheetz, M. P. Cell control by membrane–cytoskeleton adhesion. *Nat. Rev. Mol. Cell Biol.* **2,** 392–396 (2001).
50. R Core Team. R: A language and environment for statistical computing. R Foundation for Statistical Computing, Vienna, Austria. URL http://www.R-project.org/.
51. Zar, J. H. *Biostatistical Analysis.* (Pearson Education Limited, 2014).

5.10. Acknowledgments

We thank S. Weiser and J. Thoma for fibronectin fragment cloning, expression and purification, the single cell facility for help with flow cytometry, N. Beerenwinkel for help with statistical questions and J. Helenius and J. Polleux for critical discussions. This work was supported by the European Research Council (Grant Agreement no. 322652), Deutsche Forschungsgemeinschaft (SFB865-B3), and Swiss National Science Foundation (Grant 31003A_138063).

5.11. Author contributions

N.S., M.B., R.F. and D.J.M designed the experiments and wrote the paper. N.S. performed and analyzed most experiments. M.B. performed initial experiments. R.F. and M.C. provided reagents and/or analytical tools. All authors discussed the experiments, read and approved the manuscript.

5.12. Competing financial interest

The authors declare no competing financial interest.

5.13. Data and code availability statement

The data that support the findings and the code to analyse the data are available from the corresponding author upon request.

5.14. Supplementary Information

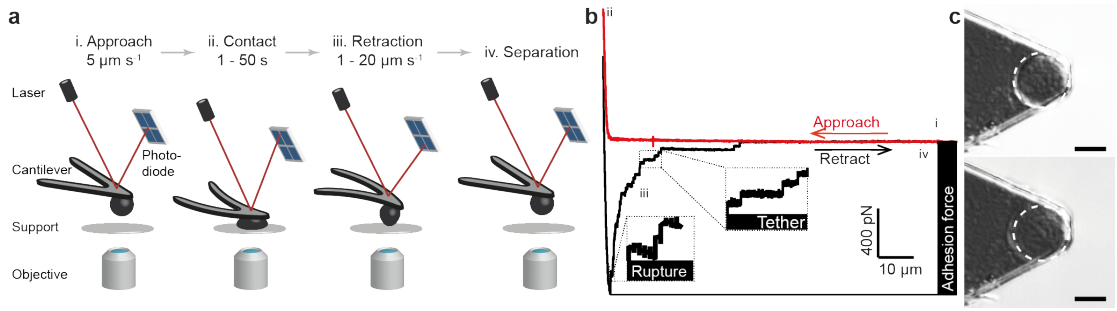

Supplementary Figure 5-1. AFM-based SCFS setup to quantify retraction speed-dependent adhesion forces of fibroblasts. a, Single-cell force spectroscopy (SCFS) setup. (i) Single fibroblasts were incubated for ~ 5 min on a ConA-coated cantilever. (ii) Subsequently, they were approached onto a fibronectin (FN) fragment-coated support. (iii and iv) After 5 s contact time, the cantilever was retracted vertically to measure the adhesion force between fibroblast and support until the fibroblasts was fully detached from the substrate. During the adhesion experiments the cantilever deflection is recorded and displayed in a force-distance curve. **b**, Force-distance curves show different features: The retraction force-distance curve (black) records the adhesion force of the fibroblast, which represents the maximum downward force deflection of the cantilever and thus, the highest force required to separate the fibroblast from the substrate[1,2]. Upon detachment of cell and substrate single receptor unbinding events are observed. Rupture events are recorded when the bond formed between a cytoskeleton-linked integrin and the substrate fails. Tether events are recorded when extruding a membrane tether from the cell membrane with the integrins at its tip. In the latter case the attachment of the integrin to the cytoskeleton is either too weak to resist the mechanical load applied or non-existent[2,3]. **c**, (top) A single round fibroblast is attached to the cantilever tip and is used for adhesion measurements until (bottom) the fibroblast shows morphological changes (i.e. spreading).

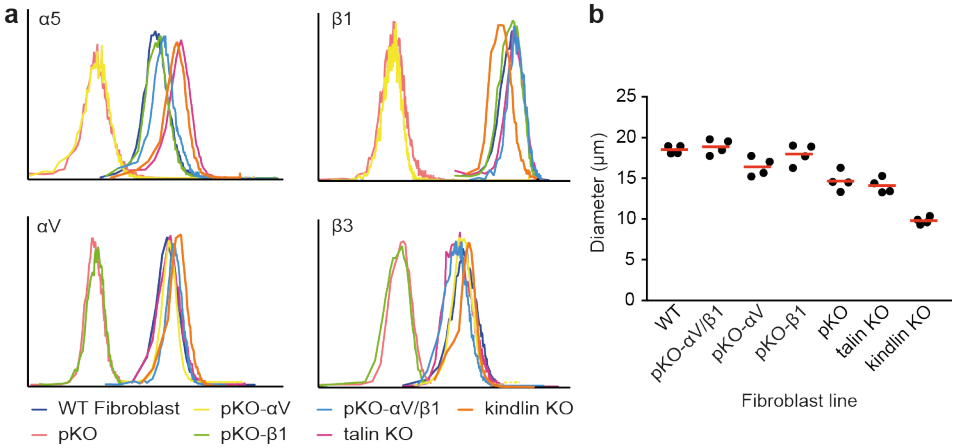

Supplementary Figure 5-2. Integrins surface expression levels and cell sizes of the fibroblasts lines. a, Every fibroblast line was incubated with phycoerythrin-labeled antibodies against αV, α5, β1 and β3 integrin subunits. Thereafter, integrin-labeled fibroblasts were analyzed using flow cytometry. pKO fibroblasts were used as negative control. **b**, The mean diameter of four independent samples of each fibroblast line was characterized using an automated cell counter device (Countess II). Each dot represents the mean diameter of an independent fibroblast sample with their mean given by the red bar. **a** and **b**, Fibroblast lines characterized were

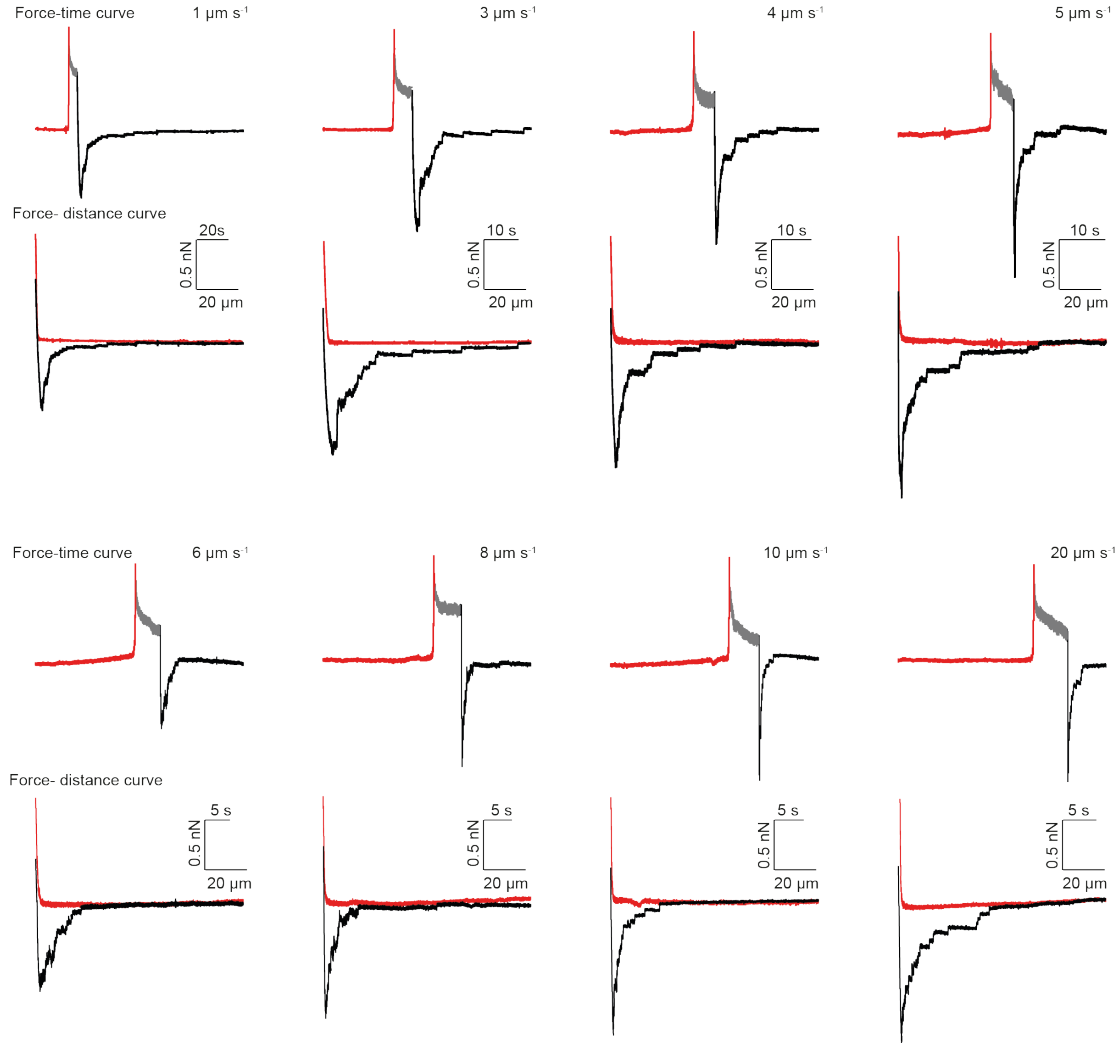

Supplementary Figure 5-3. Representative force-time and force-distance curves for all applied retraction speeds. pKO-αV/β1-fibroblasts were attached to ConA-coated cantilevers and incubated for 5 min to assure firm binding. Cantilever-bound fibroblasts were approached (red) to FNIII7-10-coated supports until recording a contact force of 1 nN. Then, the cantilever position was maintained for 5 s, allowing fibroblasts to initiate adhesion (grey). After the contact time, cantilever bound fibroblasts were retracted from the support (black). The force acting on the cantilever is shown for all retraction speeds used in relation to time (top) and distance (bottom).

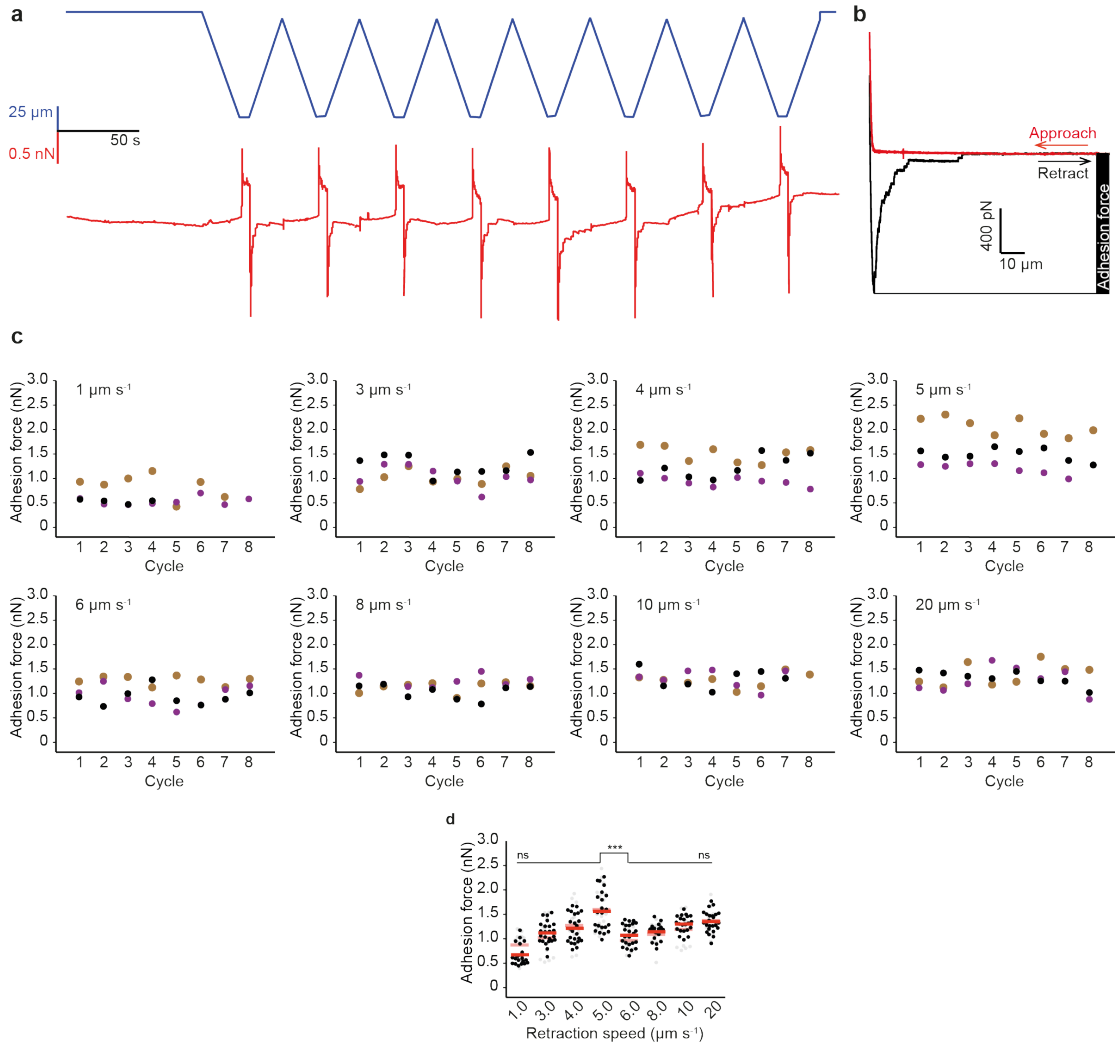

Supplementary Figure 5-4. Reproducibility of SCFS experiments to measure the retraction speed-dependent adhesion force of fibroblasts to a substrate. a-c, Single pKO-αV/β1-fibroblasts were attached to ConA-coated cantilevers and incubated for 5 min on the cantilever to assure firm binding. Thereafter, fibroblasts were approached to FNIII7-10-coated supports and were allowed to initiate adhesion for 5 s. Subsequently, the adhesion forces were quantified at the same retraction speed for eight repeated cell adhesion measurements or until the cell was fully spread on the cantilever. After each adhesion measurement, the location at which the cell was allowed to adhere to the support was changed. Each adhesion measurement was conducted at the specified retraction speed. a, The cantilever movement and the resulting force-time curve for a representative fibroblast for 5 µm s^{-1} retraction speed is shown. b, Fibroblast adhesion force quantified from a representative force-distance curve recorded at 5 µm s^{-1} retraction speed. c, Adhesion forces (dots) of pKO-αV/β1-fibroblasts for repeated measurements are shown. Dots with the same color in each panel represent the same fibroblast used. For each panel three different fibroblasts were used. d, Combined data from all adhesion measurements for all fibroblasts characterized in Supplementary Fig. 3c. The speed-dependent adhesion profile of untreated ConA-bound pKO-αV/β1 fibroblasts adhering to FNIII7-10-coated supports (Fig. 5-1a) is displayed in grey for reference. For statistical analysis, the slopes of adhesion forces from 1–5 µm s^{-1} and 6–20 µm s^{-1} were compared with the respective slopes of untreated ConA-bound pKO-αV/β1 fibroblasts adhering to FNIII7-10-coated supports. Adhesion forces of individual fibroblasts (dots) after 5 s contact time with the substrate-coated supports and their median (red bar) are given. Adhesion slopes were statistically compared based on difference in difference test. Differences of adhesion forces between 5 µm s^{-1} and 6 µm s^{-1} were evaluated applying the Mann-Whitney test. P-values are ns > 0.05, * < 0.05, ** < 0.01 and *** < 0.001.

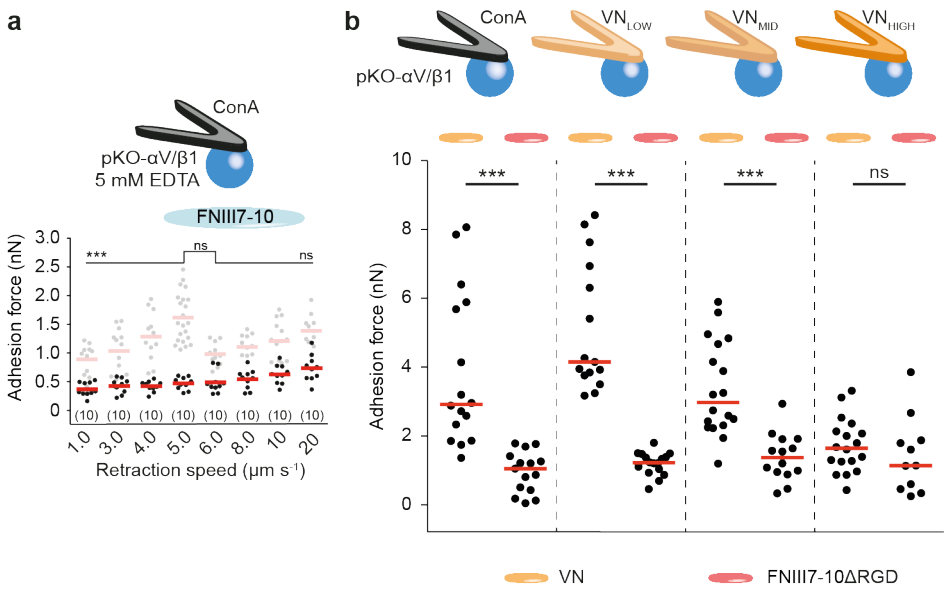

Supplementary Figure 5-5. Integrins activity and proximity are required for biphasic adhesion strengthening. a, To inactivate integrins pKO-αV/β1 fibroblasts were treated with EDTA 30 min prior to the experiments and during the adhesion measurements. Fibroblasts attached to ConA-coated cantilevers were allowed to adhere for 5 s to FNIII7-10-coated supports before being separated at the indicated retraction speed. The speed-dependent adhesion profile of untreated pKO-αV/β1 fibroblasts attached to ConA-coated cantilevers and adhering to FNIII7-10 substrates (Fig. 5-1a) is displayed in grey for reference. For statistical analysis, the slopes of adhesion forces from 1–5 µm s^{-1} and 6–20 µm s^{-1} were compared with the respective slopes of untreated pKO-αV/β1 fibroblasts attached to ConA-coated cantilevers and adhering to FNIII7-10 substrates. Adhesion slopes were compared based on difference in differences. Differences of adhesion forces between 5 µm s^{-1} and 6 µm s^{-1} were evaluated by applying the Mann-Whitney test. P-values are ns > 0.05, * < 0.05, ** < 0.01 and *** < 0.001. **b**, pKO-αV/β1 fibroblasts were attached to cantilevers either coated with ConA or ConA diluted with different concentrations of VN (0.5, 5.0 or 50 µg ml^{-1} VN (VN_{LOW}, VN_{MID} or VN_{HIGH}, respectively). After an attachment time of 7–10 min to the substrate-coated cantilever, the adhesion of the fibroblast was probed to FNIII7-10ΔRGD or VN-coated (50 µg ml^{-1}) supports. Adhesion forces of individual fibroblasts (dots) after 50 s contact time with the substrate-coated supports and their median (red bar) are given. Differences of adhesion forces between ConA- and VN-bound pKO-αV/β1 fibroblasts were evaluated by applying the Mann-Whitney test. P-values are ns > 0.05, * < 0.05, ** < 0.01 and *** < 0.001.

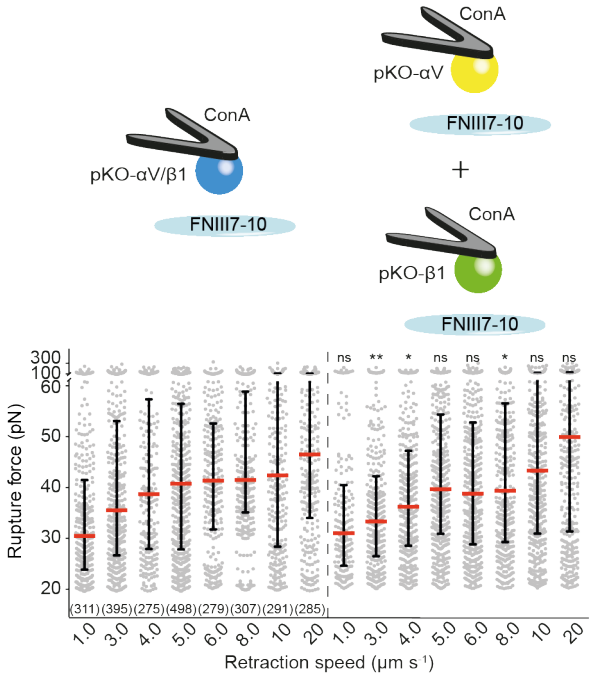

Supplementary Figure 5-6. Analysis of speed-dependent rupture forces required to separating αV-class and α5β1 integrins bound to fibronectin. pKO-αV/β1, pKO-αV or pKO-β1 fibroblasts were allowed to adhere to FNIII7-10-coated supports for 5 s before being separated at the retraction speeds indicated. All fibroblasts were attached to ConA-coated cantilevers. Analysis of single rupture events in force-distance curves (Supplementary Fig. 5-1a,b) quantified the unbinding forces of single integrin-FN bonds. The left panel shows the rupture forces recorded for pKO-αV/β1 fibroblasts (taken from data analysed in Fig. 5-2). The right panel shows rupture forces recorded for pKO-αV and pKO-β1 fibroblasts combined in one graph. The rupture forces of single integrin-FN bonds (grey dots), their median (red bars) and the interquartile range are given. (*n*) denotes the number of single unbinding events analysed. Differences of rupture forces measured at the same retraction speed were evaluated by applying the Mann-Whitney test. P-values are ns > 0.05, * < 0.05, ** < 0.01 and *** < 0.001.

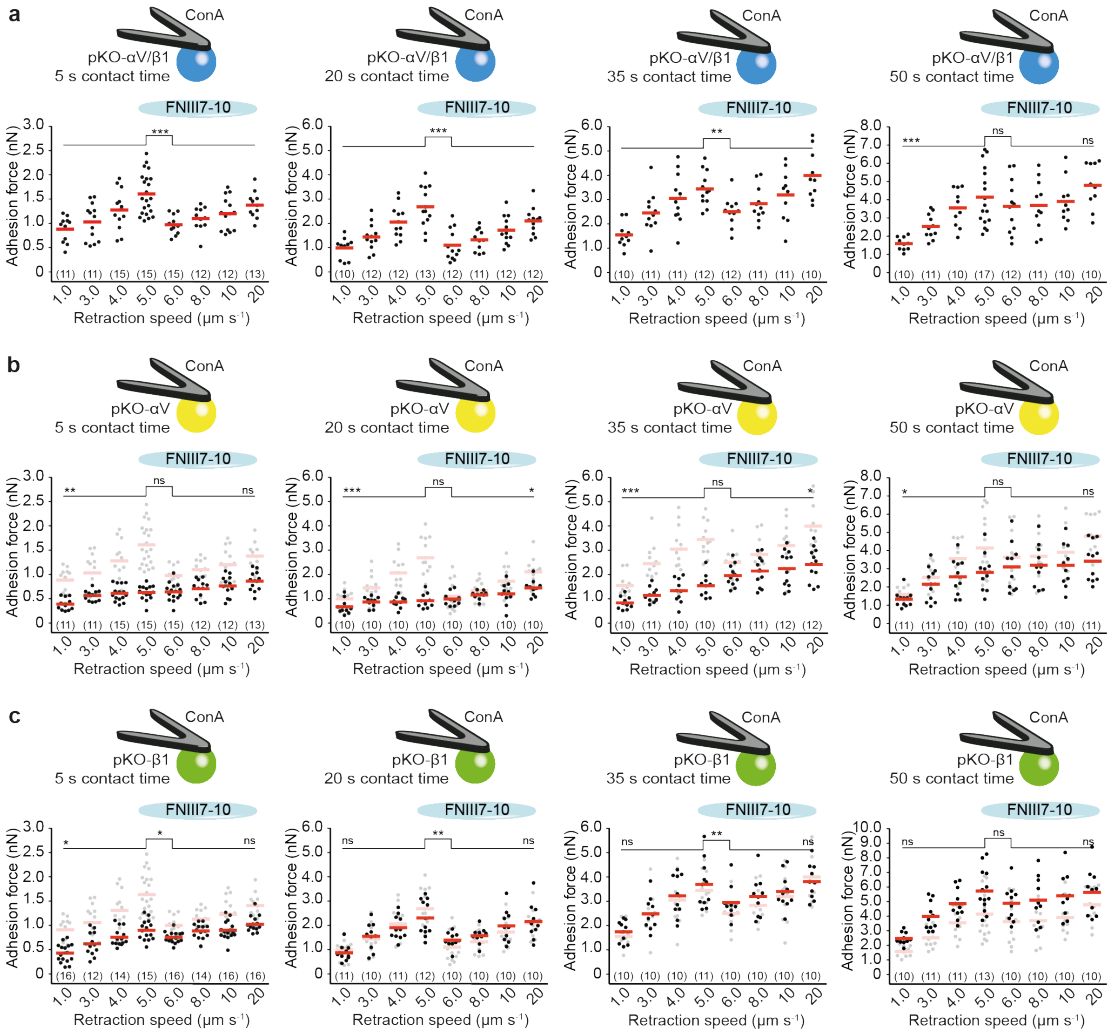

Supplementary Figure 5-7. Adhesion strengthening of pKO-αV/β1, pKO-αV or pKO-β1 fibroblasts in response to mechanical load and contact times. a, pKO-αV/β1, **b**, pKO-αV or **c**, pKO- β1 fibroblasts were attached to ConA-coated cantilevers, brought into contact with FNIII7-10-coated supports, and after contact times of 5, 20, 35 or 50 s were separated at indicated speeds. **(a)** Data taken from experiments analyzed in Fig. 5-1a and 5-3b. For each retraction speed, adhesion forces of individual fibroblasts (dots) and their mean (red bar) are given. (*n*) denotes the number of fibroblasts probed for each condition. b and c, Speed-dependent adhesion profiles of pKO-αV/β1 fibroblasts attached to ConA-coated cantilevers and adhering to FNIII7-10 substrates for the indicated contact time are displayed in grey for reference (all taken from Fig. 5-1a and 5-3b). For statistical analysis, the slopes of adhesion forces in the first (1–5 µm s^{-1}) and second (6–20 µm s^{-1}) phase were compared with the respective slopes of pKO-αV/β1 fibroblasts on ConA-coated cantilevers and adhering to FNIII7-10 substrates for the same time. Slopes were compared based on difference in differences. Differences of adhesion forces between 5 µm s^{-1} and 6 µm s^{-1} were evaluated by applying the Mann-Whitney test. P-values are ns > 0.05, * < 0.05, ** < 0.01 and *** < 0.001.

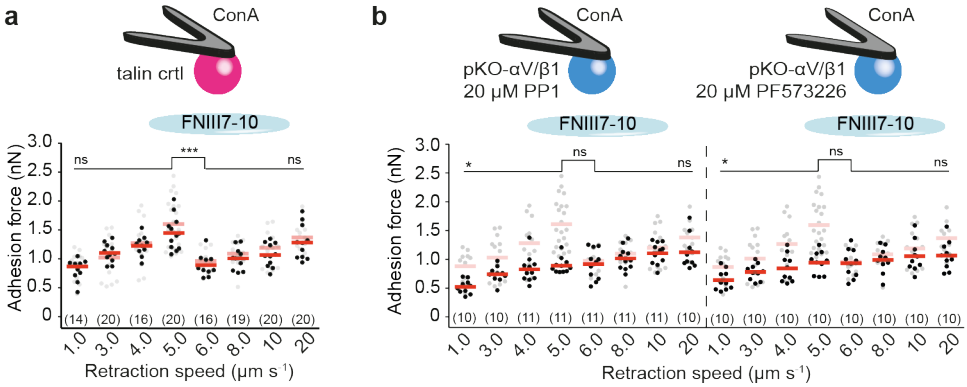

Supplementary Figure 5-8. Adhesion strengthening in response to mechanical load requires talin and FAK and c-Src mediated signalling. a, Talin control (parental *tln1*$^{fl/fl}$, *tln2*$^{-/-}$; crtl) or pKO-αV/β1 fibroblasts were attached to ConA-coated cantilever, approached to FNIII7-10-coated support and after 5 s contact time separated from the substrate at the retraction speeds indicated. **b**, To inhibit the Src-kinase family cell suspensions were incubated with 20 µM PP1 and to inhibit FAK cell suspensions were incubated with PF573228 for 30 min prior to and throughout the SCFS experiments. For each retraction speed adhesion forces of individual fibroblasts (dots) and their mean (red bar) are given. (*n*) denotes the number of fibroblasts probed for each condition. The speed-dependent adhesion profile of pKO-αV/β1 fibroblasts attached to ConA-coated cantilevers and adhering to FNIII7-10 substrates for 5 s contact time (Fig. 5-1a) is displayed in grey for reference. For statistical analysis, the slopes of adhesion forces from 1–5 µm s^{-1} and 6–20 µm s^{-1} were compared with the respective slopes of pKO-αV/β1 fibroblasts attached to ConA-coated cantilevers and adhering to FNIII7-10 substrates for 5 s. Adhesion slopes were compared based on difference in differences. Differences of adhesion forces between 5 µm s^{-1} and 6 µm s^{-1} were evaluated by applying the Mann-Whitney test. P-values are ns > 0.05, * < 0.05, ** < 0.01 and *** < 0.001.

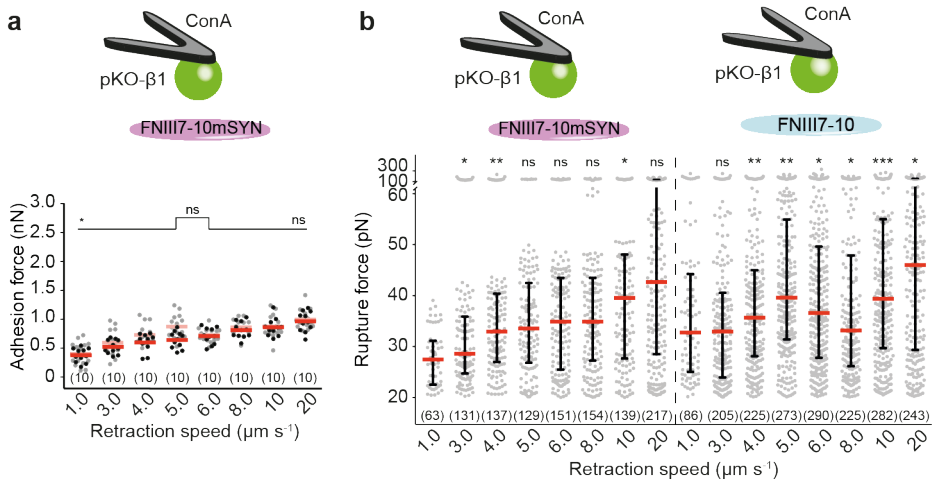

Supplementary Figure 5-9. Adhesion strengthening in response to mechanical load requires the formation of catch bonds between α5β1 integrins and fibronectin. a, Adhesion forces of pKO-β1 fibroblasts to FNIII7-10mSYN. were attached to ConA-coated cantilevers, approached to FNIII7-10mSYN-coated support and after 5 s contact time separated from the substrate at the retraction speeds indicated. For each retraction speed adhesion forces of individual fibroblasts (dots) and their mean (red bar) are given. (*n*) denotes the number of fibroblasts probed for each condition. The speed-dependent adhesion profile of pKO-αV/β1 fibroblasts attached to ConA-coated cantilevers and adhering to FNIII7-10 substrates for 5 s contact time (**Fig. 1c**) is displayed in grey for reference. For statistical analysis the slopes of adhesion forces from 1–5 μm s^{-1} and 6–20 μm s^{-1} were compared with the respective slopes of pKO-αV/β1 fibroblasts attached to ConA-coated cantilevers and adhering to FNIII7-10 substrates for 5 s. Adhesion slopes were compared based on difference in differences. Differences of adhesion forces between 5 μm s^{-1} and 6 μm s^{-1} were evaluated applying the Mann-Whitney test. **b**, Rupture forces of single α5β1 integrins. pKO-β1 fibroblasts were approached to FNIII7-10mSYN- or FNIII7-10-coated supports, allowed to adhere for 5 s and separated at the retraction speeds indicated. Rupture forces required to separating single integrin-FN bonds were taken from single rupture events detected in force-distance curves. Rupture forces of single integrin-FN bonds (grey dots), their median (red bars) and the interquartile range are given. In the right panel is taken from experiments analysed in Fig. 5-2 (*n*) denotes the number of single unbinding events analysed. Statistical significance of median differences to the slower retraction speed was tested using the Mann-Whitney-Test. P-values are ns > 0.05, * < 0.05, ** < 0.01 and *** < 0.001.

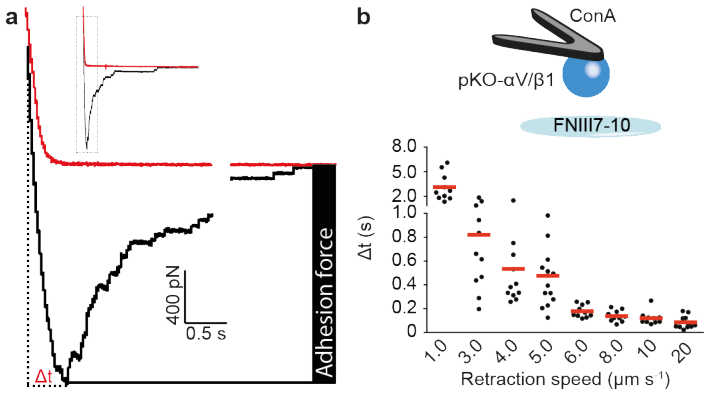

Supplementary Figure 5-10. In response to mechanical load, fibroblasts adapt adhesion within less than 0.5 seconds. a, Typical force-time curve recorded while approaching (red) and retracting (black) a pKO-αV/β1 fibroblast attached to a ConA-coated cantilever from a FNIII7-10-coated support (5 s contact time). From this retraction curve we determined the time Δ*t* the fibroblast was mechanically loaded until measuring the maximum adhesion force initiating the detachment of the cell from the substrate. **b**, time to initiate cell detachment *versus* retraction speed of pKO-αV/β1 fibroblasts attached to ConA-coated cantilevers and adhering to FNIII7-10-coated supports for 5 s. For each retraction speed, the time of individual fibroblasts (dots) and their mean (red bar) are given.

5.15. Statistical Tests

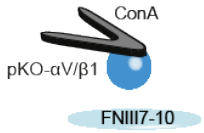

	1 µm s^{-1}	3 µm s^{-1}	4 µm s^{-1}	5 µm s^{-1}	6 µm s^{-1}	8 µm s^{-1}	10 µm s^{-1}	20 µm s^{-1}
1 µm s^{-1}		3.03E-01	**1.88E-02**	**1.44E-06**	6.06E-01	7.59E-02	**3.33E-02**	**2.75E-04**
3 µm s^{-1}	3.03E-01		1.68E-01	**2.61E-03**	7.33E-01	7.76E-01	2.80E-01	**4.74E-02**
4 µm s^{-1}	**1.88E-02**	1.68E-01		5.77E-02	6.88E-02	2.35E-01	7.05E-01	4.49E-01
5 µm s^{-1}	**1.44E-06**	**2.61E-03**	5.77E-02		**1.57E-05**	**9.67E-04**	**1.17E-02**	2.04E-01
6 µm s^{-1}	6.06E-01	7.33E-01	6.88E-02	**1.57E-05**		1.16E-01	1.49E-01	**1.04E-03**
8 µm s^{-1}	7.59E-02	7.76E-01	2.35E-01	**9.67E-04**	1.16E-01		6.47E-01	**3.36E-02**
10 µm s^{-1}	**3.33E-02**	2.80E-01	7.05E-01	**1.17E-02**	1.49E-01	6.47E-01		1.83E-01
20 µm s^{-1}	**2.75E-04**	**4.74E-02**	4.49E-01	2.04E-01	**1.04E-03**	**3.36E-02**	1.83E-01	

Statistics Table 1. Cross table of P-Values comparing adhesion forces of indicated retraction speeds from Fig. 5-1a using Mann-Whitney test. P-values smaller than 0.05 are shown bold.

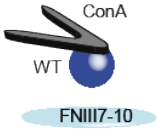

	1 µm s^{-1}	3 µm s^{-1}	4 µm s^{-1}	5 µm s^{-1}	6 µm s^{-1}	8 µm s^{-1}	10 µm s^{-1}	20 µm s^{-1}
1 µm s^{-1}		**1.15E-02**	**2.24E-04**	**9.02E-08**	1.43E-01	**2.32E-02**	**2.09E-03**	**2.09E-03**
3 µm s^{-1}	**1.15E-02**		1.44E-01	**1.75E-04**	3.53E-01	3.93E-01	1.05E-01	1.05E-01
4 µm s^{-1}	**2.24E-04**	1.44E-01		**8.99E-03**	**4.75E-02**	8.49E-01	6.43E-01	3.97E-01
5 µm s^{-1}	**9.02E-08**	**1.75E-04**	**8.99E-03**		**1.65E-05**	**1.94E-02**	**4.82E-02**	4.41E-01
6 µm s^{-1}	1.43E-01	3.53E-01	**4.75E-02**	**1.65E-05**		2.18E-01	**4.33E-02**	**2.88E-02**
8 µm s^{-1}	**2.32E-02**	3.93E-01	8.49E-01	**1.94E-02**	2.18E-01		6.31E-01	1.65E-01
10 µm s^{-1}	**2.09E-03**	1.05E-01	6.43E-01	**4.82E-02**	**4.33E-02**	6.31E-01		4.81E-01
20 µm s^{-1}	**2.09E-03**	1.05E-01	3.97E-01	4.41E-01	**2.88E-02**	1.65E-01	4.81E-01	

Statistics Table 2. Cross table of P-Values comparing adhesion forces of indicated retraction speeds from Fig. 5-1a using Mann-Whitney test. P-values smaller than 0.05 are shown bold.

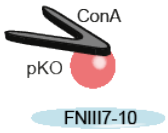

	1 µm s^{-1}	3 µm s^{-1}	4 µm s^{-1}	5 µm s^{-1}	6 µm s^{-1}	8 µm s^{-1}	10 µm s^{-1}	20 µm s^{-1}
1 µm s^{-1}		1.90E-01	6.30E-02	**1.15E-02**	**8.93E-03**	**1.50E-03**	**1.50E-03**	**1.05E-03**
3 µm s^{-1}	1.90E-01		5.79E-01	**3.55E-02**	**3.55E-02**	**3.89E-03**	**6.84E-03**	**3.89E-03**
4 µm s^{-1}	6.30E-02	5.79E-01		6.30E-02	7.53E-02	**2.09E-03**	**6.84E-03**	**5.20E-03**
5 µm s^{-1}	1.15E-02	**3.55E-02**	6.30E-02		9.12E-01	**3.55E-02**	1.05E-01	8.92E-02
6 µm s^{-1}	**8.93E-03**	**3.55E-02**	7.53E-02	9.12E-01		1.23E-01	2.18E-01	7.53E-02
8 µm s^{-1}	**1.50E-03**	**3.89E-03**	**2.09E-03**	**3.55E-02**	1.23E-01		1.00E+00	5.29E-01
10 µm s^{-1}	**1.50E-03**	**6.84E-03**	**6.84E-03**	1.05E-01	2.18E-01	1.00E+00		3.93E-01
20 µm s^{-1}	**1.05E-03**	**3.89E-03**	**5.20E-03**	8.92E-02	7.53E-02	5.29E-01	3.93E-01	

Statistics Table 3. Cross table of P-Values comparing adhesion forces of indicated retraction speeds from Fig. 5-1b using Mann-Whitney test. P-values smaller than 0.05 are shown bold.

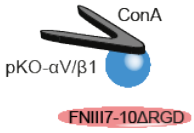

	1 µm s^{-1}	3 µm s^{-1}	4 µm s^{-1}	5 µm s^{-1}	6 µm s^{-1}	8 µm s^{-1}	10 µm s^{-1}	20 µm s^{-1}
1 µm s^{-1}		**3.00E-03**	**3.44E-04**	**3.93E-06**	**2.88E-05**	**2.96E-06**	**7.69E-07**	**7.69E-07**
3 µm s^{-1}	**3.00E-03**		3.11E-01	9.45E-02	2.39E-01	**8.85E-03**	**1.02E-02**	**6.28E-04**
4 µm s^{-1}	**3.44E-04**	3.11E-01		3.02E-01	4.58E-01	**2.57E-02**	**1.02E-02**	**1.25E-03**
5 µm s^{-1}	**3.93E-06**	9.45E-02	3.02E-01		6.67E-01	2.67E-01	2.80E-01	**2.91E-02**
6 µm s^{-1}	**2.88E-05**	2.39E-01	4.58E-01	6.67E-01		2.67E-01	1.41E-01	**2.22E-02**
8 µm s^{-1}	**2.96E-06**	**8.85E-03**	**2.57E-02**	2.67E-01	2.67E-01		8.20E-01	1.86E-01
10 µm s^{-1}	**7.69E-07**	**1.02E-02**	**1.02E-02**	2.80E-01	1.41E-01	8.20E-01		2.64E-01
20 µm s^{-1}	**7.69E-07**	**6.28E-04**	**1.25E-03**	**2.91E-02**	**2.22E-02**	1.86E-01	2.64E-01	

Statistics Table 4. Cross table of P-Values comparing adhesion forces of indicated retraction speeds from Fig. 5-1b using Mann-Whitney test. P-values smaller than 0.05 are shown bold.

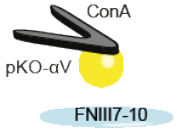

	1 µm s^{-1}	3 µm s^{-1}	4 µm s^{-1}	5 µm s^{-1}	6 µm s^{-1}	8 µm s^{-1}	10 µm s^{-1}	20 µm s^{-1}
1 µm s^{-1}		**3.18E-03**	**2.01E-03**	**5.06E-04**	**1.30E-03**	**4.01E-04**	**2.88E-04**	**5.61E-06**
3 µm s^{-1}	**3.18E-03**		5.40E-01	1.80E-01	1.64E-01	9.08E-02	**1.88E-02**	**2.17E-04**
4 µm s^{-1}	**2.01E-03**	5.40E-01		6.53E-01	6.24E-01	2.56E-01	8.32E-02	**1.03E-03**
5 µm s^{-1}	**5.06E-04**	1.80E-01	6.53E-01		9.35E-01	2.36E-01	1.03E-01	**2.63E-03**
6 µm s^{-1}	**1.30E-03**	1.64E-01	6.24E-01	9.35E-01		3.47E-01	1.26E-01	**5.18E-03**
8 µm s^{-1}	**4.01E-04**	9.08E-02	2.56E-01	2.36E-01	3.47E-01		5.90E-01	1.10E-01
10 µm s^{-1}	**2.88E-04**	**1.88E-02**	8.32E-02	1.03E-01	1.26E-01	5.90E-01		3.20E-01
20 µm s^{-1}	**5.61E-06**	**2.17E-04**	**1.03E-03**	**2.63E-03**	**5.18E-03**	1.10E-01	3.20E-01	

Statistics Table 5. Cross table of P-Values comparing adhesion forces of indicated retraction speeds from Fig. 5-1c using Mann-Whitney test. P-values smaller than 0.05 are shown bold.

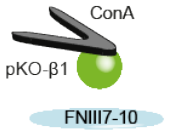

	1 µm s^{-1}	3 µm s^{-1}	4 µm s^{-1}	5 µm s^{-1}	6 µm s^{-1}	8 µm s^{-1}	10 µm s^{-1}	20 µm s^{-1}
1 µm s^{-1}		**4.73E-02**	**4.68E-05**	**1.50E-05**	**8.94E-06**	**6.19E-07**	**2.23E-07**	**3.33E-09**
3 µm s^{-1}	**4.73E-02**		9.50E-02	**1.04E-02**	1.33E-01	**5.39E-03**	**9.71E-03**	**1.32E-04**
4 µm s^{-1}	**4.68E-05**	9.50E-02		5.76E-02	5.25E-01	5.56E-02	**2.75E-02**	**1.05E-03**
5 µm s^{-1}	**1.50E-05**	**1.04E-02**	5.76E-02		**3.79E-02**	1.00E+00	8.90E-01	1.09E-01
6 µm s^{-1}	**8.94E-06**	1.33E-01	5.25E-01	**3.79E-02**		**9.06E-03**	**6.61E-03**	**1.69E-06**
8 µm s^{-1}	**6.19E-07**	**5.39E-03**	5.56E-02	1.00E+00	**9.06E-03**		8.86E-01	**5.23E-02**
10 µm s^{-1}	**2.23E-07**	**9.71E-03**	**2.75E-02**	8.90E-01	**6.61E-03**	8.86E-01		**4.26E-02**
20 µm s^{-1}	**3.33E-09**	**1.32E-04**	**1.05E-03**	1.09E-01	**1.69E-06**	5.23E-02	**4.26E-02**	

Statistics Table 6. Cross table of P-Values comparing adhesion forces of indicated retraction speeds from Fig. 5-1c using Mann-Whitney test. P-values smaller than 0.05 are shown bold.

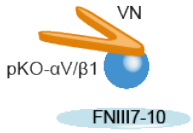

	1 µm s^{-1}	3 µm s^{-1}	4 µm s^{-1}	5 µm s^{-1}	6 µm s^{-1}	8 µm s^{-1}	10 µm s^{-1}	20 µm s^{-1}
1 µm s^{-1}		**1.49E-03**	**2.24E-04**	**2.66E-07**	**4.52E-06**	**1.73E-04**	**2.03E-06**	**1.75E-06**
3 µm s^{-1}	**1.49E-03**		**4.59E-02**	**2.01E-04**	1.01E-01	9.12E-02	**6.23E-03**	**4.49E-06**
4 µm s^{-1}	**2.24E-04**	**4.59E-02**		1.39E-01	5.20E-01	8.17E-01	2.38E-01	**4.84E-05**
5 µm s^{-1}	**2.66E-07**	**2.01E-04**	1.39E-01		**2.79E-02**	3.31E-01	8.67E-01	**2.72E-04**
6 µm s^{-1}	**4.52E-06**	1.01E-01	5.20E-01	**2.79E-02**		6.70E-01	1.47E-01	**2.01E-05**
8 µm s^{-1}	**1.73E-04**	9.12E-02	8.17E-01	3.31E-01	6.70E-01		4.60E-01	**1.04E-03**
10 µm s^{-1}	**2.03E-06**	**6.23E-03**	2.38E-01	8.67E-01	1.47E-01	4.60E-01		**1.82E-03**
20 µm s^{-1}	**1.75E-06**	**4.49E-06**	**4.84E-05**	**2.72E-04**	**2.01E-05**	**1.04E-03**	**1.82E-03**	

Statistics Table 7. Cross table of P-Values comparing adhesion forces of indicated retraction speeds from Fig. 5-1d using Mann-Whitney test. P-values smaller than 0.05 are shown bold.

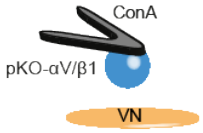

	1 µm s^{-1}	3 µm s^{-1}	4 µm s^{-1}	5 µm s^{-1}	6 µm s^{-1}	8 µm s^{-1}	10 µm s^{-1}	20µm s^{-1}
1 µm s^{-1}		**1.54E-03**	**9.72E-06**	**2.58E-08**	**4.99E-08**	**9.97E-08**	**4.24E-09**	**1.44E-09**
3 µm s^{-1}	**1.54E-03**		2.59E-01	**1.29E-02**	**3.30E-04**	**3.75E-05**	**1.52E-05**	**1.57E-07**
4 µm s^{-1}	**9.72E-06**	2.59E-01		**4.59E-02**	**2.69E-04**	**1.26E-03**	**1.95E-04**	**4.31E-08**
5 µm s^{-1}	**2.58E-08**	**1.29E-02**	**4.59E-02**		**4.11E-02**	**1.95E-02**	**3.10E-03**	**2.13E-06**
6 µm s^{-1}	**4.99E-08**	**3.30E-04**	**2.69E-04**	**4.11E-02**		8.30E-01	7.08E-02	**2.01E-04**
8 µm s^{-1}	**9.97E-08**	**3.75E-05**	**1.26E-03**	**1.95E-02**	8.30E-01		1.25E-01	**1.20E-03**
10 µm s^{-1}	**4.24E-09**	**1.52E-05**	**1.95E-04**	**3.10E-03**	7.08E-02	1.25E-01		**2.05E-02**
20 µm s^{-1}	**1.44E-09**	**1.57E-07**	**4.31E-08**	**2.13E-06**	**2.01E-04**	**1.20E-03**	**2.05E-02**	

Statistics Table 8. Cross table of P-Values comparing adhesion forces of indicated retraction speeds from Fig. 5-1d using Mann-Whitney test. P-values smaller than 0.05 are shown bold.

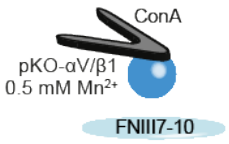

	1 µm s^{-1}	3 µm s^{-1}	4 µm s^{-1}	5 µm s^{-1}	6 µm s^{-1}	8 µm s^{-1}	10 µm s^{-1}	20 µm s^{-1}
1 µm s^{-1}		**3.29E-02**	**2.85E-03**	**5.55E-05**	**5.97E-05**	**2.97E-05**	**1.48E-05**	**1.98E-05**
3 µm s^{-1}	**3.29E-02**		5.75E-02	**4.51E-05**	**3.10E-03**	**5.18E-05**	**2.05E-05**	**5.21E-05**
4 µm s^{-1}	**2.85E-03**	5.75E-02		2.62E-01	1.71E-01	6.97E-02	8.32E-02	1.09E-01
5 µm s^{-1}	**5.55E-05**	**4.51E-05**	2.62E-01		7.41E-01	4.43E-01	8.06E-01	4.95E-01
6 µm s^{-1}	**5.97E-05**	**3.10E-03**	1.71E-01	7.41E-01		9.05E-01	9.88E-01	7.18E-01
8 µm s^{-1}	**2.97E-05**	**5.18E-05**	6.97E-02	4.43E-01	9.05E-01		9.89E-01	9.42E-01
10 µm s^{-1}	**1.48E-05**	**2.05E-05**	8.32E-02	8.06E-01	9.88E-01	9.89E-01		8.26E-01
20 µm s^{-1}	**1.98E-05**	**5.21E-05**	1.09E-01	4.95E-01	7.18E-01	9.42E-01	8.26E-01	

Statistics Table 9. Cross table of P-Values comparing adhesion forces of indicated retraction speeds from Fig. 5-3a using Mann-Whitney test. P-values smaller than 0.05 are shown bold.

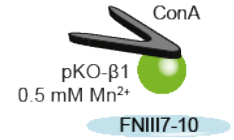

	1 µm s^{-1}	3 µm s^{-1}	4 µm s^{-1}	5 µm s^{-1}	6 µm s^{-1}	8 µm s^{-1}	10 µm s^{-1}	20 µm s^{-1}
1 µm s^{-1}		6.30E-02	**6.84E-03**	**3.80E-04**	**5.50E-04**	**3.25E-04**	**2.17E-05**	**1.70E-04**
3 µm s^{-1}	6.30E-02		1.90E-01	**2.42E-02**	**1.01E-02**	**6.84E-03**	**7.25E-04**	**4.84E-03**
4 µm s^{-1}	**6.84E-03**	1.90E-01		1.52E-01	7.20E-02	**2.88E-02**	**2.09E-03**	**7.95E-03**
5 µm s^{-1}	**3.80E-04**	**2.42E-02**	1.52E-01		4.01E-01	1.73E-01	**2.42E-02**	1.01E-01
6 µm s^{-1}	**5.50E-04**	**1.01E-02**	7.20E-02	4.01E-01		6.05E-01	3.49E-01	3.32E-01
8 µm s^{-1}	**3.25E-04**	**6.84E-03**	**2.88E-02**	1.73E-01	6.05E-01		1.00E+00	6.05E-01
10 µm s^{-1}	**2.17E-05**	**7.25E-04**	**2.09E-03**	**2.42E-02**	3.49E-01	1.00E+00		8.63E-01
20 µm s^{-1}	**1.70E-04**	**4.84E-03**	**7.95E-03**	1.01E-01	3.32E-01	6.05E-01	8.63E-01	

Statistics Table 10. Cross table of P-Values comparing adhesion forces of indicated retraction speeds from Fig. 5-3a using Mann-Whitney test. P-values smaller than 0.05 are shown bold.

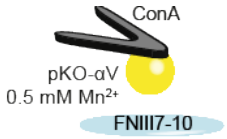

	1 µm s^{-1}	3 µm s^{-1}	4 µm s^{-1}	5 µm s^{-1}	6 µm s^{-1}	8 µm s^{-1}	10 µm s^{-1}	20 µm s^{-1}
1 µm s^{-1}		**7.58E-05**	**4.33E-05**	**1.08E-05**	**1.08E-05**	**1.08E-05**	**1.08E-05**	**1.08E-05**
3 µm s^{-1}	**7.58E-05**		5.29E-01	**2.09E-03**	2.88E-03	1.50E-03	**5.20E-03**	**1.30E-04**
4 µm s^{-1}	**4.33E-05**	5.29E-01		1.05E-01	8.92E-02	6.30E-02	8.92E-02	**3.89E-03**
5 µm s^{-1}	**1.08E-05**	**2.09E-03**	1.05E-01		7.39E-01	6.84E-01	8.53E-01	5.24E-02
6 µm s^{-1}	**1.08E-05**	**2.88E-03**	8.92E-02	7.39E-01		7.96E-01	9.71E-01	1.65E-01
8 µm s^{-1}	**1.08E-05**	**1.50E-03**	6.30E-02	6.84E-01	7.96E-01		9.12E-01	1.90E-01
10 µm s^{-1}	**1.08E-05**	**5.20E-03**	8.92E-02	8.53E-01	9.71E-01	9.12E-01		1.43E-01
20 µm s^{-1}	**1.08E-05**	**1.30E-04**	**3.89E-03**	5.24E-02	1.65E-01	1.90E-01	1.43E-01	

Statistics Table 11. Cross table of P-Values comparing adhesion forces of indicated retraction speeds from Fig. 5-3a using Mann-Whitney test. P-values smaller than 0.05 are shown bold.

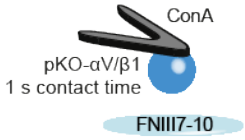

	1 µm s^{-1}	3 µm s^{-1}	4 µm s^{-1}	5 µm s^{-1}	6 µm s^{-1}	8 µm s^{-1}	10 µm s^{-1}	20 µm s^{-1}
1 µm s^{-1}		1.43E-01	**1.47E-02**	**1.50E-03**	**2.88E-03**	**1.85E-02**	**7.25E-04**	**4.11E-04**
3 µm s^{-1}	1.43E-01		4.36E-01	**1.85E-02**	1.65E-01	3.15E-01	**1.15E-02**	**1.01E-02**
4 µm s^{-1}	**1.47E-02**	4.36E-01		2.18E-01	5.29E-01	7.96E-01	6.30E-02	**6.53E-02**
5 µm s^{-1}	**1.50E-03**	**1.85E-02**	2.18E-01		4.36E-01	1.23E-01	6.31E-01	4.47E-01
6 µm s^{-1}	**2.88E-03**	1.65E-01	5.29E-01	4.36E-01		5.79E-01	1.05E-01	**3.50E-02**
8 µm s^{-1}	**1.85E-02**	3.15E-01	7.96E-01	1.23E-01	5.79E-01		8.92E-02	5.35E-02
10 µm s^{-1}	**7.25E-04**	**1.15E-02**	6.30E-02	6.31E-01	1.05E-01	**8.92E-02**		7.20E-01
20 µm s^{-1}	**4.11E-04**	**1.01E-02**	6.53E-02	4.47E-01	**3.50E-02**	**5.35E-02**	7.20E-01	

Statistics Table 12. Cross table of P-Values comparing adhesion forces of indicated retraction speeds from Fig. 5-3b using Mann-Whitney test. P-values smaller than 0.05 are shown bold.

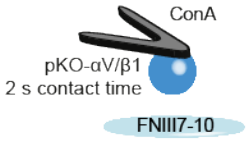

	1 µm s^{-1}	3 µm s^{-1}	4 µm s^{-1}	5 µm s^{-1}	6 µm s^{-1}	8 µm s^{-1}	10 µm s^{-1}	20 µm s^{-1}
1 µm s^{-1}		4.36E-01	7.53E-02	**1.05E-03**	3.93E-01	1.43E-01	**6.84E-03**	**4.30E-04**
3 µm s^{-1}	4.36E-01		4.36E-01	**2.88E-02**	9.71E-01	7.39E-01	2.18E-01	**2.06E-02**
4 µm s^{-1}	7.53E-02	4.36E-01		8.92E-02	3.15E-01	7.96E-01	6.31E-01	1.23E-01
5 µm s^{-1}	**1.05E-03**	**2.88E-02**	8.92E-02		1.47E-02	**4.33E-02**	1.90E-01	7.22E-01
6 µm s^{-1}	3.93E-01	9.71E-01	3.15E-01	**1.47E-02**		6.84E-01	1.90E-01	**1.38E-02**
8 µm s^{-1}	1.43E-01	7.39E-01	7.96E-01	**4.33E-02**	6.84E-01		2.18E-01	1.07E-01
10 µm s^{-1}	**6.84E-03**	2.18E-01	6.31E-01	1.90E-01	1.90E-01	2.18E-01		3.46E-01
20 µm s^{-1}	**4.30E-04**	**2.06E-02**	1.23E-01	7.22E-01	**1.38E-02**	**1.07E-01**	3.46E-01	

Statistics Table 13. Cross table of P-Values comparing adhesion forces of indicated retraction speeds from Fig. 5-3b using Mann-Whitney test. P-values smaller than 0.05 are shown bold.

	1 µm s^{-1}	3 µm s^{-1}	4 µm s^{-1}	5 µm s^{-1}	6 µm s^{-1}	8 µm s^{-1}	10 µm s^{-1}	20 µm s^{-1}
1 µm s^{-1}		**2.32E-02**	**6.84E-03**	**2.06E-04**	1.05E-01	**2.09E-03**	**8.93E-03**	5.20E-03
3 µm s^{-1}	**2.32E-02**		3.93E-01	2.18E-01	1.23E-01	9.71E-01	8.53E-01	3.53E-01
4 µm s^{-1}	**6.84E-03**	3.93E-01		5.29E-01	4.33E-02	2.47E-01	6.84E-01	7.96E-01
5 µm s^{-1}	**2.06E-04**	2.18E-01	5.29E-01		**2.32E-02**	1.05E-01	2.18E-01	6.84E-01
6 µm s^{-1}	1.05E-01	1.23E-01	**4.33E-02**	**2.32E-02**		1.05E-01	2.80E-01	7.53E-02
8 µm s^{-1}	**2.09E-03**	9.71E-01	2.47E-01	1.05E-01	**1.05E-01**		8.53E-01	1.90E-01
10 µm s^{-1}	**8.93E-03**	8.53E-01	6.84E-01	2.18E-01	2.80E-01	8.53E-01		4.81E-01
20 µm s^{-1}	**5.20E-03**	3.53E-01	7.96E-01	6.84E-01	7.53E-02	1.90E-01	4.81E-01	

Statistics Table 14. Cross table of P-Values comparing adhesion forces of indicated retraction speeds from Fig. 5-3b using Mann-Whitney test. P-values smaller than 0.05 are shown bold.

	1 µm s^{-1}	3 µm s^{-1}	4 µm s^{-1}	5 µm s^{-1}	6 µm s^{-1}	8 µm s^{-1}	10 µm s^{-1}	20 µm s^{-1}
1 µm s^{-1}		5.03E-02	**3.00E-04**	**1.22E-05**	8.63E-01	9.31E-02	**7.14E-03**	**3.71E-05**
3 µm s^{-1}	5.03E-02		**4.49E-02**	**4.51E-04**	7.92E-02	1.00E+00	3.19E-01	**1.00E-02**
4 µm s^{-1}	**3.00E-04**	**4.49E-02**		5.97E-02	**9.81E-04**	**2.42E-02**	1.98E-01	7.99E-01
5 µm s^{-1}	**1.22E-05**	**4.51E-04**	5.97E-02		**1.52E-05**	**2.59E-04**	**5.48E-03**	5.97E-02
6 µm s^{-1}	8.63E-01	**7.92E-02**	**9.81E-04**	**1.52E-05**		7.92E-02	**4.49E-03**	**2.06E-04**
8 µm s^{-1}	9.31E-02	1.00E+00	**2.42E-02**	**2.59E-04**	7.92E-02		2.19E-01	**6.81E-03**
10 µm s^{-1}	**7.14E-03**	3.19E-01	1.98E-01	**5.48E-03**	**4.49E-03**	2.19E-01		1.60E-01
20 µm s^{-1}	**3.71E-05**	**1.00E-02**	7.99E-01	5.97E-02	**2.06E-04**	**6.81E-03**	1.60E-01	

Statistics Table 15. Cross table of P-Values comparing adhesion forces of indicated retraction speeds from Fig. 5-3c using Mann-Whitney test. P-values smaller than 0.05 are shown bold.

	1 µm s^{-1}	3 µm s^{-1}	4 µm s^{-1}	5 µm s^{-1}	6 µm s^{-1}	8 µm s^{-1}	10 µm s^{-1}	20 µm s^{-1}
1 µm s^{-1}		**1.50E-03**	**1.30E-04**	**3.09E-06**	**5.50E-04**	**6.80E-05**	**2.09E-03**	**1.08E-05**
3 µm s^{-1}	**1.50E-03**		**4.33E-02**	**6.00E-04**	8.09E-01	2.82E-01	6.30E-02	**7.58E-05**
4 µm s^{-1}	**1.30E-04**	**4.33E-02**		2.03E-01	1.14E-01	4.68E-01	6.84E-01	**4.33E-02**
5 µm s^{-1}	**3.09E-06**	**6.00E-04**	2.03E-01		**2.80E-03**	**4.39E-02**	7.22E-01	1.80E-01
6 µm s^{-1}	**5.50E-04**	8.09E-01	1.14E-01	**2.80E-03**		4.01E-01	1.14E-01	**2.55E-04**
8 µm s^{-1}	**6.80E-05**	2.82E-01	4.68E-01	**4.39E-02**	4.01E-01		3.87E-01	**7.95E-03**
10 µm s^{-1}	**2.09E-03**	6.30E-02	6.84E-01	7.22E-01	1.14E-01	3.87E-01		1.90E-01
20 µm s^{-1}	**1.08E-05**	**7.58E-05**	**4.33E-02**	1.80E-01	**2.55E-04**	**7.95E-03**	1.90E-01	

Statistics Table 16. Cross table of P-Values comparing adhesion forces of indicated retraction speeds from Fig. 5-3c using Mann-Whitney test. P-values smaller than 0.05 are shown bold.

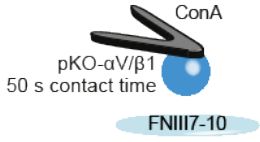

	1 µm s^{-1}	3 µm s^{-1}	4 µm s^{-1}	5 µm s^{-1}	6 µm s^{-1}	8 µm s^{-1}	10 µm s^{-1}	20 µm s^{-1}
1 µm s^{-1}		**7.88E-04**	**7.58E-05**	**4.74E-07**	**2.07E-04**	**2.55E-04**	**1.08E-05**	**1.08E-05**
3 µm s^{-1}	**7.88E-04**		**2.95E-02**	**3.48E-03**	5.95E-02	**4.73E-02**	**4.79E-03**	**2.55E-04**
4 µm s^{-1}	**7.58E-05**	**2.95E-02**		4.43E-01	9.23E-01	8.09E-01	6.84E-01	**3.55E-02**
5 µm s^{-1}	**4.74E-07**	**3.48E-03**	4.43E-01		4.71E-01	5.47E-01	9.41E-01	3.09E-01
6 µm s^{-1}	**2.07E-04**	5.95E-02	9.23E-01	4.71E-01		9.28E-01	7.22E-01	**4.26E-02**
8 µm s^{-1}	**2.55E-04**	**4.73E-02**	8.09E-01	5.47E-01	9.28E-01		8.09E-01	8.45E-02
10 µm s^{-1}	**1.08E-05**	**4.79E-03**	6.84E-01	9.41E-01	7.22E-01	8.09E-01		1.65E-01
20 µm s^{-1}	**1.08E-05**	**2.55E-04**	**3.55E-02**	3.09E-01	**4.26E-02**	8.45E-02	1.65E-01	

Statistics Table 17. Cross table of P-Values comparing adhesion forces of indicated retraction speeds from Fig. 5-3b using Mann-Whitney test. P-values smaller than 0.05 are shown bold.

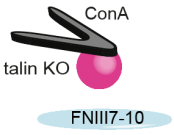

	1 µm s^{-1}	3 µm s^{-1}	4 µm s^{-1}	5 µm s^{-1}	6 µm s^{-1}	8 µm s^{-1}	10 µm s^{-1}	20 µm s^{-1}
1 µm s^{-1}		**2.55E-02**	**2.20E-02**	**6.47E-03**	**1.38E-02**	**2.24E-04**	**3.00E-04**	**4.08E-06**
3 µm s^{-1}	**2.55E-02**		5.83E-01	1.53E-01	3.47E-01	5.81E-02	**1.88E-02**	**3.72E-05**
4 µm s^{-1}	**2.20E-02**	5.83E-01		6.85E-01	4.03E-01	7.69E-02	**3.10E-02**	**1.01E-04**
5 µm s^{-1}	**6.47E-03**	1.53E-01	6.85E-01		7.69E-01	2.54E-01	7.68E-02	**1.02E-03**
6 µm s^{-1}	**1.38E-02**	3.47E-01	4.03E-01	7.69E-01		3.23E-01	1.78E-01	**1.27E-02**
8 µm s^{-1}	**2.24E-04**	5.81E-02	7.69E-02	2.54E-01	3.23E-01		6.14E-01	**4.59E-02**
10 µm s^{-1}	**3.00E-04**	**1.88E-02**	**3.10E-02**	7.68E-02	1.78E-01	6.14E-01		2.52E-01
20 µm s^{-1}	**4.08E-06**	**3.72E-05**	**1.01E-04**	**1.02E-03**	**1.27E-02**	**4.59E-02**	2.52E-01	

Statistics Table 18. Cross table of P-Values comparing adhesion forces of indicated retraction speeds from Fig. 5-4a using Mann-Whitney test. P-values smaller than 0.05 are shown bold.

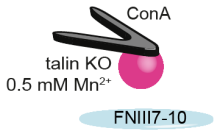

	1 µm s^{-1}	3 µm s^{-1}	4 µm s^{-1}	5 µm s^{-1}	6 µm s^{-1}	8 µm s^{-1}	10 µm s^{-1}	20 µm s^{-1}
1 µm s^{-1}		**1.47E-02**	**7.25E-04**	**2.06E-04**	**6.19E-06**	**7.58E-05**	**2.17E-05**	**1.08E-05**
3 µm s^{-1}	**1.47E-02**		1.43E-01	**4.33E-02**	**3.00E-04**	**3.89E-03**	**4.87E-04**	**1.08E-05**
4 µm s^{-1}	**7.25E-04**	1.43E-01		4.81E-01	**4.26E-02**	1.05E-01	**1.47E-02**	**1.50E-03**
5 µm s^{-1}	**2.06E-04**	**4.33E-02**	4.81E-01		2.54E-01	3.53E-01	5.24E-02	**3.89E-03**
6 µm s^{-1}	**6.19E-06**	**3.00E-04**	**4.26E-02**	2.54E-01		1.00E+00	1.80E-01	**4.30E-04**
8 µm s^{-1}	**7.58E-05**	**3.89E-03**	1.05E-01	3.53E-01	1.00E+00		3.53E-01	**1.47E-02**
10 µm s^{-1}	**2.17E-05**	**4.87E-04**	**1.47E-02**	5.24E-02	1.80E-01	3.53E-01		2.47E-01
20 µm s^{-1}	**1.08E-05**	**1.08E-05**	**1.50E-03**	**3.89E-03**	**4.30E-04**	**1.47E-02**	2.47E-01	

Statistics Table 19. Cross table of P-Values comparing adhesion forces of indicated retraction speeds from Fig. 5-4a using Mann-Whitney test. P-values smaller than 0.05 are shown bold.

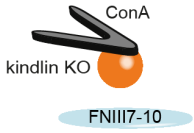

	1 µm s^{-1}	3 µm s^{-1}	4 µm s^{-1}	5 µm s^{-1}	6 µm s^{-1}	8 µm s^{-1}	10 µm s^{-1}	20 µm s^{-1}
1 µm s^{-1}		**2.70E-02**	**5.92E-05**	**2.24E-06**	**4.96E-04**	**1.23E-03**	**7.17E-05**	**6.19E-06**
3 µm s^{-1}	**2.70E-02**		**5.19E-03**	**5.80E-05**	1.06E-01	1.16E-01	**3.71E-03**	**1.02E-06**
4 µm s^{-1}	**5.92E-05**	**5.19E-03**		2.66E-01	3.02E-01	3.08E-01	9.45E-01	**1.03E-02**
5 µm s^{-1}	**2.24E-06**	**5.80E-05**	2.66E-01		**1.71E-02**	**3.42E-02**	3.68E-01	**4.00E-02**
6 µm s^{-1}	**4.96E-04**	1.06E-01	3.02E-01	**1.71E-02**		9.79E-01	1.60E-01	**2.07E-04**
8 µm s^{-1}	**1.23E-03**	1.16E-01	3.08E-01	**3.42E-02**	9.79E-01		2.47E-01	**1.96E-03**
10 µm s^{-1}	**7.17E-05**	**3.71E-03**	9.45E-01	3.68E-01	1.60E-01	2.47E-01		**4.43E-03**
20 µm s^{-1}	**6.19E-06**	**1.02E-06**	**1.03E-02**	**4.00E-02**	**2.07E-04**	**1.96E-03**	**4.43E-03**	

Statistics Table 20. Cross table of P-Values comparing adhesion forces of indicated retraction speeds from Fig. 5-4b using Mann-Whitney test. P-values smaller than 0.05 are shown bold.

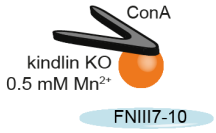

	1 µm s^{-1}	3 µm s^{-1}	4 µm s^{-1}	5 µm s^{-1}	6 µm s^{-1}	8 µm s^{-1}	10 µm s^{-1}	20 µm s^{-1}
1 µm s^{-1}		**3.25E-04**	**1.08E-05**	**1.08E-05**	**7.58E-05**	**1.08E-05**	**1.08E-05**	**1.08E-05**
3 µm s^{-1}	**3.25E-04**		**1.85E-02**	**1.15E-02**	**1.85E-02**	**2.06E-04**	**5.20E-03**	**7.58E-05**
4 µm s^{-1}	**1.08E-05**	**1.85E-02**		7.39E-01	3.53E-01	**2.88E-02**	**2.88E-02**	**2.88E-03**
5 µm s^{-1}	**1.08E-05**	**1.15E-02**	7.39E-01		5.79E-01	2.47E-01	2.80E-01	5.24E-02
6 µm s^{-1}	**7.58E-05**	**1.85E-02**	3.53E-01	5.79E-01		7.96E-01	6.31E-01	3.53E-01
8 µm s^{-1}	**1.08E-05**	**2.06E-04**	**2.88E-02**	2.47E-01	7.96E-01		7.96E-01	2.47E-01
10 µm s^{-1}	**1.08E-05**	**5.20E-03**	**2.88E-02**	2.80E-01	6.31E-01	7.96E-01		4.36E-01
20 µm s^{-1}	**1.08E-05**	**7.58E-05**	**2.88E-03**	5.24E-02	3.53E-01	2.47E-01	4.36E-01	

Statistics Table 21. Cross table of P-Values comparing adhesion forces of indicated retraction speeds from Fig. 5-4b using Mann-Whitney test. P-values smaller than 0.05 are shown bold.

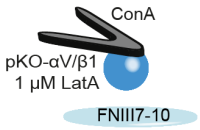

	1 µm s^{-1}	3 µm s^{-1}	4 µm s^{-1}	5 µm s^{-1}	6 µm s^{-1}	8 µm s^{-1}	10 µm s^{-1}	20 µm s^{-1}
1 µm s^{-1}		**1.45E-02**	**1.26E-03**	**5.18E-06**	**3.84E-04**	**3.75E-05**	**2.40E-06**	**3.73E-05**
3 µm s^{-1}	**1.45E-02**		6.03E-01	**6.83E-03**	2.20E-01	**1.45E-02**	**7.65E-04**	**4.48E-03**
4 µm s^{-1}	**1.26E-03**	6.03E-01		**2.59E-02**	3.50E-01	**4.27E-02**	**2.26E-03**	**6.45E-03**
5 µm s^{-1}	**5.18E-06**	**6.83E-03**	**2.59E-02**		3.39E-01	8.56E-01	3.45E-01	1.39E-01
6 µm s^{-1}	**3.84E-04**	2.20E-01	3.50E-01	3.39E-01		4.18E-01	**4.13E-02**	**4.57E-02**
8 µm s^{-1}	**3.75E-05**	**1.45E-02**	**4.27E-02**	8.56E-01	4.18E-01		2.54E-01	1.37E-01
10 µm s^{1}	**2.40E-06**	**7.65E-04**	**2.26E-03**	**3.45E-01**	**4.13E-02**	**2.54E-01**		**3.47E-01**
20 µm s^{-1}	**3.73E-05**	**4.48E-03**	**6.45E-03**	1.39E-01	**4.57E-02**	1.37E-01	3.47E-01	

Statistics Table 22. Cross table of P-Values comparing adhesion forces of indicated retraction speeds from Fig. 5-4c using Mann-Whitney test. P-values smaller than 0.05 are shown bold.

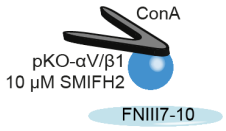

	1 µm s^{-1}	3 µm s^{-1}	4 µm s^{-1}	5 µm s^{-1}	6 µm s^{-1}	8 µm s^{-1}	10 µm s^{-1}	20 µm s^{-1}
1 µm s^{-1}		1.09E-01	**3.01E-02**	**3.01E-04**	**4.73E-02**	**5.94E-03**	**5.24E-03**	**1.90E-04**
3 µm s^{-1}	1.09E-01		3.16E-01	**4.94E-02**	7.99E-01	1.70E-01	**4.14E-02**	**8.22E-04**
4 µm s^{-1}	**3.01E-02**	3.16E-01		3.98E-01	5.31E-01	7.62E-01	3.03E-01	**2.18E-02**
5 µm s^{-1}	**3.01E-04**	**4.94E-02**	3.98E-01		**3.01E-02**	5.03E-01	6.10E-01	8.89E-02
6 µm s^{-1}	**4.73E-02**	7.99E-01	5.31E-01	**3.01E-02**		2.28E-01	1.16E-01	**8.33E-03**
8 µm s^{-1}	**5.94E-03**	1.70E-01	7.62E-01	5.03E-01	2.28E-01		3.31E-01	**4.10E-02**
10 µm s^{-1}	**5.24E-03**	**4.14E-02**	3.03E-01	6.10E-01	1.16E-01	3.31E-01		2.17E-01
20 µm s^{-1}	**1.90E-04**	**8.22E-04**	**2.18E-02**	8.89E-02	**8.33E-03**	**4.10E-02**	2.17E-01	

Statistics Table 23. Cross table of P-Values comparing adhesion forces of indicated retraction speeds from Fig. 5-4c using Mann-Whitney test. P-values smaller than 0.05 are shown bold.

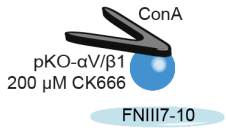

	1 µm s^{-1}	3 µm s^{-1}	4 µm s^{-1}	5 µm s^{-1}	6 µm s^{-1}	8 µm s^{-1}	10 µm s^{-1}	20 µm s^{-1}
1 µm s^{-1}		**8.60E-03**	**2.87E-03**	**7.17E-05**	**2.97E-04**	**6.78E-05**	**1.89E-06**	**8.65E-06**
3 µm s^{-1}	**8.60E-03**		3.90E-01	**1.40E-02**	8.11E-02	**3.32E-02**	**1.54E-03**	**4.93E-04**
4 µm s^{-1}	**2.87E-03**	3.90E-01		4.79E-01	4.79E-01	4.02E-01	4.27E-02	**3.38E-02**
5 µm s^{-1}	**7.17E-05**	**1.40E-02**	4.79E-01		5.45E-01	9.43E-01	3.25E-01	7.23E-02
6 µm s^{-1}	**2.97E-04**	8.11E-02	4.79E-01	5.45E-01		5.83E-01	1.55E-01	5.68E-02
8 µm s^{-1}	**6.78E-05**	**3.32E-02**	4.02E-01	9.43E-01	5.83E-01		3.29E-01	1.28E-01
10 µm s^{-1}	**1.89E-06**	**1.54E-03**	**4.27E-02**	3.25E-01	1.55E-01	3.29E-01		5.50E-01
20 µm s^{-1}	**8.65E-06**	**4.93E-04**	**3.38E-02**	**7.23E-02**	5.68E-02	1.28E-01	5.50E-01	

Statistics Table 24. Cross table of P-Values comparing adhesion forces of indicated retraction speeds from Fig. 5-4c using Mann-Whitney test. P-values smaller than 0.05 are shown bold.

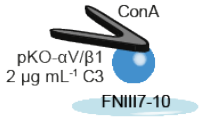

	1 µm s^{-1}	3 µm s^{-1}	4 µm s^{-1}	5 µm s^{-1}	6 µm s^{-1}	8 µm s^{-1}	10 µm s^{-1}	20 µm s^{-1}
1 µm s^{-1}		8.92E-02	**2.17E-05**	**7.58E-05**	**8.93E-03**	7.53E-02	**7.25E-04**	**7.58E-05**
3 µm s^{-1}	8.92E-02		**7.25E-04**	**4.87E-04**	4.81E-01	4.36E-01	**2.88E-02**	**2.88E-03**
4 µm s^{-1}	**2.17E-05**	**7.25E-04**		4.36E-01	**2.32E-02**	**4.33E-02**	1.90E-01	1.00E+00
5 µm s^{-1}	**7.58E-05**	**4.87E-04**	4.36E-01		**5.20E-03**	**2.32E-02**	8.92E-02	3.93E-01
6 µm s^{-1}	**8.93E-03**	4.81E-01	**2.32E-02**	**5.20E-03**		1.00E+00	1.65E-01	**2.32E-02**
8 µm s^{-1}	7.53E-02	4.36E-01	**4.33E-02**	**2.32E-02**	1.00E+00		3.53E-01	7.53E-02
10 µm s^{-1}	**7.25E-04**	**2.88E-02**	1.90E-01	8.92E-02	1.65E-01	3.53E-01		3.15E-01
20 µm s^{-1}	**7.58E-05**	**2.88E-03**	1.00E+00	3.93E-01	**2.32E-02**	**7.53E-02**	3.15E-01	

Statistics Table 25. Cross table of P-Values comparing adhesion forces of indicated retraction speeds from Fig. 5-4d using Mann-Whitney test. P-values smaller than 0.05 are shown bold.

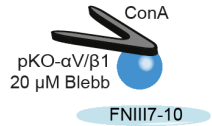

	1 µm s^{-1}	3 µm s^{-1}	4 µm s^{-1}	5 µm s^{-1}	6 µm s^{-1}	8 µm s^{-1}	10 µm s^{-1}	20 µm s^{-1}
1 µm s^{-1}		**2.09E-03**	**9.28E-05**	**1.22E-05**	5.24E-02	**1.05E-03**	**3.80E-04**	**2.55E-04**
3 µm s^{-1}	**2.09E-03**		1.23E-01	**3.06E-02**	3.15E-01	9.71E-01	6.54E-01	1.52E-01
4 µm s^{-1}	**9.28E-05**	1.23E-01		3.47E-01	**2.06E-02**	2.83E-01	4.13E-01	8.33E-01
5 µm s^{-1}	**1.22E-05**	**3.06E-02**	3.47E-01		**1.91E-03**	**1.85E-02**	8.47E-02	2.44E-01
6 µm s^{-1}	5.24E-02	3.15E-01	**2.06E-02**	**1.91E-03**		1.23E-01	5.13E-02	5.13E-02
8 µm s^{-1}	**1.05E-03**	9.71E-01	2.83E-01	**1.85E-02**	1.23E-01		5.12E-01	1.73E-01
10 µm s^{-1}	**3.80E-04**	6.54E-01	4.13E-01	8.47E-02	5.13E-02	5.12E-01		5.19E-01
20 µm s^{-1}	**2.55E-04**	1.52E-01	8.33E-01	2.44E-01	5.13E-02	1.73E-01	5.19E-01	

Statistics Table 26. Cross table of P-Values comparing adhesion forces of indicated retraction speeds from Fig. 5-4d using Mann-Whitney test. P-values smaller than 0.05 are shown bold.

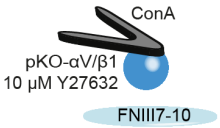

	1 µm s^{-1}	3 µm s^{-1}	4 µm s^{-1}	5 µm s^{-1}	6 µm s^{-1}	8 µm s^{-1}	10 µm s^{-1}	20 µm s^{-1}
1 µm s^{-1}		**1.11E-03**	**8.51E-05**	**1.84E-06**	**1.07E-02**	**7.07E-04**	**2.81E-05**	**9.61E-06**
3 µm s^{-1}	**1.11E-03**		2.91E-01	**1.18E-02**	3.25E-01	9.43E-01	4.32E-01	**2.91E-02**
4 µm s^{-1}	**8.51E-05**	2.91E-01		9.89E-02	**4.74E-02**	2.28E-01	5.66E-01	4.94E-01
5 µm s^{-1}	**1.84E-06**	1.18E-02	9.89E-02		**2.52E-03**	**1.16E-02**	5.93E-02	3.51E-01
6 µm s^{-1}	**1.07E-02**	3.25E-01	**4.74E-02**	**2.52E-03**		4.48E-01	1.52E-01	**2.35E-03**
8 µm s^{-1}	**7.07E-04**	9.43E-01	2.28E-01	**1.16E-02**	4.48E-01		7.28E-01	**2.21E-02**
10 µm s^{-1}	**2.81E-05**	4.32E-01	5.66E-01	5.93E-02	1.52E-01	7.28E-01		1.23E-01
20 µm s^{-1}	**9.61E-06**	**2.91E-02**	4.94E-01	3.51E-01	**2.35E-03**	**2.21E-02**	1.23E-01	

Statistics Table 27. Cross table of P-Values comparing adhesion forces of indicated retraction speeds from Fig. 5-4d using Mann-Whitney test. P-values smaller than 0.05 are shown bold.

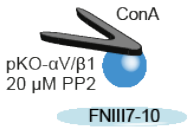

	1 μm s^{-1}	3 μm s^{-1}	4 μm s^{-1}	5 μm s^{-1}	6 μm s^{-1}	8 μm s^{-1}	10 μm s^{-1}	20 μm s^{-1}
1 μm s^{-1}		**6.84E-03**	**1.01E-02**	**2.43E-04**	**3.25E-04**	**4.33E-05**	**2.55E-04**	**2.17E-05**
3 μm s^{-1}	**6.84E-03**		5.57E-01	**3.58E-02**	**3.55E-02**	**4.87E-04**	**3.65E-03**	**1.30E-04**
4 μm s^{-1}	**1.01E-02**	5.57E-01		3.03E-01	1.73E-01	**7.95E-03**	**2.33E-02**	**3.80E-04**
5 μm s^{-1}	**2.43E-04**	**3.58E-02**	3.03E-01		7.84E-01	**4.93E-02**	6.29E-02	**6.40E-04**
6 μm s^{-1}	**3.25E-04**	**3.55E-02**	1.73E-01	7.84E-01		1.05E-01	1.52E-01	**1.50E-03**
8 μm s^{-1}	**4.33E-05**	**4.87E-04**	**7.95E-03**	**4.93E-02**	1.05E-01		9.73E-01	**3.55E-02**
10 μm s^{-1}	**2.55E-04**	**3.65E-03**	**2.33E-02**	6.29E-02	1.52E-01	9.73E-01		**1.59E-02**
20 μm s^{-1}	**2.17E-05**	**1.30E-04**	**3.80E-04**	**6.40E-04**	**1.50E-03**	**3.55E-02**	**1.59E-02**	

Statistics Table 28. Cross table of P-Values comparing adhesion forces of indicated retraction speeds from Fig. 5-5a using Mann-Whitney test. P-values smaller than 0.05 are shown bold.

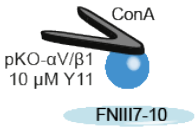

	1 μm s^{-1}	3 μm s^{-1}	4 μm s^{-1}	5 μm s^{-1}	6 μm s^{-1}	8 μm s^{-1}	10 μm s^{-1}	20 μm s^{-1}
1 μm s^{-1}		**1.47E-02**	**6.19E-03**	**5.20E-03**	**2.06E-03**	**2.27E-05**	**7.58E-05**	**4.33E-05**
3 μm s^{-1}	**1.47E-02**		4.26E-01	1.43E-01	6.10E-02	**3.65E-03**	**2.88E-03**	**1.05E-03**
4 μm s^{-1}	**6.19E-03**	4.26E-01		2.23E-01	1.01E-01	**6.63E-03**	**1.01E-02**	**3.65E-03**
5 μm s^{-1}	**5.20E-03**	1.43E-01	2.23E-01		9.73E-01	3.49E-01	1.90E-01	7.53E-02
6 μm s^{-1}	**2.06E-03**	**6.10E-02**	1.01E-01	9.73E-01		2.43E-01	2.82E-01	7.20E-02
8 μm s^{-1}	**2.27E-05**	**3.65E-03**	**6.63E-03**	3.49E-01	2.43E-01		6.54E-01	1.97E-01
10 μm s^{-1}	**7.58E-05**	**2.88E-03**	**1.01E-02**	1.90E-01	2.82E-01	6.54E-01		3.53E-01
20 μm s^{-1}	**4.33E-05**	**1.05E-03**	**3.65E-03**	7.53E-02	7.20E-02	1.97E-01	3.53E-01	

Statistics Table 29. Cross table of P-Values comparing adhesion forces of indicated retraction speeds from Fig. 5-5b using Mann-Whitney test. P-values smaller than 0.05 are shown bold.

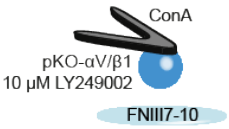

	1 μm s^{-1}	3 μm s^{-1}	4 μm s^{-1}	5 μm s^{-1}	6 μm s^{-1}	8 μm s^{-1}	10 μm s^{-1}	20 μm s^{-1}
1 μm s^{-1}		**1.12E-02**	**2.06E-02**	**1.22E-05**	**1.52E-03**	**1.30E-04**	**5.88E-05**	**1.13E-05**
3 μm s^{-1}	**1.12E-02**		4.78E-01	**1.73E-02**	9.76E-01	2.03E-01	1.14E-01	**1.06E-02**
4 μm s^{-1}	**2.06E-02**	4.78E-01		1.18E-01	5.25E-01	5.82E-01	3.78E-01	1.34E-01
5 μm s^{-1}	**1.22E-05**	**1.73E-02**	1.18E-01		**3.33E-02**	3.71E-01	4.32E-01	8.93E-01
6 μm s^{-1}	**1.52E-03**	9.76E-01	5.25E-01	**3.33E-02**		1.73E-01	1.18E-01	**4.10E-03**
8 μm s^{-1}	**1.30E-04**	2.03E-01	5.82E-01	3.71E-01	1.73E-01		8.72E-01	1.14E-01
10 μm s^{-1}	**5.88E-05**	1.14E-01	3.78E-01	4.32E-01	1.18E-01	8.72E-01		2.88E-01
20 μm s^{-1}	**1.13E-05**	**1.06E-02**	1.34E-01	8.93E-01	**4.10E-03**	1.14E-01	2.88E-01	

Statistics Table 30. Cross table of P-Values comparing adhesion forces of indicated retraction speeds from Fig. 5-5c using Mann-Whitney test. P-values smaller than 0.05 are shown bold.

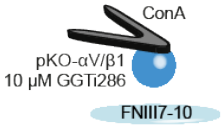

	1 µm s^{-1}	3 µm s^{-1}	4 µm s^{-1}	5 µm s^{-1}	6 µm s^{-1}	8 µm s^{-1}	10 µm s^{-1}	20 µm s^{-1}
1 µm s^{-1}		**1.85E-02**	**1.05E-03**	**3.32E-05**	1.65E-01	**2.88E-03**	**4.87E-04**	**7.58E-05**
3 µm s^{-1}	**1.85E-02**		2.80E-01	**9.89E-03**	1.43E-01	9.12E-01	1.90E-01	**2.32E-02**
4 µm s^{-1}	**1.05E-03**	2.80E-01		1.01E-01	**4.33E-02**	3.15E-01	8.53E-01	5.29E-01
5 µm s^{-1}	**3.32E-05**	**9.89E-03**	1.01E-01		**4.70E-04**	**2.54E-03**	1.01E-01	4.10E-01
6 µm s^{-1}	1.65E-01	1.43E-01	**4.33E-02**	**4.70E-04**		2.18E-01	**6.84E-03**	**7.25E-04**
8 µm s^{-1}	**2.88E-03**	9.12E-01	3.15E-01	**2.54E-03**	2.18E-01		5.24E-02	**5.20E-03**
10 µm s^{-1}	**4.87E-04**	1.90E-01	8.53E-01	1.01E-01	**6.84E-03**	5.24E-02		8.92E-02
20 µm s^{-1}	**7.58E-05**	**2.32E-02**	5.29E-01	4.10E-01	**7.25E-04**	**5.20E-03**	8.92E-02	

Statistics Table 31. Cross table of P-Values comparing adhesion forces of indicated retraction speeds from Fig. 5-5d using Mann-Whitney test. P-values smaller than 0.05 are shown bold.

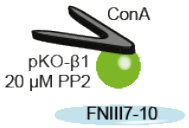

	1 µm s^{-1}	3 µm s^{-1}	4 µm s^{-1}	5 µm s^{-1}	6 µm s^{-1}	8 µm s^{-1}	10 µm s^{-1}	20 µm s^{-1}
1 µm s^{-1}		1.23E-01	**1.50E-03**	**1.30E-04**	**3.89E-03**	**4.87E-04**	**1.08E-04**	**4.33E-05**
3 µm s^{-1}	1.23E-01		1.23E-01	**3.89E-03**	3.53E-01	**2.32E-02**	**1.01E-02**	**3.89E-03**
4 µm s^{-1}	**1.50E-03**	1.23E-01		1.65E-01	5.29E-01	6.31E-01	3.14E-01	1.65E-01
5 µm s^{-1}	**1.30E-04**	**3.89E-03**	1.65E-01		**1.47E-02**	3.15E-01	7.56E-01	8.53E-01
6 µm s^{-1}	**3.89E-03**	3.53E-01	5.29E-01	**1.47E-02**		1.90E-01	**4.30E-02**	**8.93E-03**
8 µm s^{-1}	**4.87E-04**	**2.32E-02**	6.31E-01	3.15E-01	1.90E-01		6.54E-01	1.23E-01
10 µm s^{-1}	**1.08E-04**	**1.01E-02**	3.14E-01	7.56E-01	**4.30E-02**	6.54E-01		4.26E-01
20 µm s^{-1}	**4.33E-05**	**3.89E-03**	1.65E-01	8.53E-01	**8.93E-03**	1.23E-01	4.26E-01	

Statistics Table 32. Cross table of P-Values comparing adhesion forces of indicated retraction speeds from Fig. 5-5e using Mann-Whitney test. P-values smaller than 0.05 are shown bold.

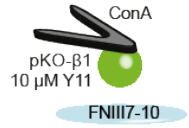

	1 µm s^{-1}	3 µm s^{-1}	4 µm s^{-1}	5 µm s^{-1}	6 µm s^{-1}	8 µm s^{-1}	10 µm s^{-1}	20 µm s^{-1}
1 µm s^{-1}		4.26E-01	3.93E-01	**4.33E-02**	**1.15E-02**	**5.20E-03**	**1.05E-03**	**2.09E-03**
3 µm s^{-1}	4.26E-01		8.09E-01	6.10E-02	**2.95E-02**	**3.65E-03**	**1.52E-03**	**2.76E-03**
4 µm s^{-1}	3.93E-01	8.09E-01		1.90E-01	1.05E-01	**4.33E-02**	**2.88E-03**	**5.20E-03**
5 µm s^{-1}	**4.33E-02**	6.10E-02	1.90E-01		9.71E-01	8.53E-01	8.92E-02	**1.85E-02**
6 µm s^{-1}	**1.15E-02**	**2.95E-02**	1.05E-01	9.71E-01		6.84E-01	6.30E-02	**1.15E-02**
8 µm s^{-1}	**5.20E-03**	**3.65E-03**	**4.33E-02**	8.53E-01	6.84E-01		1.05E-01	**2.32E-02**
10 µm s^{-1}	**1.05E-03**	**1.52E-03**	**2.88E-03**	8.92E-02	6.30E-02	1.05E-01		2.47E-01
20 µm s^{-1}	**2.09E-03**	**2.76E-03**	**5.20E-03**	**1.85E-02**	**1.15E-02**	**2.32E-02**	2.47E-01	

Statistics Table 33. Cross table of P-Values comparing adhesion forces of indicated retraction speeds from Fig. 5-5f using Mann-Whitney test. P-values smaller than 0.05 are shown bold.

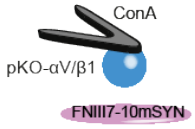

	1 µm s^{-1}	3 µm s^{-1}	4 µm s^{-1}	5 µm s^{-1}	6 µm s^{-1}	8 µm s^{-1}	10 µm s^{-1}	20 µm s^{-1}
1 µm s^{-1}		**1.47E-02**	**7.25E-04**	**1.15E-03**	**3.80E-04**	**4.87E-04**	**1.22E-05**	**4.33E-05**
3 µm s^{-1}	**1.47E-02**		1.05E-01	9.56E-02	8.45E-02	8.92E-02	**9.89E-03**	**2.06E-04**
4 µm s^{-1}	**7.25E-04**	1.05E-01		8.86E-01	4.68E-01	8.53E-01	2.32E-01	**1.15E-02**
5 µm s^{-1}	**1.15E-03**	9.56E-02	8.86E-01		7.27E-01	7.96E-01	3.50E-01	**3.06E-02**
6 µm s^{-1}	**3.80E-04**	8.45E-02	4.68E-01	7.27E-01		9.18E-01	9.10E-01	7.20E-02
8 µm s^{-1}	**4.87E-04**	8.92E-02	8.53E-01	7.96E-01	9.18E-01		3.76E-01	8.92E-02
10 µm s^{-1}	**1.22E-05**	**9.89E-03**	2.32E-01	3.50E-01	9.10E-01	3.76E-01		**4.71E-02**
20 µm s^{-1}	**4.33E-05**	**2.06E-04**	**1.15E-02**	**3.06E-02**	7.20E-02	8.92E-02	**4.71E-02**	

Statistics Table 34. Cross table of P-Values comparing adhesion forces of indicated retraction speeds from Fig. 5-5g using Mann-Whitney test. P-values smaller than 0.05 are shown bold.

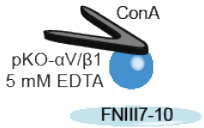

	1 µm s^{-1}	3 µm s^{-1}	4 µm s^{-1}	5 µm s^{-1}	6 µm s^{-1}	8 µm s^{-1}	10 µm s^{-1}	20 µm s^{-1}
1 µm s^{-1}		4.36E-01	4.36E-01	7.53E-02	3.93E-01	**1.47E-02**	**2.09E-03**	**1.30E-04**
3 µm s^{-1}	4.36E-01		7.39E-01	4.36E-01	7.39E-01	1.05E-01	**6.84E-03**	**2.09E-03**
4 µm s^{-1}	4.36E-01	7.39E-01		3.15E-01	7.39E-01	6.30E-02	**5.20E-03**	**7.25E-04**
5 µm s^{-1}	7.53E-02	4.36E-01	3.15E-01		6.84E-01	2.80E-01	**2.32E-02**	**6.84E-03**
6 µm s^{-1}	3.93E-01	7.39E-01	7.39E-01	6.84E-01		2.80E-01	8.92E-02	**2.32E-02**
8 µm s^{-1}	**1.47E-02**	1.05E-01	6.30E-02	2.80E-01	2.80E-01		3.15E-01	7.53E-02
10 µm s^{-1}	**2.09E-03**	**6.84E-03**	**5.20E-03**	**2.32E-02**	8.92E-02	3.15E-01		3.53E-01
20 µm s^{-1}	**1.30E-04**	**2.09E-03**	**7.25E-04**	**6.84E-03**	**2.32E-02**	7.53E-02	3.53E-01	

Statistics Table 35. Cross table of P-Values comparing adhesion forces of indicated retraction speeds from Supplementary Fig. 5-5a using Mann-Whitney test. P-values smaller than 0.05 are shown bold.

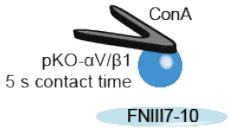

	1 µm s^{-1}	3 µm s^{-1}	4 µm s^{-1}	5 µm s^{-1}	6 µm s^{-1}	8 µm s^{-1}	10 µm s^{-1}	20 µm s^{-1}
1 µm s^{-1}		3.03E-01	**1.88E-02**	**1.44E-06**	6.06E-01	7.59E-02	**3.33E-02**	**2.75E-04**
3 µm s^{-1}	3.03E-01		1.68E-01	**2.61E-03**	7.33E-01	7.76E-01	2.80E-01	**4.74E-02**
4 µm s^{-1}	**1.88E-02**	1.68E-01		5.77E-02	6.88E-02	2.35E-01	7.05E-01	4.49E-01
5 µm s^{-1}	**1.44E-06**	**2.61E-03**	5.77E-02		**1.57E-05**	**9.67E-04**	**1.17E-02**	2.04E-01
6 µm s^{-1}	6.06E-01	7.33E-01	6.88E-02	**1.57E-05**		1.16E-01	1.49E-01	**1.04E-03**
8 µm s^{-1}	7.59E-02	7.76E-01	2.35E-01	**9.67E-04**	1.16E-01		6.47E-01	**3.36E-02**
10 µm s^{-1}	**3.33E-02**	2.80E-01	7.05E-01	**1.17E-02**	1.49E-01	6.47E-01		1.83E-01
20 µm s^{-1}	**2.75E-04**	**4.74E-02**	4.49E-01	2.04E-01	**1.04E-03**	**3.36E-02**	1.83E-01	

Statistics Table 36. Cross table of P-Values comparing adhesion forces of indicated retraction speeds from Supplementary Fig. 5-7a using Mann-Whitney test. P-values smaller than 0.05 are shown bold.

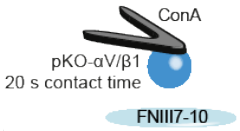

	1 µm s^{-1}	3 µm s^{-1}	4 µm s^{-1}	5 µm s^{-1}	6 µm s^{-1}	8 µm s^{-1}	10 µm s^{-1}	20 µm s^{-1}
1 µm s^{-1}		5.03E-02	**3.00E-04**	**1.22E-05**	8.63E-01	9.31E-02	**7.14E-03**	**3.71E-05**
3 µm s^{-1}	5.03E-02		**4.49E-02**	**4.51E-04**	7.92E-02	1.00E+00	3.19E-01	**1.00E-02**
4 µm s^{-1}	**3.00E-04**	**4.49E-02**		5.97E-02	**9.81E-04**	**2.42E-02**	1.98E-01	7.99E-01
5 µm s^{-1}	**1.22E-05**	**4.51E-04**	5.97E-02		**1.52E-05**	**2.59E-04**	**5.48E-03**	5.97E-02
6 µm s^{-1}	8.63E-01	**7.92E-02**	**9.81E-04**	**1.52E-05**		7.92E-02	**4.49E-03**	**2.06E-04**
8 µm s^{-1}	9.31E-02	1.00E+00	**2.42E-02**	**2.59E-04**	7.92E-02		2.19E-01	**6.81E-03**
10 µm s^{-1}	**7.14E-03**	3.19E-01	1.98E-01	**5.48E-03**	**4.49E-03**	2.19E-01		1.60E-01
20 µm s^{-1}	**3.71E-05**	**1.00E-02**	7.99E-01	5.97E-02	**2.06E-04**	**6.81E-03**	1.60E-01	

Statistics Table 37. Cross table of P-Values comparing adhesion forces of indicated retraction speeds from **Supplementary Fig. 7a** using Mann-Whitney test. P-values smaller than 0.05 are shown bold.

	1 µm s^{-1}	3 µm s^{-1}	4 µm s^{-1}	5 µm s^{-1}	6 µm s^{-1}	8 µm s^{-1}	10 µm s^{-1}	20 µm s^{-1}
1 µm s^{-1}		**1.50E-03**	**1.30E-04**	**3.09E-06**	**5.50E-04**	**6.80E-05**	**2.09E-03**	**1.08E-05**
3 µm s^{-1}	**1.50E-03**		**4.33E-02**	**6.00E-04**	8.09E-01	2.82E-01	6.30E-02	**7.58E-05**
4 µm s^{-1}	**1.30E-04**	**4.33E-02**		2.03E-01	1.14E-01	4.68E-01	6.84E-01	**4.33E-02**
5 µm s^{-1}	**3.09E-06**	**6.00E-04**	2.03E-01		**2.80E-03**	**4.39E-02**	7.22E-01	1.80E-01
6 µm s^{-1}	**5.50E-04**	8.09E-01	1.14E-01	**2.80E-03**		4.01E-01	1.14E-01	**2.55E-04**
8 µm s^{-1}	**6.80E-05**	2.82E-01	4.68E-01	**4.39E-02**	4.01E-01		3.87E-01	**7.95E-03**
10 µm s^{-1}	**2.09E-03**	6.30E-02	6.84E-01	7.22E-01	1.14E-01	3.87E-01		1.90E-01
20 µm s^{-1}	**1.08E-05**	**7.58E-05**	**4.33E-02**	1.80E-01	**2.55E-04**	**7.95E-03**	1.90E-01	

Statistics Table 38. Cross table of P-Values comparing adhesion forces of indicated retraction speeds from **Supplementary Fig. 7a** using Mann-Whitney test. P-values smaller than 0.05 are shown bold.

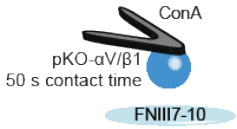

	1 µm s^{-1}	3 µm s^{-1}	4 µm s^{-1}	5 µm s^{-1}	6 µm s^{-1}	8 µm s^{-1}	10 µm s^{-1}	20 µm s^{-1}
1 µm s^{-1}		**7.88E-04**	**7.58E-05**	**4.74E-07**	**2.07E-04**	**2.55E-04**	**1.08E-05**	**1.08E-05**
3 µm s^{-1}	**7.88E-04**		**2.95E-02**	**3.48E-03**	5.95E-02	**4.73E-02**	**4.79E-03**	**2.55E-04**
4 µm s^{-1}	**7.58E-05**	**2.95E-02**		4.43E-01	9.23E-01	8.09E-01	6.84E-01	**3.55E-02**
5 µm s^{-1}	**4.74E-07**	**3.48E-03**	4.43E-01		4.71E-01	5.47E-01	9.41E-01	3.09E-01
6 µm s^{-1}	**2.07E-04**	5.95E-02	9.23E-01	4.71E-01		9.28E-01	7.22E-01	**4.26E-02**
8 µm s^{-1}	**2.55E-04**	**4.73E-02**	8.09E-01	5.47E-01	9.28E-01		8.09E-01	8.45E-02
10 µm s^{-1}	**1.08E-05**	**4.79E-03**	6.84E-01	9.41E-01	7.22E-01	8.09E-01		1.65E-01
20 µm s^{-1}	**1.08E-05**	**2.55E-04**	**3.55E-02**	3.09E-01	**4.26E-02**	8.45E-02	1.65E-01	

Statistics Table 39. Cross table of P-Values comparing adhesion forces of indicated retraction speeds from Supplementary Fig. 5-7a using Mann-Whitney test. P-values smaller than 0.05 are shown bold.

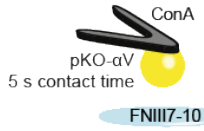

	1 µm s^{-1}	3 µm s^{-1}	4 µm s^{-1}	5 µm s^{-1}	6 µm s^{-1}	8 µm s^{-1}	10 µm s^{-1}	20 µm s^{-1}
1 µm s^{-1}		**3.18E-03**	**2.01E-03**	**5.06E-04**	**1.30E-03**	**4.01E-04**	**2.88E-04**	**5.61E-06**
3 µm s^{-1}	**3.18E-03**		5.40E-01	1.80E-01	1.64E-01	9.08E-02	**1.88E-02**	**2.17E-04**
4 µm s^{-1}	**2.01E-03**	5.40E-01		6.53E-01	6.24E-01	2.56E-01	8.32E-02	**1.03E-03**
5 µm s^{-1}	**5.06E-04**	1.80E-01	6.53E-01		9.35E-01	2.36E-01	1.03E-01	**2.63E-03**
6 µm s^{-1}	**1.30E-03**	1.64E-01	6.24E-01	9.35E-01		3.47E-01	1.26E-01	**5.18E-03**
8 µm s^{-1}	**4.01E-04**	9.08E-02	2.56E-01	2.36E-01	3.47E-01		5.90E-01	1.10E-01
10 µm s^{-1}	**2.88E-04**	**1.88E-02**	8.32E-02	1.03E-01	1.26E-01	5.90E-01		3.20E-01
20 µm s^{-1}	**5.61E-06**	**2.17E-04**	**1.03E-03**	**2.63E-03**	**5.18E-03**	1.10E-01	3.20E-01	

Statistics Table 40. Cross table of P-Values comparing adhesion forces of indicated retraction speeds from Supplementary Fig. 5-7b using Mann-Whitney test. P-values smaller than 0.05 are shown bold.

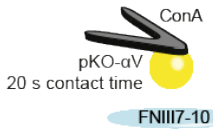

	1 µm s^{-1}	3 µm s^{-1}	4 µm s^{-1}	5 µm s^{-1}	6 µm s^{-1}	8 µm s^{-1}	10 µm s^{-1}	20 µm s^{-1}
1 µm s^{-1}		1.05E-01	1.23E-01	5.24E-02	**1.47E-02**	**2.88E-03**	**1.47E-02**	**2.06E-04**
3 µm s^{-1}	1.05E-01		9.71E-01	9.12E-01	6.31E-01	**2.09E-03**	**3.55E-02**	**1.30E-04**
4 µm s^{-1}	1.23E-01	9.71E-01		9.71E-01	4.81E-01	**8.93E-03**	**3.55E-02**	**2.06E-04**
5 µm s^{-1}	5.24E-02	9.12E-01	9.71E-01		5.29E-01	**4.33E-02**	8.92E-02	**2.09E-03**
6 µm s^{-1}	**1.47E-02**	6.31E-01	4.81E-01	5.29E-01		1.23E-01	1.43E-01	**2.88E-03**
8 µm s^{-1}	**2.88E-03**	**2.09E-03**	**8.93E-03**	**4.33E-02**	1.23E-01		7.39E-01	**4.33E-02**
10 µm s^{-1}	**1.47E-02**	**3.55E-02**	**3.55E-02**	8.92E-02	1.43E-01	7.39E-01		2.80E-01
20 µm s^{-1}	**2.06E-04**	**1.30E-04**	**2.06E-04**	**2.09E-03**	**2.88E-03**	**4.33E-02**	2.80E-01	

Statistics Table 41. Cross table of P-Values comparing adhesion forces of indicated retraction speeds from Supplementary Fig. 5-7b using Mann-Whitney test. P-values smaller than 0.05 are shown bold.

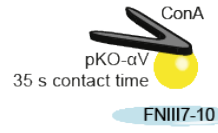

	1 µm s^{-1}	3 µm s^{-1}	4 µm s^{-1}	5 µm s^{-1}	6 µm s^{-1}	8 µm s^{-1}	10 µm s^{-1}	20 µm s^{-1}
1 µm s^{-1}		**1.97E-02**	**1.85E-02**	**7.25E-04**	**5.67E-06**	**1.13E-05**	**6.19E-06**	**3.09E-06**
3 µm s^{-1}	**1.97E-02**		2.51E-01	**2.95E-02**	**1.28E-04**	**1.90E-04**	**2.06E-04**	**2.81E-05**
4 µm s^{-1}	**1.85E-02**	2.51E-01		4.81E-01	**1.27E-02**	**1.01E-02**	**1.12E-02**	**6.00E-04**
5 µm s^{-1}	**7.25E-04**	**2.95E-02**	4.81E-01		5.13E-02	**3.57E-02**	**2.49E-02**	**7.14E-03**
6 µm s^{-1}	**5.67E-06**	**1.28E-04**	**1.27E-02**	5.13E-02		4.78E-01	4.49E-01	1.04E-01
8 µm s^{-1}	**1.13E-05**	**1.90E-04**	**1.01E-02**	**3.57E-02**	4.78E-01		6.95E-01	3.79E-01
10 µm s^{-1}	**6.19E-06**	**2.06E-04**	**1.12E-02**	**2.49E-02**	4.49E-01	6.95E-01		7.13E-01
20 µm s^{-1}	**3.09E-06**	**2.81E-05**	**6.00E-04**	**7.14E-03**	1.04E-01	3.79E-01	7.13E-01	

Statistics Table 42. Cross table of P-Values comparing adhesion forces of indicated retraction speeds from Supplementary Fig. 5-7b using Mann-Whitney test. P-values smaller than 0.05 are shown bold.

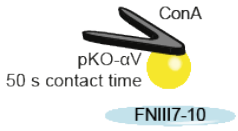

	1 µm s^{-1}	3 µm s^{-1}	4 µm s^{-1}	5 µm s^{-1}	6 µm s^{-1}	8 µm s^{-1}	10 µm s^{-1}	20 µm s^{-1}
1 µm s^{-1}		**4.87E-02**	**5.40E-03**	**1.05E-03**	**3.75E-04**	**2.86E-04**	**4.89E-04**	**1.81E-04**
3 µm s^{-1}	**4.87E-02**		3.07E-01	1.93E-01	1.13E-01	6.19E-02	5.27E-02	**2.55E-02**
4 µm s^{-1}	**5.40E-03**	3.07E-01		7.39E-01	3.15E-01	2.80E-01	2.47E-01	8.45E-02
5 µm s^{-1}	**1.05E-03**	1.93E-01	7.39E-01		6.84E-01	3.93E-01	4.81E-01	3.87E-01
6 µm s^{-1}	**3.75E-04**	1.13E-01	3.15E-01	6.84E-01		8.53E-01	9.12E-01	3.49E-01
8 µm s^{-1}	**2.86E-04**	6.19E-02	2.80E-01	3.93E-01	8.53E-01		9.71E-01	6.54E-01
10 µm s^{-1}	**4.89E-04**	5.27E-02	2.47E-01	4.81E-01	9.12E-01	9.71E-01		6.54E-01
20 µm s^{-1}	**1.81E-04**	**2.55E-02**	8.45E-02	3.87E-01	3.49E-01	6.54E-01	6.54E-01	

Statistics Table 43. Cross table of P-Values comparing adhesion forces of indicated retraction speeds from Supplementary Fig. 5-7b using Mann-Whitney test. P-values smaller than 0.05 are shown bold.

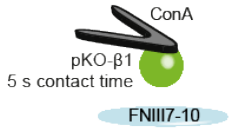

	1 µm s^{-1}	3 µm s^{-1}	4 µm s^{-1}	5 µm s^{-1}	6 µm s^{-1}	8 µm s^{-1}	10 µm s^{-1}	20 µm s^{-1}
1 µm s^{-1}		**4.73E-02**	**4.68E-05**	**1.50E-05**	**8.94E-06**	**6.19E-07**	**2.23E-07**	**3.33E-09**
3 µm s^{-1}	**4.73E-02**		9.50E-02	**1.04E-02**	1.33E-01	**5.39E-03**	**9.71E-03**	**1.32E-04**
4 µm s^{-1}	**4.68E-05**	9.50E-02		5.76E-02	5.25E-01	5.56E-02	**2.75E-02**	**1.05E-03**
5 µm s^{-1}	**1.50E-05**	**1.04E-02**	5.76E-02		**3.79E-02**	1.00E+00	8.90E-01	1.09E-01
6 µm s^{-1}	**8.94E-06**	1.33E-01	5.25E-01	**3.79E-02**		**9.06E-03**	**6.61E-03**	**1.69E-06**
8 µm s^{-1}	**6.19E-07**	**5.39E-03**	5.56E-02	1.00E+00	**9.06E-03**		8.86E-01	**5.23E-02**
10 µm s^{-1}	**2.23E-07**	**9.71E-03**	**2.75E-02**	8.90E-01	**6.61E-03**	8.86E-01		**4.26E-02**
20 µm s^{-1}	**3.33E-09**	**1.32E-04**	**1.05E-03**	1.09E-01	**1.69E-06**	5.23E-02	**4.26E-02**	

Statistics Table 44. Cross table of P-Values comparing adhesion forces of indicated retraction speeds from Supplementary Fig. 5-7c using Mann-Whitney test. P-values smaller than 0.05 are shown bold.

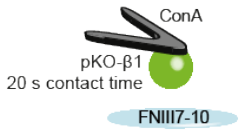

	1 µm s^{-1}	3 µm s^{-1}	4 µm s^{-1}	5 µm s^{-1}	6 µm s^{-1}	8 µm s^{-1}	10 µm s^{-1}	20 µm s^{-1}
1 µm s^{-1}		**7.95E-03**	**5.39E-05**	**5.92E-06**	**3.65E-03**	**3.80E-04**	**6.80E-05**	**2.27E-05**
3 µm s^{-1}	**7.95E-03**		2.51E-01	**2.49E-02**	3.93E-01	9.71E-01	2.47E-01	6.30E-02
4 µm s^{-1}	**5.39E-05**	2.51E-01		1.90E-01	**3.57E-02**	1.32E-01	9.18E-01	5.12E-01
5 µm s^{-1}	**5.92E-06**	**2.49E-02**	1.90E-01		**1.52E-03**	**7.14E-03**	3.81E-01	6.74E-01
6 µm s^{-1}	**3.65E-03**	3.93E-01	**3.57E-02**	**1.52E-03**		2.80E-01	3.55E-02	**6.84E-03**
8 µm s^{-1}	**3.80E-04**	9.71E-01	1.32E-01	**7.14E-03**	2.80E-01		1.90E-01	**3.55E-02**
10 µm s^{-1}	**6.80E-05**	2.47E-01	9.18E-01	3.81E-01	**3.55E-02**	1.90E-01		6.31E-01
20 µm s^{-1}	**2.27E-05**	6.30E-02	5.12E-01	6.74E-01	**6.84E-03**	**3.55E-02**	6.31E-01	

Statistics Table 45. Cross table of P-Values comparing adhesion forces of indicated retraction speeds from Supplementary Fig. 5-7c using Mann-Whitney test. P-values smaller than 0.05 are shown bold.

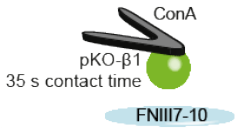

	1 µm s^{-1}	3 µm s^{-1}	4 µm s^{-1}	5 µm s^{-1}	6 µm s^{-1}	8 µm s^{-1}	10 µm s^{-1}	20 µm s^{-1}
1 µm s^{-1}		**1.85E-02**	**3.25E-04**	**5.67E-06**	**7.58E-05**	**4.33E-05**	**2.17E-05**	**1.08E-05**
3 µm s^{-1}	**1.85E-02**		7.53E-02	**4.79E-03**	1.65E-01	**4.33E-02**	**1.15E-02**	**1.05E-03**
4 µm s^{-1}	**3.25E-04**	7.53E-02		3.49E-01	6.31E-01	9.71E-01	4.81E-01	1.23E-01
5 µm s^{-1}	**5.67E-06**	**4.79E-03**	3.49E-01		3.57E-02	2.51E-01	7.05E-01	5.57E-01
6 µm s^{-1}	**7.58E-05**	1.65E-01	6.31E-01	**3.57E-02**		3.93E-01	6.30E-02	**6.84E-03**
8 µm s^{-1}	**4.33E-05**	**4.33E-02**	9.71E-01	2.51E-01	3.93E-01		6.84E-01	7.53E-02
10 µm s^{-1}	**2.17E-05**	**1.15E-02**	4.81E-01	7.05E-01	6.30E-02	6.84E-01		3.53E-01
20 µm s^{-1}	**1.08E-05**	**1.05E-03**	1.23E-01	5.57E-01	**6.84E-03**	7.53E-02	3.53E-01	

Statistics Table 46. Cross table of P-Values comparing adhesion forces of indicated retraction speeds from Supplementary Fig. 5-7c using Mann-Whitney test. P-values smaller than 0.05 are shown bold.

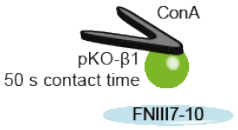

	1 µm s^{-1}	3 µm s^{-1}	4 µm s^{-1}	5 µm s^{-1}	6 µm s^{-1}	8 µm s^{-1}	10 µm s^{-1}	20 µm s^{-1}
1 µm s^{-1}		**3.97E-05**	**5.67E-06**	**1.75E-06**	**1.08E-05**	**2.17E-05**	**1.08E-05**	**1.08E-05**
3 µm s^{-1}	**3.97E-05**		6.52E-02	**3.89E-03**	6.10E-02	1.32E-01	**2.42E-02**	**7.95E-03**
4 µm s^{-1}	**5.67E-06**	6.52E-02		1.67E-01	9.73E-01	7.56E-01	3.87E-01	3.49E-01
5 µm s^{-1}	**1.75E-06**	**3.89E-03**	1.67E-01		2.32E-01	2.84E-01	6.48E-01	9.27E-01
6 µm s^{-1}	**1.08E-05**	6.10E-02	9.73E-01	2.32E-01		9.71E-01	6.31E-01	2.18E-01
8 µm s^{-1}	**2.17E-05**	1.32E-01	7.56E-01	2.84E-01	9.71E-01		5.79E-01	5.29E-01
10 µm s^{-1}	**1.08E-05**	**2.42E-02**	3.87E-01	6.48E-01	6.31E-01	5.79E-01		6.31E-01
20 µm s^{-1}	**1.08E-05**	**7.95E-03**	3.49E-01	9.27E-01	2.18E-01	5.29E-01	6.31E-01	

Statistics Table 47. Cross table of P-Values comparing adhesion forces of indicated retraction speeds from Supplementary Fig. 5-7c using Mann-Whitney test. P-values smaller than 0.05 are shown bold.

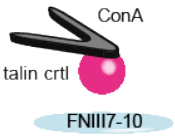

	1 µm s^{-1}	3 µm s^{-1}	4 µm s^{-1}	5 µm s^{-1}	6 µm s^{-1}	8 µm s^{-1}	10 µm s^{-1}	20 µm s^{-1}
1 µm s^{-1}		**1.27E-02**	**5.50E-04**	**1.78E-05**	8.09E-01	9.86E-02	2.81E-02	**3.94E-04**
3 µm s^{-1}	**1.27E-02**		1.05E-01	**1.52E-03**	**1.47E-02**	2.80E-01	7.56E-01	1.97E-01
4 µm s^{-1}	**5.50E-04**	1.05E-01		8.04E-02	**2.09E-03**	**2.88E-02**	1.32E-01	8.63E-01
5 µm s^{-1}	**1.78E-05**	**1.52E-03**	8.04E-02		**5.88E-05**	**4.30E-04**	**1.69E-03**	1.90E-01
6 µm s^{-1}	8.09E-01	**1.47E-02**	**2.09E-03**	**5.88E-05**		2.80E-01	**4.30E-02**	**1.52E-03**
8 µm s^{-1}	9.86E-02	2.80E-01	**2.88E-02**	**4.30E-04**	2.80E-01		6.05E-01	**4.30E-02**
10 µm s^{-1}	**2.81E-02**	7.56E-01	1.32E-01	**1.69E-03**	**4.30E-02**	6.05E-01		1.51E-01
20 µm s^{-1}	**3.94E-04**	1.97E-01	8.63E-01	1.90E-01	**1.52E-03**	**4.30E-02**	1.51E-01	

Statistics Table 48. Cross table of P-Values comparing adhesion forces of indicated retraction speeds from Supplementary Fig. 5-8a using Mann-Whitney test. P-values smaller than 0.05 are shown bold.

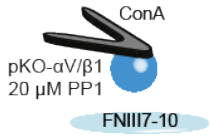

	1 µm s^{-1}	3 µm s^{-1}	4 µm s^{-1}	5 µm s^{-1}	6 µm s^{-1}	8 µm s^{-1}	10 µm s^{-1}	20 µm s^{-1}
1 µm s^{-1}		**1.50E-03**	**1.10E-03**	**5.67E-06**	**5.50E-04**	**5.67E-06**	**5.67E-06**	**1.08E-05**
3 µm s^{-1}	**1.50E-03**		4.26E-01	**1.01E-02**	1.52E-01	**1.52E-03**	**1.08E-04**	**3.25E-04**
4 µm s^{-1}	**1.10E-03**	4.26E-01		2.17E-01	4.38E-01	**4.73E-02**	**6.63E-03**	**7.95E-03**
5 µm s^{-1}	**5.67E-06**	**1.01E-02**	2.17E-01		7.97E-01	1.01E-01	**1.04E-02**	**1.59E-02**
6 µm s^{-1}	**5.50E-04**	1.52E-01	4.38E-01	7.97E-01		4.01E-01	1.16E-01	2.82E-01
8 µm s^{-1}	**5.67E-06**	**1.52E-03**	**4.73E-02**	1.01E-01	4.01E-01		2.70E-01	5.12E-01
10 µm s^{-1}	**5.67E-06**	**1.08E-04**	**6.63E-03**	**1.04E-02**	1.16E-01	2.70E-01		7.05E-01
20 µm s^{-1}	**1.08E-05**	**3.25E-04**	**7.95E-03**	**1.59E-02**	2.82E-01	5.12E-01	7.05E-01	

Statistics Table 49. Cross table of P-Values comparing adhesion forces of indicated retraction speeds from Supplementary Fig. 5-8b using Mann-Whitney test. P-values smaller than 0.05 are shown bold.

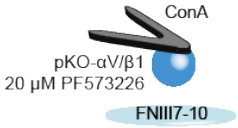

	1 µm s^{-1}	3 µm s^{-1}	4 µm s^{-1}	5 µm s^{-1}	6 µm s^{-1}	8 µm s^{-1}	10 µm s^{-1}	20 µm s^{-1}
1 µm s^{-1}		5.24E-02	5.24E-02	**3.89E-03**	**1.15E-02**	**1.05E-03**	**7.25E-04**	**2.06E-04**
3 µm s^{-1}	5.24E-02		7.39E-01	7.53E-02	2.47E-01	**2.88E-02**	**6.84E-03**	**8.93E-03**
4 µm s^{-1}	5.24E-02	7.39E-01		2.47E-01	3.93E-01	1.90E-01	1.05E-01	5.24E-02
5 µm s^{-1}	**3.89E-03**	7.53E-02	2.47E-01		1.00E+00	5.29E-01	6.31E-01	2.80E-01
6 µm s^{-1}	**1.15E-02**	2.47E-01	3.93E-01	1.00E+00		6.31E-01	4.36E-01	3.15E-01
8 µm s^{-1}	**1.05E-03**	**2.88E-02**	1.90E-01	5.29E-01	6.31E-01		8.53E-01	6.31E-01
10 µm s^{-1}	**7.25E-04**	**6.84E-03**	1.05E-01	6.31E-01	4.36E-01	8.53E-01		8.53E-01
20 µm s^{-1}	**2.06E-04**	**8.93E-03**	5.24E-02	2.80E-01	3.15E-01	6.31E-01	8.53E-01	

Statistics Table 50. Cross table of P-Values comparing adhesion forces of indicated retraction speeds from Supplementary Fig. 5-8b using Mann-Whitney test. P-values smaller than 0.05 are shown bold.

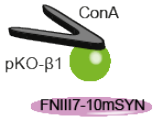

	1 µm s^{-1}	3 µm s^{-1}	4 µm s^{-1}	5 µm s^{-1}	6 µm s^{-1}	8 µm s^{-1}	10 µm s^{-1}	20 µm s^{-1}
1 µm s^{-1}		**2.33E-02**	**3.18E-03**	**3.94E-04**	**3.40E-05**	**2.84E-06**	**2.84E-06**	**2.84E-06**
3 µm s^{-1}	**2.33E-02**		1.71E-01	6.52E-02	**3.18E-03**	**3.40E-05**	**1.13E-05**	**1.13E-05**
4 µm s^{-1}	**3.18E-03**	1.71E-01		7.48E-01	1.93E-01	**4.10E-03**	**2.75E-04**	**8.51E-05**
5 µm s^{-1}	**3.94E-04**	6.52E-02	7.48E-01		3.32E-01	**2.81E-02**	**3.18E-03**	**2.75E-04**
6 µm s^{-1}	**3.40E-05**	**3.18E-03**	1.93E-01	3.32E-01		1.33E-01	**4.73E-02**	**4.10E-03**
8 µm s^{-1}	**2.84E-06**	**3.40E-05**	**4.10E-03**	**2.81E-02**	1.33E-01		6.06E-01	5.57E-02
10 µm s^{-1}	**2.84E-06**	**1.13E-05**	**2.75E-04**	**3.18E-03**	**4.73E-02**	6.06E-01		1.93E-01
20 µm s^{-1}	**2.84E-06**	**1.13E-05**	**8.51E-05**	**2.75E-04**	**4.10E-03**	5.57E-02	1.93E-01	

Statistics Table 51. Cross table of P-Values comparing adhesion forces of indicated retraction speeds from Supplementary Fig. 5-9a using Mann-Whitney test. P-values smaller than 0.05 are shown bold.

6. Conclusions and Outlook

6.1. Conclusions

In order to increase the throughput of atomic force microscopy (AFM)-based single cell force spectroscopy (SCFS), we developed a PDMS mask that is easy to produce and allows adhesion characterization of a single cell to multiple substrates of interest (Chapter 2). This mask allows better comparison of cell adhesion formation on different substrates as adhesion parameters of a single cell can characterize. Thereby the influence on results of cell to cell differences in adhesion formation are minimized. Hence, less experiments are required for statistically sound results. Further, the reproducibility and thus reliability of SCFS experiments are increased by understanding how cell detachment from the culture flask prior to adhesion experiments influences adhesion formation (Chapter 3). Detaching fibroblast with trypsin increases adhesion forces during early cell adhesion formation to fibronectin in subsequent SCFS experiments within about 45 minutes of detachment. This indicates that trypsin induces a signaling cascade, likely dependent on the protease activated receptor 2 (PAR2), which ultimately induces integrin ligand binding and/or integrin clustering.

To form new adhesion to fibronectin, fibroblasts employ α5β1 and αVβ3 integrins, both of which differentially regulate adhesion maturation and cytoskeleton dynamics when expressed exclusively[1,2]. However, the cooperation between these two integrins in adhesion initiation has not been studied. In this thesis, two distinct crosstalks between α5β1 and αVβ3 integrins are described that regulate early fibroblasts adhesion (Figure 6-1). In the first crosstalk (Chapter 4), clustered αVβ3 integrins signal to increase the avidity of α5β1 integrins in mixed adhesion sites over long distances, likely by engaging additional α5β1 integrins and inducing their clustering. Thereby, the signaling of αVβ3 integrins relies on the actin polymerization machinery Arp2/3 and on myosin II-mediated contractility, which is regulated by RhoA. The second crosstalk (Chapter 5) employs α5β1 integrins that sense mechanical load after two seconds of adhesion formation. Hence, already the onset adhesion of fibroblasts to fibronectin is tightly regulated by physical parameters, which results in a reinforcement of fibroblast adhesion. Although this crosstalk may not be required in stationary cells, dynamic cells, such as migrating fibroblasts during wound healing, require to attach newly formed protrusions to the extracellular matrix. At the periphery of the lamellipodium in a migrating fibroblast, mainly α5β1 integrins bind to the substrate[1]. When α5β1 integrins bind fibronectin, and are connected to actin by talin, α5β1 integrins sense force applied to them by the extracellular matrix, retrograde actin flow or actomyosin driven contractions. Due to a triggered signaling cascade additional fibronectin-binding integrins in the proximity of α5β1 integrins are engaged. This adhesion reinforcement requires fast signaling of FAK and Src and induces the formation mixed adhesion sites of α5β1 and αVβ3

integrins. These mixed adhesion sites are than reinforced by contractility dependent signaling of matured αVβ3 integrins-rich focal adhesions. This signaling enhances α5β1 integrin binding and clustering in the mixed adhesion sites. Hence, adhesion in protrusions and the newly formed lamellipodium is reinforced to ensure a persistent migration. When adhesion sites are more matured, α5β1 integrins are internalized in the high affinity conformation, stabilized by talin and FAK[3]. Subsequently, they are recycled to the leading edge of a migrating cell, which depends on Src kinase activety[3]. At the leading edge, the exocytosed α5β1 integrins can readily bind the ligand again, thereby forming a new adhesion site. Both described crosstalks in early adhesion reinforcement may also contribute in different physiological cell attachment processes, such as platelet clotting, and diseases, such as metastasis formation in cancer. Although we now better understand the cooperation of fibronectin-binding integrins to form new adhesions in migrating cells, many questions in the process of adhesion initiation remain to be answered.

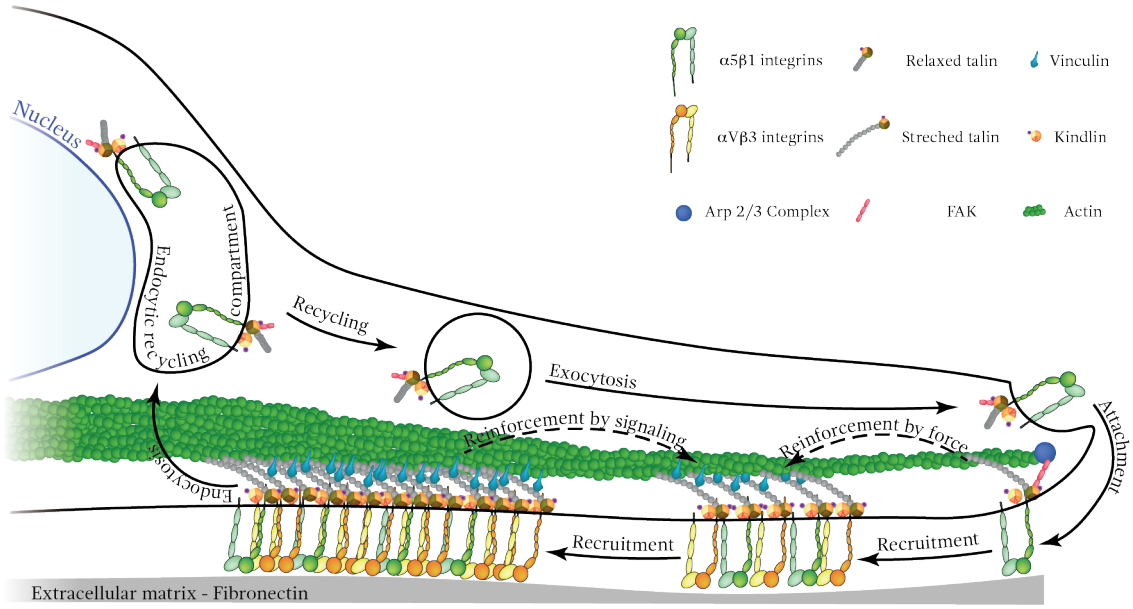

Figure 6-1 Two distinct integrin crosstalks regulate adhesion initiation and early adhesion formation in fibroblasts to fibronectin. Upon ligand binding at the leading edge of a migrating fibroblasts, α5β1 integrins are connected to actin by talin and the ligand bound conformation is stabilized by kindlin binding. These ligand-bound integrins sense forces applied to them, thereby inducing signaling that engages additional fibronectin-binding integrins to reinforce the adhesion. Due to that mixed adhesion sites are formed, containing α5β1 and αVβ3 integrins. These nascent adhesion sites are reinforced by signaling of matured adhesions that contain mainly αVβ3 integrins but also some α5β1 integrins. From matured adhesion sites α5β1 integrins are internalized in the high-affinity conformation with FAK and Src bound to their β-tail[3]. After internalization, these integrins are recycled to the leading edge, where they are exocytozed and can readily bind fibronectin.

6.2. Outlook

There are multiple challenges in fully understanding cell adhesion initiation and maturation on a molecular level, since the complexity of the cellular system is incredibly high. At the early stage of adhesion initiation, integrin conformations are important as the state of integrin dictates the ligand binding rate. However, the evaluation of integrin conformational changes is hampered due many different factors that influence integrin conformation. The documented

high flexibility of integrins argues for constantly changing conformations in the extracellular domains. However, a recent report suggested, that 99.7% of α5β1 integrins on the cell surface are in the closed, bend conformation and only 0.15% are in the extended, head piece open state[4]. This indicates a major energy barrier that needs to be overcome in order to switch integrins form the low to the high affinity conformation. So far it is not known how the energy is provided to integrin extracellular domains. However, it is likely that integrin conformation is influenced by multiple parameter, including intra- or extracellular proteins and the glycocalyx. A synthetic cell approach could be used to study integrin conformation in a defined system, in which integrin conformations are independent from other factors. Our lab has recently shown that soluble proteins can be used to oriented the insertion of membrane proteins into preformed liposomes[5]. This is an approach that could be used to reconstitute integrins into liposomes. Further, a microfluidics approach was reported that reconstituted integrins into giant unilamellar vesicles (GUVs)[6]. In combination with the increasing availability of cryo-electron microscopy devices, these approaches would allow the characterization of integrin conformation at an atomic level, which is not available yet. These synthetic cell systems can be supplemented with different cellular components, such as actin[6], integrins, actin regulatory proteins or glycoproteins to understand how these components alone and in synergy control integrin conformation and affinity. This bottom up approach could be used to fundamentally understand how adhesion is regulated by avidity or affinity changes and how the cohort of integrin regulatory proteins influences the adhesion formation and maturation without the complexity of the cell. However, a drawback of this technique would be the synthetic lipid composition, which may influence the movement of the transmembrane domain and membrane proximal domains of integrins. Nevertheless, this approach is promising in order to understand how integrin conformational changes regulate adhesion initiation.

Another challenge of understanding adhesion initiation is the dependence on optically resolvable adhesion structures. Although super-resolution microscopy has evolved in studying cell adhesion over the last years[7-9], still very little is known about exact mechanisms of adhesion initiation due to the lack of sensitive adhesion readouts. To study adhesion initiation, very soft substrates were used on which force transduction does not occure[7]. However, very soft substrates do not allow the formation of force dependent adhesion clusters and hence limit the understanding of early adhesion maturation. The combination of traction force microscopy, high resolution florescence microscopy and force sensitive measurements, which could either be single cell force spectroscopy or multiparametric characterization[10,11], would give more detailed insights into the mechanisms of early adhesion formation. A long-standing question, how traction forces and adhesion are linked and further, how increasing traction forces regulate adhesion independent from integrin recruitment could be answered.

Although kindlin and talin are indispensable for adhesion, their interplay in order to induce or maintain integrins in the high affinity conformation. Moreover, the synergetic effect

talin and kindlin in adhesion initiation is still not fully understood[12]. Using fibroblasts deficient of all talin and kindlin isoforms[13], allows the reconstitution of different combinations of talin and kindlin. The impact on binding kinetics of kindlin or talin to integrins, their dimerization or other features can be studied by genetic modification of both proteins. This may ultimately allow to understand the interplay of both proteins in integrin activation. Further, it will give more detailed information about functional domains in both proteins. Especially, the debated influence on adhesion of the hierarchy of actin binding to talin at ABS2 and ABS3 can be investigated. Further it is not clear, whether the integrin binding site in the talin rod (IBS2) can induce or maintain the active conformation of integrins. Although talin deficient fibroblasts that re-express the talin rod are non-adherent, adhesion initiation is indistinguishable from wild-type talin and significantly higher than in fibroblasts lacking talin (Figure 6-2). This indicates that IBS2 can induce or maintain integrins in the high affinity conformations, however adhesion maturation is strongly impaired. Whether other proteins are recruited to the talin rod domain remains to be understood. The role of this integrin binding site and whether it plays an important role in integrin mediated adhesion remains to be investigated. Fibroblasts expressing only the talin head domain show a strengthened early adhesion to fibronectin, which indicates that adhesion initiation is regulated by talin conformation and how it is regulated. This cellular system allows to identify proteins that are recruited to the adhesion site independently of talin transmitted force.

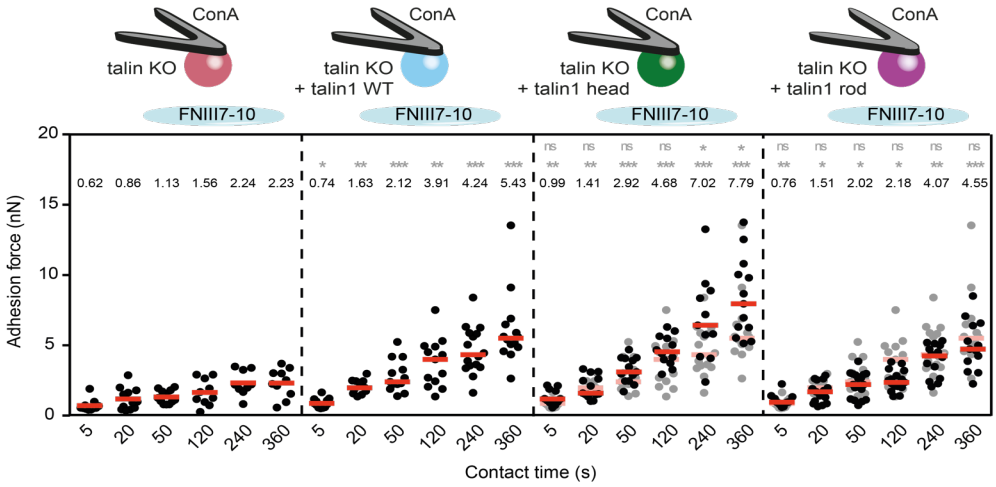

Figure 6-2 Talin head and rod domain can induce integrin mediated adhesion. Talin KO with or without reconstituted wild type talin1 and talin KO fibroblasts reconstituted with either talin1 head or rod domain were attached to a ConA-coated cantilever. Fibroblasts were approached onto a FNIII7-10-coated substrate and allowed to initiate adhesion for the given contact times. Subsequently, fibroblasts were detached from the substrate and their adhesion forces measured. Adhesion forces of individual fibroblasts (dots) and their median is given (red bar). *n* denotes median adhesion forces. As reference adhesion forces of fibroblasts expressing talin 1 (second panel) is given in the background. Differences of adhesion forces were evaluated by using Mann-Whitney test. *P*-values are given as ns – P <0.05, * – P ≦ 0.05, ** – P ≦ 0.01 or *** – P ≦ 0.001. Top row compares the given data with data from talin KO + talin 1 WT and bottom row with talin KO fibroblasts.

Although talin is widely studied, research is focused on talin 1 and about talin 2 very little is known. However, talin 2 is widely expressed[14], partially in tissue that is subjected to high mechanical load including heart, lung and skin. Moreover, it was suggested that talin 2 modulates

the adhesion in prostate cancer[15]. Recently it was shown that fibroblasts expressing exclusively talin 2, instead of talin 1, induces higher forces applied to talin and hence higher traction forces at adhesion sites[16]. Whether integrin-mediated adhesion is reinforced and single integrin-binding is modulated by talin 2 has not been evaluated. We have preliminary evaluated the adhesion initiation and maturation of fibroblasts expressing talin 1 or talin 2 (Figure 6-3). It was reported that talin 2 binds stronger to integrin intracellular domains[17], these experiments indicate that both isoforms of talin have similar mechanisms of integrin tail binding. However, fibroblast expressing talin 2 exceed adhesion forces of talin 1 expressing fibroblasts with increasing contact time. An increased vinculin recruitment to talin 2 (Ref. 16) could induce the increased adhesion forces by talin 2 expression. However, biophysical aspects, such as talin stretching that regulate protein binding to talin 2 as well as differences in adhesome formation that induce higher actin contraction remain to be understood.

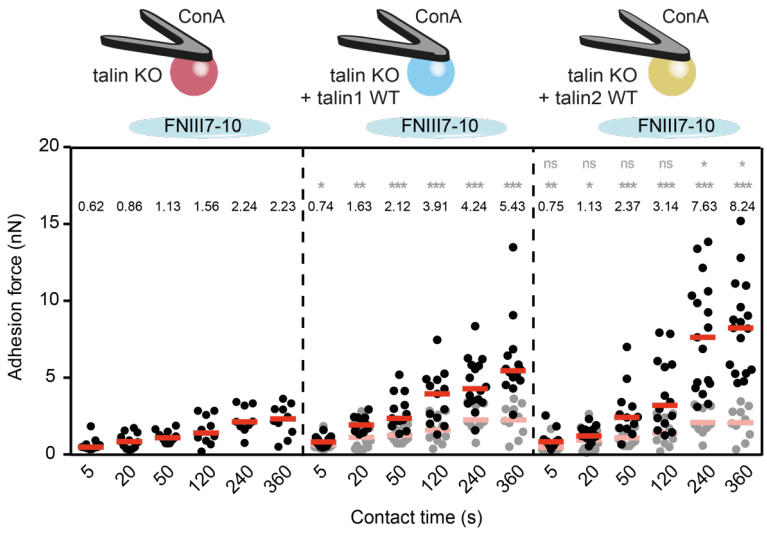

Figure 6-3 Talin head and rod domain can induce integrin mediated adhesion. Talin KO with or without reconstituted wild type talin1 and talin KO fibroblasts reconstituted with either talin1 head or rod domain were attached to a ConA-coated cantilever. Fibroblasts were approached onto a FNIII7-10-coated substrate and allowed to initiate adhesion for the given contact times. Subsequently, fibroblasts were detached from the substrate and their adhesion forces measured. Adhesion forces of individual fibroblasts (dots) and their median is given (red bar). *n* denotes median adhesion forces. As reference adhesion forces of fibroblasts expressing talin 1 (second panel) is given in the background. Differences of adhesion forces were evaluated by using Mann-Whitney test. *P*-values are given as ns – P <0.05, * – P ≦ 0.05, ** – P ≦ 0.01 or *** – P ≦ 0.001. Top row compares the given data with data from talin KO + talin 1 WT and bottom row with talin KO fibroblasts.

In this thesis, it is shown that with increasing contact time up to two minutes, α5β1 integrins from stronger adhesion than αVβ3 integrins, although individual α5β1 integrin-fibronectin bonds dissociate at lower forces from the ligand, have lower binding rates and require more time to form optically visible paxillin rich clusters than αVβ3 integrins. The delayed ligand binding of α5β1 integrins may be due to impaired stabilization in the active conformation by talin and/or kindlin, either due to competitive inhibition or a competitive binding of talin/kindlin to β3-tails. However, that α5β1 integrins form stronger adhesion during early adhesion formation indicates that either α5β1 integrins are recruited faster to the adhesion site or intracellular signaling

regulates adhesion maturation of α5β1 integrins at earlier stages compared to αVβ3 integrins. It remains unclear, how α5β1 integrin meditated adhesion initiation is regulated and further how it differs from αVβ3 integrins. Although α5β1 integrins are mechanosensitive already at the onset of adhesion and that these integrins induce actomyosin dependent cell contractility[1], it remains to be understood at which stage of adhesion initiation contractility regulates adhesion and how this is induced by α5β1 integrins. Very likely the composition of the adhesome of these two integrins is different during adhesion initiation and maturation and needs to be investigated in order to understand regulatory processes of adhesion initiation.

6.3. References

1. Schiller, H. B. *et al.* β1- and αv-class integrins cooperate to regulate myosin II during rigidity sensing of fibronectin-based microenvironments. *Nat. Cell Biol.* **15,** 625–636 (2013).
2. Schiller, H. B. & Fässler, R. Mechanosensitivity and compositional dynamics of cell–matrix adhesions. *EMBO Rep.* **14,** 509–519 (2013).
3. Nader, G., Ezratty, E. J. & Gundersen, G. G. FAK, talin and PIPKIγ regulate endocytosed integrin activation to polarize focal adhesion assembly. *Nat. Cell Biol.* **18,** 491–503 (2016).
4. Li, J. *et al.* Conformational equilibria and intrinsic affinities define integrin activation. *EMBO J.* **36,** 629–645 (2017).
5. Ritzmann, N. *et al.* Fusion Domains Guide the Oriented Insertion of Light-Driven Proton Pumps into Liposomes. *Biophys. J.* **113,** 1181–1186 (2017).
6. Weiss, M. *et al.* Sequential bottom-up assembly of mechanically stabilized synthetic cells by microfluidics. *Nat. Mater.* **409,** 387 (2017).
7. Changede, R., Xu, X., Margadant, F. & Sheetz, M. P. Nascent Integrin Adhesions Form on All Matrix Rigidities after Integrin Activation. *Dev. Cell* **35,** 614–621 (2015).
8. Theodosiou, M. *et al.* Kindlin-2 cooperates with talin to activate integrins and induces cell spreading by directly binding paxillin. *eLIFE* **5,** e10130 (2016).
9. Kanchanawong, P. *et al.* Nanoscale architecture of integrin-based cell adhesions. *Nature* **468,** 580–584 (2010).
10. Laskowski, P. R. *et al.* High-Resolution Imaging and Multiparametric Characterization of Native Membranes by Combining Confocal Microscopy and an Atomic Force Microscopy-Based Toolbox. *ACS Nano* **11,** 8292–8301 (2017).
11. Alsteens, D. *et al.* Atomic force microscopy-based characterization and design of biointerfaces. *Nat. Rev. Mater.* **2,** 17008 (2017).
12. Calderwood, D. A., Campbell, I. D. & Critchley, D. R. Talins and kindlins: partners in integrin-mediated adhesion. *Nat. Rev. Mol. Cell Biol.* **14,** 503–517 (2013).
13. Böttcher, R. T. *et al.* Kindlin-2 recruits paxillin and Arp2/3 to promote membrane protrusions during initial cell spreading. *J. Cell Biol.* (2017). doi:10.1083/jcb.201701176
14. Debrand, E. *et al.* Talin 2 is a large and complex gene encoding multiple transcripts and protein isoforms. *The FEBS Journal* **276,** 1610–1628 (2009).
15. Formosa, A. *et al.* DNA methylation silences miR-132 in prostate cancer. *Oncogene* **32,** 127–134 (2012).
16. Austen, K. *et al.* Extracellular rigidity sensing by talin isoform-specific mechanical linkages. *Nat. Cell Biol.* **17,** 1597–1606 (2015).
17. Qi, L. *et al.* Talin2-mediated traction force drives matrix degradation and cell invasion. *J. Cell Sci.* **129,** 3661–3674 (2016).

7. Acknowledgements

During the time that I worked on this PhD thesis, I was supported by many people that ensured this time to be successful. I might not list everyone in person here, but to everyone that was closely or remotely involved in or away from the work: Thank you very much.

To start with I would like to thank Daniel Müller, who gave me the opportunity to work in his lab not only once but twice. It has been a long journey, in which you gave me the freedom to shape and drive projects. I really appreciate your trust in my judgements, decisions and gut feeling, as well as in me as a mentor for students. Thanks to your support, in which ever form it was, I could grow not only professionally but also personally.

I would also like to thank Reinhard Fässler, with whom we have a very fruitful collaboration. I very much enjoyed our regular meetings, whether they were in Germany, Switzerland, Italy or Spain. I value your input in everything related to my work very much, without these nothing written in this thesis would have been possible. But I also enjoyed every discussion we had besides work. Thank you for being like a second mentor.

In addition, I would like to thank Michael Nash for completing the committee and for dedicating valuable time to my thesis.

A very special thank you goes to Mitasha. Thank you for the great time while working with you and at several conferences, for your open ears and valuable advises. Thank you for being a good friend. Since you'll leave the lab soon, I wish you all the best for your future; it's not gonna be the same without you.

The whole Müller Lab, contributed tremendously to this work. Thank you all for being great colleagues, for you inputs in lab meetings, great retreats and coffee discussions. Especially I have to name the adhesion group with Mitasha, Patrizia, Max, Marilia and Kevin. Together, we somehow understood how integrins may work, although I guess this is only a wishful thinking, but we are getting there! I thank Jonne, not only for his programming skills and critical questions, which occasionally gave me a hard time thereby always improving my work, but also for (partially off-topic) discussions. I have to specially mention Yosh and Moritz here. Spending time with you in the lab, but especially also outside the lab was great fun.

A big thank you goes to the molecular medicine group at the Max-Planck Institute in Munich for their great hospitality, scientific discussions and for providing all important reagents and cells that we needed. It was great discussing our work.

I would like to thank my parents and brother, for supporting and believing in me, even in times when I didn't. Thank you for always being there for me.

At the end, I thank the most special person in my life. Marie thank you for ... everything